# STUDIES ON THE DIGLYCOLAMIDE-FUNCTIONALIZED EXTRACTANTS CONTAINING POLYMER INCLUSION MEMBRANE FOR ACTINIDE SEPARATION AND SENSOR DEVELOPMENT

**By**

**Bholanath Mahanty**

**CHEM01201204010**

**Bhabha Atomic Research Centre, Mumbai-85**

***A Thesis submitted to the***

***Board of Studies in Chemical Sciences***

***In partial fulfillment of requirements***

***for the Degree of***

**DOCTOR OF PHILOSOPHY**

***of***

**HOMI BHABHA NATIONAL INSTITUTE**

**November, 2017**

# Homi Bhabha National Institute

## Recommendations of the Viva Voce Committee

As members of the Viva Voce Committee, we certify that we have read the dissertation prepared by **Shri Bholanath Mahanty** entitled **"Studies on the diglycolamide-functionalized extractants containing polymer inclusion membrane for actinide separation and sensor development"** and recommend that it may be accepted as fulfilling the thesis requirement for the award of Degree of Doctor of Philosophy.

Chairman - Dr. A. Dash Dash **Date:** 28.9.17

Guide / Convener - Dr. P. K. Mohapatra **Date:** 28.9.2017

Examiner – Dr. U. K. Kharul **Date:** 28.09.17

Member 1- Dr. S. C. Tripathi **Date:**

Member 2- Dr. A. K. Pandey Pandey **Date:** 28.9.2017

Technology Adviser- Dr. A. K. Satpati **Date:** 28.9.17

Final approval and acceptance of this thesis is contingent upon the candidate's submission of the final copies of the thesis to HBNI.

***I hereby certify that I have read this thesis prepared under my direction and recommend that it may be accepted as fulfilling the thesis requirement.***

**Date:** 28.9.17
**Place:** Mumbai

**Signature**

**Guide**

# STATEMENT BY AUTHOR

This dissertation has been submitted in partial fulfillment of requirements for an advanced degree at Homi Bhabha National Institute (HBNI) and is deposited in the Library to be made available to borrowers under rules of the HBNI.

Brief quotations from this dissertation are allowable without special permission, provided that accurate acknowledgement of source is made. Request for permission for extended quotation from or reproduction of this manuscript in whole or in part may be granted by the Competent Authority of HBNI when in his or her judgement the proposed use of the material is in the interests of schloraship. In all other instances, however, permission must be obtained from the author.

Bholanath Mahanty

**(Bholanath Mahanty)**

# DECLARATION

I, hereby declare that the investigation presented in the thesis has been carried out by me. The work is original and has not been submitted earlier as a whole or in part for a degree / diploma at this or any other Institution / University.

Bholanath Mahanty
**(Bholanath Mahanty)**

## List of Publications arising from the Thesis

### Journal

1. Comparative evaluation of actinide ion uptake by polymer inclusion membranes containing TODGA as the carrier extractant; **B. N. Mahanty**, D. R. Raut, P. K. Mohapatra, D. K. Das, P. G. Behere, Md. Afzal; ***J. Hazard. Mater.***, 275 (**2014**) 146–153.
2. Novel Polymer Inclusion Membranes Containing T2EHDGA as Carrier Extractant for Actinide Ion Uptake from Acidic Feeds; **Bholanath Mahanty**, P. K. Mohapatra, D. R. Raut, D. K. Das, P. G. Behere, Md. Afzal; ***Radiochim. Acta***, 103(4) (**2015** ) 257–264.
3. Actinide Ion Specific Polymer Inclusion Membranes Containing T2EHDGA: Uptake Isotherm and Transport Studies; **B. N. Mahanty**, P. K. Mohapatra, D. R. Raut, D. K. Das, P. G. Behere, Md. Afzal; ***Ind. Eng. Chem. Res***., 54 (12) (**2015**) 3237–3246.
4. Comparative Evaluation of Polymer Inclusion Membranes Containing Several Substituted Diglycolamides for Actinide ion Separations; **B. N. Mahanty**, P. K. Mohapatra , D. R. Raut, D. K. Das, P. G. Behere, Md. Afzal; ***J. Membr. Sci.*** 501 **(2016)** 134–143.
5. Polymer Inclusion Membrane Containing a Tripodal Diglycolamide Ligand: Actinide Ion Uptake and Transport Studies; **Bholanath Mahanty**, P. K. Mohapatra, D. R. Raut, D. K. Das, P. G. Behere, Md. Afzal, W. Verboom; ***Ind. Eng. Chem. Res.,*** 55 (7) **(2016)** 2202–2209.
6. Polymer inclusion membrane containing a tripodal diglycolamide (T- DGA): Characterization and sorption isotherm studies; **B. N. Mahanty**, P. K. Mohapatra, D. R. Raut, D. K. Das, P. G. Behere, Md. Afzal, W. Verboom; ***J. Environ. Chem. Eng.*** 4 **(2016)** 1826–1838.
7. Polymer inclusion membrane containing a diglycolamide- functionalized calix[4]arene for actinide ion uptake and transport; **B. N. Mahanty**, P. K. Mohapatra, D. R. Raut, D. K. Das, P. G. Behere, Md.Afzal , W.Verboom, ***J. Membr. Sci.*** 516 **(2016)** 194–201.

**8.** Development of a *N,N,N',N'*-tetra-*n*-octyl diglycolamide (TODGA) based Potentiometric Sensor for $Eu^{3+}$; **B. Mahanty**, A. K. Satpati, P. K.Mohapatra; ***J. Electroanal. Chem*** (**Communicated**).

**Conferences / Symposia**

**i.** Studies on uptake and transport of actinide ions using polymer inclusion membranes containing multiple diglycolamide-functionalized ligands; **B. N. Mahanty**, D. R. Raut, P. K. Mohapatra, D. K. Das, P. G. Behere, Md. Afzal, W. Verboom; In proceedings of DAE-BRNS Theme Meeting on Membrane Separations for Fuel Cycle Applications (***MEMSEP-2013***) held at Bhabha Atomic Research Centre, Mumbai, during September 16-18, 2013, Paper No. O-28.

**ii.** Studies on actinide ion uptake and transport using polymer inclusion membranes containing TODGA as the extractant: **B.N. Mahanty**, D.R. Raut, D.K. Das, P.G. Behere, Md. Afzal, P.K. Mohapatra; In proceedings of DAE-BRNS Fifth Symposium on Nuclear Analytical Chemistry (***NAC-V***), held at Bhabha Atomic Research Centre, Mumbai, during January 20-24, 2014, Paper No. G-7.

**iii.** Evaluation of a Novel PIM Containing T2EHDGA as a Carrier for Uptake and Transport of Actinides from Acidic Feeds: **B. N. Mahanty**, D. R. Raut, D. K. Das, P. G. Behere, Md. Afzal, P. K. Mohapatra; In proceedings of DAE-BRNS Theme meeting on Emerging Trends in Separation Science and Technology (***SESTEC-2014***) held at Bhabha Atomic Research Centre, Mumbai, during February 25-28, 2014, Paper No. SNFC-45.

**iv.** Comparative Studies on Uranyl Ion Uptake and Transport from Acidic Feeds by Several Diglycolamides employing Polymer Inclusion Membrane Technique. **B. N. Mahanty**, D. R. Raut, D. K. Das, P. G. Behere, Md. Afzal, P. K. Mohapatra; In proceedings of

National Conference on Rare Earth Processing and Utilization (***REPUT-2014***) held at Bhabha Atomic Research Centre, Mumbai, during May 2-3, 2014, Paper No. B-1.

**v.** Evaluation of a Polymer Inclusion Membrane Containing a C-pivot Tripodal Diglycolamide for Am(III) Extraction: **B. N. Mahanty**, D. R. Raut, P. K. Mohapatra, D. K. Das, P. G. Behere, Md. Afzal, W. Verboom; In proceedings of DAE-BRNS 5th Interdisciplinary Symposium in Materials Chemistry (***ISMC-2014***) held at Bhabha Atomic Research Centre, Mumbai, December 9-13, 2014, Paper No. A-137.

**vi.** Experimental and Modeling Study of $Eu^{3+}$ Uptake by Polymer Inclusion Membrane Containing C-Pivot Tripodal Diglycolamide from Acidic Feed. **B. N. Mahanty**, D. R. Raut, P. K. Mohapatra, D. K. Das, P. G. Behere, Md. Afzal, W. Verboom; In Proceedings of DAE-BRNS Symposium on Nuclear and Radiochemistry (***NUCAR-2015***), held at Bhabha Atomic Research Centre, Mumbai, during Feburary 9-13, 2015, Paper No. B-30.

**vii.** Uptake and Transport of Actinides by a Polymer Inclusion Membrane Containing a Diglycolamide Functionalized Calix[4]arene; **B. N. Mahanty**, D. R. Raut, P. K. Mohapatra, W. Verboom; In Proceedings of DAE-BRNS Symposium on Nuclear and Radiochemistry (***NUCAR-2015***), held at Bhabha Atomic Research Centre, Mumbai, during Feburary 9-13, 2015, Paper No. B-34.

**viii.** Separations of Actinide Ions by Polymer Inclusion Membranes Containing Several Substituted Diglycolamides: **B. N. Mahanty**, D. R. Raut, D. K. Das, P. G. Behere, Md. Afzal, P. K. Mohapatra; In Proceedings of DAE-BRNS Symposium on Nuclear and Radiochemistry (***NUCAR-2015***), held at Bhabha Atomic Research Centre, Mumbai, during Feburary 9-13, 2015, Paper No. B-49.

**ix.** Uptake of Eu(III) by a Polymer Inclusion Membrane Containing T2EHDGA: Sorption Isotherm Analysis; **B. N. Mahanty**, D. R. Raut, D. K. Das, P. G. Behere, Md. Afzal, P. K. Mohapatra; In Proceedings of DAE-BRNS Symposium on Nuclear and Radiochemistry (***NUCAR-2015***), held at Bhabha Atomic Research Centre, Mumbai, during Feburary 9-13, 2015, Paper No. D-8.

**x.** Evaluation of a Polymer Inclusion Membrane containing N,N,N',N'-tetraoctyl diglycolamide (TODGA) for Europium Ion Selective Electrode: **B. N. Mahanty**, A. K. Satpati, P. K. Mohapatra, D. K. Das, P. G. Behere, Md. Afzal; In proceedings of first DAE-BRNS first symposium on Recent Advances in Nuclear Fuel Cycle Activities (***NUFUC-2015***), held at Bhabha Atomic Research Centre, Tarapur, during August 20-21, 2015, Paper No.-A 12.

**xi.** Studies on Actinide ion uptake and transport using Polymer inclusion membrane containing Multiple diglycolamide-functionalized extractant; D. R. Raut, **Bholanath Mahanty**, P. K. Mohapatra, W. Verboom; In proceedings of ***GLOBAL-2015***, held at Paris, France, during September 21-24, 2015, Paper No. 5283.

**xii.** Development of a N, N, N', N'-tetraoctyl diglycolamide (TODGA) based Potentiometric Sensor for Europium Ion; **B. N. Mahanty**, A. K. Satpati, P. K. Mohapatra, D. K. Das, P. G. Behere, Md. Afzal; In proceedings of International Conference on Recent Advances in Analytical Sciences (***RAAS-2016***), held at Department of Chemistry, Indian Institute of Technology, Banars Hindu University, Varanasi, during April 7-9, 2016, Paper No.-CS-14.

Bholanath Mahanty

**(Bholanath Mahanty)**

*DEDICATED To*

*My Parents and Family*

# ACKNOWLEDGEMENT

Finally I am writing the acknowledgement part of my ph.d thesis. Completion of ph.d is a challengeing task and also a dream come true for me.

First and foremost, I would like to extend my sincere gratitude to my research guide, Prof. P.K.Mohapatra, Head, Actinide Chemistry Section for giving me an opportunity to participate in the interesting and challenging work in his research laboratory. I am deeply indebted to him for his invaluable guidance, critical comments and constant encouragement during the entire course of this study. This work would not have been possible without his sincere guidance, support and motivation. I take this opportunity to state that his keen interest and valuable suggestions were of immense help in improving the quality of work as well as enriching my knowledge.

I especially thank Dr. D. R. Raut for his immense help during execution of the work. It was always a pleasant experience to work with him and gives me an opportunity to learn many things from him.

It is my pleasure to express my sincere thanks to Dr. A.K.Satpati who is also my technology adviser of the doctoral committee for giving me an opportunity to work in his laboratory and his active support during the course of the work.

I would like to thank all the doctoral committee members including respected chairman, Dr. A. Dash for their constructive and critical evaluation of my work during the course of the studies.

I am thankful to Director, Radiochemistry and Isotope (RC & I) group, BARC, Mumbai and Head, Radiochemistry Division, B.A.R.C., Mumbai for allowing me to avail all the facilities at the division required for the completion of the work. I wish to express my sincere gratitude to Shri P. G. Behere, Chief Superintendent, Advanced Fuel Fabrication Facility (AFFF), Nuclear Recycle Board (NRB) and Shri R. B. Bhatt, Plant Superintendent, AFFF for allowing

me to persue the research work. My special thanks also go to Dr. Amrit Prakash who has introduced me to my research guide. I also wish to sincerely thank Dr. R. B.Gujar, Dr. S. A. Ansari, Dr. A. Bhattacharya, Mr. D. R. Prabhu, Mr. P. K. Verma and Mr. A. S. Kanekar for their co-operation during the course of this study. I would also like to thank my batchmate Shri Chetan Baghra from 48th batch OCES training school, for helping me in few characterization studies of my samples. I am thankful to my colleagues Dr. A. Kumar, Dr. A. Kelkar, Shri V. R. Sonar, Shri C. D. Karekar, Mrs. R. S. Gaikwad, Mrs. S. S. Raul, Shri K. Sadhukhan, Shri A. Pandey, Mr. F. A. Khan and Shri G. Singh for their invaluable support during the course of this study. I thank to all persons who helped me directly or indirectly during this work.

My parents are my constant source of inspiration for me. What I am today is because of their support and blessing. I am forever indebted to them. I would also like to thank my uncles, aunties, sisters, brother and in-laws for their good wishes. I am thankful to my son, Rudraneel Mahanty who has been the source of my vitality. Last but not least I am thankful to my beloved wife, Mrs Rinku Mahanty for her support all along this journey.

I thank GOD for making dream come true, and helping me realize my goal.

Bholanath Mahanty
Bholanath Mahanty

## CHAPTER 4: SEPARATION OF ACTINIDES BY POLYMER INCLUSION MEMBRANES CONTAINING MULTIPLE DIGLYCOLAMIDE-FUNCTIONALIZED LIGANDS AS THE CARRIER EXTRACTANTS 110-154

# SYNOPSIS

## "Studies on the diglycolamide-functionalized extractants containing polymer inclusion membrane for actinide separation and sensor development"

As a consequence of factors such as nuclear weapon testing, accidents at nuclear plant site or leaching of vitrified waste blocks containing radionuclides due to possible failure, phase incompatibility etc., there is a possibility of release of radioactivity into the Environment. Since, the half lives of actinides (Th, U, Pu, Am, Np) ranges from about hundreds of years to several millions of years, there is long term radiation hazard to the Environment. Thus, efficient separation methods for the removal of actinides from a variety of samples, such as soil, rock, food, air, biological samples, radioactive waste, etc are required. All these separations involve nitric acid feed solutions and suitable extractants. Though U and Pu are conveniently extracted using TBP based extraction processes, the minor actinide (Np, Am, Cm) removal is a challenging task and usually requires efficient tailor made extractants such as octyl-(phenyl)-*N*,*N*-diisobutylcarbamoylmethylphosphine oxide (CMPO), tetralkylmalonamides, diisodecylphosphoric acid (DIDPA), trialkyl phosphine oxide (TRPO), etc. [1]. However, these extractants are associated with problems such as third phase formation, poor back extraction which made search for alternative extractants. Diglycolamide (Fig. 1) (DGA) based extractants such as TODGA (N,N,N',N'-tetraoctyl diglycolamide) have been suggested to overcome these problems and quite a few studies have been carried out to demonstrate separation of these metal ions from "hot" solutions [2].

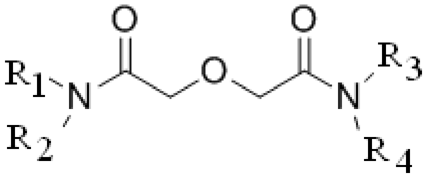

**Fig. 1: Structure of a diglycolamide (R = Alkyl group)**

It has been reported that TODGA extracts metal ions based on a size selective extraction mechanism. Factors which make TODGA a promising extractant for actinide partitioning include (i) high distribution coefficient of trivalent actinides / lanthanides from moderately acidic aqueous medium, (ii) complete incineration as it contains C, H, N, O as the constituent atoms (iii) radiolytic and hydrolytic stability, (iv) ease of preparation. In view of a possible lesser aggregation tendency, which may have significant effects on the metal ion extraction, the branched homolog of TODGA, namely T2EHDGA (N,N,N',N'-tetra(2-ethyl hexyl) diglycolamide) has also been extensively studied by different research groups with encouraging results [3]. Analogous DGA extractants such as N,N,N',N'-tetrapentyl diglycolamide (TPDGA), N,N,N',N'-tetrahexyl diglycolamide (THDGA) and N,N N',N'-tetradecyl diglycolamide (TDDGA) [4] and multiple DGAs, such as tripodal diglycolamides (T-DGA) and DGA functionalized calix[4]arene (C4DGA) (Fig. 2) [5] have also been studied for actinide ion separations. Though solvent extraction based separation methods have been found promising, there is a need to develop eco-friendly separation methods with low ligand inventory.

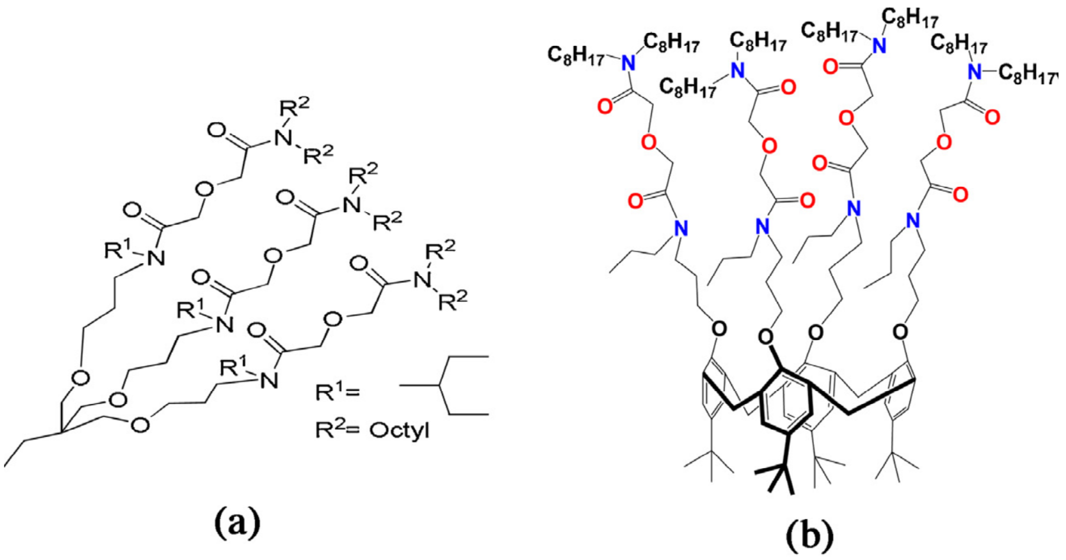

**Fig. 2: Structural formulae of (a) T-DGA and (b) C4DGA**

Liquid membrane (LM) based separation methods [6] have been suggested as viable alternatives to solvent extraction based methods due to advantages such as low ligand inventory, easy scale up, simultaneous extraction and stripping, etc. However, a major disadvantage associated with the LMs is their poor stability under experimental conditions which limits their use in large-scale applications. Polymer inclusion membranes (PIMs), on the other hand, retain most of the advantages of LM and have been suggested as alternatives to the LMs and have been extensively studied for metal ion separations by many research groups. In PIMs, the carrier is held in the membrane by molecular entanglement due to which the loss of carrier from the membrane is minimized and the stability of the membrane is enhanced [7]. These PIMs were formed by casting a solution containing polymer, carrier and plasticizer to form a thin, mechanically strong and flexible film. The PIM based methods are extensively employed in the extraction of metal ions from waste solution, separation of anions, construction of ion selective electrodes, optodes, as a template for nano particle synthesis, [8-12]. DGA (Fig. 1) based extractants such as TODGA, T2EHDGA, TPDGA, THDGA, etc., and ligands containing multiple DGA groups such as T-DGA and C4DGA have been extensively studied for actinides separation from acidic radioactive feeds using supported liquid membrane (SLM) methods. However, studies on PIMs containing DGAs are very limited. Similarly, PIMs containing DGA as ionophore in the electrochemical sensing of lanthanide ions is also lacking which has relevance in environmental sample analysis.

This doctoral thesis describes the application of the PIMs in the field of actinide separation and electrochemical sensing of Europium(III) ion using DGAs as the carrier extractant in a systematic manner. In the present study, PIMs were prepared using the above mentioned DGAs as carrier, cellulose triacetate (CTA) or polyvinyl chloride (PVC) as the base polymer and 2-nitrophenyl octyl ether (2-NPOE) as the plasticizer. The present work is divided into two parts. In the first part, the PIMs containing different DGA as carrier extractant were used to study the uptake and transport of actinides ($Am^{3+}$, $Pu^{4+}$, $Th^{4+}$ and $UO_2^{2+}$) from acidic feed solutions. The different DGAs and multiple-DGA ligands used for the preparation of the PIMs are TODGA, T2EHDGA, TPDGA, THDGA, TDDGA, T-DGA and C4DGA. In the second part, the PIMs containing TODGA were explored for the development of ion selective electrodes for the Europium(III) ion. This doctoral Thesis has been structured in different Chapters and each Chapter contains the following information.

## CHAPTER 1: GENERAL INTRODUCTION

This Chapter includes an overview of the nuclear fuel cycle, chemistry of the actinide elements with emphasis on elements such as Th, U, Pu and Am, classification of radioactive wastes, and an introduction to different separation techniques such as solvent extraction, liquid membrane and polymer inclusion membranes, etc. The theory of facilitated transport of metal ions across the PIMs was described. A brief description on the different types of extractants involved in the separation of minor actinides (Am, Cm, Np) and their advantage/disadvantage are also included in this Chapter. The DGA based ligands are very versatile extractant for the removal of trivalent actinides/lanthanides from nuclear waste solution. The background of the development of the DGA based ligands is briefly mentioned in this Chapter as well.

The theory of ion selective electrode is briefly described in this Chapter. Additionally, the role of different constituents of the polymer based ion selective electrode on the electrode potential is explained [13, 14]. Finally, the aims and objectives of the work are presented in this Chapter.

## CHAPTER 2: EXPERIMENTAL

A general outline of the various experimental techniques and instrumentations used in the study are discussed in this Chapter. A general procedure for the synthesis, purification and characterization of DGA ligands used in the present work are included in this Chapter. The radiometric assay for $^{241}$Am, $^{234}$Th and $^{152, 154}$Eu were done by gamma ray counting using NaI(Tl) scintillation detector while liquid scintillation counting was carried out for assaying alpha emitting radio nuclides, such as Pu, $^{233}$U. The basic principles of these radiation detectors are briefly discussed. The various steps followed for the separation and purification of the radio tracer, including oxidation state adjustment are also included in this Chapter. The experimental procedure for the uptake and transport studies of the actinides used in the present study is given in this Chapter. The physical characterizations of the PIMs are carried out using various techniques, such as thermogravimetric analysis (TGA), x-ray diffraction (XRD) study, transmission infrared mapping microscopy (TIMM), Fourier transform infrared (FT-IR) spectroscopy, atomic force microscopy (AFM) and scanning electron microscopy (SEM). The basic principles of these techniques are described briefly in this Chapter. The experimental part of potentiometry study is also included in this chapter.

## CHAPTER 3: ACTINIDE ION UPTAKE AND TRANSPORT BY THE POLYMER INCLUSION MEMBRANES CONTAINING DIFFERENT DIGLYCOLAMIDES AS THE CARRIER EXTRACTANTS

This Chapter deals with the studies on the uptake and transport of actinide ions from acidic feed solutions by polymer inclusion membranes (PIM) containing DGA based carrier extractants such as TODGA, T2EHDGA, TPDGA, THDGA and TDDGA. The actinide ions studied are Am(III), Pu(IV), Th(IV) and U(VI). The effect of plasticizer (NPOE), polymer (CTA) and carrier extractant (different DGAs) on the uptake of the actinide ions ($Am^{3+}$ has been used as the representative actinide) by the PIMs were studied in detail in order to find the optimized composition of the PIMs. The uptake studies of the actinide ions were carried out with a small piece of the PIM (usually 4 $cm^2$) in dilute acidic feed solutions (1 M $HNO_3$) while the transport studies were carried out using 1 M $HNO_3$ as the feed and 1 M α-HIBA (*alpha*-hydroxy-*iso*-butyric acid) as the strip solution.

Out of the different DGAs, TODGA was found to be the most promising extractant for the uptake of actinide ions from acidic feed solutions [2]. The comparative uptake and transport behaviour of the actinides by the optimized PIMs were studied in this Chapter which showed the trend: Am(III) > Pu(IV) > Th(IV) > U(VI). The comparatively lower uptake of Pu(IV) as compared to that of Am(III) indicated prevalence of the well known reverse micellar mechanism reported in case of TODGA [15]. The diffusion coefficient and permeability coefficient values for different actinides were experimentally determined and the results are included in this Chapter along with the relevant discussion.

T2EHDGA is a branched homolog of TODGA and has been reported to be a promising extractant for the actinides [3] and is reported to favour the extraction of trivalent actinides with higher decontamination factor values (with respect to fission products) due to stereo-chemical hindrance. The comparative uptake and transport study of different actinide ions by the optimized PIMs indicated the trend: Pu(IV) > Am(III) > Th(IV) > U(VI) which was different from that found with TODGA based PIM (*vide supra*). The reason for the higher transport of Pu(IV) than Am(III) could be due to the lower possibility of aggregate formation by the branched chain T2EHDGA molecules and thus, indicates the absence of reverse micellar mechanism. This Chapter also gives a detailed account of the kinetics and extraction isotherm studies for the batch extraction studies with macro amounts of $Eu^{3+}$ (used as a surrogate of $Am^{3+}$) using the T2EHDGA based PIM. The batch uptake data conformed to the pseudo-second order kinetic model and the Langmuir sorption isotherm model, both of which propose chemisorption as the extraction mechanism.

The physico-chemical properties of the DGA-based ligands can be tuned by judicious choice of the alkyl group attached to the nitrogen atom of the ligand. Therefore, in this Chapter several substituted diglycolamide viz. TPDGA, THDGA and TDDGA were used for the preparation of PIMs which were subsequently evaluated for the uptake and transport studies of the actinide ions from acidic feed solutions under identical experimental conditions mentioned above. The effect of the alkyl chain length on the uptake of the actinides is significant with TDDGA based PIMs as comparatively lower uptake efficiencies were noticed with the TDDGA based PIM. This may be due to the lower availability of the carrier molecules due to more DGA-$HNO_3$ types adduct with TDDGA as compared to TPDGA and THDGA. Different transport parameters such as diffusion coefficient, permeability coefficient, etc. were experimentally determined and used for the comparison of the transport efficiency of the PIMs used and the results are included in this Chapter. Stability and reusability of the PIMs were also investigated.

## CHAPTER 4: SEPARATION OF ACTINIDES BY POLYMER INCLUSION MEMBRANES CONTAINING MULTIPLE DIGLYCOLAMIDES AS THE CARRIER EXTRACTANTS

In order to discount the effect of the organic diluents in the formation of reverse micellar aggregates, it was of interest to evaluate the performance of several DGA-based extractant for the extraction of the actinide ions in the absence of any aggregation effect. Moreover, the extraction efficiency also increases due to a cooperative action of in case of multiple-DGA-functionalized extractants resulting from entropy stabilization. In the view of these, PIMs containing multiple DGA-functionalized carrier extractants, such as, tripodal diglycolamides (T-DGA) (Fig.2) and DGA-functionalized calix[4]arenes containing 4 DGA pendent arms (C4DGA) (Fig.2) based PIMs were evaluated for the uptake and transport of actinide ions from acidic feed solutions. The actinide ions studied were, Am(III), Pu(IV), Th(IV) and

U(VI). This Chapter deals with the studies on the uptake and transport of actinide ions using CTA based PIMs containing T-DGA as well as C4DGA as the carrier extractant while 2-NPOE was used as the plasticizer.

The effects of the concentrations of T-DGA and NPOE in the PIMs on the uptake of Am(III) at 1 M $HNO_3$ are studied and the results are discussed in this Chapter. The effect of the feed composition (the feed acidity as well as the salt composition) on Am(III) uptake was also investigated. The comparative uptake of different actinide ions followed the trend: Pu(IV) > Am(III) >> U(VI) > Th(IV) while their transport behaviour followed the trend: Am(III) > Pu(IV) > Th(IV) > U(VI). This Chapter also describes in detail the batch extraction of Eu-radiotracer in the presence of macro concentrations of $Eu^{3+}$ (used as a surrogate of $Am^{3+}$) on to the T-DGA based PIMs. The experimental uptake data were fitted to different isotherms (Langmuir, Freundlich, Dubinin−Radushkevich, Redlich-Peterson) and kinetic (pseudo-first-order, pseudo-second order, Elovich) models. The various parameters of the different model equations were determined from the fitted plots and the results are included in this Chapter.

The best extraction efficiency of different DGA-functionalized calix[4]arenes for the extraction of actinide / lanthanide ions has been thoroughly investigated [5] and the results indicated that the C4DGA ligand with *n*-octyl groups as the most efficient. The effects of NPOE and C4DGA content in the PIMs on the uptake and transport efficiencies of Am(III) from dilute nitric acid feeds was investigated in detail and the results are presented in this Chapter. The comparative uptake and transport behaviour of the actinide ions by the C4DGA based PIMs were also studied and the results are included in this Chapter. The stability and reusability possibility of the T-DGA and C4DGA based PIMs, which are crucial for their long term use, were also evaluated.

## CHAPTER 5: DEVELOPMENT OF AN EUROPIUM (III) ION SENSOR BASED ON TODGA AS THE IONOPHORE

A polymeric membrane can become a suitable sensor membrane for a given metal ion, provided it shows very fast interfacial reaction at the membrane - feed interface and very slow transport of the metal ion through the polymeric membrane in a measurable time scale as required for an ion selective electrode. The polymeric membrane should also show preferential interfacial reaction of the given metal ion as compared to other metal ions since it primarily decides the selectivity of the given metal ion in the presence of other metal ions. It has been observed that PIMs containing TODGA as the carrier extractant showed not only faster extraction kinetics but also preferential extraction of the trivalent actinides over the other tetravalent and hexavalent actinide ions from dilute acidic feeds. Thus, it was of interest to evaluate PIMs containing TODGA as a potential membrane for sensing trivalent actinide / lanthanide ions from acidic feed solutions. This Chapter deals with the development of a potentiometric ion sensor for Europium(III) ion based on TODGA as the ionophore. The initial part of this Chapter presents a feasibility study in the construction of a CTA based PIM containing TODGA as the ionophore for electrochemical sensing of Eu(III) ion from dilute nitric acidic solutions while the second part of this Chapter deals with the development of a polyvinyl chloride (PVC) based Eu(III) ion sensor containing TODGA as the ionophore, 2-NPOE as plasticizer and sodium tetra phenyl borate (NaTPB) as the anion excluder. The effect of pH, concentration of inner filling solution and the interference effects of different metal ions on the electrode response are presented in this part of the Chapter. The possibility of the sensor electrode as an indicator electrode for the potentiometric titration of $Eu^{3+}$ has also been presented in this Chapter. Finally, the determination of $Eu^{3+}$ in a synthetic mixture containing a known amount of added $Eu^{3+}$ in the uranyl nitrate sample by the proposed sensor as well as its comparison with ICP-AES result are also discussed.

## CHAPTER 6: SUMMARY AND CONCLUSIONS

This thesis work mainly demonstrates the possible application of PIM based separation of U(VI), Pu(IV), Th(IV) and Am(III) from dilute nitric acid feed solutions using several DGA ligands viz. TODGA, T2EHDGA, TPDGA, THDGA and TDDGA and multiple DGA-functionalized ligands viz., T-DGA and C4DGA as the carrier extractants. The PIMs were prepared following standard methods and their physical characterization was carried out using techniques, e.g., TGA, XRD, SEM, AFM, FTIR and TIMM. The effect of the concentrations of the carriers, the plasticizer and the polymer on the uptake of the actinide ions ($Am^{3+}$ has been used as a representative in most studies) by the PIMs was investigated in detail to get the optimum composition of the PIMs. The uptake and transport profiles of actinide ions were evaluated at varying feed compositions by the PIMs.

The uptake and transport studies suggested that the uranyl ion was least effectively extracted by the DGA based PIMs indicating possible steric constraints in accommodating the ligand molecules along the equatorial plane of the metal ion which hindered the extraction. The transport studies of the actinides ions using the above mentioned PIMs indicated that significant amounts of the actinide ions are held up within the PIM and longer time was required for >90% transport. The T-DGA-containing PIMs were found to be more efficient than the TODGA-based PIMs in the batch uptake studies. A comparable uptake (~90%) of Pu(IV) was observed at 10 times lower concentration with the T-DGA based PIMs as compared to those containing TODGA / T2EHDGA or other substituted-DGAs as the extractant. A comparatively slow uptake and transport of actinide ions was observed with the C4DGA containing PIM.  Different transport parameters e.g., permeability coefficients, diffusion coefficient for the actinides with the PIMs were determined experimentally and compared with the available data obtained with analogous SLMs. The reusability and stability studies of the DGA-based PIMs indicate the limited life time of the PIMs. The mechanism of extraction of trivalent actinide ions ($Eu^{3+}$ was taken as a surrogate of $Am^{3+}$) was studied in detail with T2EHDGA and T-DGA based PIMs by fitting the uptake data with various kinetic and isotherm equations. Finally, a polymeric membrane electrode containing TODGA as the ionophore was prepared and studied for possible potentiometric determination of Eu (III) ions.

## REFERENCES

1. J.N. Mathur, M.S. Murali and K.L. Nash, *Solv. Extr. Ion Exch.*, 19 (2001) 357.
2. Y. Sasaki, Y. Sugo, S. Suzuki and T. Kimura, Conference Proceedings Atalante 2004, Nimes, France, 2004.
3. S. Manohar, J.N. Sharma, B.V. Shah and P.K. Wattal, *Nucl. Sci. Eng.* 156 (2007) 96.
4. S. Panja, P.K. Mohapatra, S.C. Tripathi, G.D. Dhekane, P.M. Gandhi and P. Janardan, *J. Membr. Sci.*, 399– 400 (2012) 28
5. M. Iqbal, Ph. D. Thesis; University of Twente, The Netherlands, 2012.
6. P. K. Mohapatra and V. K. Manchanda, *Indian J. Chem.* 42A (2003) 2925.
7. L. D. Nghiem, P. Mornane, I. D. Potter, J. M. Perera, R. W. Cattrall and S. D. Kolev, *J. Membr. Sci.,* 281 (2006) 7.
8. P. K. Mohapatra, D. S. Lakshmi, A. Bhattacharyya and V. K. Manchanda, *J. Hazard. Mater.* 169 (2009) 472.
9. J. S. Gardner, Q. P. Peterson, J. O. Walker, B. D. Jensen, B. Adhikary, R.G. Harrison and J. D. Lamb, *J. Membr. Sci.* 277 (2006) 165.
10. F. Faridbod, M. R. Ganjali, R. Dinarvand and P. Norouzi, *Afr. J. Biotechnol.* 6 (2007) 2960.
11. F. B. Mohd Suah, M. Ahmad and L.Y. Heng, *Sens. Actuators B* 201 (2014) 490.
12. Y.Y.N. Bonggotgetsakul, R.W. Cattrall and S.D. Kolev, *J. Membr. Sci.* 428 (2013) 142.

13. P. Buhlmann and L.D. Chen, in: A.W. Steed, P. Gale (Eds.), vol. 5, John Wiley & Sons, Ltd, New York, (2012) 2539.
14. E. Lindner and B. D. Pendley, *Analytica Chimica Acta* 762 (2013) 1.
15. M. P. Jensen, T. Yaita and R. Chiarizia; *Langmuir* 23 (2007) 4765.

# List of figures

**Page No.**

# List of tables

# CHAPTER 1

# GENERAL INTRODUCTION

Actinides are heavy metals with atomic numbers ranging from 89 through to 103 [**1**]. Most of their isotopes are alpha active with long half lives, and are, therefore, highly radiotoxic in nature. These elements can enter into the food chain through various pathways and even in small amounts can cause serious health hazards. The nuclear weapon tests have produced global fallouts detectable in different parts of the world. The use of nuclear power in energy production also creates actinides which might be released to the Environment during different activities of the nuclear fuel cycle. The consequences of the accidents involving nuclear power plants at Chernobyl in the former Soviet Union, and more recently at Fukushima Daiichi in Japan increased interest in understanding the behaviour of radionuclides in the Environment and on their hazards to the ecosystem [**2**]. One of the important sources of actinides found in the environment is from the waste products that are left behind after the use of radioactive substances. Radioactive wastes are usually resultant of activities related to the nuclear fuel cycle [**3**].

Due to the neutron induced nuclear fission of fissile elements (such as $^{235}$U, $^{233}$U, $^{239}$Pu, etc.), an enormous amount of energy is released along with the production of a host of fission product nuclides (most of which are highly radioactive) including some lanthanide elements. In this process, long-lived alpha emitting actinides such as $^{241}$Am, $^{243}$Am, $^{245}$Cm and $^{237}$Np (referred to as minor actinides) also produced as activation products are present in significant quantities in the spent fuel along with the unreacted fissile elements. Since, the half lives of actinides (Th, U, Pu, Am, Np, Cm) ranges from 100 years to millions of years, there is long term radiological risk to the Environment [**4**]. Thus, efficient separation methods for the removal of actinides from a variety of samples, such as soil, rock, food, air, biological samples, radioactive wastes, etc are required. The sustainability of future nuclear energy programmes for the welfare of humanity largely depends on the safe management of nuclear waste which includes the removal of long-lived radionuclides and safe disposal of the lean waste under deep geological repositories. Hence, it is desirable to understand the source and composition of radioactive waste generated at various stages of nuclear fuel cycle.

## 1.1. NUCLEAR FUEL CYCLE

The steps involved in the production of electricity from nuclear fission of a fissile radionuclide in a controlled manner in a reactor are referred, collectively, to as the nuclear fuel cycle. The nuclear fuel cycle is broadly comprised of two parts, viz. the front end and the back end. The front end of the nuclear fuel cycle includes mining of the ore, milling, conversion, enrichment, fuel fabrication, reactor operation, etc.

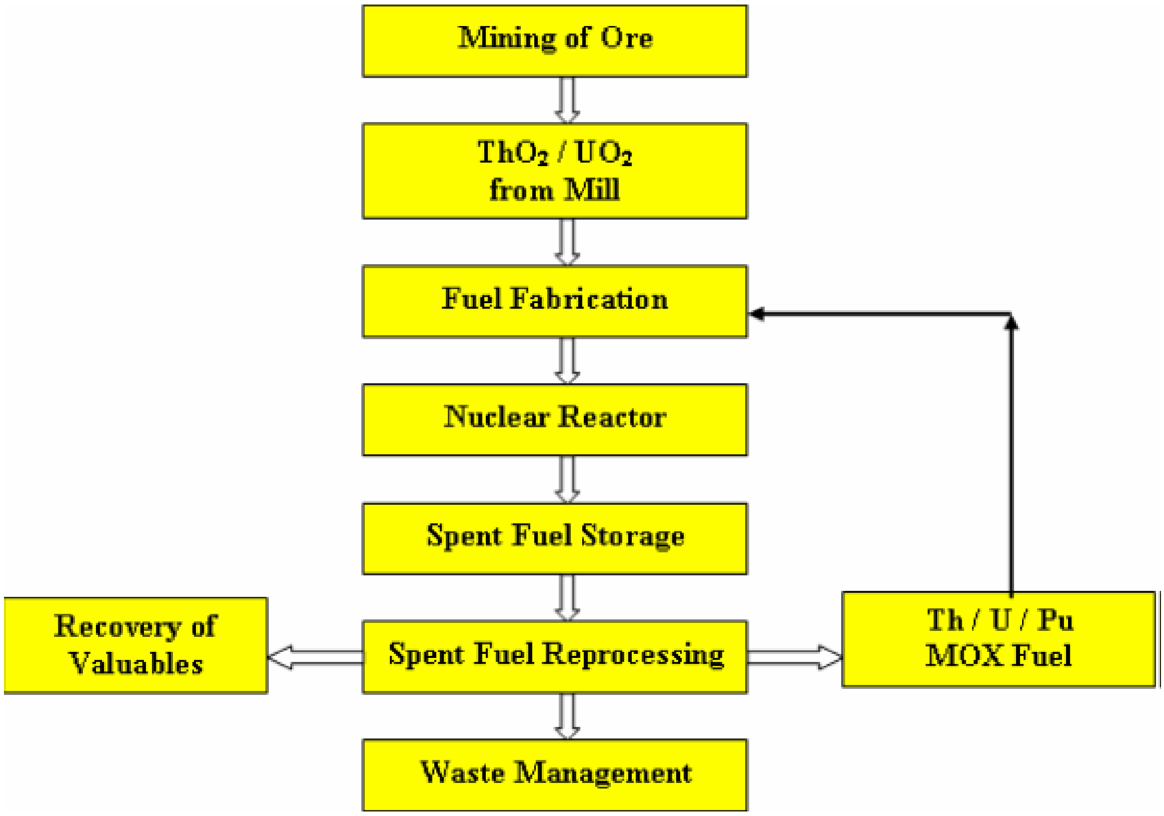

Fig.1.1. Nuclear fuel cycle

The back end of nuclear fuel cycle includes removal of the spent fuel from the reactor, temporary storage, reprocessing to recover the valuables, and treatment and subsequent disposal of the high level waste. At each stage of the fuel cycle, radioactivity can be released into the Environment. Fig. 1.1 shows the schematic of the nuclear fuel cycle.

### 1.1.1. Waste from the "Front End"

Uranium is mined in open or in underground. The ores contain generally 0.1% to 0.2% of uranium; therefore, a large quantity of uranium ore has to be mined. Waste rock is produced during mining when overburden is removed. The piles of this waste rock may contain elevated concentrations of the radioisotopes compared to normal rocks. The piles releases radon gas continuously due to the decay of long-lived $^{226}$Ra and radioactivity can be released into the environment even after shut down of the mine due to the seepage of water.

Table 1.1. Major contributors to the radioactivity in the spent fuel after a cooling period of 50 days

| Nuclides | Half life | Nuclides | Half life |
|---|---|---|---|
| $^{3}$H | 12.3 y | $^{131}$I | 8.05 d |
| $^{85}$Kr | 10.8 y | $^{137}$Cs | 30.0 y |
| $^{89}$Sr | 50.6 d | $^{140}$Ba | 12.8 d |
| $^{90}$Sr | 28.8 y | $^{140}$La | 40.2 d |
| $^{90}$Y | 64.4 h | $^{141}$Ce | 32.4 d |
| $^{91}$Y | 58.8 d | $^{143}$Pr | 13.6 d |
| $^{95}$Zr | 65 d | $^{144}$Ce | 285 d |
| $^{95}$Nb | 35 d | $^{144}$Pr | 17.3 m |
| $^{103}$Ru | 39.6 d | $^{147}$Nb | 11.1 d |
| $^{106}$Ru | 367 d | $^{147}$Pm | 2.62 y |
| $^{129m}$Te | 34 d | | |

Ores obtained from uranium mines are milled, leached and subjected to various separation processes to get uranium in the form of yellow cake ($U_3O_8$) leaving behind a large quantity of liquid waste tailing containing small amounts of un-extracted uranium and other decay products of uranium. The yellow cake contained only a fraction of the total concentration of the decay products as most of those are retained in the tailing itself. The uranium tailings emit gamma-radiations 20 to 100 times of the natural background levels on the deposit surface. The $^{226}$Ra in the tailing pile continuously decays to the radioactive gas $^{222}$Rn which is a major concern for uranium tailing even after shut down of the mill. Tailing piles are also subjected to erosion and seepage which contaminates the ground and surface water. The steps accompanied in the conversion of yellow cake to the usable form of the fuel do not produce significant radioactive waste. A significant quantity of the radioactive elements is produced when the fuel is subjected to fission in the reactor (Table 1.1). Normally, more than 99.9% radioactivity is retained in the fuel rods while 0.1% of the total radioactivity is distributed in other parts of the reactor.

### 1.1.2. Waste from the "Back End"

Most of the radioactive wastes emanating from various activities in the nuclear fuel cycle are generated in the reprocessing of the spent fuel. A nuclear fuel that has been sufficiently used in the reactor is referred as the "spent fuel". In uranium fuelled reactor, $^{235}$U undergoes neutron induced fission to produce fission products which are mostly highly radioactive and contribute to major part of the radiation dose of the waste. Apart from this, due to the neutron capture reaction with $^{238}$U followed by sequential beta emission and also neutron capture reaction of the daughter nuclei, long-lived alpha emitting transuranic elements such as Np, Pu, Am and Cm are formed and retained in the spent fuel. The spent fuel is usually allowed to cool for a few years in a water pool to allow the decay of the short lived radionuclides and also, to reduce the decay heat. The major contributors to the radioactivity after a cooling period of 50 days are included in Table 1.1. In the spent fuel, the dominant sources of heat and radioactivity which lasts for ~300 years are due to the presence of two fission product nuclides such as $^{137}$Cs and $^{90}$Sr. After 300 years, the major sources of radioactivity are $^{239}$Pu, $^{240}$Pu, $^{238}$Pu, $^{241}$Am, $^{151}$Sm, $^{237}$Np, $^{99}$Tc, etc. The main radionuclides concerned after 10,000 years are $^{239}$Pu, $^{240}$Pu, $^{243}$Am, $^{237}$Np, and $^{99}$Tc whereas after 100,000 years the major contribution to the radioactivity in the spent fuel is due to the presence of fission product nuclides viz. $^{99}$Tc, $^{135}$Cs, $^{93}$Zr, $^{129}$I, and actinides viz. $^{234,235,238}$U, $^{242}$Pu, $^{237}$Np, etc and their decay products. In a closed fuel cycle, the spent fuel is subjected to reprocessing (PUREX process) to recover the valuable plutonium and depleted uranium. A flow sheet for the reprocessing of the spent fuel is shown in Fig. 1.2.

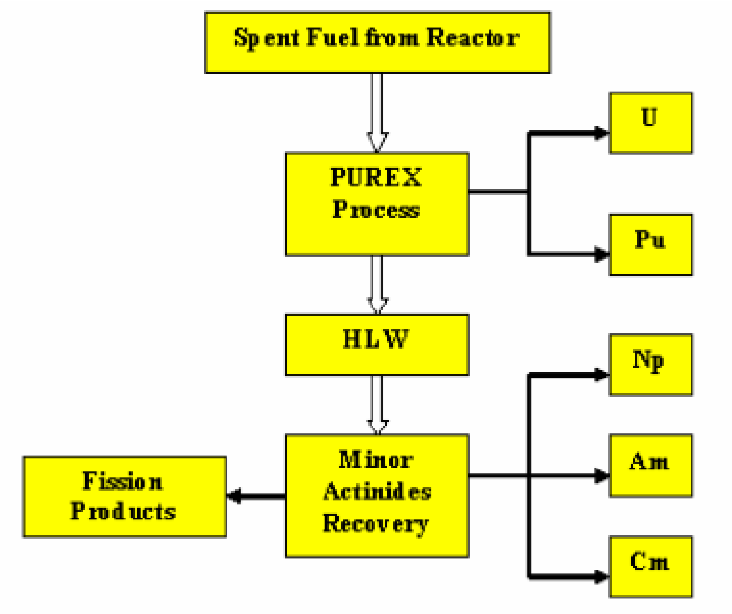

Fig. 1.2. Reprocessing of spent fuel

The aqueous raffinate of PUREX process is concentrated to result in the high-level radioactive waste (HLW) containing the unextracted U, Pu, the minor actinides (Am, Cm, Np), the fission and the activation products along with the structural elements and process chemicals. This HLW is potentially hazardous for tens of thousands to millions of years due to the presence of long-lived actinides and therefore, a safe disposal of the HLW is a challenging task in the back end of the nuclear fuel cycle. Apart from this, the other sources of radioactive waste in the back end of nuclear fuel cycle are ion exchange resins used for water purification in PHT / coolant channels, chemical sludges, reactor components, reprocessing equipments, etc.

## 1.2. CATAGORIZATION OF NUCLEAR WASTE

Radioactive wastes can be broadly categorized into low level waste (LLW), intermediate level waste (ILW) and high level waste (HLW) based on the radioactivity content in the waste. A brief description of the different types of radioactive waste is given below.

### 1.2.1. Low level waste

The waste containing radioactivity of less than millicurie / litre is called low level waste (LLW). It is generated from the decontamination of equipments, radioactive laboratories, hospitals using radiopharmaceuticals, various chemical treatments in the nuclear fuel cycle, etc. The low level waste contains small amounts of (mostly) short-lived radionuclides and therefore, when stored for a few months, most of the radioactive isotopes decay to their stable daughter products. It is not very dangerous to handle but must be disposed off carefully as compared to the normal wastes. The LLW comprises of about 90% of the total volume of the radioactive wastes generated, but only < 1% radioactivity of all the wastes. Generally, the solid LLWs are compressed or incinerated before their final burial in shallow landfill sites.

### 1.2.2. Intermediate level waste

Intermediate level waste (ILW) is the category of nuclear waste which contains the radioactivity in the range of millicuries/litre to curie/litre and may require special shielding. The waste contains long-lived radionuclides in moderate to large quantities. It comprises of chemical sludges, resins, nuclear reactor parts, reprocessing equipments, contaminated equipments of weapon decommissioning. It comprises of 7% of the total volume of the waste and only 4% of the total radioactive waste. The waste may be solidified in the concrete form and the disposal can be in the facility at the depth of between a few tens and a few hundreds of meters.

### 1.2.3. High level waste

High level waste (HLW) is defined to contain radioactivity in quantities greater than curie/litre of the waste. HLW is generated in the reprocessing of nuclear fuels. It makes up 3% of the total volume while it contains more than 95% of the total radioactivity generated in the nuclear fuel cycle. HLW contains minor actinides (Np, Am, Cm), uranium, plutonium and fission product nuclides. It generates a considerable amount of heat and requires interim cooling as well requires special shielding during handling and transportation. Due to the presence of long-lived minor actinides in HLW, it possesses major challenges in the final disposal. Efforts are being made by separation scientists to meet the challenges in the development of a suitable method to separate the minor actinides from HLW.

## 1.3. IMPACT OF RADIONUCLIDES ON THE ENVIRONMENT

The impact of a radionuclide on the Environment is influenced by the behavior of the former in the natural environment, quantity, chemical form, nature of radiation and half life of the radionuclide. A long-lived radionuclide has an impact on the environment that exists for longer duration as compared to the short-lived radionuclide. The radioactive waste, whether natural or artificial, is a potential source of radiation exposure to the living beings through different pathways. The mining and processing of uranium and thorium bearing ores gives rise to the production of wastes which possess potential radiological hazards to the Environment. For example, the mining of uranium bearing ore leaves a residue which contains an elevated concentration of $^{226}$Ra compared to that present in the original mined ore and thus, presenting a source of radon progeny. Events like nuclear explosion or major accident in the reactor result in the release of different radionuclides having different physical and radiological characteristics. The impact of long-lived radionuclides, such as $^{137}$Cs, $^{90}$Sr and actinides on the Environment can be observed many years after such events. The other potential sources of radiation hazard are from processes involved in the management of spent fuel in the back end of the nuclear fuel cycle. The raffinate of PUREX process after reprocessing of the spent fuels in the closed fuel cycle generally contains un-extracted U, Pu and bulk of minor actinides such as Am, Np, Cm and a host of fission products like $^{99}$Tc, $^{107}$Pd, $^{93}$Zr, $^{135,137}$Cs, $^{90}$Sr and lanthanides as well as activation products. The long-lived radionuclides present in the raffinate of the PUREX process are of great environmental concern. At present, the most accepted conceptual approach for the management of HLW is to vitrify it in a glass matrix followed by its burial in deep geological repositories [**5, 6**]. Since the half lives of minor actinides concerned range between a few hundred to millions of years, the surveillance of high active waste for such a long period is practically impossible from economical as well as environmental safety point of view. Moreover, the possibility of heat and radiation damage of the vitrified mass of HLW due to the decay of the beta / gamma emitting fission products such as $^{137}$Cs and $^{90}$Sr cannot be ruled out during the first 100-300 years. Therefore, it may create a possible risk of leaching and migration of long-lived alpha emitting minor actinides from the repository to the environment. As recommended, a waste containing alpha activity of 4000 Bq per gram or less is considered to be benign enough to be treated as LLW.

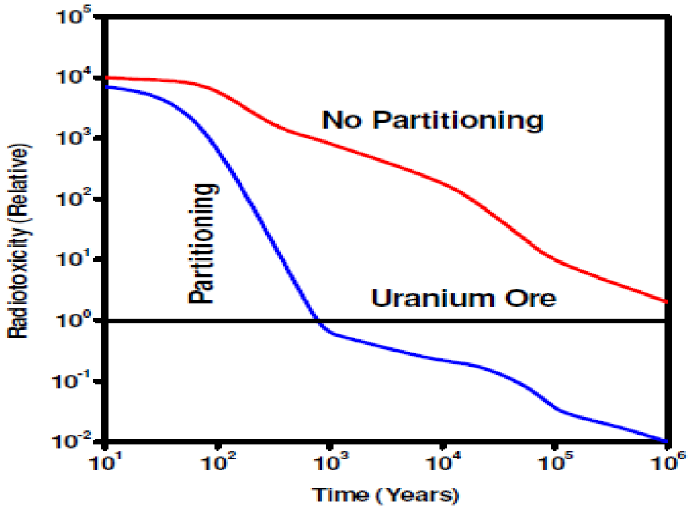

Fig. 1.3. Partitioning of minor actinides-impact on waste management

As represented in Fig. 1.3, if the actinides are not removed from the HLW, it will require millions of years to reduce its radiotoxicity to the level of uranium ore. However, if one can separate U, Pu and minor actinides from the waste, the radiotoxicity of the HLW would reach to the acceptable level after few hundreds of years. Therefore, P&T (partitioning of long-lived actinides followed by transmutation) strategy is being considered by many countries around the world prior to the disposal of HLW [**7, 8**]. The P&T strategy envisages complete removal of the long-lived minor actinides from the HLW followed by its burning in high flux reactors / accelerators as mixed oxide fuel. This would lead to the generation of extra energy in the reactor and at the same time long term surveillance of the repository may not be required. After partitioning of the actinides along with long-lived fission products from HLW, the residual waste can be vitrified in the glass matrix and buried in subsurface repositories at a much reduced risk and cost.

## 1.4. CHEMISTRY OF ACTINIDES AND LANTHANIDES

The work carried out in this Thesis pertains to the separation chemistry of actinides from radioactive waste solutions and electrochemical sensing of Eu(III) from its aqueous solutions. The actinides include thorium, uranium, plutonium and americium whereas europium was the representative lanthanide element chosen for the electrochemical studies. It is quite essential to understand the chemistry of actinides and lanthanides before their separation / analysis from the aqueous waste solution. A brief survey of the chemistry of actinide and lanthanide elements is, therefore, considered relevant.

### 1.4.1. History

#### 1.4.1.1. Actinides

The existence of a rare earth like series in the seventh row of the periodic table, which was suggested as early as 1926, gained wider acceptance with the discovery of the transuranium elements [**9**]. In 1945, Seaborg proposed that actinium and transactinium elements form such a series in which the 5*f* electron shell is being filled in a manner analogous to the filling of the 4*f* shell in the lanthanides [**10**]. Except for uranium and thorium, which are well known actinide elements discovered in 1789 and 1828, respectively, all the other elements were discovered in the twentieth century. Amongst the actinide elements, uranium and thorium have isotopes with half-lives exceeding the estimated life of this planet and hence occur in nature. Actinium and protactinium owe their existence to the decay of long lived isotopes of uranium, thorium and their daughter products. The rest of the elements in this series are essentially “man made” with some evidence for the trace occurrence of neptunium and plutonium in the nature formed by nuclear reactions involving uranium [**11**, **12**]. Amongst the man made elements, plutonium, and to a lesser extent, neptunium, americium and curium are produced in the nuclear power reactors and are recovered from the spent nuclear fuels. The elements beyond curium are generally produced through heavy ion reactions of transplutonium elements in accelerators. With increasing atomic number of the actinides, the nuclei become increasingly less stable and only einsteinium has an isotope with a half-life long enough to offer any possibility for conventional chemical studies.

The fourteen 5*f* electrons enter the actinide elements beginning formally with Th (Z=90) and ending with Lr (Z=103). These fourteen elements following Ac are placed in the 7th row of the periodic table separately analogous to the lanthanides. Intensive chemical studies have revealed many similarities between the lanthanides and actinides. One of the major similarities is their existence in the +3 oxidation states (more common for the heavier actinides) which is a consequence of their electronic configuration. The ground state electronic configurations of lanthanides and actinides are presented in Table 1.2.

Table 1.2. Electronic configuration of lanthanide and actinide elements

| Lanthanides | | | Actinides | | |
|---|---|---|---|---|---|
| Elements | Atomic numbers | Electronic configuration | Elements | Atomic numbers | Electronic configuration |
| La | 57 | $5d^1\ 6s^2$ | Ac | 89 | $6d^1\ 7s^2$ |
| Ce | 58 | $4f^1\ 5d^1\ 6s^2$ | Th | 90 | $6d^2\ 7s^2$ |
| Pr | 59 | $4f^3\ 6s^2$ | Pa | 91 | $5f^2\ 6d^1\ 7s^2$ |
| Nd | 60 | $4f^4\ 6s^2$ | U | 92 | $5f^3\ 6d^1\ 7s^2$ |
| Pm | 61 | $4f^5\ 6s^2$ | Np | 93 | $5f^4\ 6d^1\ 7s^2$ |
| Sm | 62 | $4f^6\ 6s^2$ | Pu | 94 | $5f^6\ 7s^2$ |
| Eu | 63 | $4f^7\ 6s^2$ | Am | 95 | $5f^7\ 7s^2$ |
| Gd | 64 | $4f^7\ 5d^1\ 6s^2$ | Cm | 96 | $5f^7\ 6d^1\ 7s^2$ |
| Tb | 65 | $4f^9\ 6s^2$ | Bk | 97 | $5f^9\ 7s^2$ |
| Dy | 66 | $4f^{10}\ 6s^2$ | Cf | 98 | $5f^{10}\ 7s^2$ |
| Ho | 67 | $4f^{11}\ 6s^2$ | Es | 99 | $5f^{11}\ 7s^2$ |
| Er | 68 | $4f^{12}\ 6s^2$ | Fm | 100 | $5f^{12}\ 7s^2$ |
| Tm | 69 | $4f^{13}\ 6s^2$ | Md | 101 | $5f^{13}\ 7s^2$ |
| Yb | 70 | $4f^{14}\ 6s^2$ | No | 102 | $5f^{14}\ 7s^2$ |
| Lu | 71 | $4f^{14}\ 5d^1\ 6s^2$ | Lr | 103 | $5f^{14}\ 6d^1\ 7s^2$ |

Though there is overall similarity between the two groups of elements, some important differences also exist mainly due to the similar energies of the 5*f* and 6*d* shells in the actinides and the 5*f* electrons are not as well shielded as the 4*f* electrons in the lanthanides [**13**]. The lighter actinides (Ac to Np) show greater tendency to retain their 6*d* electrons due to smaller energy differences between the 6*d* and the 5*f* orbitals relative to that between the

5*d* and the 4*f* orbitals of lanthanides. In case of transition series, the relative energy of the orbitals undergoing the filling process becomes lower as the successive electrons are added. For actinides also, the 5*f* orbitals of plutonium and subsequent elements are of lower energy than the 6*d* orbitals and, therefore, the subsequent electrons are filled in the 5*f* orbitals with no electrons in the 6*d* orbitals.

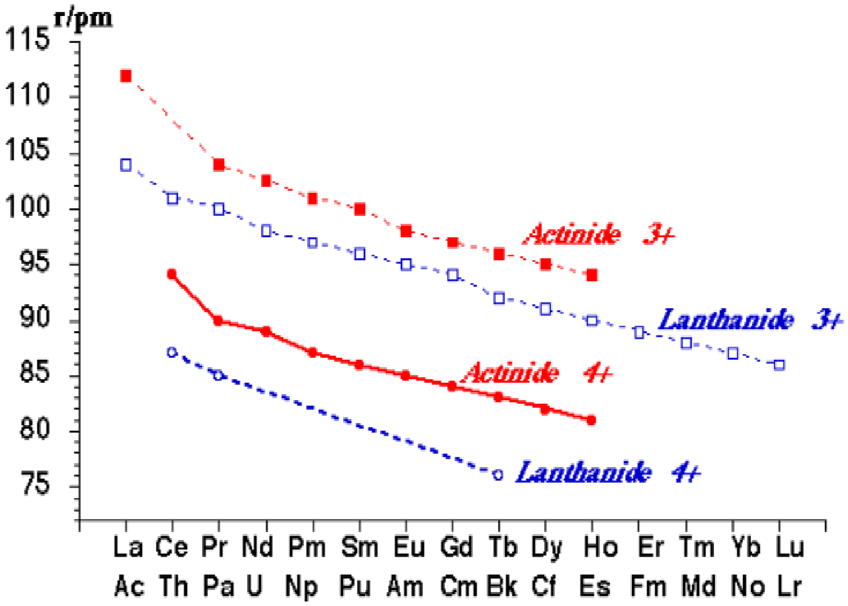

Fig. 1.4. Lanthanide and actinide contraction in 3+ and 4+ oxidation states

The size of the actinide ions decreases with increasing atomic number (Fig. 1.4) similar to the lanthanides, which is termed as the ‘actinide contraction’ analogous to the famously known ‘lanthanide contraction’.

### 1.4.2. Solution chemistry of actinides

As the processes of separation and purification of actinides on large scale are essentially based on hydrometallurgical techniques, the study of solution chemistry of actinides has received considerable attention. The actinide elements exist in multiple oxidation states and most of their separation processes are based on the effective exploitation of this property. It is, therefore, desirable to understand the various oxidation states of actinides in solution.

### 1.4.2.1. Oxidation states

The trivalent oxidation state is the most stable for all lanthanides. However, this is not so at least in the case of the early members of the actinide series. The 5*f* electrons of the actinides are subjected to a lesser attraction from the nuclear charge than the corresponding 4*f* electrons of the lanthanides. The greater stability of the tetra positive ions of the early actinide series is attributed to the smaller values of fourth ionization potential for the 5*f* electrons compared to those for the 4*f* electrons of the lanthanides, an effect which has been observed experimentally in the case of Th and Ce [**14**]. Thus, thorium exists in the aqueous phase only as Th(IV) while the oxidation state 3+ becomes dominant only for transplutonium elements. The actinides existing in different oxidation states are shown in Table 1.3, where the most stable oxidation states are also indicated [**13**]. All the oxidation states are well known except for the 7+ states for Np and Pu which exist in alkaline solutions [**15**]. Penta and hexavalent actinide ions exist in acid solution as oxygenated cations, viz. $MO_2^+$ and $MO_2^{2+}$.

Table 1.3. Oxidation states of actinide elements

| 89 | 90 | 91 | 92 | 93 | 94 | 95 | 96 | 97 | 98 | 99 | 100 | 101 | 102 | 103 |
|---|---|---|---|---|---|---|---|---|---|---|---|---|---|---|
| Ac | Th | Pa | U | Np | Pu | Am | Cm | Bk | Cf | Es | Fm | Md | No | Lr |
|  |  |  |  |  |  | (2) |  | (2) |  |  |  | 2 | 2 |  |
| 3 | (3) | (3) | 3 | 3 | 3 | 3 | 3 | 3 | 3 | 3 | 3 | 3 | 3 | 3 |
|  | 4 | 4 | 4 | 4 | 4 | 4 | 4 | 4 |  |  |  |  |  |  |
|  |  | 5 | 5 | 5 | 5 | 5 |  |  |  |  |  |  |  |  |
|  |  |  | 6 | 6 | 6 | 6 |  |  |  |  |  |  |  |  |
|  |  |  |  | 7 | 7 |  |  |  |  |  |  |  |  |  |

**Those underlined are the most stable oxidation states in aqueous solution; those in parentheses refer to oxidation states which are not known in solutions.*

Actinide elements such as Pu are known to exist in different oxidation states simultaneously. This has been attributed to their very close redox potentials. The redox potential diagrams of early actinides such as Th, U, Np and Pu at 25°C in 1 M $HClO_4$ are shown in Fig. 1.5 [**16**, **17**].

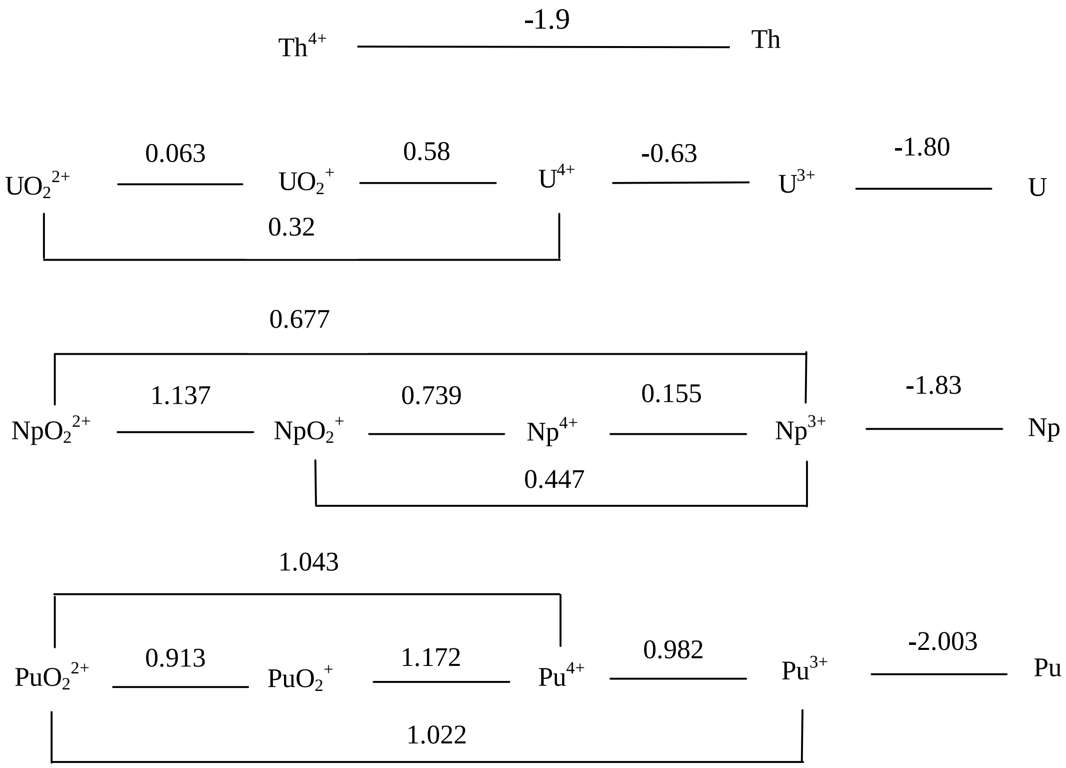

Fig. 1.5. Redox potential of actinide ions in 1 M $HClO_4$ (volts)

It has been found that the $M^{3+}/M^{4+}$ and $MO_2^{+}/MO_2^{2+}$ couples are reversible and fast as they involve the transfer of only single electron. On the other hand, the other couples, such as the $M^{4+}/MO_2^{+}$ couple, are irreversible and achieve equilibrium slowly as they involve the formation or rupture of the metal oxygen bonds.

### 1.4.2.2. Hydrolysis of actinides

In view of their large ionic potentials, the actinide ions in various oxidation states exist as strongly hydrated ions in the absence of complexing anions. The actinide ions in the divalent to the tetravalent oxidation states are present as $M^{2+}$, $M^{3+}$ and $M^{4+}$, respectively. The penta and hexavalent oxidation states are prone to more hydrolysis as compared to the lower oxidation states and exist as partially hydrolyzed actinyl ions, viz. $MO_2^+$ and $MO_2^{2+}$ which can get further hydrolyzed under high pH conditions. The oxygen atoms of these ions are not basic in nature and thus do not co-ordinate with protons. The degree of hydrolysis for the actinide ions decreases in the order: $M^{4+} > MO_2^{2+} > M^{3+} > MO_2^+$ which is similar to their complex formation properties [**18**]. In general, the hydrolysis of the actinide ions can be represented by the following generic equation:

$$M^{n+} + xH_2O \leftrightarrow M(H_2O)_x^{n+} \leftrightarrow M(OH)_x^{(n-x)+} + xH^+ \qquad (1.1)$$

The hydrolytic behaviour of Th(IV) is quite different from that of other tetravalent actinide ions [**19**]. For U(IV) and Pu(IV), the metal ion hydrolyses first in a simple monomeric reaction (Eq. 1.1) followed by a slow irreversible polymerization of hydrolyzed products. For Th(IV), however, various polymeric species exist even in very dilute solutions. Whereas the polymer formation of Pu(IV) is irreversible, that of Th(IV) is reversible. The hydrolysis of some of the trivalent actinides such as Am(III), Cm(III) and Cf(III) is well studied which revealed higher hydrolysis constant values for the trivalent actinides as compared to their lanthanides analogs [**13**].

### 1.4.2.3. Complexation of actinides

The actinide ions in the aqueous solutions exhibit strong tendency to form complexes. This property of actinides is widely exploited in devising methods for their separation and purification. One of the most important factors that determines the strength of the complex formed is the ionic potential (or charge density expressed as charge to ionic radius ratio) of the metal ions, which is defined as the ratio of the ionic charge to the ionic radius of a given actinide ion. Higher the ionic potential, greater is the electrostatic attraction between cations and anions and hence stronger is the complex formed. The complexing strength of actinide ions in different oxidation states follows the order: $M^{4+} > MO_2^{2+} > M^{3+} > MO_2^{+}$. Similarly, for the given metal ions of the same oxidation state, the complexing ability increases with the atomic number due to increase in the ionic potential as a result of the ‘actinide contraction’ phenomenon [**13**]. However, the above generalized statement may be valid when complexation is primarily ionic in nature. There are a large number of instances where hybridization involving 5*f* orbitals, steric effects and hydration of metal ions affect the tendency of complexation. For anions, the tendency to form complexes with the given actinide ion generally vary in the same manner as their abilities to bind with hydrogen ion [**20**]. For monovalent ligands, the complexing tendency decreases in the order: $F^- > CH_3COO^- > SCN^- > NO_3^- > Cl^- > Br^- > I^- > ClO_4^-$. The divalent anions usually from stronger complexes than the monovalent anions and their complexing ability decreases in the order: $CO_3^{2-} > SO_3^{2-} > C_2O_4^{2-} > SO_4^{2-}$. The complexing ability of some of the commonly used organic ligands with Th(IV) varies as: EDTA > Citrate> Oxalate > HIBA > Lactate > Acetate.

## 1.5. METHODS FOR THE SEPARATION OF METAL IONS

The scientific principles that govern the separation of metal ions from solutions are chemical reaction equilibrium kinetics, fluid mechanics and mass transfer from one phase to another. The theory of separation utilizes these principles in different techniques including solvent extraction, extraction chromatography as well as liquid membranes. The principles behind these techniques are discussed in this Section. Out of these techniques, solvent extraction is the most versatile technique and is extensively used for separation, preparation, purification, enrichment and analysis on micro scale to industrial scale.

### 1.5.1. Solvent extraction

Solvent or liquid-liquid extraction is based on the principle that a solute can distribute itself in a certain ratio between the two immiscible solvents, one of which is usually water and the other is an organic solvent. In certain cases, the solute can be more or less completely transferred into the organic phase. Thus, when molecular species of the solute is same in the two phases, its concentration in one phase is related to that in the other phase (the distribution law). Consider the following equilibrium reaction,

$$M_{(aq.)} \leftrightarrow M_{(org.)} \tag{1.2}$$

where the subscripts (aq.) and (org.) represent aqueous and organic phases, respectively. According to the distribution law, the distribution coefficient ($K_d$) is represented as,

$$K_d = \frac{[M]_{(org)}}{[M]_{(aq)}} \tag{1.3}$$

However, it has been observed that, in most cases, the chemical species of metal ions are not the same in both the phases. Therefore, the term “distribution ratio ($K_d$)” is used in the solvent extraction which is defined as the ratio of the total concentration of metal ion (in all forms) in the organic phase to that in the aqueous phase. In order to achieve efficient extraction of the metal ion, a proper choice of the extractant is required.

#### 1.5.1.1. Criteria for the selection of the extractants

A number of factors are taken into consideration while selecting or designing a particular extractant for the separation of metal ions for industrial applications. Some of the important considerations are listed as follows,

(i) High solubility in paraffinic solvents (non-polar solvents),

(ii) Low solubility in the aqueous phase,

(iii) Non-volatile, non-toxic and non-inflammable,

(iv) High complexation ability with the metal ions of interest,

(v) High solubility of the metal-ligand complex in the organic phase, i.e. high metal loading capacity in the organic phase,

(vi) Ease of stripping of metal ions from the organic phase,

(vii) Reasonably high selectivity for the metal ion of interest over the other metal ions present in the aqueous solution,

(viii) Optimum viscosity for ease of flow and optimum interfacial tension (IFT) to enable a faster rate of phase disengagement,

(ix) Ease of regeneration of the extractant for recycling,

(x) High resistance to radiolytic and chemical degradation during operation, and

(xi) Ease of synthesis / availability of the extractant at a reasonable cost.

### 1.5.2. Membrane separations

Membranes are barriers that separate two liquid phases and allow the mass transfer from one side of the barrier to the other [**21**]. The membrane material could be solid as well as liquid. When a liquid is used as the membrane material it is referred to as liquid membrane. There are myriad examples of liquid membranes in various forms in our daily life, e.g., an oil layer on a water surface is a typical organic liquid membrane of an immiscible liquid phase, beer froth, foam on soap, detergent or surfactant solutions, oil films coated on a metal surface – popularly used in rust protection and lubrication are familiar liquid films separating two phases [**22**]. Membrane based separation technique has the advantages of low energy requirements, low capital and operating costs, the possibility of achieving high volume reduction factors, low inventory of carrier ligand (thus possibility of using costly tailored made ligand), simultaneous extraction and stripping, continuous flow, possibility to achieve high volume reduction factor, easy scale up possibility, higher selectivity and simple modular design [**23, 24**]. From a practical point of view, membranes based separations find applications in the industrial [**25-29**], biomedical [**30**], and analytical fields [**31-33**] as well as in waste water treatment [**34**]. The use of liquid membranes containing a carrier has been proposed as an alternative to solvent extraction for selective separation and concentration of metal ions from dilute aqueous solutions [**35-37**]. The required carrier can be the same extractant used in the solvent extraction process. One of the major advantages of carrier facilitated transport in LM is the larger selectivity that is achieved than in other membrane processes. One of the important features of the liquid membrane based technique is that unlike solvent extraction, the extraction and stripping of the metal ion as well as regeneration of the carrier are combined in a single stage. Supported liquid membranes (SLM), where the liquid membrane is supported on a porous polymer matrix, are found to be highly efficient so far as the ligand inventory and metal ion throughput are concerned. However, the major disadvantage of the SLM is the membrane stability which can be alleviated by the use of polymer inclusion membranes [**31**].

#### 1.5.2.1. Polymer inclusion membrane (PIM)

PIMs are very simple in structure and are formed by casting a solution containing an extractant, a plasticizer and a base polymer such as cellulose triacetate (CTA) or poly(vinyl chloride) (PVC) to form a thin, flexible and stable film. The resulting self-supporting PIMs resemble, to some extent, to the SLMs although the extraction mechanism may be very different. In PIMs, the base polymer provides mechanical strength to the PIMs, the plasticizer provides elasticity and acts as the solvent in which the carrier molecule can diffuse while the carrier extracts the analyte of interest and transports it across the membrane. In PIMs, the carrier is physically immobilized into the plasticized polymer matrix and thus, the possibility of its leaching out from the matrix is rather difficult. A good PIM is homogeneous in microscopic level, optically transparent to construct an optical chemical sensor (optodes) and it is flexible and mechanically strong so that it can withstand mechanical stress such as bending without visual deformation. The choice of different constituents of the membrane is crucial to ensure its separation efficiency, so it is important to know the role of different constituents of the PIM.

#### 1.5.2.1.1. Base polymers

The base polymers play a crucial role in providing mechanical strength to the PIM. These are thermoplastic polymers consisting of linear polymer strands and devoid of cross-linkers between the strands. They can be dissolved in a suitable organic solvent where the polymer strands become separated. The mechanical strength of the membrane is the result of a combination of the intermolecular forces among the polymer strands and the process of entanglement [**38**]. Higher the intermolecular force among the polymer strands, greater is the rigidity of the membrane and lesser is the flexibility of the membrane. On the other hand, entanglement is the result of random diffusion of the flexible polymer strands in a sol as the solvent evaporates. Although the polymer provides the mechanical support to the membrane, their bulk properties appear to be highly important in deciding the metal ion transport through the membrane. The glass transition temperature ($T_g$) for an amorphous polymer or the melting temperature ($T_m$) for a crystalline polymer is often used to characterize its inherent flexibility and microstructural characteristics. Below the glass transition temperature ($T_g$), the polymer is rigid and glassy and the individual polymer strands are unable to change their conformation. This condition is considered to be an unfavorable condition for metal ion transport in the PIMs and a plasticizer is often added to the polymer to decrease its $T_g$ value and create more flexible and less brittle PIMs. In the absence of any plasticizer, the $T_g$ of the pure polymer is usually much higher than the room temperature and hence, the membrane without plasticizer is rigid in its structure. Some of the carriers also act as plasticizer and in that case, the addition of an extra plasticizer to the polymer is generally not required. The suitability of a base polymer for the PIM depends on (a) it can be cast in the molds to the desired thickness (b) are mechanically strong (c) are resistant to hydrolysis (d) to offer low resistance to cation transport, (e) may be cast with higher plasticizer content and (f) ready availability.

Among the various polymers available, cellulose triacetate (CTA) and polyvinyl chloride (PVC) are the polymers which are widely used in the construction of PIMs. Both are thermoplastic polymers though the $T_g$ ($T_m$) of the polymers are different. The different physical characteristics of the base polymers frequently used in the PIMs are included in Table 1.4.

Table 1.4. Physical characteristics of three polymers most frequently used in PIMs [**31**]

| Polymer | MW used in PIMs (kDa) | $MW_c$ (kDa) | $T_g$ (°C) | $T_m$ (°C) | Polymeric characteristics |
|---|---|---|---|---|---|
| Poly(vinyl chloride) (PVC) | 90-180 | 12.7 | 80 | - | Slightly crystalline, mostly amorphus |
| Cellulose triacetate (CTA) | 72-74 | 17.3 | - | 302 | Infusible, high degree of crystallinity, excellent strength |
| Cellulose tributyrate (CTB) | 120 | 47.4 | - | 207 | Infusible, high degree of crystallinity, excellent strength |

*MW: molecular weight of the polymer; MWc: critical entanglement molecular weight of the polymer*

CTA contains polar groups like hydroxyl and acetyl groups and thus, forms highly oriented hydrogen bond while PVC contains relatively less polar C-Cl bond and hence, non-specific dispersion forces dominate the intermolecular forces between the polymer strands. Consequently, PVC is an amorphous polymer with a small degree of crystallinity whereas CTA is highly crystalline in structure. Moreover, CTA is slightly hydrated and due to the presence of polar groups, it is very prone to hydrolysis particularly in acidic medium whereas PVC is not hydrated and it can be useful in harsher conditions. In addition, due to the presence of crystallinity in CTA, it has excellent mechanical strength [**31**].

#### 1.5.2.1.2. Plasticizer

Plasticizers are substances which, when added to a material (usually a plastic), make it flexible, resilient and easier to handle and ensure durability. In PIMs, the plasticizer provides elasticity and acts as a solvent in which the carrier can diffuse. It interposes itself between the polymer molecules to neutralize the polar groups of the polymer with its own polar groups or to merely increase the distance between the polymer molecules and hence, reduce the strength of the intermolecular forces of the polymer. For many plasticized polymers, the $T_g$ is typically a function of the plasticizer content.

Plasticizers are organic compounds which have a hydrophobic alkyl backbone and one or several highly solvating polar groups in its structure. The former governs the compatibility of the plasticizer with the membrane phase while the latter interacts with the polar groups of the base polymer molecule and hence, neutralizes them. A proper ratio between the polar and non-polar groups of the plasticizer determines enhanced plasticizing properties. An increase in the carbon chain length of the plasticizer results in more hydrophobic and viscous plasticizer that eventually suppresses the polar properties of the plasticizer whereas an increase in the number of polar groups of the plasticizer decreases the viscosity and increases the hydrophilicity of the plasticizer which eventually make it unsuitable as the plasticizer [**31**]. Membrane performance depends on the the physicochemical properties of the plasticizer as well as the concentration of the latter. Structures of some commonly used plasticizers are depicted in Fig. 1.6.

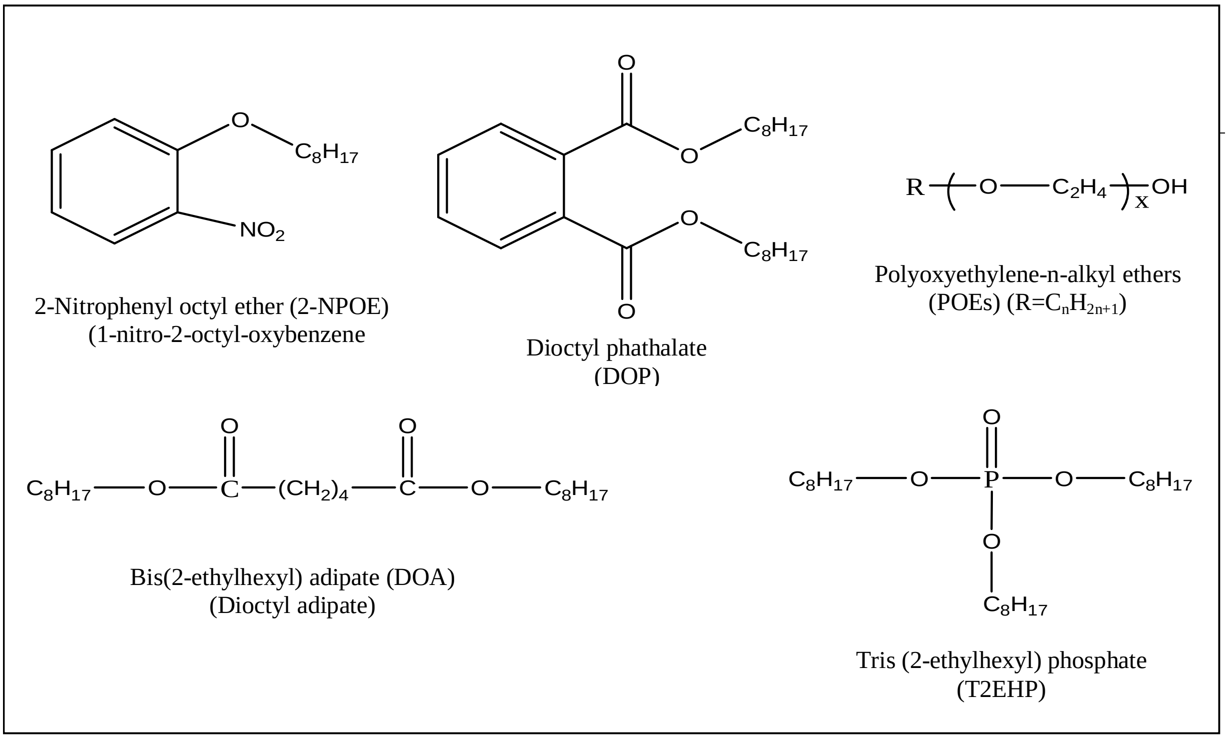

Fig. 1.6. Few examples of plasticizers commonly used in PIMs

However, for a good plasticizer to be adequate for its use in PIMs, it should gather certain physicochemical properties such as good compatibility with the base polymer, low vapor pressure, high capacity to dissolve the substrate and other additives present in the polymeric membrane, high lipophilicity, high molecular weight, low tendency for exudation from the polymeric matrix, low viscosity, high dielectric constant, low cost and low toxicity. While there is a large number of commercially available plasticizers, 2-nitrophenyl octyl ether (2-NPOE) and 2-nitrophenyl pentyl ether (2-NPPE) are quite common and have been used in the majority of successful PIMs studies currently available. It was found that 2-NPOE suffers virtually no loss from the membrane into the adjacent water phases. It has the further advantageous properties such as non-volatile, high boiling point, high dielectric constant, low viscosity, insoluble in water, etc. Generally, NPOE is a common plasticizer in CTA-based PIMs. The performance of the membrane is influenced by the concentration and physicochemical properties of the plasticizer. Therefore, it is necessary to discuss it in this Chapter in greater detail.

#### 1.5.2.1.2.1. Role of plasticizer concentration

Low plasticizer concentration leads to the formation of a more rigid and brittle membrane due to the phenomenon commonly referred to as the “anti-plasticizing effect” [**39**]. The minimum concentration which results in better performance of a membrane widely varied depending on both plasticizer and the base polymer. The minimum concentration required for a given plasticizer to neutralize all the polar groups of the base polymer is defined by $\mathrm{phr}_{\mathrm{min}}$ (parts of plasticizer per 100 parts of polymer by mass). The $\mathrm{phr}_{\mathrm{min}}$ depends on molecular weight (MW) of plasticizer and molecular weight of one helical unit of the base polymer as given by the following equation.

$$\mathrm{phr}_{\mathrm{min}} = \frac{\text{MW of plasticizer}}{\text{MW of one helical unit of base polymer}} \times 100 \qquad (1.4)$$

Excessive plasticizer concentration in the PIM leads to exudation of the plasticizer to the membrane / aqueous interface and forms a thin membrane, which would create an additional barrier to the transport of metal ions across the membrane. In case of poor compatibility between the base polymer and the plasticizer, plasticizer exudation is observed [**40**]. Furthermore, presences of excessive plasticizer in the membrane make the membrane very flexible and thus, make it unsuitable for practical purposes. Generally, increasing the plasticizer concentration increases the metal ion transport across the membrane. However, considering wider range of plasticizer concentration, it is not always true and there exists a convex shape relationship of metal ion flux with the plasticizer concentration.

#### 1.5.2.1.2.2. Role of plasticizer viscosity

The transport of metal ion across the membrane may be accompanied by diffusion and therefore, the diffusion coefficient is expected to depend on the viscosity of the membrane phase. This behavior can be explained by the diffusion-dependent relation of the Stokes–Einstein relation [**41**] for diffusion coefficient,

$$D = \frac{KT}{6\pi\eta r} \tag{1.5}$$

Where η is the viscosity of the solvent, D is the diffusion coefficient of the solute, r is the radius of the solute, k is the Boltzman constant, and T is absolute temperature.

### 1.5.2.1.2.3. Role of plasticizer dielectric constant

Plasticizer dielectric constant plays an important role in the metal ion transport across the membrane. Higher the dielectric constant of the plasticizer, more readily the ion-pair can dissociates. The diffusion coefficients of the individual cations and anions are higher than those of the respective undissociated ion-pair species [**42**]. This is also reflected in the faster relocation of the ions between the active sites in the PIMs. The polarity of the plasticizer had a greater influence on the diffusion of the complex in the membrane compared to that with respect to the viscosity.

### 1.5.2.1.3. Carriers

Carrier plays the most important role in the extraction and transport of metal ions across the PIMs. The complex or the ion-pair formed between the metal ion and the carrier is extracted at the membrane-aqueous phase interface, solubilized in the membrane and facilitates metal ion transport across the membrane. The different classes of carrier molecules commonly used in solvent extraction processes are also studied in PIMs.

The selectivity and the transport efficiency in the PIM system are influenced by the properties of the carrier because of the differences in their complexation mechanisms with a given metal ion. The carrier molecular structure can markedly influence the rate of transport of the target solute across the membrane. The basic and the neutral carriers exhibit low selectivity for the metal ions. The basic carrier reacts with the metal ion via an ion-pair mechanism while the neutral carrier reacts with the metal ion by a solvating mechanism. Both of these mechanisms are based on electrostatic interactions between the ions. Acidic carriers extract the metal ion by forming an uncharged complex with the cation by exchanging their proton for the cation. The selectivity exhibited by acidic carriers is relatively low and is normally controlled by pH of the aqueous feed [**43**]. On the other hand, the selectivity achieved by certain chelating carrier is much better due to their specific and conformational interaction with the metal ions [**44**]. Similarly, excellent selectivity can be achieved with macrocyclic carriers, although it may vary significantly depending on the size of the macrocyclic carriers.

### 1.5.2.1.4. Transport mechanism

One or more driving forces facilitate the transport of the particular species through the membrane. Species can be transported from a region of high solute concentration to that of low solute concentration following the Fick's first law of diffusion:

$$J = -D\left(\frac{\partial C}{\partial X}\right) \tag{1.6}$$

Where $\frac{\partial C}{\partial X}$ is the concentration gradient, 'J' is flux and 'D' is diffusion co-efficient. The flux is proportional to the concentration gradient across a phase with thickness 'X'. This means that the diffusion of a species through a liquid membrane will stop as soon as the concentration at both sides of the membrane becomes equal. This is called unfacilitated transport. There is another type of transport mechanism termed as the facilitated transport mechanism.

### 1.5.2.1.4.1. Theory of facilitated transport of metal ions across PIM

The facilitated transport which can cause uphill transport leading to near quantitative metal ion transport can follow two mechanisms.

a. Type I facilitation

In order to maintain the transport of solutes from bulk phase ‘I’ towards bulk phase ‘II’, the diffusing species reacts with a complexing / decomplexing species in the receiving phase resulting in a compound that cannot move back towards phase ‘I’.

b. Type II facilitation

Another type of transport mechanism is needed in the case that the species to be removed are not soluble in the organic membrane phase. This type of transport is also called carrier mediated transport. The addition of a carrier extractant to the membrane phase accelerates the transport of a specific component. Both coupled and uncoupled transport can be distinguished. The majority of liquid membranes, such as SLM and PIM for metal ion separation follow a coupled transport mechanism, which involves the presence of two components. This Chapter will discuss the mechanism of carrier mediated transport of solutes through PIM.

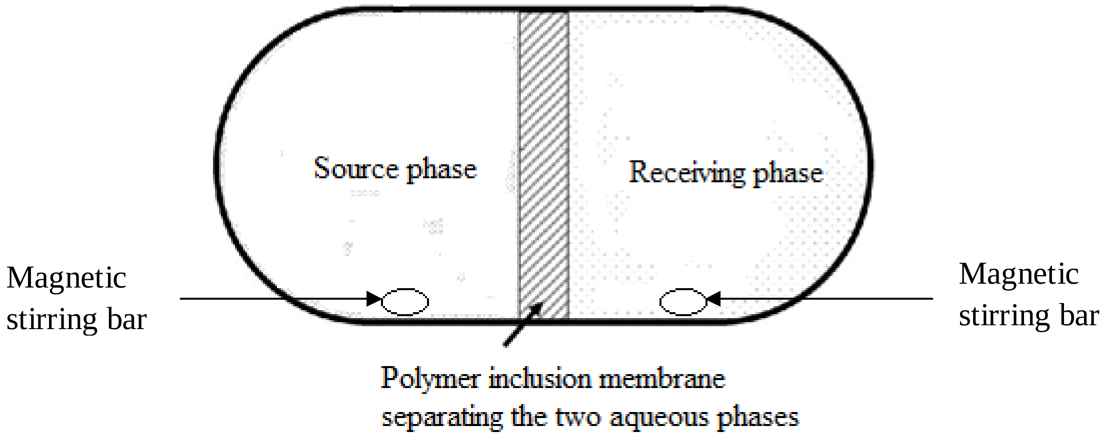

Fig. 1.7. Schematic diagram of the transport cell

The mechanism of metal ion transport across PIM is based on facilitated carrier mediated coupled transport [**31**]. The carrier molecules present in the membrane phase selectively bind the metal ion from the aqueous source phase and transport through the organic membrane phase to the aqueous strip phase. A schematic diagram of the transport cell is presented in Fig. 1.7. The following mechanisms can be considered for the carrier mediated transport of metal ion through the polymer inclusion membrane.

#### 1.5.2.1.4.1.1. Interfacial transport mechanism

The uphill transport of the solute from the bulk of the aqueous source phase through the polymeric membrane to the bulk of aqueous receiving phase takes place in three steps. In the first step, the target solute after diffusing through the aqueous stagnant layer at the source - membrane interface reacts with the carrier to form a solute – carrier complex, which is then transported across this interface and replaced by another molecule of the carrier. In the next step, this solute-carrier complex diffuses across the membrane towards the interface between the membrane and the receiving solution where it dissociates at the yield the carrier (which remains in the membrane) and the solute (which is released in to the receiveing phase). The last step resembles with the reverse of the step occurring at the source-membrane interface. Generally, the diffusion processes occurring through the aqueous stagnant layer at the two aqueous - membrane interfaces are relatively fast and can be ignored if suitable hydrodynamic condition is maintained. The different possibilities of the coupled transport processes in the PIM system are shown in Fig. 1.8.

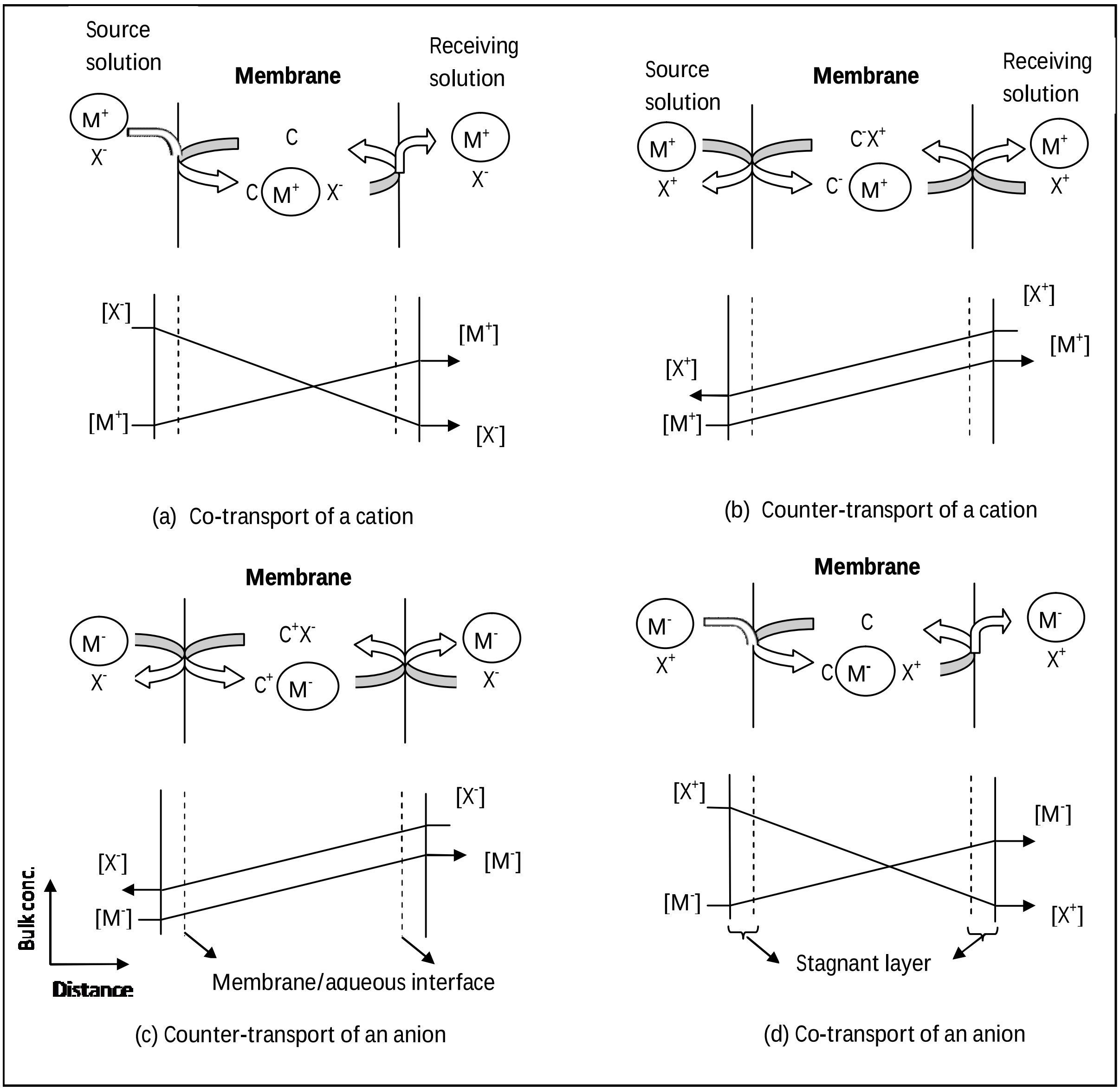

Fig.1.8. Schematic description of coupled transport of a positively charged ($M^+$) or negatively charged ($M^-$) species through a PIM. C represents the carrier and X is an aqueous soluble coupled-transport ion. [$M^+$], [$M^-$], [$X^-$] and [$X^+$] represent the total analytical concentrations of the respective solute in the bulk aqueous phases.

As presented in Fig. 1.8, the different possibilities of transport are: (a) the target solute is a cation and is co-transported with an anion involving a neutral carrier in the membrane; (b) the target solute is a cation and is counter-transported with a cation involving an anionic carrier; (c) the target solute is an anion and is counter-transported with an anion involving a cationic carrier; (d) the target solute is an anion and is co-transported with a cation involving a neutral carrier in the membrane.

In co-transport (Fig. 1.8 a), both metal ions and counter ions are transported from the feed solution through PIM into the strip solution. The chemical reactions for this separation process are shown below.

$M^{n+} + nX^- + C\ (\text{membrane}) \rightarrow CMX_n\ (\text{membrane})$ (at source-membrane interface) (1.7)

$CMX_n\ (\text{membrane}) \rightarrow C\ (\text{membrane}) + M^{n+} + nX^-$ (at membrane-strip interface) (1.8)

In counter-transport (Fig. 1.8 b), an acidic carrier (HC) is used for complexation with the metal ion and subsequent transport as already mentioned above. The chemical reactions involved in this coupled transport are shown below.

$M^{n+} + nHC\ (\text{membrane}) \rightarrow MC_n\ (\text{membrane}) + nH^+$ (at source-membrane interface) (1.9)

$MC_n(\text{membrane}) + nH^+ \rightarrow nHC(\text{membrane}) + M^{n+}$ (at membrane-strip interface) (1.10)

The distribution ratio ($K_d$) of the extracted metal ion between the organic membrane phase and the aqueous source phase should be high enough to favour the metal ion extraction into the membrane phase. Also, the $K_d$ of the extracted metal ion between the membrane phase and the aqueous receiving phase must be sufficiently low to facilitate the transfer of the solute into the receiver phase. It appears that the concentration gradient of the target solute/carrier complex (or the ion-pair within the membrane phase) acts as a driving force for its transport across the membrane phase despite the fact that the total analytical concentration of the target solute in the source phase can be substantially lower than that in the receiving solution. The total analytical concentration is the sum of the concentrations of all chemical species containing the target ion. For better results, complexing agents in the receiving phase are used to destabilize the metal-carrier complex present in the membrane phase. The transport process of the target ion for the PIM system containing solvating type carrier (like diglycolamide studied in the present study) is an example where the driving force for the transport of the target ion is achieved by keeping a large difference in the $K_d$ values.

Another driving force for the uphill transport of target ion through the membrane is achieved by keeping a concentration gradient of a coupled-transport ion across the membrane. The target solute is transported across the PIM in association with the coupled-transport ion to maintain the electroneutrality. This coupled-transport phenomenon could be co-transport or counter-transport depending on the transport direction of coupled-transport ion with respect to the transport of target ion. Typical examples of this can be found by considering PIM systems containing basic, acidic or chelating carriers.

#### 1.5.2.1.4.1.2. Bulk transport mechanism

Although the transport of target solute through the aqueous solution / membrane interface is similar in SLM and PIM, the actual bulk transport mechanism through both membranes can be different. This is because of the different chemical composition and morphology of the two systems. The carrier molecule in the SLM is mobile and plays the role of a shuttle, freely moving within the membrane. The PIM is essentially a quasi-solid homogeneous thin film and it is not a true liquid and hence, the movement of the carrier is restricted.

Cussler et al. [**45**] modeled the facilitated transport in solid membranes and postulated a “chained carrier” theory which restricts the carrier molecule movement. The model demonstrates the existence of a percolation threshold for the membrane with immobilized carrier, i.e., a minimum concentration of the carrier molecule in the membrane is required to make a continuous chain of carriers across the membrane to initiate the target solute transport. The model also indicated the presence of some local mobility for the carrier molecules. However, the model is not perfect to describe the transport in PIMs. Presence of a percolation threshold which depends on the concentration of the solute was reported in several studies [**46, 47**]. The limitation of the ‘chained carrier model’ is the assumption that the free uncomplexed solute cannot enter the membrane phase and the carrier sites must be within reach of one another so that the transfer of the target solute can take place.

Fixed-site jumping model is an extended bulk diffusion model which is essentially an improvement of chained carrier theory. In addition to the requirement for locally mobile carrier species, this new model assumed that the target solute can jump from one carrier to another. Similar to the chained carrier theory, a percolation threshold exists. When carrier concentration is below the threshold concentration, the distance between fixed-sites becomes too great to allow solute jumping and the flux is close to zero. When the carrier concentration exceeds the threshold concentration, flux may increase linearly with it or a higher power which is determined by the experimental conditions. The model explicitly includes the complexation reaction between the carrier and the target solute as an integral part of the bulk transport across the PIM unlike the carrier diffusion model which assumes that the complex formation and dissociation occur only at the membrane - aqueous solution (feed or receiver) interface. Both the carrier diffusion model and the fixed site jumping follow a Fickian diffusion pattern and therefore, the overall transport process is similar.

It may be possible that an increase in the carrier concentration in the PIM can result in a variation in the membrane morphology, which may ultimately influence the nature of the diffusion process across the PIMs. Though different mechanisms have been proposed, the actual diffusion mechanism may be assumed to be in between the “mobile carrier diffusion” and “fixed-site jumping” mechanisms explained above.

## 1.6. MINOR ACTINIDE EXTRACTION

HLW management is required to mitigate the long term hazards of the minor actinides which not only have long half lives but also have very large radiotoxicity values. This has been achieved by ‘Actinide Partitioning’ using a variety of extractants selective for the minor actinides. Some of these minor actinide partitioning processes are discussed below.

### 1.6.1. The TRUEX process

The Trans Uranium Extraction (TRUEX) process is a solvent extraction process designed to separate transuranic elements from various types of high level waste solutions. The key ingredient in this process is a phosphine oxide based extractant, viz octyl(phenyl)-*N*,*N*-diisobutyl carbamoyl methyl phosphine oxide (CMPO, Fig. 1.9(a)) [**48**]. The TRUEX extractant is usually 0.2 M CMPO + 1.2 M TBP (used as the phase modifier) in paraffinic hydrocarbon like *n*-dodecane [**49**]. In the TRUEX solvent, TBP suppresses the third phase formation, contributes to better acid dependencies for $D_{Am}$, improves phase compatibility, and reduces hydrolytic and radiolytic degradation of CMPO [**50**]. High distribution ratio of tri-, tetra- and hexavalent actinides from solutions of moderate acid concentration and good selectivity over fission products is the key feature of this extractant. Lanthanides such as Eu, Ce and Pr behave in a chemically similar manner to the trivalent actinides, viz. Am(III). Other fission products, except Zr, show relatively small distribution values.

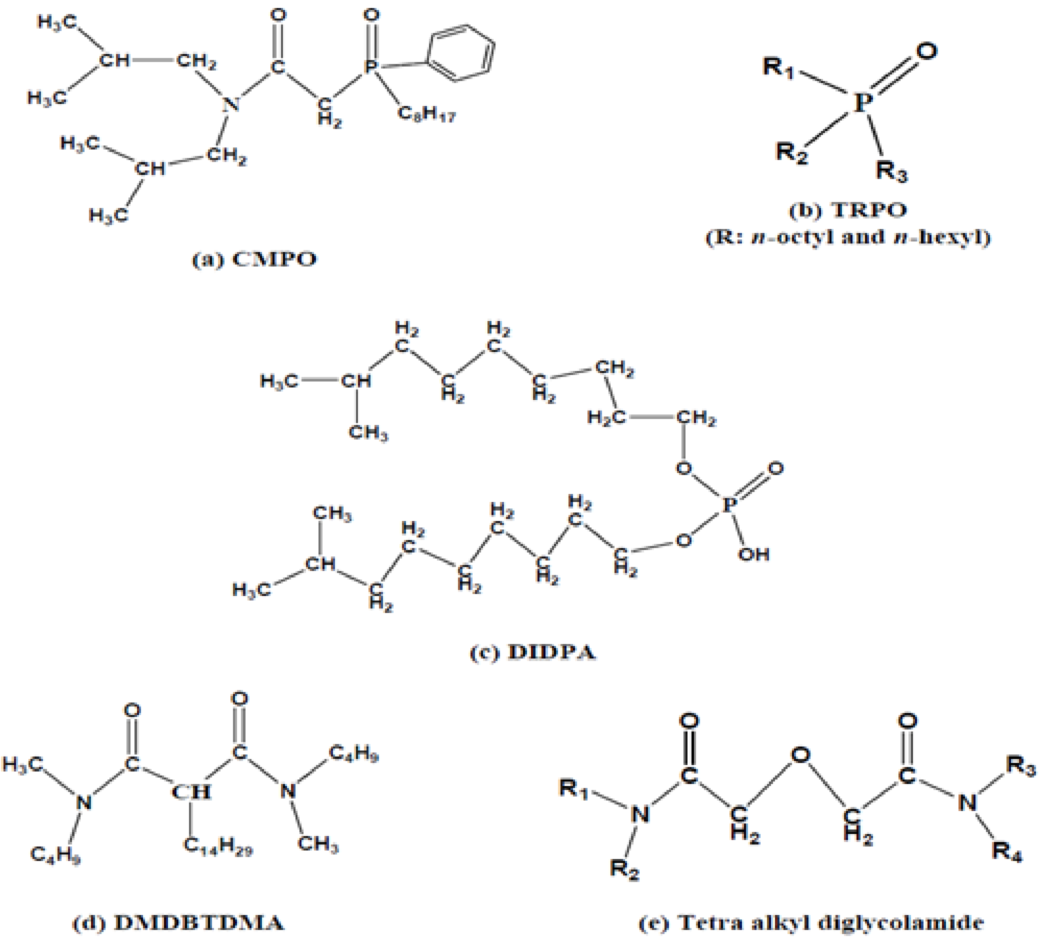

(a) CMPO

(b) TRPO
(R: *n*-octyl and *n*-hexyl)

(c) DIDPA

(d) DMDBTDMA

(e) Tetra alkyl diglycolamide

Fig. 1.9. Structural formulae of some of the proposed extractants for actinide partitioning

Due to high extraction of tetra- and hexavalent actinides such as Pu(IV) and U(VI) by CMPO in a wide range of acidity, the stripping of these metal ions with dilute nitric acid is difficult. A mixture of formic acid, hydrazine hydrate and citric acid has shown promise for efficient stripping of Am and Pu from TRUEX solvent loaded with the actinide ions in both batch as well as counter current modes [**51**, **52**].

### 1.6.2. TRPO process

Trialkyl Phosphine Oxide (TRPO) process utilizes a mixture of four alkyl phosphine oxides (Fig. 1.9(b)) as the extractant. The TRPO solvent has been tested for the extraction of actinides, lanthanides and other fission products from $HNO_3$ and HLW solutions [**53**, **54**]. It was observed that >99% of U(VI), Np(IV), Np(VI) and Pu(IV) were extracted from 0.2–1 M $HNO_3$ through a single extraction with 30% (v/v) TRPO in kerosene [**55**]. Also >95% of Pu(III), Am(III) and Ln(III) could be extracted, while fission products such as Cs, Sr, Ru were not extracted. Trivalent lanthanides and actinides are generally stripped with 5 M $HNO_3$. On the other hand, tetravalent (Np and Pu) and hexavalent (U) actinides are stripped with 0.5 M oxalic acid and 5% $Na_2CO_3$, respectively.

### 1.6.3. The DIDPA process

The extraction behavior of actinides and other fission products with di-*iso*-decyl phosphoric acid (DIDPA, Fig. 1.9(c)) has been studied by Morita et al. [**56**, **57**], at Japan Atomic Energy Research Institute (JAERI) It has been shown that DIDPA can simultaneously extract Am(III), Cm(III), U(VI), Pu(IV) and even Np(V) from a solution of low acidity such as 0.5 M $HNO_3$ [56,57]. The trivalent cations can be separated from their tetravalent counterparts by appropriate back-extraction procedures the details of which are out of scope of this Thesis work.

### 1.6.4. Processes with amide based extractants

#### 1.6.4.1. The DIAMEX process

The DIAMide EXtraction (DIAMEX) process was developed in France for the extraction of transuranic elements from the HLW solutions. One of the major drawbacks of using organophosphorus extractants is the solid residue that results upon their incineration at the end of their useful life. French researchers utilized the CHON (carbon, hydrogen, oxygen and nitrogen) principle for designing the extractants, which can be completely incinerated into gaseous products, thereby minimizing the generation of solid secondary wastes at the end of the process. Among the numerous diamides synthesized and tested for the extraction of actinides, *N*,*N'*-dimethyl-*N*,*N'*-dibutyl tetradecyl malonamide (DMDBTDMA, Fig. 1.9(d)) and *N*,*N'*-dimethyl-*N*,*N'*-dioctylhexylethoxymalonamide (DMDOHEMA) have shown the most promising results [**58-64**]. In France, these reagents are extensively evaluated for actinide partitioning from HLW solutions.

### 1.6.4.2. Digylycolamides: A class of promising extractants for actinide partitioning

In order to improve the efficiency of diamides in the extraction of trivalent actinides from HLW, several structural modifications have been attempted. Recently, a series of diamide compounds have been synthesized by introducing different substituents on amide nitrogen or by introducing an etheric oxygen into the bridging chain of the malonamide [**65**]. It has been observed that the introduction of the etheric oxygen between the two amide groups (diglycolamides, Fig. 1.9(e)) causes significant enhancement in the extraction of trivalent actinides / lanthanides. The work on diglycolamides was started after Stephan et al., reported the extraction of various metal ions with multidentate amido podands [**66, 67**]. Sasaki and Choppin were probably the first to report the extraction of lanthanides and actinides with diglycolamides [**68-72**]. They used dimethyl dihexyl diglycolamide and its analogs for the solvent extraction studies on lanthanides and actinides. These preliminary studies, however, were focused on the extraction of metal ions from aqueous solutions of pH ranging from 1 to 4. Narita et al., studied the extraction of lanthanides from acidic solutions employing *N*,*N'*-dimethyl-*N*,*N'*-diphenyl diglycolamide [**73**]. They proved by XRD and EXAFS studies that the diglycolamide forms tridentate complex with lanthanides in solid complexes as well as in solution [**74**]. Sasaki et al. [**75**] synthesized a series of diglycolamides having the same central frame with different alkyl chains (ranging from *n*-propyl to *n*-dodecyl) attached to amidic nitrogen atoms (Fig. 1.9(e)). Various properties of the synthesized diglycolamide derivatives are listed in Table 1.5.

Table 1.5. Various properties of tetra- *n*-propyl, *n*-butyl, *n*-amyl, *n*-hexyl, *n*-octyl, *n*-decyl and *n*-dodecyl diglycolamide

| Diglycolamide (DGA) | Solubility in water [mM] | Solubility in n-dodecane | $D_{Am}$ by 0.1M DGA in n-dodecane (1M $HNO_3$) |
|---|---|---|---|
| TPDGA | 57.0 | Very poor | -- |
| TBDGA | 2.3 | poor | -- |
| TADGA | 0.27 | Soluble | 100 |
| THDGA | 0.11 | Soluble | 40 |
| TODGA | 0.042 | Freely soluble | 30 |
| TDDGA | 0.042 | Freely soluble | 18 |
| TDDDGA | 0.040 | Freely soluble | 11 |

Diglycolamides with lower alkyl chain (*n*-propyl and *n*-butyl) were found to be not soluble in paraffinic solvents like *n*-dodecane due to the presence of three polar oxygen atoms. Though the higher homologs of diglycolamide were freely soluble in *n*-dodecane, the distribution ratio values for Am(III) were found to decrease due to the steric hindrance during complexation of the bulky molecules. Amongst the different derivatives synthesized, *N,N,N',N'*-tetra-*n*-octyl diglycolamide (TODGA) was found to be the most suitable with respect to its free solubility in *n*-dodecane and significantly high distribution ratio values of trivalent actinides. Another diglycolamide extractant, which is a branched homolog of TODGA, is *N,N,N',N'*-tetra-(2-ethylhexyl) diglycolamide (T2EHDGA) which also gives satisfactory results [**76**].

## 1.7. ION SELECTIVE ELECTRODE (ISE)

### 1.7.1. Theory of ion selective electrode

A chemical sensor can be defined as a small device that allows the transformation of chemical information into an optical or electrical signal that can be processed by an instrument.

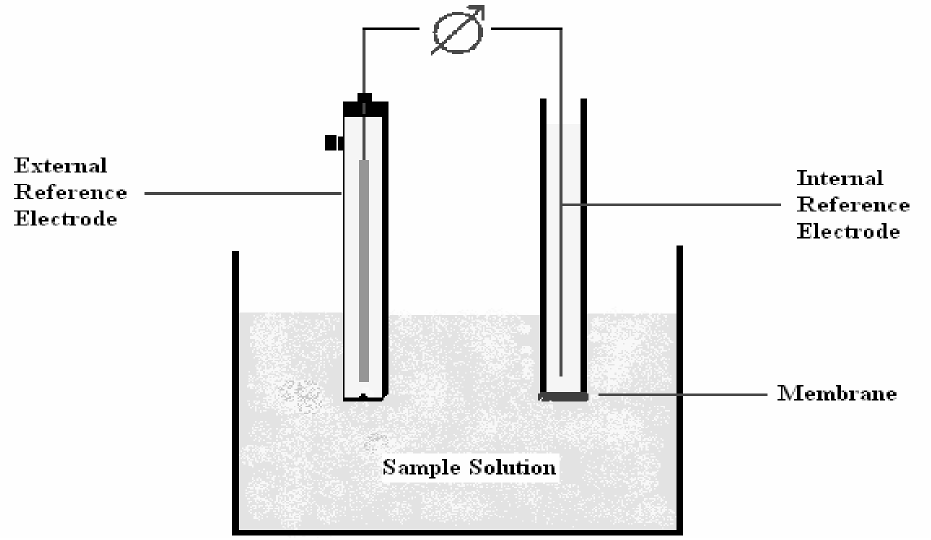

Fig. 1.10. Typical set up of an ion selective electrode based potentiometric sensor

Ion selective electrodes (ISEs) are potentiometrie ion sensors based on ion-selective membranes such as the PIMs discussed above. They respond to the activity of the analyte ion, whose logarithmic value is proportional to the membrane electrical potential measured relative to a reference electrode. A potentiometric (a galvanic cell) set up consist of an indicator (ISE) and a reference electrode that are immersed into the sample solution and connected to the two terminals of a potentiometer as shown in Fig.1.10. The most versatile ion-selective membrane consists of an organic polymeric matrix containing a lipophilic ionic species and a lipophilic ionophore.

#### 1.7.1.1. Components of the polymeric ion-selective membrane

The polymeric membrane of an ion selective electrode shall have the selectivity for a particular analyte ion accompanied by minimal electrical resistivity, solubility and swelling. It consists of the following components.

##### 1.7.1.1.1. Polymeric matrix

The polymeric matrix provides mechanical stability to the membrane. In ideal cases it is inert and has no chemical interaction with the sensed ions. Polymeric ISE-membranes are commonly prepared with poly(vinyl chloride) (PVC). The polymer cannot have many polar groups as it may become soluble in water. The examples of other polymers that are also used in ISEs include silicone rubbers, polyurethanes, acrylates, perfloropolymers and many others.

##### 1.7.1.1.2. Membrane solvent or plasticizer

The membrane solvent reduces the viscosity and ensures a relatively high mobility of the membrane constituents. In order to provide homogeneity of the organic phase it must be compatible with the other membrane components and acts as a plasticizer. The plasticizer has been elaborated above and need not be discussed here.

##### 1.7.1.1.3. Lipophilic ion

The prerequisite for a theoretical Nernstian response of the ISE is that no significant amount of primary ions may be coextracted together with counter ions (ions with opposite charge sign of the measuring ion) from the sample into the membrane phase. This means that the membrane is permeable only for ions with the same charge sign of the measuring ion. This membrane characteristic is called permselectivity or Donnan exclusion [**77, 78**]. The hydrophobic ion in the membrane phase suppresses the extraction of the counter ion into the organic membrane phase. The presence of non-exchangeable lipophilic ions in the membrane phase garantees the operation of the ISE by keeping the total concentration of measuring ions in the membrane constant. Cation-selective ISE-membranes contain normally a tetraphenylborate derivate as the lipophilic site and anion-selective membranes contain a tetraalkylammonium salt.

#### 1.7.1.1.4. Ionophore

The ionophore, or ion carrier, or ligand, has the main influence on the selectivity of the ISE membrane. It ideally forms relatively strong, selective and reversible complexes only with the target ion, so that no ion-exchange between the measuring and the interfering ions occurs in the membrane. Additionally, the ionophore structure must contain numerous lipophilic groups in order to keep its leaching rate from the membrane to the sample phase as low as possible.

### 1.7.1.2. Membrane potential

The total potential difference (electromotive force, EMF) measured under zero-current condition between the two electrodes is the sum of individual potential contributions and is usually described as:

$$\mathrm{EMF} = E_{const} + E_J + E_M \qquad (1.11)$$

Where $E_J$, $E_M$ and $E_{const}$ are termed as liquid junction potential of the reference electrode, membrane potential and a constant to account for all other potentials, respectively. The liquid junction potential at the sample / reference electrode interface ($E_J$) is kept reasonably small and constant under well defined conditions. The membrane potential ($E_M$), is the electrical potential difference developed across two electrolyte solutions (analyte test solution and internal reference solution) separated by ion selective membrane. It is the sum of the three contributions, viz., the phase boundary potentials at the membrane / inner filling solution interface, $E_{PB''}$, the diffusion potential, $E_{D,M}$ and the phase boundary potential at the membrane/sample interface, $E_{PB'}$ [**79**]. As the analyte ion concentration remains constant in the internal reference solution and varies only in test solution, the potential ($E_{PB''}$) on the inner side of the membrane remains constant and is independent of the analyte ion concentration in the test solution. The diffusion potential arises from charge separations within the membrane due to the different mobilities of the ionic species. In most cases of practical relevance, the contribution of $E_{D,M}$ to $E_M$ can be neglected [**80**] since membranes showing a Nernstian response contain only homogeneously distributed primary and lipophilic ions of opposite charge. Moreover, even if more than one kind of exchangeable ions are simultaneously present in the membrane, they are usually quantitatively complexed by the ionophore, and, therefore, have the same mobility. The phase boundary potential ($E_{PB'}$) arises from a charge separation, due to a non-uniform distribution of ionic species between the organic membrane and the aqueous sample phase. Considering, the diffusion potential, $E_{D,M}$ is zero, the membrane potential can be given as:

$$E_M = E_{M,const} + E_{PB'} \tag{1.12}$$

Taking into account the chemical and the electrical potential contributions, the electrochemical potential $\bar{\mu}_I$ for the primary ion I in a solution can be formulated as:

$$\bar{\mu}_I = \mu_I + z_I F\varphi = \mu_I^O + RT\ln a_I + z_I F\varphi \tag{1.13}$$

Where $z_I$ and $a_I$ are the charge and activity of the ion I; $\mu_I^O$ is the standard chemical potential, $\mu_I$ is chemical potential and $\varphi$ the electric potential. At thermodynamic equilibrium the electrochemical potential of the ion I in the membrane, $\bar{\mu}_{I,M}$, and in the sample, $\bar{\mu}_{I,S}$ , are equal. Thus, the phase boundary potential, $E_{PB'}$ can be given as

$$E_{PB'} = \varphi_M - \varphi_S = \frac{\mu_{I,S}^0 - \mu_{I,M}^0}{z_I F} + \frac{RT}{z_I F}\ln\frac{a_{I,S}}{a_{I,M}} \tag{1.14}$$

where the subscripts ‘S’ and ‘M’ indicate the aqueous sample and the organic membrane phase, respectively while R, T, F and $z_I$ are the gas constant, absolute temperature, Faraday constant and the valency of the ion I, respectively.

On combining Eq.(1.12) and Eq.(1.14), the following equation for the membrane potential is obtained.

$$E_M = E_{const} + \frac{\mu^0_{I,S} - \mu^0_{I,M}}{z_I F} + \frac{RT}{z_I F} \ln a_{I,S} - \frac{RT}{z_I F} \ln a_{I,M} \tag{1.15}$$

Under the condition that $a_{I,M}$ remains unaltered, and it can, together with all other sample independent potential contributions, be included in one term ($E^0$) and one can get the Nernst equation as follows:

$$E_M = E^0 + \frac{RT}{z_I F} \ln a_{I,S} \tag{1.16}$$

$$E_M = E^0 + \frac{2.303RT}{z_I F} \log a_{I,S} \tag{1.17}$$

At 25°C, the value of $2.303RT/z_I F$ is $0.059/z_I$ volts. For an ideal ion selective electrode, slope of the plot between cell potential and log $a_{I,S}$ comes out to be $0.059/z_I$ volts and the membrane is said to be exhibiting Nernstian response.

### 1.7.2. Characteristic of an ion selective electrode

Properties of an ion selective electrode are characterized by parameters like calibration plot and slope, total measuring range, detection limit, response time and selectivity. A brief description of these electrode characteristics is given below.

#### 1.7.2.1. Calibration plot and slope

It is a plot of emf (E) versus logarithm of the concentration of a given ionic species (Fig. 1.11). Slope of the calibration plot is expressed in terms of change in the potential per decade of concentration change (mV/decade). Nernstian value of slope for an electrode is given by 59.16/$z_I$ mV/decade of concentration change at 298 K, where '$z_I$' stands for the charge on the primary ion.

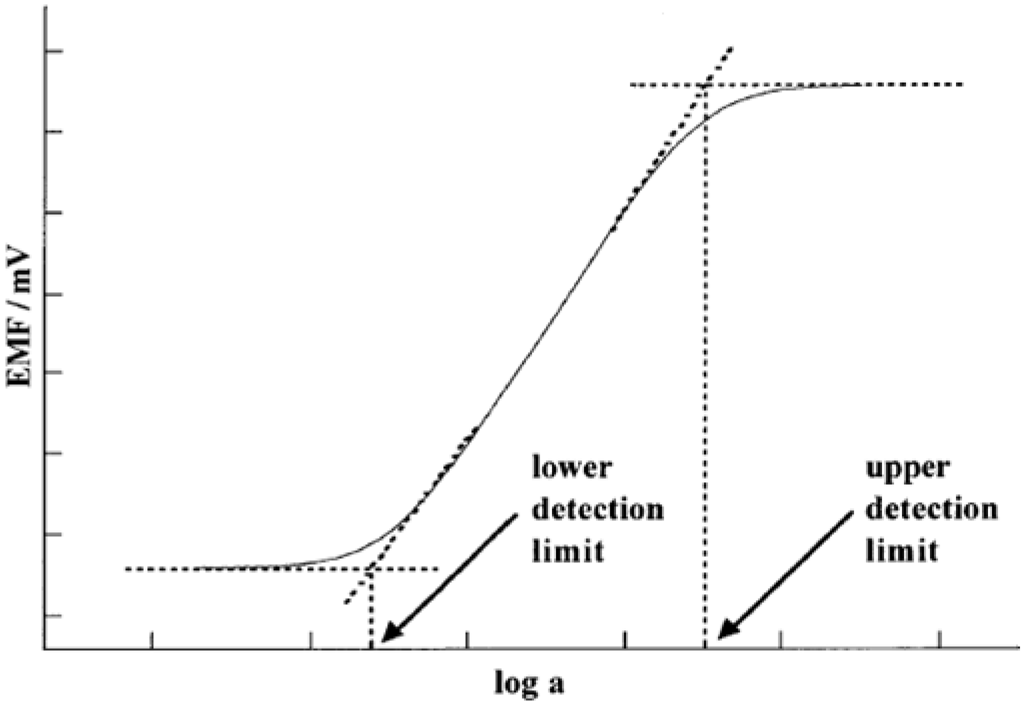

Fig.1.11. The detection limits of an ion-selective electrode are defined according to the IUPAC recommendations by the cross section of the two extrapolated linear segments of the calibration curve.

### 1.7.2.2. Total measuring range

Total measuring range includes the linear range of the calibration graph together with the lower curved portion where the response of the electrode to primary ions becomes progressively less with concentration changes. Samples can be measured in this lower range however more closely spaced calibration points are required in order to define the curve accurately and the percentage error per mV on the calculated concentration will be progressively higher as the slope reduces.

#### 1.7.2.3. Detection limit

Deviations of the electrode function from the linear response are normally observed at high and low activities of the measuring ion. According to the IUPAC recommendations [**81, 82**], the corresponding upper and lower detection limits are defined by the cross-section of the two extrapolated linear segments of the calibration curves (Fig. 1.11). The upper detection limit is caused by the loss of membrane permselectivity, owing to the coextraction of the primary ion together with a counter ion from the sample into the membrane. The lower detection limit can be dictated by two processes namely, (i) interference by the competing ions present in the sample and (ii) perturbation of the interfacial sample activity by the membrane due to leaching of lower amounts of primary ion from the membrane phase into the sample solution.

#### 1.7.2.4. Response time

In IUPAC recommendations, response time is defined as the length of time between the instant at which the ion selective electrode and the reference electrode are brought into contact with sample solution and the first instant at which the cell potential becomes equal to its steady state value within ± 1 mV or has reached 90% of the final value [**81, 82**].

#### 1.7.2.5. Lifetime

Lifetime of an ion selective electrode is defined as the period over which there is no significant change in the performance characteristics (slope, concentration range, lower detection limit etc.) of the electrode. The primary reason for limited lifetime of carrier based ion selective electrodes is the loss of plasticizers, carrier or ionic site from the polymeric film due to leaching into the sample. The main consequence of this limited lifetime is the slow deterioration of the selectivity and the response of the ISE.

### 1.7.2.6. Selectivity

Selectivity is one of the most important characteristic of the ISEs. It measures the extent to which the sensor may be employed in the determination of the primary ion in the presence of other interfering ions. It is measured in terms of the potentiometric selectivity coefficient value, $K_{A,B}^{Pot}$ . If $K_{A,B}^{Pot}$ is larger than 1, the ISE responds to the interfering ions more selectively than to the primary ions. In most cases, $K_{A,B}^{Pot}$ is smaller than 1, which means that such ISEs respond to the primary ions more selectively than to interfering ions.

## 1.8. SCOPE OF THE THESIS

There is a growing risk of environmental contamination with actinides, such as U(VI), Th(IV), Pu(IV) and Am(III) due to increasing nuclear fuel cycle activity associated with the ever increasing number of nuclear reactors in the world. This is not only due to the possible leaching of the radionuclides from the underground radioactive waste burial sites but also due to the accidental events such as Chernobyl and Fukushima. So, there is a long term radiation hazard due to the presence of long lived actinides in the environment. Therefore, an efficient separation method for the removal of actinides from the environment is required. An eco-friendly separation method such as membranes in view of very low ligand inventory can be considered as a viable alternative to the solvent extraction method. However, the major drawbacks of liquid membrane-based separation / pre-concentration methods include the LM stability, which can be alleviated by employing PIM based separation.

This thesis includes the work carried out for the separation / pre-concentration of actinides, viz. U(VI), Th(IV), Pu(IV) and Am(III) from dilute nitric acid solution by PIMs employing different diglycolamides as the carrier extractants. The different DGAs employed in the PIMs as the carrier extractants for the separation / pre-concentration study include TODGA, T2EHDGA, TPDGA, THDGA, TDDGA and multiple DGAs such as T-DGA and

C4DGA. The composition of the PIMs were optimized by the uptake studies of actinide ions ($Am^{3+}$ as representative actinide ion) with PIMs of varying concentration of plasticizer, polymer and carrier extractant. The physical characterization of the PIMs was carried out using techniques, e.g., TGA, XRD, FTIR, TIMM, AFM and SEM. The uptake and transport profile of the actinides have been investigated in dilute nitric acid medium using the optimized PIMs. The effects of the feed composition on the uptake and transport profile of the actinide ions by the PIMs were also investigated in this thesis. The different transport parameters, e.g., diffusion coefficient, permeability coefficient were evaluated experimentally. The sorption kinetics and isotherms studies were carried out with the PIMs using Eu(III) as a surrogate ion for Am(III) ion. The second part of the Thesis includes the work pertaining to the development of a polymeric membrane based potentiometric sensor for Eu(III) ion using TODGA as the ionophore.

# CHAPTER 2

# EXPERIMENTAL

In the present work, uptake and transport of various actinides such as U(VI), Am(III), Pu(IV) and Th(IV) have been investigated under different experimental conditions employing polymer inclusion membrane (PIM) containing various diglycolamides (DGA) viz., *N*,*N*,*N*´,*N*´-tetra-*n*-octyldiglycolamide (TODGA), *N*,*N*,*N*´,*N*´-tetra (2-ethyl hexyl) diglycolamide (T2EHDGA), *N*,*N*,*N*´,*N*´-tetra-*n*-pentyldiglycolamide (TPDGA), *N*,*N*,*N*´,*N*´-tetra-*n*-hexyldiglycolamide (THDGA) and *N*,*N*,*N*´,*N*´-tetra-*n*-decyldiglycolamide (TDDGA) and multiple diglycolamides like tripodal diglycolamides (T-DGA) and DGA functionalized calix[4]arene (C4DGA) as extractant/carrier. In the second part of the Thesis, DGA containing PIM was evaluated for the development of a potentiometric sensor for Europium(III) ion. This Chapter gives deals of synthesis protocol and characterization of different DGAs used in the present thesis work. It also includes experimental techniques for uptake and transport studies with PIMs and potentiometric studies. The details of various apparatus, materials, experimental techniques as well as analytical techniques used in the present work are also discussed in this Chapter. The physical characterizations of the PIMs are carried out using various techniques, such as thermogravimetric analysis (TGA), x-ray diffraction (XRD), transmission infrared mapping microscopy (TIMM), Fourier transform infrared (FT-IR) spectroscopy, atomic force microscopy (AFM), scanning electron microscopy (SEM), etc. The basic principles of these techniques are described briefly in this Chapter.

## 2.1. SYNTHESIS OF DIFFERENT DGA$_S$ AND MULTIPLE DGAs

### 2.1.1. Synthesis of different DGAs (TODGA, T2EHDGA, TPDGA, THDGA, TDDGA)

Di-glycolamides (DGAs) were synthesized with slight modification of the method reported elsewhere [**75**]. In a reaction flask containing 1 mol of diglycolic anhydride (dissolved in 600 mL of dichloromethane) connected with moisture and oxygen free nitrogen gas stream, 1 mol of di-alkyl (alkyl = pentyl/hexyl/octyl/2-ethyl hexyl/ decyl) amine dissolved in ~300 mL of dichloromethane was added dropwise with constant stirring maintaining the temperature in the range of 0-5$^o$ C. After complete addition of the amine, the reaction mixture was stirred for 16 h at room temperature. Subsequently, 1.3 mol of *N,N*-dicyclohexylcarbodiimide (DCC), dissolved in 100 mL dichloromethane, was added dropwise to the reaction mixture (at 0-5° C) with constant stirring. It should be noted that ~30% extra DCC was added (DCC was used as a dehydrating agent) as it is liable to decompose easily. After complete addition of DCC, the reaction mixture was stirred at the same temperature for 30 minutes followed by the addition of the next batch of the required amine (1 mol dissolved in dichloromethane) in a dropwise manner with constant stirring and maintaining the temperature in the range of 0- 5° C. After complete addition of the required amine, the reaction mixture was stirred for six days at room temperature. The white precipitate of *N,N*-dicyclohexyl urea formed was discarded after filtering and washing with excess of dichloromethane. The dichloromethane was then removed from the filtrate by a rotavapor (Buchi) to get the crude product. The crude product, thus obtained, was purified by ethyl acetate and the insoluble impurities were discarded. The other soluble volatile impurities were removed by vacuum distillation (2.5 mm) at 120-140° C to get the desired product in the flask. The product was further purified by column chromatography using silica gel. The final pure product of DGA was obtained as a pale yellow viscous liquid with about 70% yield. The synthesis scheme for DGAs is represented in Scheme 2.1.

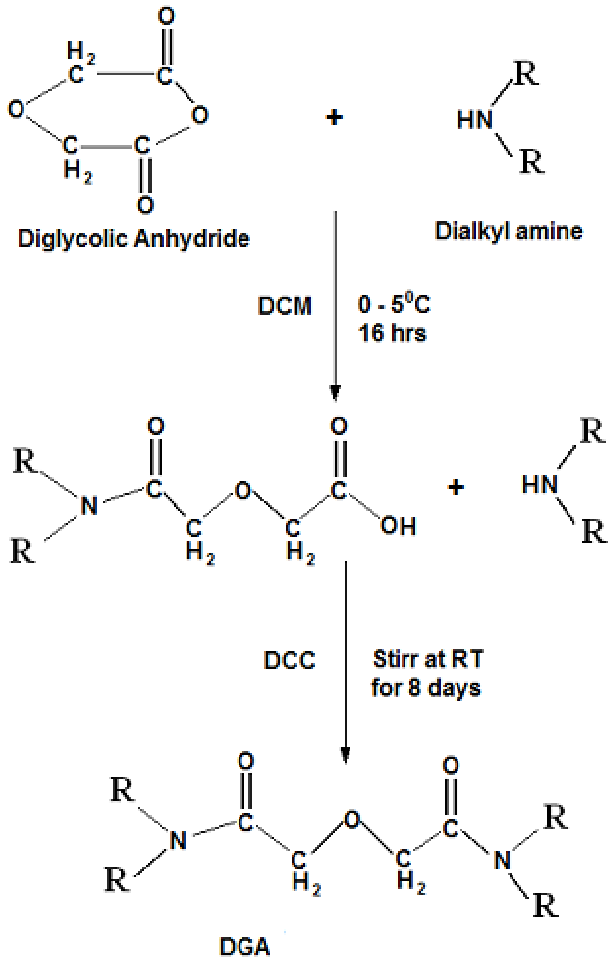

Scheme 2.1. Generic synthesis scheme of DGAs

### 2.1.2. Synthesis of multiple diglycolamides

#### 2.1.2.1. Synthesis of tripodal diglycolamide (T-DGA)

The tripodal diglycolamide (T-DGA) was synthesized using the known tripodal amine **1** following a reported method [**83**]. The glycolamide unit was introduced in two steps, viz. reaction with diglycolic anhydride and subsequent amide formation by reaction with dioctylamine. The detailed procedure is given below.

A solution of tripodal amine **1** (1.70 g, 3.29 mmol) and diglycolic anhydride (1.14 g, 9.89 mmol) in THF (60 mL) was stirred at room temperature for 3 days. The solvent was evaporated and the residue was dissolved in chloroform (50 mL) and the resulting solution washed with 1M HCl solution (2× 30 mL) and water (3× 30 mL). Evaporation of the solvent resulted in tripodaltricarboxylic acid, **2** as an oil. A solution of **2** (1.70 g, 1.96 mmol), dioctylamine (1.42 g, 5.90 mmol), N,N-dicyclohexylcarbodiimide or DCC (1.24 g, 5.96 mmol),1-hydroxybenzotriazole or HOBT (0.80 g, 5.96 mmol), and triethylamine (0.64 g, 6.33 mmol) in $CHCl_3$ (60 mL) was stirred at room temperature for 2 days. The solvent was evaporated and the residue was dissolved in *n*-hexane (100 mL) and filtered. The solvent was evaporated and the residue purified with column chromatography ($SiO_2$, $CH_2Cl_2$: MeOH= 95:5→7:3) to yield T-DGA as a viscous oil (1.50 g, 50%). The synthesis scheme for T-DGA is represented in Scheme 2.2.

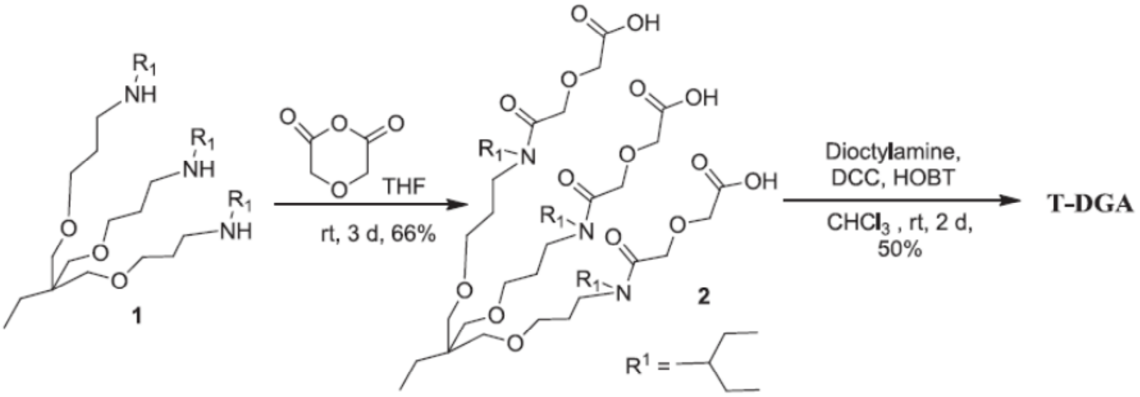

Scheme 2.2. Synthesis scheme of T-DGA

### 2.1.2.2. Synthesis of DGA functionalized calix[4]arene (C4DGA)

DGA functionalized calix[4]arene was synthesized by the reaction of amino-functionalized calix[4]arenes with the *p*-nitrophenol-activated diglycolamide.

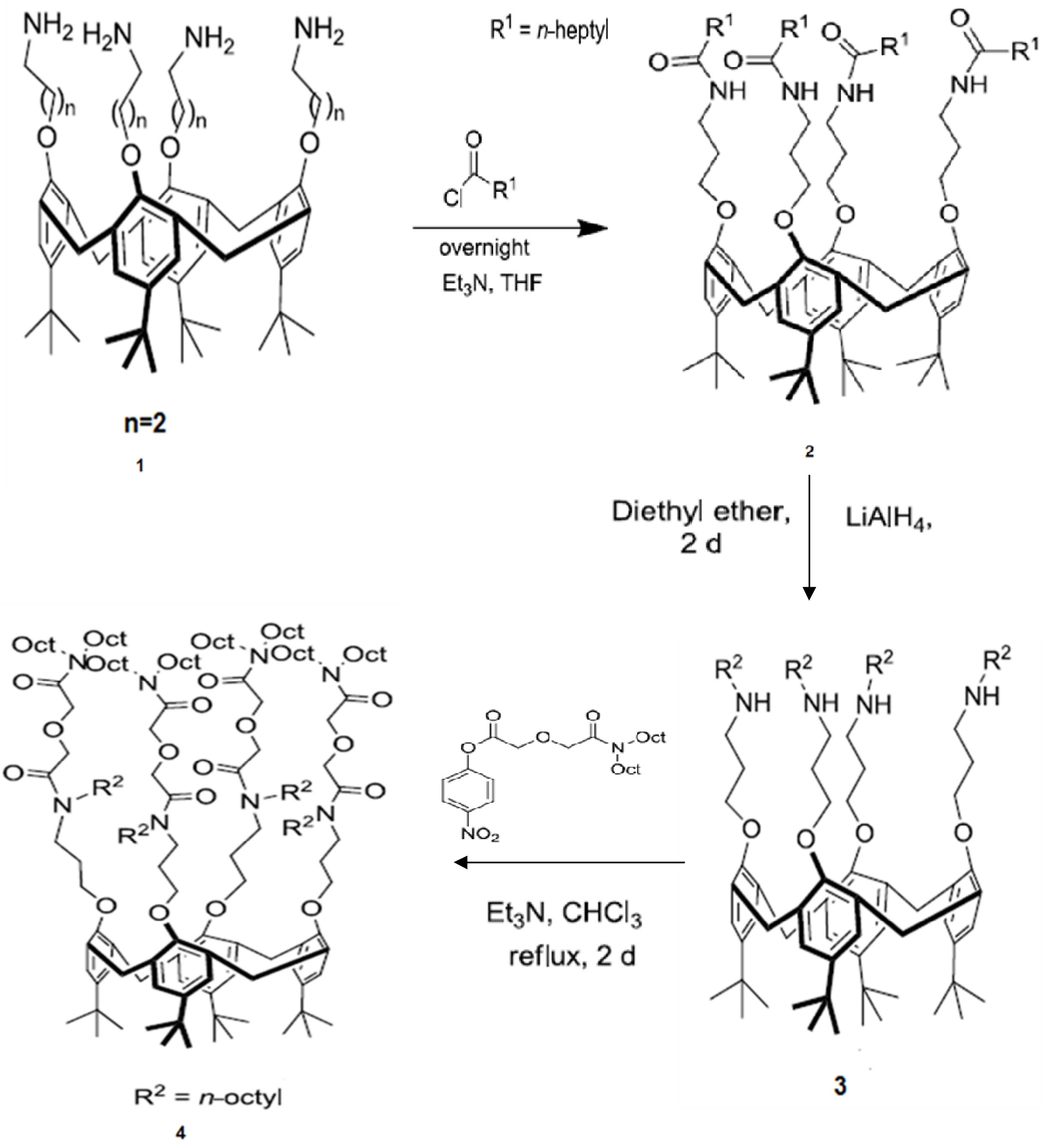

Scheme 2.3. Synthesis scheme of C4DGA

The starting tetrakis(aminoalkoxy)calix[4]arenes (**1**) was allowed to react with octanoyl chloride to produce **2** followed by reduction of the amide carbonyl groups with $LiAlH_4$ to produce tetrakis(alkylaminoalkoxy)calix[4]arenes, **3**. Finally, **3** was further reacted with *p*-nitrophenol-activated DGAto convert it into the tetra-DGA-calix[4]arenes, **4**. The synthesis scheme for C4DGA is represented in Scheme 2.3.

## 2.2. CHARACTERIZATION OF THE DGA LIGANDS

### 2.2.1. Characterization of *N, N, N', N'*-tetra-*n*-octyldiglycolamide (TODGA)

The product was characterized by GC–MS, FTIR and elemental analyzer. The results are as follows: GC–MS: 7.12 min, 1.59%, m/z 241 calculated for $HN(C_8H_{17})_2$; 22.00 min, 98.01%, m/z 582 calculated for $O[CH_2C(O)N(C_8H_{17})_2]_2$. Similarly, the analytical data of the synthesized TODGA are presented in Table 2.1. The appearance of the characteristic vibrational frequency at 1640 $cm^{-1}$ in the recorded FT-IR spectra suggested the presence of the carbonyl groups of the diglycolamide. The CHN elemental analysis of the synthesized product yielded values close to the theoretical values. The FT-IR and CHN analysis confirmed the formation of the product in good yield (70%). The other DGAs were also characterized in a similar way.

Table 2.1. Analytical data of TODGA

| | |
|---|---|
| Formula | $C_{36}H_{72}N_2O_3$ |
| Product Yield | ~70% |
| C (%) | 73.1 (74.5)$^{\#}$ |
| H (%) | 12.8 (12.4)$^{\#}$ |
| N (%) | 5.2 (4.8)$^{\#}$ |
| $\nu_{>C=O}$ | 1640 $cm^{-1}$ |

\# *Values in parentheses are the theoretical values*

## 2.3. RADIOTRACERS (PREPARATION AND PURIFICATION)

The separation studies on metal ions reported in the present thesis were carried out with radiotracers. Procurement, preparation as well as purification of various radiotracers are given below.

### 2.3.1. Uranium-233

$^{233}$U tracer ($t_{1/2}$ = 1.59 x $10^5$ years) was produced by the irradiation of $^{232}$Th followed by its purification using a reported method [**84**]. $^{233}$U was purified using an anion exchange method (Dowex 1x8, $Cl^-$ form resin was used) as reported previously to get rid of its major decay products such as $^{228}$Th (daughter product of $^{232}$U which is present in small quantity along with $^{233}$U) and its daughter products. It is well known that in 6 M HCl, anionic complexes of U are held onto the column while $^{232}$Th and its daughter products pass through [**85**]. The loaded U was subsequently eluted using dilute HCl. The U in HCl medium was converted to $HNO_3$ medium by repeated evaporation in concentrated $HNO_3$ and finally used as stock solution (in 0.5 M $HNO_3$). The purity of $^{233}$U tracer was ensured by alpha spectrometry.

### 2.3.2. Thorium-234

$^{234}$Th was obtained from natural uranium which contained a small fraction of $^{234}$Th in secular equilibrium with the long-lived parent $^{238}$U. As Th(IV) does not form any anionic chloro complexes in HCl medium while U(VI) forms anionic complexes such as $UO_2Cl_3^-$ and $UO_2Cl_4^{2-}$, this was used to selectively extract $^{238}$U from the mixture of the radionuclides in 6 M HCl using 30% Aliquat 336 in chloroform. For quantitative separation, the extraction was repeated several times till the aqueous phase appeared completely colorless. The aqueous phase, containing $^{234}$Th was washed two times with chloroform to remove traces of the organic extractant and the diluent. Finally, the aqueous phase was dried under infrared lamp. One mL of concentrated $HNO_3$ and a few drops of concentrated $HClO_4$ were added and further dried to oxidize and destroy the traces of the organic. This step was repeated to convert $Th^{4+}$ in the chloride form to the nitrate form. The purity of the purified product was confirmed by gammaray spectrometry.

### 2.3.3. Plutonium-239

Plutonium (mixture of isotopes but mainly $^{239}$Pu) is separated from spent fuel obtained from research reactors CIRUS and DHRUVA using PUREX process. Table 2.2 shows the typical range of isotopic composition of Pu obtained from research and Indian Pressurized Heavy Water Reactors (PHWRs) [**86**]. Pu was finally purified from its major decay product $^{235}$U and $^{241}$Am (from beta decay of $^{241}$Pu) by TTA (2-thenoyltrifluoro acetone) extraction (using 0.5 M TTA in xylene) from an aqueous phase containing 1 M $HNO_3$. Under these conditions, $Am^{3+}$ and $UO_2^{2+}$ are not extracted while $Pu^{4+}$ is extracted quantitatively. Pu was subsequently stripped by 8 M $HNO_3$. Its radiochemical purity was ascertained by alpha as well as gamma ray spectrometry to check the absence of $^{241}$Am [**87**].

Table 2.2. Range of isotopic composition data of Pu of Research and Power reactors

| Reactor type | Range of atom% abundance | | | | |
|---|---|---|---|---|---|
| | $^{238}$Pu | $^{239}$Pu | $^{240}$Pu | $^{241}$Pu | $^{242}$Pu |
| Research | 0.003-0.031 | 89.930-94.540 | 5.180-8.980 | 0.243-0.796 | 0.013-0.154 |
| PHWR | 0.072-0.160 | 69.570-77.640 | 19.140-25.400 | 1.917-3.475 | 0.702-1.659 |

### 2.3.4. Americium-241

$^{241}$Am was purified from its daughter product, $^{237}$Np, by first reducing Np to its +4 state using hydroxylamine hydrochloride at 1 M $HNO_3$ and subsequently extracting $Np^{4+}$ by TTA (similar to the extraction of $Pu^{4+}$ mentioned above). The aqueous phase was evaporated to dryness and a few drops of a mixture of concentrated $HNO_3$ and $HClO_4$ (5:1 ratio) was added to destroy the organic impurities. Alpha spectrometry of the purified $^{241}$Am stock was carried out to rule out the presence of the impurities.

### 2.3.5. Other radiotracer

The radiochemical tracer such as $^{152,154}Eu$ was procured from BRIT (Board of Radiation and Isotope Technology), Mumbai and its radiochemical purity was ascertained by gamma ray spectrometry.

## 2.4. OXIDATION STATE ADJUSTMENT

The oxidation state of Pu was adjusted to the +4 state by first drying a known amount of Pu (about 20 microgram) under an infrared lamp. The dried activity was dissolved in one mL of 1 M $HNO_3$ and a few drops of 0.005 M $NaNO_2$ solution was added to change the oxidation state from +3 and +6 state to the +4 state. The aqueous solution was contacted with one mL of 0.5 M TTA in xylene for 30 minutes. The extracted $Pu^{4+}$ (the unconverted $Pu^{3+}$ and $PuO_2^{2+}$ were not extracted under these conditions) was subsequently stripped using 7 M $HNO_3$ and kept for subsequent studies involving $Pu^{4+}$. The oxidation state of $Pu^{4+}$ was intermittently checked by TTA extraction (log D *vs* log TTA concentration plot gave slope close to 4). $Pu^{4+}$ was found to be stable for about one month and was used as the stock solution of $Pu^{4+}$.

## 2.5. METHODS

### 2.5.1. Preparation of PIM

Preparation of the polymer inclusion membrane (PIM) was done following literature method [**88**]. For the preparation of the PIM, 1.62 % solution of the polymer solution was prepared by dissolving cellulose triacetate (CTA) in 100 ml of dichloromethane. The required amount of CTA solution was mixed with the respective carrier ligand (different diglycolamides), plasticizer (2-nitrophenyl octyl ether (NPOE) and sonicated for few minutes in a beaker to ensure the homogeneity of PIM. The resulting solution was poured into a Petri dish of 9 cm diameter. The dichloromethane was allowed to evaporate slowly for overnight. The resulting PIM was peeled out by spreading few ml of water on it. It was cut in to the required sizes (exposed membrane area was 4.94 cm$^2$) and fitted in membrane cell for transport studies and 4 cm$^2$ (2cm x 2cm) for uptake studies.

### 2.5.2. Uptake studies

Uptake studies of the actinide ions, $Am^{3+}$, $Pu^{4+}$, $UO_2^{2+}$ and $Th^{4+}$ were conducted using a conical flask (Fig.2.1) where a small piece of PIM (total area of the PIM was fixed at 4 cm$^2$) was immersed into the feed solution (20 mL) containing the target radio tracer in dilute nitric acid (0.5-3.0 M). The solution was stirred at a fixed speed of 200 rpm using a high-speed precise magnetic stirrer. Samples of fixed volume (0.1 mL) were taken out at regular time intervals for their subsequent assay by radiometry. The percentage uptake of the metal ion by the PIM at a given time‘t’ was determined by the following equation,

$$\% \text{ Uptake } = \frac{C_0 - C_t}{C_0} X100 \qquad (2.1)$$

where, $C_0$ and $C_t$ are the metal ion concentrations in the aqueous phase at the start of the experiment (t = 0) and at time ‘t’, respectively. The uptake studies were carried out in duplicate at ambient temperature (24 ± 1$^o$C) and the reproducibility of the results was observed to be within ±5% of the average value.

Fig. 2.1. A typical arrangement for the uptake studies

### 2.5.3. Transport studies

The transport experiments were conducted in a two compartment cylindrical Pyrex glass transport cell (Fig. 2.2) in which, the PIM was tightly clamped between two cell compartments. The feed compartment contained the target radionuclide in 1 M nitric acid and the receiver compartment contained the strippant solution of 1 M *alpha*-hydroxyisobutyric acid (α-HIBA) (pH 3.0 ± 0.1). The volumes of the aqueous feed and strip solutions were kept constant (20 mL) in all the experiments and the exposed membrane area was 4.94 cm$^2$. Both the phases were stirred at 200 rpm using a high speed magnetic stirrer equipped with precise speed control which ensured minimum thickness of the aqueous diffusion boundary layers without causing any damage to the membrane [**37**]. Aliquots (usually 0.1 mL) were removed from both the phases via the sampling ports with a micropipette at suitable time intervals for subsequent radiometric assay. All the PIM transport studies were carried out at ambient temperatures (24 ± 1$^{o}$C) and the results were found to be reproducible within ± 5%.

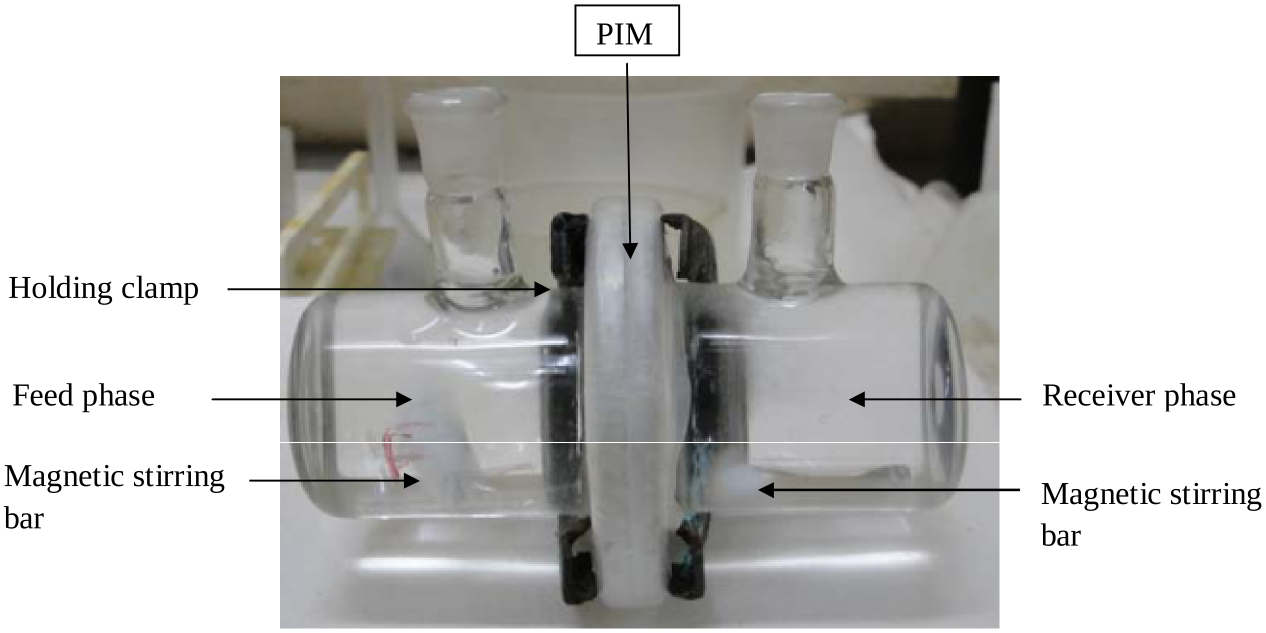

Fig. 2.2. A typical membrane transport cell used in the present studies

The cumulative percentage transport (% T) of the metal ions at a given time was obtained from the following equation:

$$\% \mathrm{T} = 100.\frac{C_{r,t}}{C_{f,0}} \tag{2.2}$$

The removal percentage of the actinide ion from the feed phase by the PIM during the transport was given by the following equation

$$\% \mathrm{R} = 100.\frac{C_{f,0} - C_{f,t}}{C_{f,0}} \tag{2.3}$$

where, $C_{r,t}$ and $C_{f,t}$ are the concentration of the actinide ion in the receiver compartment and feed compartment at any given time ‘t’ of the transport, respectively and $C_{f,0}$ is the concentration of the actinide in the feed compartment at the beginning of the experiment (t = 0). The permeability coefficient, P was obtained using the following equation,

$$\frac{\ln C_{f,t}}{C_{f,0}} = -P\left(\frac{A}{V}\right)t \tag{2.4}$$

where, the terms $C_{f,0}$ and $C_{f,t}$ have their usual meanings while V is the volume of the feed phases in $cm^3$, and A is the total exposed surface area of the membrane.

A plot of $\ln(C_{f,t}/ C_{f,0})$ versus time allows calculating the P value from the slope of the linear fit. It should be noted that the above equation is valid only when the membrane is not saturated with the carrier. In the present work, since all the experiments were carried out at tracer metal concentrations, Eq. (2.4) was applicable for the calculation of P.

## 2.6. INSTRUMENTS

### 2.6.1. Radioanalytical instruments / techniques

The radio analytical technique employed for the analysis of alpha emitting radionuclides such as $^{233}$U and Pu was liquid scintillation counter, whereas NaI(Tl) scintillation counter was used for the estimation of the gamma ray emitting radionuclides such as $^{234}$Th and $^{241}$Am.

### 2.6.1.1. Liquid scintillation counter (LSC)

LSC is the most widely used detector for the quantitative analysis of the alpha emitting radionuclides. Nearly 100% detection efficiency of this detector is of great advantage and even as low as few Bq of alpha activity can be assayed with good precision. A scintillator is a material that luminesces in a suitable wavelength region when ionizing radiation interacts with it. Interaction of the charged particles (alpha particles) with the scintillator results in emission of photons and the intensity of the emitted light is a quantitative measure of the incident radiation. The light emitted from scintillator is then collected by the photomultiplier tube (PMT) which produces signal representative of the primary radiation. Generally, the scintillator emits photons in the UV region and hence, a ‘wavelength shifter’ is added to the scintillator which has intermediate energy levels. In such cases, the de-excitation takes place via these intermediate energy levels and hence, the wavelength of the emitted photons is shifted from the UV to the visible region which is subsequently recorded in the PMT (as photo cathodes of most PMTs are compatible with the visible light). The liquid scintillation counter is used to monitor gross alpha activity as it cannot distinguish between alpha energies and thus, cannot be used for alpha spectrometry.

Many organic compounds are versatile scintillators for radiation measurements [**89, 90**]. The liquid scintillation cocktail comprises of a solvent such as dioxane or toluene, a scintillator such as PPO (2,5-diphenyl oxazole) and a wavelength shifter such as POPOP (1,4-bis-2-(5-phenyl oxazolyl)-benzene). The solvent is the main stopping medium for radiation and must be chosen to give efficient energy transfer to the scintillating solute. In case of toluene based scintillator, a suitable extractant such as di(2-ethylhexyl) phosphoric acid (HD2EHP) is added to facilitate the aqueous samples determinations by transferring the radionuclides from the aqueous phase to the organic phase. In the present work, a toluene based liquid scintillator cocktail was employed which consisted of 10 % (v/v) HD2EHP, 0.7 % (w/v) PPO and 0.03 % (w/v) POPOP. Suitable aliquots (25-100 µL) containing alpha activity were taken in glass vials containing ca. 5 mL of the liquid scintillator cocktail. When aqueous phase was added to the toluene scintillator, the two phases were sonicated for ca. 2 min using an ultrasonic agitator to transfer the radionuclides into the organic phase. Each sample was counted for sufficient time so as to get more than 10,000 counts to restrict the statistical counting error to < 1%.

### 2.6.1.2. NaI(Tl) scintillation counter

Sodium iodide activated with 0.1–0.2% of thallium, NaI(Tl), is by far the most widely used inorganic scintillator for the assay of gamma emitting radionuclides. Salient features of the detectors are the low cost, ease of operation and ruggedness [**91, 92**]. The band gap in the NaI crystal is of the order of 5-6 eV. When a charged particle (or gamma ray) falls on the detector its energy is used up either for excitation of electrons from the valence band to the conduction band or for the ionization of atom. De-excitation of these electrons from the conduction band to valance band leads to the emission of photons in the UV region as the band gap is large. To shift the emitted photons such that they fall in the visible region, which is the requisite of PMT, NaI crystal is doped with an activator impurity like Tl which forms the intermediate level conduction band. The resolution of NaI(Tl) detector is about 7% at 662 keV. In the present work, a 3” x 3” well type NaI(Tl) detector (Para Electronics) coupled with a multichannel analyzer (ECIL, India) has been used for gamma ray counting. Nearly 100 % detection efficiency for moderate energy photons in a well type NaI(Tl) detector offers great advantages for counting of low activity samples. A suitable aliquot (0.1 - 0.5 mL) of the desired analyte solution was taken in glass counting tubes (10 mm dia) which was then placed in the cavity of detector coupled with the PMT and the associated electronics. Each sample was counted for sufficient time so as to get more than 10,000 counts to restrict the statistical counting error within 1%.

### 2.6.2. Analytical instruments / techniques

#### 2.6.2.1. Equipments for the characterization of the diglycolamides

Elemental (C, H, N) analysis was performed using an elemental analyzer EA 1110 from Carlo-Erba Instruments. The FT-IR spectra were recorded as thin film in IR spectrophotometer in the wavelength range of 4000 – 400 cm$^{-1}$. The PMR spectra of the diglycolamide products were recorded in $CDCl_3$ medium using Bruker 200 MHz instrument employing TMS (tetramethylsilane) as an internal standard. GC– MS was performed using a Thermo Finnigan Trace DSQ GC–MS instrument with a single quadrupole mass spectrometer.

### 2.6.2.2. Equipments for the characterization of PIMs

Different techniques, viz., TIMM (Transmission Infrared Mapping Microscopy), FTIR (Fourier Transform Infrared), XRD (x-ray diffraction), TGA (Thermogravimetric analysis), SEM (Scanning Electron Microscopy), AFM (Atomic Force Microscopy), etc. were employed for the physical characterization of the PIMs. A brief description of these techniques and the corresponding instruments employed are discussed here.

#### 2.6.2.2.1. Fourier transform infrared (FTIR) spectroscopy with Transmission infrared mapping microscopy (TIMM)

Membrane mapping of PIM was performed using a Perkin Elmer (USA) FTIR microscope. TIMM studies were carried out in the wavelength range of 4000–750 $cm^{-1}$, with a resolution of 4 $cm^{-1}$, coupled with a mercury-cadmium telluride detector. The mapping was carried out in the area of 150 µm x 193 µm of the PIM with 16 scans per pixel. The membrane made from pure CTA was taken as the blank for all subsequent composite PIMs. The distribution profiles of the membrane components in the membrane were determined by monitoring the right frequency band of the components. The FTIR measurements were carried out in the wavelength range of 4000– 650 $cm^{-1}$, with a resolution of 4 $cm^{-1}$, coupled with a TriglycineSulfate (TGS) detector. Eight scans were required for the FT-IR measurements, while 16 scans were done per pixel for the TIMM studies.

#### 2.6.2.2.2. X-ray diffraction (XRD)

The membrane samples (2cm x 2cm) were mounted as such and the X-ray diffraction patterns were recorded for angles ranges ($2\theta$) from 5° to 40° of the membrane under study using a XRD instrument (GBC scientific equipment) equipped with Cu $K_\alpha$ radiation ($\lambda$=1.5418Å) target and Xe-proportional detector. XRD scans were carried out with a step size of 0.008°

(2θ) with a speed of 0.229° $\text{min}^{-1}$. A standard silicon sample was used to calibrate the instrument. The accuracy of the equipment for X-ray intensity is ± 5%.

#### 2.6.2.2.3. Thermogravimetric analysis (TGA)

TG analysis was carried out to investigate the thermal decomposition of the PIMs. Weight loss of a small piece of the PIM (usually 1 mg) was recorded in the temperature range of 25-600 ºC at a heating rate of 10 ºC $\text{min}^{-1}$ using a high resolution (0.04 µg) thermogravimetric analyzer (SetaramSetsys Evolution) under a constant flow (100 mL/min) of high purity (99.995%) argon gas.

#### 2.6.2.2.4. Scanning electron microscope (SEM)

The morphology of the surface and the cross section of the PIMs were determined by SEM analysis. The SEM studies were carried out with a JSM 840 Scanning Electron Microscope (SEM) from JEOL, Japan, with a 1000–5000 times magnification of the membrane surface/cross section. The samples were prepared by mounting the PIM samples on a carbon tape on top of a stub and both sides of the dry membrane were coated with gold using a Polaron E5100 sputter coater.

#### 2.6.2.2.5. Atomic force microscope (AFM)

The surface roughness was investigated using AFM for the pristine PIMs as well as the PIMs loaded with the metal ions, the PIMs stripped off loaded metal ions and the PIMs treated with dilute nitric acid. The small square PIM sample pieces (1 $\text{cm}^2$) were cut from each prepared membranes and glued on metal disks. The topographic, amplitude and phase AFM images of the PIM samples were taken with an Asylum MFP-3D classic AFM instrument using an AC 160 TS-R3 silicon cantilever probe in tapping mode (AC mode). The membrane surface was imaged in two different scan sizes: large (3µm x 3µm) and small (600nm x 600nm). The roughness was determined in terms of root mean square roughness ($R_q$) defined as the standard deviation of the Z values within a given area and is calculated as:

$$R_q = \sqrt{\frac{\Sigma(Z_i - Z_{avg})^2}{N}} \qquad (2.5)$$

where, $Z_{avg}$ is the average of the Z values within the given area; $Z_i$, the current $Z$ value; and $N$, the number of points within a given area.

### 2.6.2.2.6. Thickness measurements

Thickness of the membranes was measured using a digimatic micrometer (Mitutoyo Corporation, Japan) of a resolution of 0.001 mm.

### 2.6.2.3. Inductively coupled plasma-atomic emission spectroscopy (ICP-AES)

Inductively Coupled Plasma-Atomic Emission Spectrometry (ICP-AES) is an emission spectrophotometric technique, working on the principle that the excited electrons emit energy at a given wavelength as they return to their corresponding ground states after excitation at high temperature Argon Plasma [**93, 94**]. The fundamental characteristic of this process is that each element emits energy at specific wavelengths peculiar to its atomic character. The energy transfer for electrons when they are de-exited back to the ground state is unique to each element as it depends upon the electronic configuration of the orbital. The energy transfer is inversely proportional to the wavelength of the electromagnetic radiation, Eq. (2.6)

$$E = \frac{hc}{\lambda} \qquad (2.6)$$

(where, h is Planck's constant, c is the velocity of light and $\lambda$ is the wavelength), and hence, the wavelength of light emitted is also unique.

Although each element emits energy at multiple wavelengths, in the ICP-AES technique it is most common to select a single wavelength (or a very few) for a given element. The intensity of the energy emitted at the chosen wavelength is proportional to the amount (concentration) of that element in the sample being analyzed. Thus, by determining which wavelengths are emitted by a sample and by determining their intensities, the analyst can qualitatively and quantitatively find the elements from the given sample relative to a reference standard.

The wavelengths used in the AES measurements range from the upper part of the vacuum ultraviolet (160 nm) to the limit of visible light (800 nm). As borosilicate glass absorbs light below 310 nm and oxygen in air absorbs light below 200 nm, optical lenses and prisms are generally fabricated from quartz glass and optical paths are evacuated or filled by a non-absorbing gas such as Argon. In the present studies, Ultima 2CHR, Horibajobinyvon ICP-AES has been used for the determination of the metal ion concentrations in the given samples.

#### 2.6.2.4. Potentiometry

##### 2.6.2.4.1. Membrane preparation

The polymeric membrane was prepared following the literature method [**88**]. In case of CTA based membrane no ionic additives was added and the PIM contains CTA as the base polymer, NPOE as the plasticizer and TODGA as the ionophore, whereas in case of PVC (polyvinyl chloride) based membrane, apart from PVC, NPOE and TODGA in the membrane, NaTPB (Sodium tetraphenyl borate) was added as the ionic additive during the preparation of the membrane. The details of composition of different PVC and CTA based sensor membranes were given in Chapter-5.

##### 2.6.2.4.2. Sensor preparation

Potentiometric sensor electrode was fabricated using the PIMs of varying compositions. A small piece of the PIM was cut and attached at the base of a plastic tube with the help of an adhesive. After drying of the adhesive, the PIM was tightly held with the tube body by the help of Para film. The sensor, thus fabricated, was filled (3/4 th of the volume) with 0.1 M Eu(NO$_3$) solution and the inner filling liquid. The electrode was conditioned for overnight by soaking in 0.1 M Eu(NO$_3$)$_3$ solution.

### 2.6.2.4.3. Electromotive force (EMF) measurement

Real time EMF measurements were performed using a high impedance digital potentiometer (Radiometer Ion 85 Ion Analyser) (Fig. 2.3) at 25.0 ± 0.5 ºC. A silver/silver chloride electrode was used as an internal reference electrode. A saturated calomel electrode was used as the external reference electrode in conjunction with the sensor electrode to measure the cell potential.

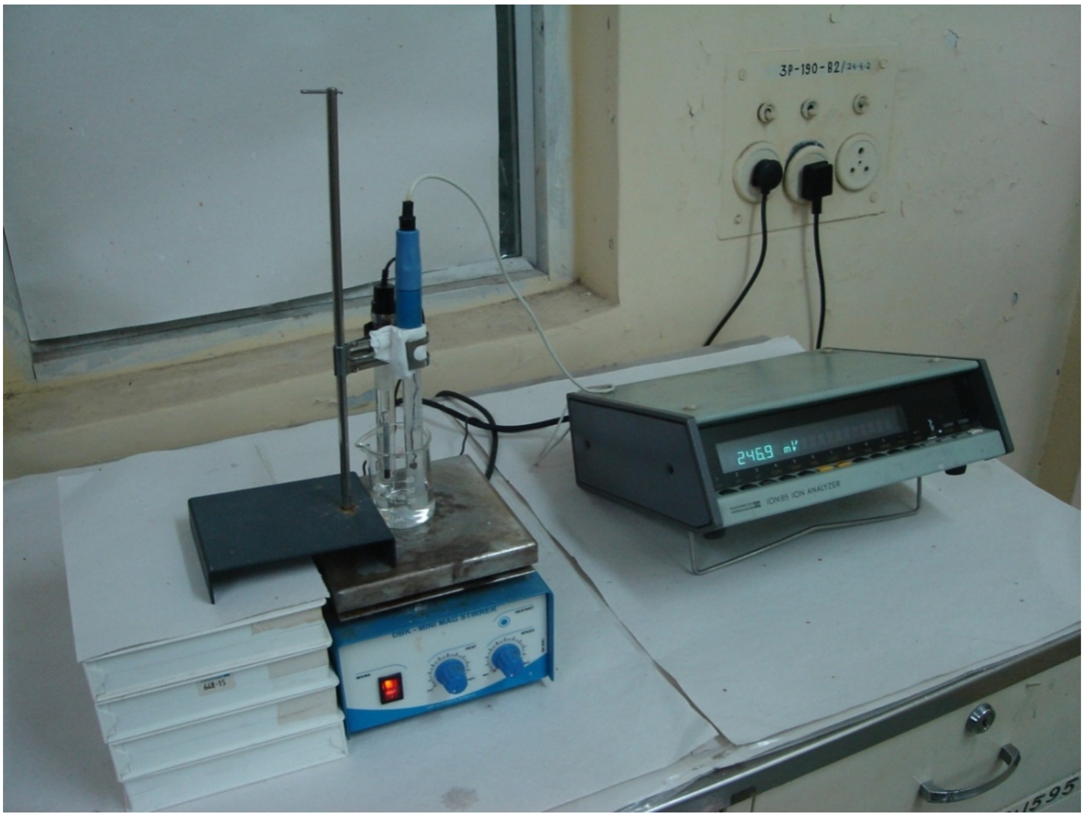

Fig. 2.3. Experimental set up for EMF measurement

The ionic strength and pH of the solution were maintained constant throughout the experimental studies by using an acetate buffer solution at pH 5.0 ± 0.1. The EMF generated from the sensor out of the test solution has the following cell assembly:

Ag-AgCl (3 M KCl) /0.1 M $Eu(NO_3)_3$/Membrane/Test solution/Hg-$Hg_2Cl_2$, KCl (sat.)

The pH of the solution was measured using a pH-electrode (Micro pH Analytica, SDFCL, India).

# CHAPTER 3

# ACTINIDE ION UPTAKE AND TRANSPORT BY THE POLYMER INCLUSION MEMBRANES CONTAINING DIFFERENT DIGLYCOLAMIDES AS THE CARRIER EXTRACTANTS

## 3.1. INTRODUCTION

In view of the long term radiation hazard due to the presence of long lived radionuclides such as the actinides in the environment arising due to factors such as accidents, weapon testing, milling mining activities, escape from geological repositories, etc, efficient separation methods for the removal of actinides from a variety of samples, such as soil, rock, food, air, biological samples, etc, are required. However, the separation of actinides, particularly those of minor actinides (Am, Cm, Np), is a challenging task [**95**] and needs efficient separation methods. Though U and Pu are conveniently extracted using TBP based extraction processes, the removal of the minor actinides (Np, Am, Cm) is quite a task and usually requires efficient tailor made extractantssuch as octyl-(phenyl)-$N$,$N$-diisobutylcarbamoylmethylphosphine oxide (CMPO), diisodecylphosphoricacid (DIDPA) or trialkyl phosphine oxide (TRPO) [**95-98**]. However, the use of these extractants is associated with problems such as third phase formation, poor back extraction, etc. Completely incinerable substituted diamides extractants offer several advantages over organophosphorus compounds, especially with respect to (i) the innocuous nature of their degradation products, viz. carboxylic acids / amines and (ii) the possibility of complete incineration of the spent solvent leading to reduced volume of the secondary waste volumes [**99-101**]. In addition, the physico-chemical properties of this class of ligands can be tuned by the judicious choice of the alkyl substituents. In the last decade, several investigations have been conducted on the modification of diamide structure in order to further improve its extracting properties. It was observed that the introduction of an etheric oxygen between the two amide groups of a diamide can lead to the formation of a diglycolamide caused significant enhancement in the extraction of trivalent actinides / lanthanides. The diglycolamide (DGA) extractants were initially introduced by Stephan et al. [**66, 67**] for the extraction of divalent and trivalent cations. Subsequent studies involving various DGA derivatives concerning fundamental as well as applied research have been reported extensively [**102-106**]. The physico-chemical properties of the DGAs can be changed by the attachment of different alkyl chains to N atoms. For example, DGA ligands with short alkyl groups (-$CH_3$, -$C_2H_5$) are water soluble and have been utilized as masking agents [**107**]. On the other hand, DGA molecules with long alkyl chains (-$C_8H_{17}$, -$C_{10}H_{21}$, -$C_{12}H_{25}$) can be dissolved in non-polar organic diluents and hence, can be utilized in solvent extraction processes for the separation of metal ions including the trivalent actinide ions.

Solvent extraction based processes involve large quantities of toxic and inflammable solvents with added disadvantages of third phase formation, phase entrainment, etc. Therefore, there is a need for an alternative "green" and efficient process for the recovery of these hazardous metal ions. Liquid membrane (LM) based separation methods [**108-111**] have been suggested as viable alternatives to solvent extraction based methods due to advantages such as low ligand inventory, easy scale up, simultaneous extraction and stripping, etc. However, a major disadvantage associated with the supported liquid membranes (SLMs) is their poor stability under experimental conditions which limits their use in large-scale applications. Polymer inclusion membranes (PIMs), on the other hand, have been reported to have superior stability while retaining most of the advantages of the SLMs and have been suggested as alternatives to the SLMs and have been evaluated for metal ion separations by many research groups [**112-114**]. Diglycolamide based extractants such as *N,N,N′,N′*-tetra-*n*-octyldiglycolamide (TODGA), *N,N,N',N'*-tetra(2-ethylhexyl) diglycolamide (T2EHDGA) and different substituted diglycolamides, such as *N,N,N',N'*-tetra-*n*-pentyldiglycolamide (TPDGA), *N,N,N',N'*-tetra-*n*-hexyl diglycolamide (THDGA), *N,N,N',N'*-tetra-*n*-decyldiglycolamide (TDDGA) have been extensively studied for actinide ion separations from acidic radioactive feeds using SLM based methods [**115-121**]. However, studies on PIMs containing diglycolamides are very limited [**122, 123**]. This Chapter describes the comparative uptake and transport behaviour of actinide ions, viz. Am(III), Pu(IV), Th(IV) and U(VI) from acidic feed solutions by PIMs containing carrier extractants such as TODGA, T2EHDGA, TPDGA, THDGA and TDDGA. The PIMs contained different DGAs as the carrier extractant, 2-nitrophenyloctylether (NPOE) as the plasticizer and cellulose triacetate (CTA) as the base polymer matrix. Generally, the effect of membrane components, viz., plasticizer, polymer and carrier extractant (different DGAs) on the uptake of the actinide ions ($Am^{3+}$ was used as the representative trivalent actinide) by the PIMs were studied to find the optimized composition of the PIMs and subsequently, the optimized PIMs were employed to study the comparative uptake and transport behavior of the above mentioned actinide ions. A detailed physical characterization of the PIMs was done using different techniques such as thermogravimetric analysis (TGA), x-ray diffraction (XRD), atomic force microscopy (AFM), Fourier transform infrared (FTIR) spectroscopy and transmission infrared mapping microscopy (TIMM) and the results are included in this Chapter. Different transport parameters, viz., diffusion coefficient (D), permeability coefficient (P) were experimentally determined. This Chapter also gives a detailed account of the kinetics and sorption isotherm studies for the batch sorption studies with macro amounts of $Eu^{3+}$ (used as a surrogate of $Am^{3+}$) using the T2EHDGA based PIMs.

## 3.2. PHYSICAL CHARACTERIZATION OF THE PIM

Physical characterization of the PIMs containing TODGA, T2EHDGA, TPDGA, THDGA and TDDGA as the carrier extractants was carried out using different techniques such as TGA, XRD, AFM, FTIR and TIMM.

### 3.2.1. Thermogravimetric analysis

The thermogravimetric analysis (TGA) suggested DGA based PIMs are generally stable upto 150°C and nearly 100% decomposition is seen at 370°C with major mass losses at 180, 230 and 330°C corresponding to the combustion of NPOE, DGA and CTA. Fig. 3.1 shows a typical thermogram of a TODGA containing PIM with the optimized composition (vide infra) of 58% TODGA, 30% NPOE, 12% CTA.

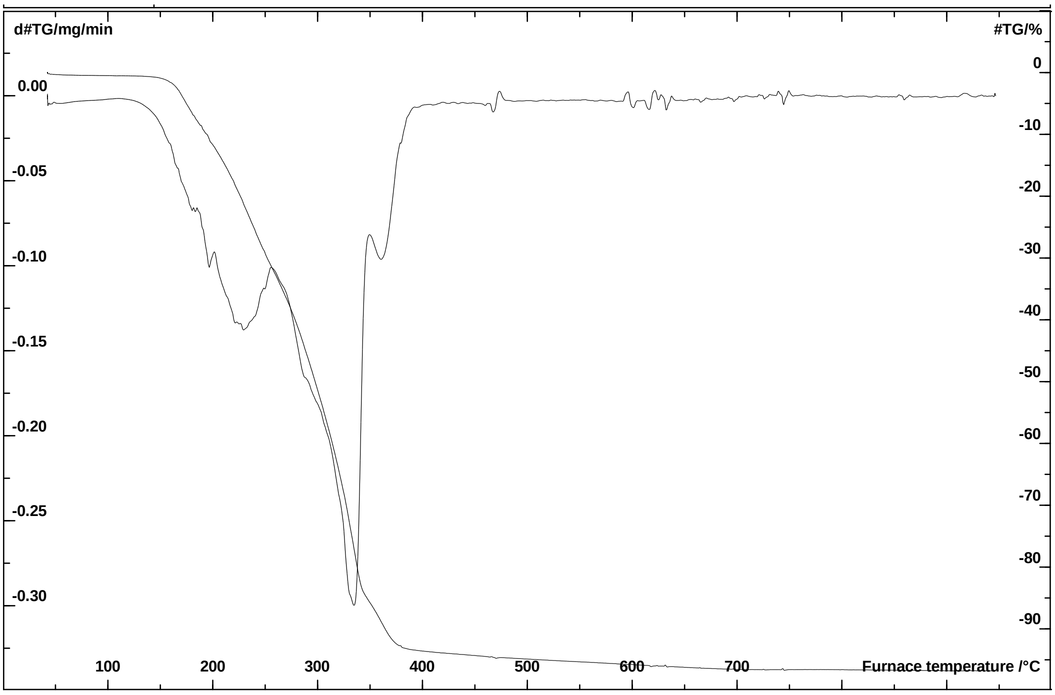

Fig. 3.1. TG-DTG profile of the PIM containing 58% TODGA, 30% NPOE, 12% CTA, heating rate: 10°C/min.; carrier gas: high purity Ar, flow rate: 100 mL/min.

The thermal study of other PIMs containing different diglycolamides as the carrier extractants is given in *Annexure-I* (Fig.A1.1 and Fig.A1.2).

### 3.2.2. XRD studies

XRD study of the different DGA based PIMs showed a broad peak centered around 20° corresponding to the Van der Waals halo found in all polymers [**124, 125**]. This suggested amorphous character of the membranes suggesting no crystallization of the components. A previous publication has also shown similar results with CTA based PIMs [**126**]. This also indicated that a carrier-metal ion diffusion mechanism might be operative for the transport of metal ions across the PIMs.

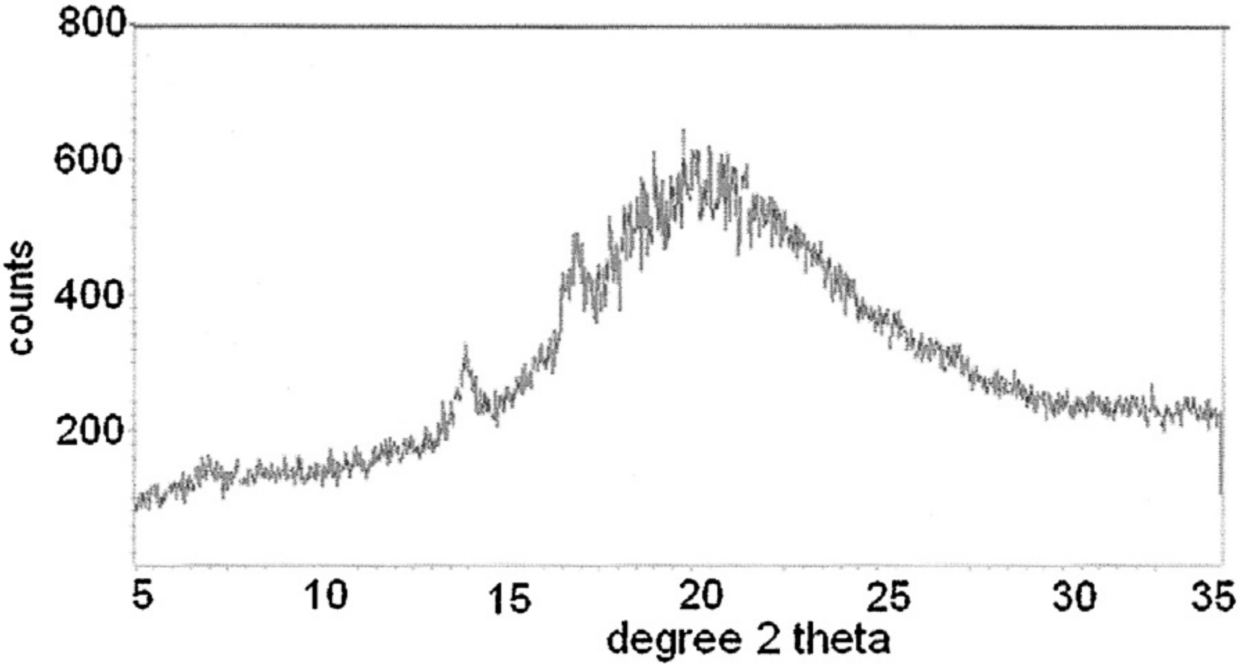

Fig. 3.2. XRD pattern of the PIM containing 58% TODGA, 30% NPOE, 12% CTA.

A typical XRD pattern of the PIM containing 58% TODGA, 30% NPOE, 12% CTA is given in Fig. 3.2. The XRD patterns of the other PIMs containing T2EHDGA, TPDGA and THDGA were analogous and are given in *Annexure-I* (Fig.A1.6 and Fig.A1.7)

### 3.2.3. AFM studies

The morphology of the PIMs containing TODGA as the carrier extractant is analyzed using AFM which showed roughness characteristics of similar to the CTA based membranes showing reasonably high mass transfer rates (Fig. 3.3a). Apparently, a PIM treated with 1 M $HNO_3$ for 10 days did not show appreciable changes in its morphology and roughness as shown by the AFM profile picture (Fig. 3.3b). However, when the PIMs were loaded with $Eu(NO_3)_3$ solution ($Eu^{3+}$ has been taken as a surrogate for $Am^{3+}$) in 1 M $HNO_3$, the profile changed drastically with clear decrease in the roughness (Fig. 3.3c).

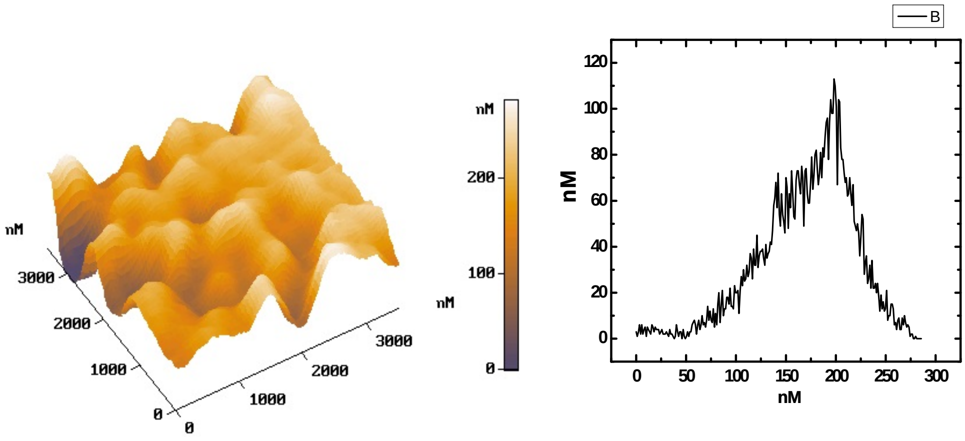

(a): Fresh PIM

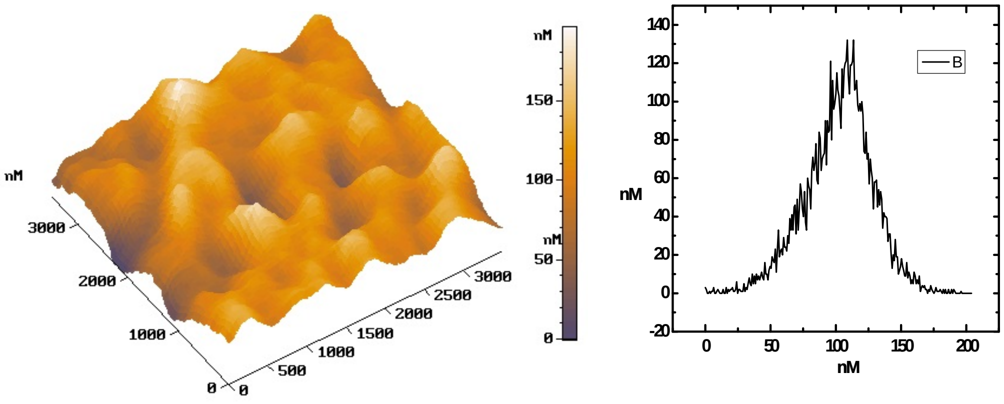

(b): 1 M $HNO_3$ treated TODGA PIM

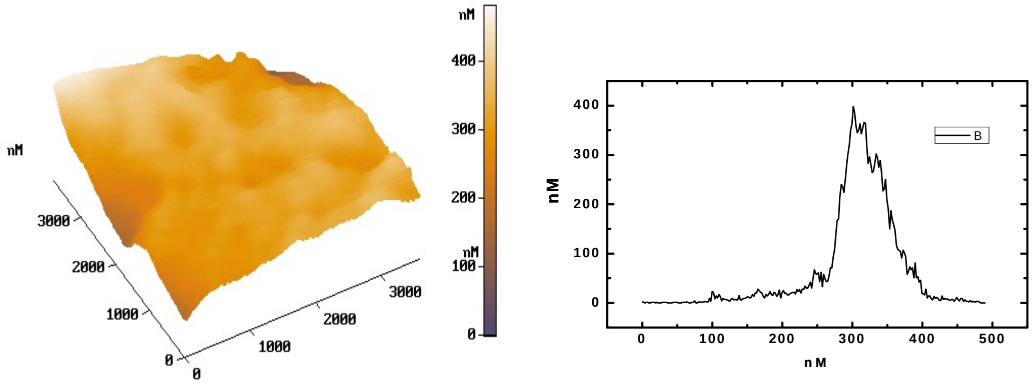

(c): Eu loaded PIM containing TODGA

Fig. 3.3. 3D atomic force micrographs along with the roughness parameters of the PIMs containing 58% TODGA, 30% NPOE, 12% CTA. (a) Fresh PIM; (b) PIM contacted with $HNO_3$; (c) Eu loaded PIM

### 3.2.4. FTIR studies

The FTIR spectra of the respective membranes, viz. CTA, NPOE+CTA and NPOE+CTA+DGA were analyzed. The comparison of the spectra of the membranes containing NPOE and CTA with that of the membrane containing only CTA indicated similarities between the two spectra at all wave lengths except at 1529 cm$^{-1}$ (corresponding to the –NO stretching) where CTA did not absorb. It indicated that CTA and NPOE were present as separate entities in the membrane and any chemical interaction was lacking. The comparison of the FTIR spectra of NPOE + CTA and NPOE + CTA + T2EHDGA showed perfect matching of the two spectra except for the band at 1651 cm$^{-1}$ which corresponded to the absorption due to the >C=O stretching (Fig. 3.4).

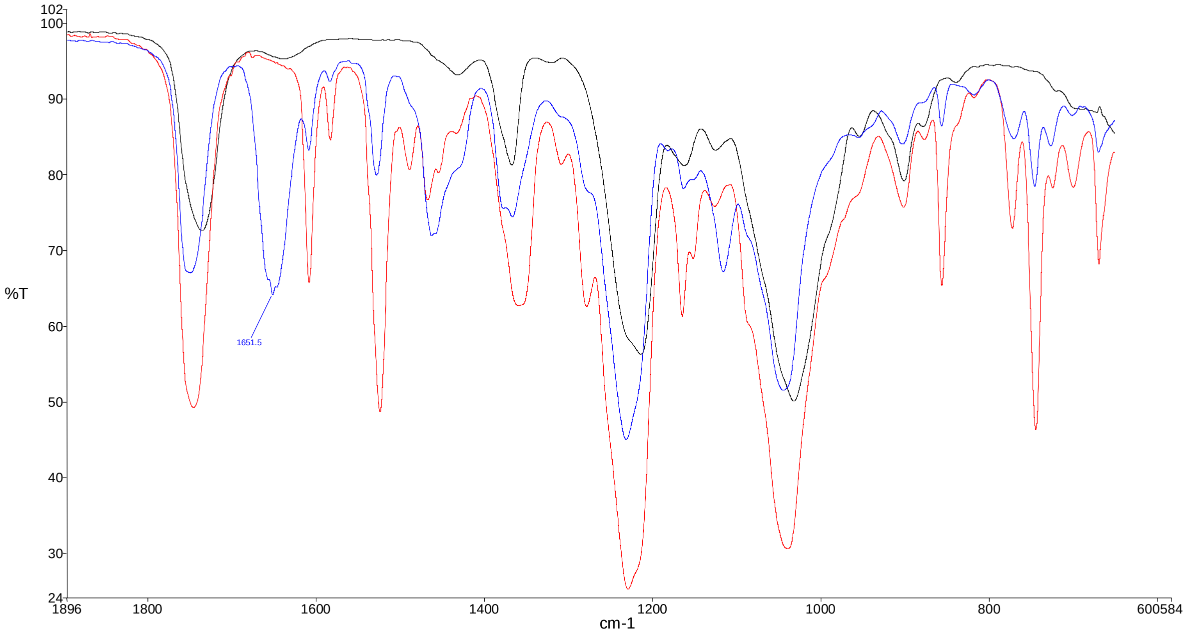

Fig. 3.4. FT-IR spectra of the PIMs. Black line: Blank CTA; Red line: PIM containing CTA + NPOE; Blue line: PIM containing CTA + NPOE + T2EHDGA

Similarly, the FTIR spectra of the respective membranes containing TPDGA (or THDGA) + NPOE + CTA also showed perfect matching of the spectra with the CTA+NPOE membrane except for the band at 1645cm$^{-1}$(or 1651cm$^{-1}$) (*Annexure-I*, Fig.A1.9). Thus, the

FTIR spectra of all the membranes indicated that all the membrane components, viz., CTA, NPOE and T2EHDGA (or TPDGA or THDGA) existed in the membrane as separate entities and no chemical interaction was operating between those.

### 3.2.5. TIMM studies

TIMM was used to elucidate the distribution of the components within the PIMs unlike SEM and AFM which provided basic information about the surfaces of the PIMs [**127**]. Fig. 3.5 presents the TIMM plots for PIMs containing CTA + NPOE and CTA + NPOE + T2EHDGA. As shown in the FT-IR spectra, it was not possible to monitor the CTA profile alone without interference from NPOE. The NPOE profile was monitored in both the PIMs at 1529 $cm^{-1}$ (where T2EHDGA also absorbs), and the results are presented in Fig. 3.5a and 3.5b. Some limited spikes are seen in Fig. 3.5b, suggesting reasonably homogeneous distribution of the plasticizer. On the other hand, the T2EHDGA distribution profile was obtained by monitoring the 1651 $cm^{-1}$ band where there was no interference from NPOE. As shown in Fig. 3.5c, the distribution of T2EHDGA was found to be homogeneous. This suggested that there should not be any “percolation threshold” in the composition of the PIM used and “carrier diffusion” type mechanism for the metal ion transport should be operative. The TIMM studies with TPDGA and THDGA based PIMs indicated similar reasonably homogeneous distribution for NPOE while the distribution profile of TPDGA and THDGA was found to be homogeneous (*Annexure-I*, Fig.A1.12-A1.15). TIMM studies were also carried out with the PIMs kept in 1 M $HNO_3$ for 24 h and the results showed no significant change suggesting no leaching out of the carrier or the plasticizer from the PIMs (*Annexure-I*, Fig.A1.16-A1.17). The TDDGA based PIMs appeared inhomogeneous with subsequent evidence of extractant leaching out of the PIM and hence, not used for TIMM measurements.

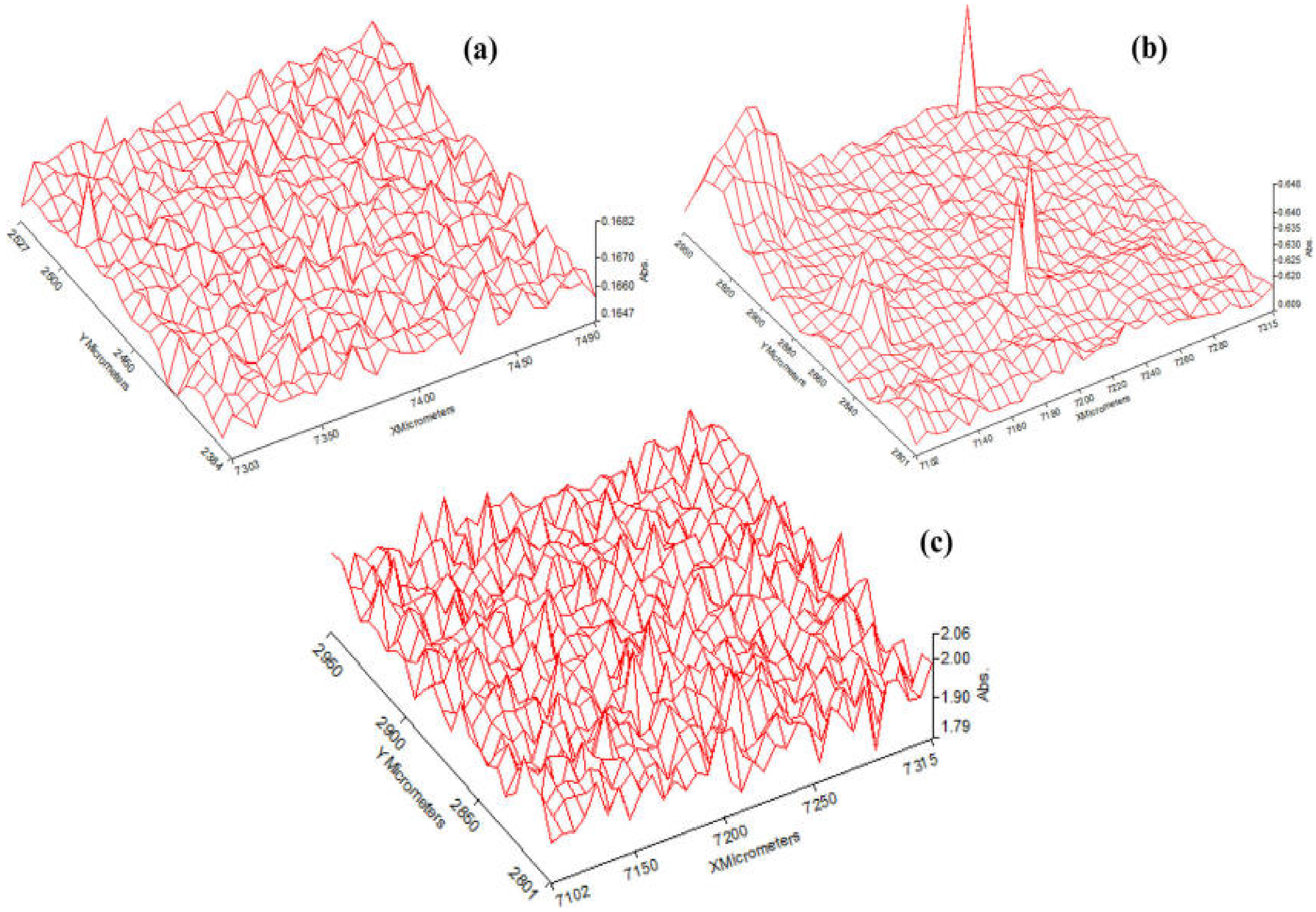

Fig. 3.5. TIMM plots of T2EHDGA-containing PIMs. Mapping done at 1529 cm$^{-1}$ for PIMs containing (a) CTA + NPOE and (b) CTA + NPOE+ T2EHDGA and that done at 1651 cm$^{-1}$ using (c) CTA + NPOE + T2EHDGA membrane.

## 3.3. UPTAKE STUDIES

The uptake studies were carried out using a small piece of the PIM (usually 4 cm$^2$) containing the diglycolamide extractants from a feed solution containing 1 M $HNO_3$ spiked with the respective actinide ion. The percentage of metal ion uptake by the PIM at a given time ‘t’ was determined by the following equation.

$$\%\,\mathbf{Uptake} = \frac{C_0 - C_t}{C_0} x100 \qquad (3.1)$$

where $C_0$ and $C_t$ are the metal ion concentrations in the aqueous phase at the beginning of the experiment and at time t, respectively. The uptake studies were carried out in duplicate at ambient temperature (ca. 24 °C); the errors in the uptake data were limited to <5%. Uptake studies included optimization of the composition of the PIMs, feed composition variation, reusability study, sorption isotherm and kinetics studies and comparative uptake behavior of different actinides.

### 3.3.1. Optimization of the composition of the PIM

Optimization of the composition of the PIM was carried out from a series of uptake studies involving Am(III) tracer where a 4 $cm^2$ PIM was stirred in a vial containing 20 mL solution of 1 M $HNO_3$ spiked with $^{241}Am$ tracer. These studies included the uptake of Am(III) by PIMs made with varying concentrations of the carrier extractant (different DGAs), NPOE or CTA keeping the other two constant. These studies indicated that the optimum composition of TODGA containing PIM was 58% TODGA, 30% NPOE and 12% CTA which corresponded to 400 mg TODGA, 210 mg NPOE and 80 mg CTA used to prepare the PIM. A similar study with T2EHDGA containing PIM revealed an optimum composition of 68.4% T2EHDGA, 17.9% NPOE and 13.7% CTA which corresponded to 400 mg T2EHDGA, 105 mg NPOE and 80 mg CTA in the PIM. A general trend, as seen from Fig. 3.6 (or Fig. 3.7), was that the uptake efficiency for Am(III) ion increased with increasing the carrier extractant (TODGA or T2EHDGA) content in the PIM. The extraction mechanism for the trivalent and tetravalent actinide ions is generally given as [**123**]:

$$M_{aq}^{n+} + mDGA_{org} + nNO_{3,aq}^{-} \backslash{==}\backslash \quad M(NO_3)_n \bullet mDGA_{org} \tag{3.2}$$

where, the subscripts ‘aq’ and ‘org’ refer to the species in the aqueous and the membrane phases, respectively.

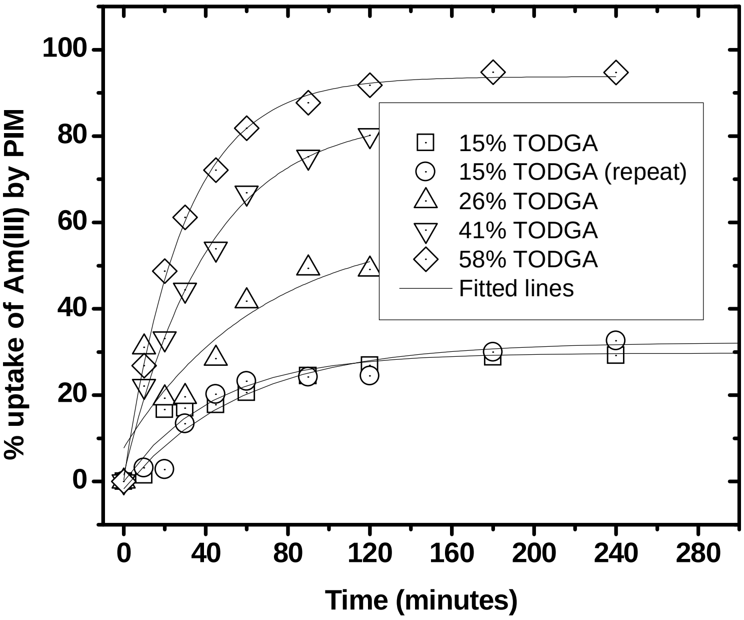

Fig. 3.6. Effect of TODGA content in the PIMs on Am(III) uptake keeping other parameters such as CTA (80 mg) and NPOE (210 mg) content fixed. Feed: 1 M $HNO_3$

Though a sharp increase in the uptake of Am(III) ion was noted at the initial stages of the uptake profile, a plateau was seen beyond 3 h. Similar plateau like behavior has been reported in several membrane transport studies as well [**128**].

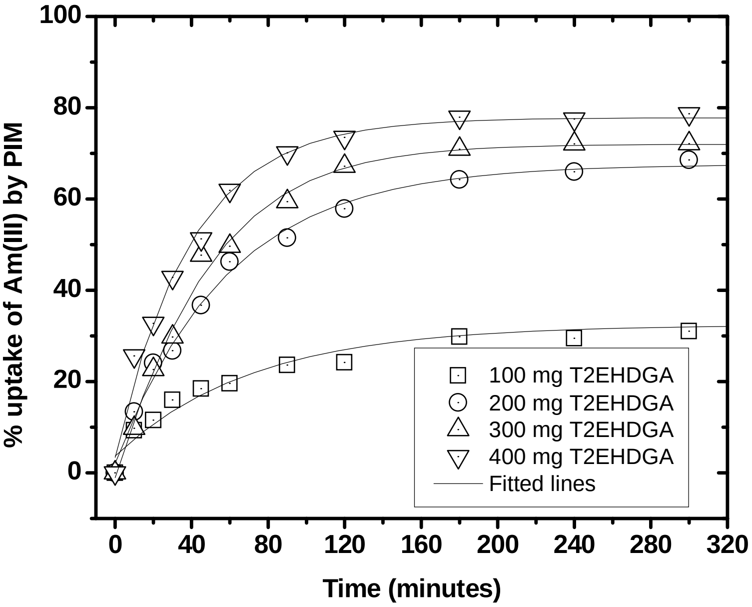

Fig. 3.7. Effect of T2EHDGA content in the PIMs on Am(III) uptake keeping other parameters such as CTA (80 mg) and NPOE (105 mg) content fixed. Feed: 1 M $HNO_3$.

From Fig. 3.6 and Fig. 3.7, it can also be seen that there is a tendency to deviate from the steep rise at lower ligand concentrations to a much less steep increase in the metal ion uptake at higher ligand content in the PIM which may be attributed to factors such as molecular aggregation in diglycolamides [**129**]. Any further increase in the TODGA (or T2EHDGA) content in the PIM reduces its mechanical strength and thus, was difficult to handle for the uptake studies. Lower TODGA (or T2EHDGA) containing PIMs than those used in the uptake studies (with the optimized composition) were not studied in view of the well known 'percolation threshold' [**44**] prevalent in case of polymer inclusion membranes which may restrict metal ion diffusion into the bulk of the membrane due to the prevention of the 'site jumping' mechanism [**130**]. The details of the optimization studies which include the effect of NPOE and CTA variation on Am(III) uptake by the PIMs containing various DGAs are described in the *Annexure-II* (Fig.A2.1-A2.5, Table A2.1). It was of interest to see the performance of other diglycolamides (TPDGA, THDGA and TDDGA) substituted PIMs under similar compositions. Therefore, PIMs containing 400 mg of the DGA ligand (TPDGA, THDGA, TDDGA with *n*-pentyl, *n*-hexyl and *n*-decyl groups as the alkyl substituents, respectively), 100 μL NPOE and 80 mg CTA were employed for the subsequent studies and the results were compared with those obtained with the TODGA and T2EHDGA containing PIMs.

### 3.3.2. Effect of feed composition on the uptake of metal ions by the PIM

In view of the fact that most of the radioactive wastes containing Am are acidic in nature, it was thought of interest to investigate the role of feed acidity on metal ion extraction. From Eq. (3.2), it is clear that with increasing feed nitric acid concentration, the metal ion complexation tendency with DGA increases due to higher availability of the nitrate ions which in turn is expected to increase the metal ion extraction. On the other hand, increase in nitric acid concentration can decrease the availability of free DGA due to the formation of DGA.$HNO_3$ adduct as per the following equilibrium:

$$DGA + H^{+}_{aq} + NO^{-}_{3(aq)} \overset{K_H}{\Leftrightarrow} DGA \cdot HNO_{3,org} \tag{3.3}$$

Thus, the availability of the free DGA depends on the basicity (quantified in terms of log $K_H$) of the diglycolamide extractant which usually depends on the alkyl chain length. Therefore, a linear increase in the metal ion extraction with increasing feed nitric acid concentration is not expected for a given extractant. The effect of $HNO_3$ concentration variation on the uptake of actinide ions by TODGA and T2EHDGA containing PIMs are shown in Table 3.1 and Table 3.2, respectively.

Table 3.1. Uptake of actinide ions by TODGA containing PIM at varying concentrations of $HNO_3$. Composition of PIM: 58% TODGA, 30% NPOE, 12% CTA.

| [$HNO_3$], M | % Uptake[a,b] | | | |
|---|---|---|---|---|
| | Am(III) | Pu(IV) | U(VI) | Th(IV) |
| 0.5 | 82.3 | 88.2 | 9.3 | 48.9 |
| 1.0 | 91.6 | 95.4 | 7.4 | 57.7 |
| 2.0 | 95.4 | 92.9 | 19.4 | 58.8 |
| 3.0 | 89.2 | 89.7 | 17.7 | 53.1 |

*Note:* [a]*2 h data;* [b]*Using 4 cm*$^2$ *PIM pieces with average wt.: 34 ± 1 mg;*

As it can be seen from Table 3.1, the uptake increased with increasing feed nitric acid concentration, for all the actinide ions, up to 2 M $HNO_3$ beyond which a slight decrease was seen at 3 M and also the uptake trend was: Am(III) > Pu(IV) > Th(IV) > U(VI). On the other hand, as indicated in Table 3.2, for the T2EHDGA containing PIM, the uptake increased with increasing feed nitric acid concentration, for all the actinide ions, up to 3 M $HNO_3$ and the uptake trend was Pu(IV) > Am(III) > Th(IV) > U(VI). This suggested that while the reverse micellar mechanism of extraction with a preference for the extraction of Am(III) over Pu(IV) is prevalent in TODGA based PIMs, it may be operative to a lesser extent in the branched diglycolamide, T2EHDGA, especially in the PIM matrix where NPOE, a relatively polar diluent, was used as the solvent medium.

Table 3.2. Uptake of actinide ions by T2EHDGA based PIMs at varying concentrations of nitric acid in the feed. Composition of PIM: 68.4% T2EHDGA, 17.9% NPOE and 13.7% CTA.

| [$HNO_3$], M | % Uptake (2h)[a] | | | |
|---|---|---|---|---|
| | Am(III) | Pu(IV) | U(VI) | Th(IV) |
| 0.5 | 44.7 | 56.7 (74.7)[b] | 4.9 (8.3)[b] | 8.7 |
| 1.0 | 73.8 | 72.2 (94.4)[b] | 4.8 (6.8)[b] | 60.4 |
| 2.0 | 77.8 (94.5)[b] | 97.2 (99.0)[b] | 8.4 (10.7)[b] | 73.7 (92.5)[b] |
| 3.0 | 84.4 | 95.0 (97.8)[b] | 27.9 (62.6)[b] | 74.5 |

*Note: [a]Using 4 $cm^2$ PIMs with average wt.:34 ± 1 mg; [b]Values in brackets indicate the respective metal ion uptakes after 24 h.*

Though increasing the $HNO_3$ concentration increased Am(III) uptake significantly and near quantitative recovery was possible, there was a detrimental effect on the PIM integrity due to the hydrolysis of CTA [**31**]. In view of this, a mixture of $NaNO_3$ and $HNO_3$ was used while maintaining the nitrate ion concentration at 3 M and the results are plotted in Fig. 3.8 and 3.9 for the PIMs containing TODGA and T2EHDGA, respectively. As seen from Fig. 3.8, the highest uptake efficiency was seen for a feed containing 2 M $NaNO_3$+ 1 M $HNO_3$. While comparable uptake efficiencies were recorded for 1 M $HNO_3$ and 1 M $NaNO_3$ + 2 M $HNO_3$, the feed containing 3 M $NaNO_3$+ 0.01 M $HNO_3$ (to prevent hydrolysis of the metal ions) was the least effective. Apparently, the presence of $Na^+$ ion is not helping in the metal ion extraction which could be due to dehydrating nature of the former is not facilitating the reverse micelle formation [**131**].

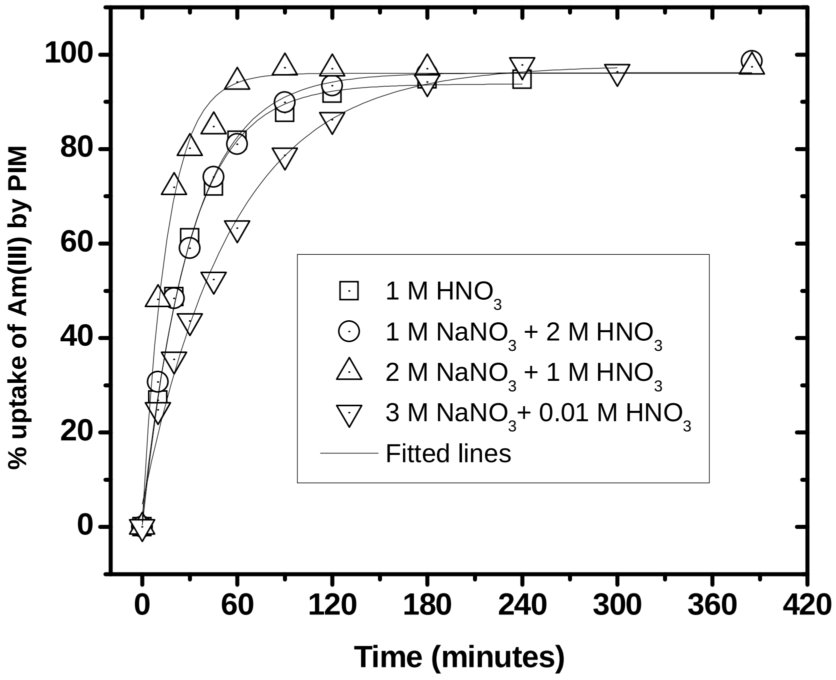

Fig. 3.8. Uptake of Am(III) from feeds containing varying fractions of $HNO_3$ and $NaNO_3$. Membrane composition: 58% TODGA, 30% NPOE and 12% CTA

On the other hand, for the T2EHDGA containing PIM (Fig. 3.9), the % Am(III) uptake data after 1 h of equilibration showed the trend: 1 M $NaNO_3$ + 2 M $HNO_3$ > 2 M $NaNO_3$ + 1 M $HNO_3$ > 3 M $HNO_3$ > 3 M $NaNO_3$ + 0.01 M $HNO_3$ and the trend changed somewhat after 5 h where, though 1 M $NaNO_3$ + 2 M $HNO_3$ was still the most suitable feed, the least metal ion uptake was seen with 2 M $NaNO_3$ + 1 M $HNO_3$ as the feed.

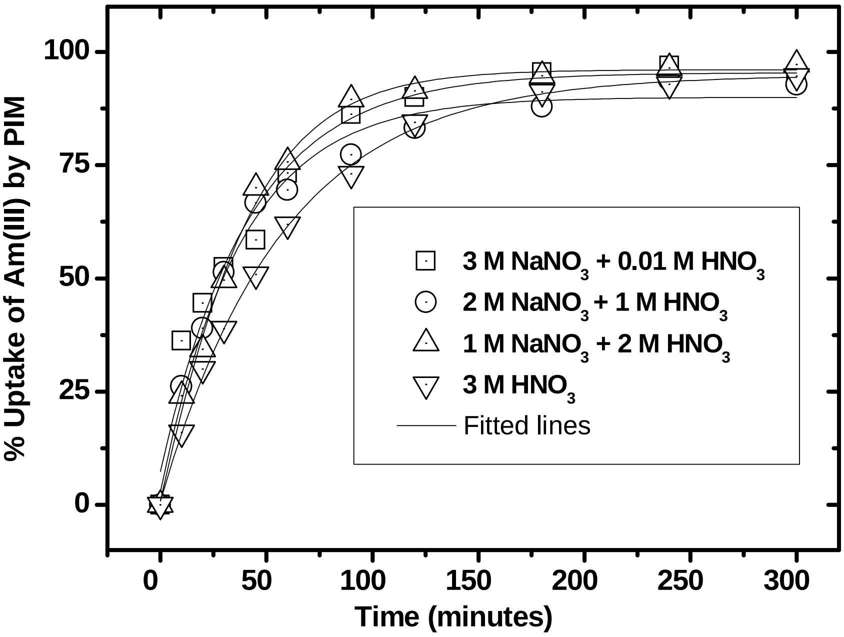

Fig. 3.9. Uptake of Am(III) from feeds containing varying fractions of $HNO_3$ and $NaNO_3$. Membrane composition: 68.4% T2EHDGA, 17.9% NPOE and 13.7% CTA.

### 3.3.3. Comparative evaluation of the uptake data for various actinide ions by PIMs containing different DGAs

The uptake data of various actinide ions, viz. Am(III), Pu(IV), Th(IV) and U(VI) from 1 M $HNO_3$ as the feed solution by different PIMs containing TODGA, T2EHDGA, TPDGA, THDGA and TDDGA are given in Table 3.3. A common feature found amongst all the PIMs was that U(VI) was poorly extracted and its uptake trend by the PIMs at 1 M $HNO_3$ can be given as: TPDGA > THDGA ~ TODGA > TDDGA > T2EHDGA. On the other hand, Am(III) uptake trend may be given as: TODGA > TPDGA ~ THDGA > TDDGA > T2EHDGA. It may be noted that the TODGA containing PIMs contained lower fraction of the extractant (58%) and much higher uptake may be expected at the weight fraction used for the rest of the DGA ligands. The poor uptake of U(VI) by all the PIMs may be attributed to steric constraints associated with the uranyl ion while accommodating the ligands for coordination along the equatorial plane. The steric factors were also clearly visible as the

DGA ligands with longer alkyl chain showing lower uptake (Table 3.3**)**. Also, lower uptake in case of the branched DGA ligand, T2EHDGA may be attributed to stereochemical factors due to the lower possibility to form reverse micelles.

Table 3.3. Uptake of various actinide ions by substituted DGA based PIMs of the composition, 68.4% Carrier + 17.9% NPOE + 13.7% CTA; Feed solution: 1 M $HNO_3$; (20 mL)

| Metal ion | % Uptake (2 h)[a,b] | | | | |
|---|---|---|---|---|---|
| | TPDGA[c] | THDGA[c] | TODGA[d] | T2EHDGA[c] | TDDGA[c] |
| U(VI) | 19.3 (25.5) | 15.8 (19.2) | 15.3 | 8.6 (42.9) | 9.8 (12.6) |
| Pu(IV) | 86.9 (94.8) | 80.6 (94.1) | 87.1 | 83.6 (96.9) | 45.7 (48.1) |
| Th(IV) | 88.3 (95.9) | 92.3 (96.5) | 60.6 | 38.8 (86.5) | 37.1 |
| Am(III) | 90.3 (97.5) | 90.4 (97.9) | 93.8 | 63.8 (97.9) | 85.3 (90.4) |

*[a]Values inside brackets indicate respective metal ion uptake at 24 h; [b] PIM weight: 34±1 mg, 4 $cm^2$ PIM piece; [c]PIM composition: 68.4% carrier + 17.9% NPOE + 13.7% CTA; [d]PIM composition: 58% TODGA + 30% NPOE + 12% CTA*

The uptake results with other actinides showed a near quantitative uptake (~90% after 2 h) with the TPDGA and THDGA based PIMs while with the TDDGA based PIM the uptake of Pu(IV) and Th(IV) was comparatively less. The uptake efficiency for Am(III) followed the trend: TPDGA ~ THDGA > TDDGA at 1 M $HNO_3$ (Table 3.3 and *Annexure-II*, Fig.A2.6). Similarly, the uptake efficiency for Pu(IV) and Th(IV) at 1 M $HNO_3$ followed the trend: TPDGA >THDGA > TDDGA and TPDGA ~THDGA > TDDGA, respectively (Table 3.3 and *Annexure-II*, Fig.A2.6). This indicated that the extraction of a given actinide does not differ much when *n*-pentyl and *n*-hexyl group present at the acyl nitrogen atom of the DGA carrier while the presence of *n*-decyl group significantly decreases the extraction of actinide.

Though a previously reported solvent extraction study using several substituted diglycolamides for the extraction of Am(III) from 1 M nitric acid medium showed $D_{Am}$ followed the trend: TPDGA > THDGA > TDDGA in the presence of 30% *iso*-decanol as the phase modifier [**132**], the low uptake in the present study can also be attributed to the leaching out of TDDGA from the PIMs as seen from the floating oily organic matter after equilibrating for about 2 h. As shown in Table 3.3, the uptake efficiency of the actinides by TPDGA and THDGA based PIMs followed the trends, Am(III) ~ Pu(IV) ~ Th(IV) > U(VI) and Am(III) ~ Th(IV) > Pu(IV) > U(VI), respectively whereas the TDDGA based PIM followed the trend: Am(III) > Pu(IV) > Th(IV) > U(VI). On the other hand, studies with the PIMs containing TODGA and T2EHDGA had indicated the uptake trend as: Am(III) > Pu(IV) > Th(IV) > U(VI) and Pu(IV) > Am(III) > Th(IV) > U(VI), respectively (Table 3.3).

### 3.3.4. Sorption isotherm and kinetic modeling studies with T2EHDGA containing PIM

Kinetic modeling studies were required to be investigated for PIMs containing the DGA ligands, and T2EHDGA based PIMs were chosen in view of the unique properties of the ligand. The batch uptake studies were carried out using a reported procedure [**133, 134**] in which a known weight (37 ± 1 mg) of the T2EHDGA containing PIM of a known surface area was cut into small pieces and equilibrated with a 1.0 M $HNO_3$ solution (25 mL) containing Eu carrier (taken as a surrogate of Am), taken in a stoppered conical flask and spiked with $^{152}$Eu tracer (for convenient assaying by radiometry) for over 4 days using the magnetic stirrer (*vide supra*). Four different concentrations of Eu were used, viz., 25, 50, 75, and 100 mg/L. Samples were intermittently removed from the conical flask and assayed radiometrically. The percentage metal ion uptake by the PIM at a given time t was determined by the equation (3.1). The uptake data are presented in Table 3.4. The time required to obtain the equilibrium uptake data was about 16 h (Fig. 3.10). The data treatment was done using different kinetic and isotherm model equations as reported in the literature [**133, 134**].

Table 3.4. Uptake of Eu(III) feed solution (spiked with $^{152}$Eu Tracer) in 1 M $HNO_3$ by PIMs of the composition 69% T2EHDGA, 17% NPOE, and 14% CTA; Size of the PIMs: 2 cm x 2 cm; Average weight of the PIMs: 37 mg

| Eu concentration in feed (1 M $HNO_3$) | % uptake of Eu(III) after 2 h (24 h) |
|---|---|
| 100 mg/L | 24.4±0.1 (43.3±0.3) |
| 75 mg/L | 23.0±0.1 (41.2±0.2) |
| 50 mg/L | 35.5±0.1 (52.5±0.1) |
| 25 mg/L | 43.1±0.2 (60.1±0.3) |

### 3.3.4.1. Kinetic modeling of the Eu uptake data

It was intended to model the kinetics of the metal ion uptake data by the T2EHDGA-containing PIMs. Three different kinetic models, viz., the Lagergren’s pseudo-first-order, the Ho’s pseudo-second-order (under the assumption that the chemical sorption is the rate limiting step of the sorption processes), and the Elovich models (under the assumption that the sorption of the metal ion occurs by some sort of chemical reaction) were evaluated for the metal ion uptake (for linear equations representing the kinetic models, Table 3.5) and the results are presented in Figure 3.10.

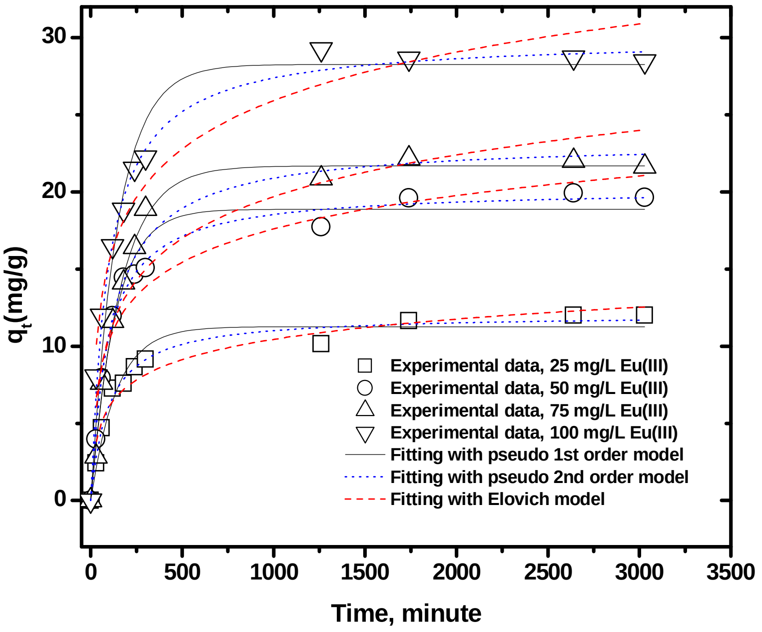

Fig. 3.10. Fitting of the Eu(III) uptake data to the pseudo-first-order, pseudo-second-order, and Elovich models. The PIMs contain 69% T2EHDGA, 17% NPOE, and 14% CTA. Feed acidity: 1 M $HNO_3$.

Table 3.5. Linearized forms of the three different kinetic models [a]

| kinetic model | linearized form | plot | parameters |
|---|---|---|---|
| pseudo-first order | $\ln(q_e-q_t)=\ln q_e-k_1t$ | $\ln(q_e-q_t)$ versus t | slope=$k_1$ |
| pseudo-second order | $t/q_t = 1/(k_2q_e^2) + t/q_e$ | $t/q_t$ versus t | slope=1/ $q_e$ |
| Elovich | $q_t=(\ln(\alpha\beta))/\beta +(\ln t)/\beta$ | $q_t$ versus ln t | slope=1/β;<br>intercept=(ln(αβ))/β |

[a] *$q_e$ and $q_t$ are the concentration of Eu(III) sorbed per gram of the T2EHDGA-containing PIM at equilibrium and at time t, respectively; $k_1$, pseudo-first-order rate constant; $k_2$, pseudo-second-order rate constant; α, initial absorption rate; β, desorption constant*

The linear fits shown in Fig. 3.11 suggested that out of the three kinetic models, the pseudo-second-order kinetic model (Figure 3.11b) fits perfectly as compared to the pseudo-first-order (Figure 3.11a) as well as the Elovich model (Figure 3.11c). This kinetic model suggests that chemisorption is the rate-limiting step. The parameters are calculated and are listed in Table 3.6, which suggested that the equilibrium uptake capacity ($q_e$) values obtained from the linear plots of the pseudo-second-order kinetic model (Fig. 3.11b) are very close to the experimentally obtained saturation uptake capacity of the PIMs. Also, the $R^2$ values for the least squares lines of the pseudo-second-order kinetic model are close to unity (Table 3.6). On the other hand, the pseudo-first order kinetic model (Fig. 3.11a) does not show linear behavior, and a clear curved nature of the data points is seen. Therefore, the $q_e$ values obtained from the pseudo-first-order kinetic model (Table 3.6) do not match at all with the experimentally obtained $q_{exp}$ values shown in the table, and the $R^2$ values for the least-squares lines deviate from unity. Finally, when the data points are fitted to the linearized form of the Elovich equation (Table 3.5), straight line plots are obtained with slight deviations at the higher ln t values (Fig. 3.11c), which corroborates the chemisorption model concluded from the pseudo-second order kinetic model [**135**]. Similar deviations were also observed by Gherasim et al. [**133**] in their studies involving Pb(II) sorption onto PIMs containing 50% D2EHPA and 50% PVC.

Table 3.6. Kinetic parameters for the sorption of Eu(III) on to T2EHDGA based PIM of the composition, 69% T2EHDGA, 17% NPOE, and 14% CTA

| | | Pseudo-first order model | | | | Pseudo-second order model | | | | Elovich model | | | |
|---|---|---|---|---|---|---|---|---|---|---|---|---|---|
| Eu (mg/L) | $q_{e,exp}$ (mg/g) | $q_1$ (µg/mg) | $k_1$x $10^3$ ($min^{-1}$) | $R^2$ | $\chi^2$ | $q_1$ (µg/mg) | $k_2$x$10^3$ (mg/µg min) | $R^2$ | $\chi^2$ | α (µg/mg min) | β (mg/µg) | $R^2$ | $\chi^2$ |
| 25 | 12.01 | 8.84 | 2.24 | 0.920 | 53.9 | 12.38 | 0.677 | 0.997 | 0.417 | 0.469 | 0.528 | 0.929 | 0.975 |
| 50 | 19.64 | 14.46 | 3.09 | 0.942 | 32.5 | 20.41 | 0.480 | 0.999 | 0.447 | 0.876 | 0.320 | 0.908 | 2.083 |
| 75 | 21.65 | 14.35 | 2.76 | 0.973 | 86.2 | 22.86 | 0.377 | 0.998 | 1.199 | 0.606 | 0.256 | 0.886 | 3.638 |
| 100 | 28.48 | 18.31 | 2.81 | 0.992 | 157 | 29.63 | 0.402 | 0.999 | 0.292 | 1.386 | 0.221 | 0.941 | 1.376 |

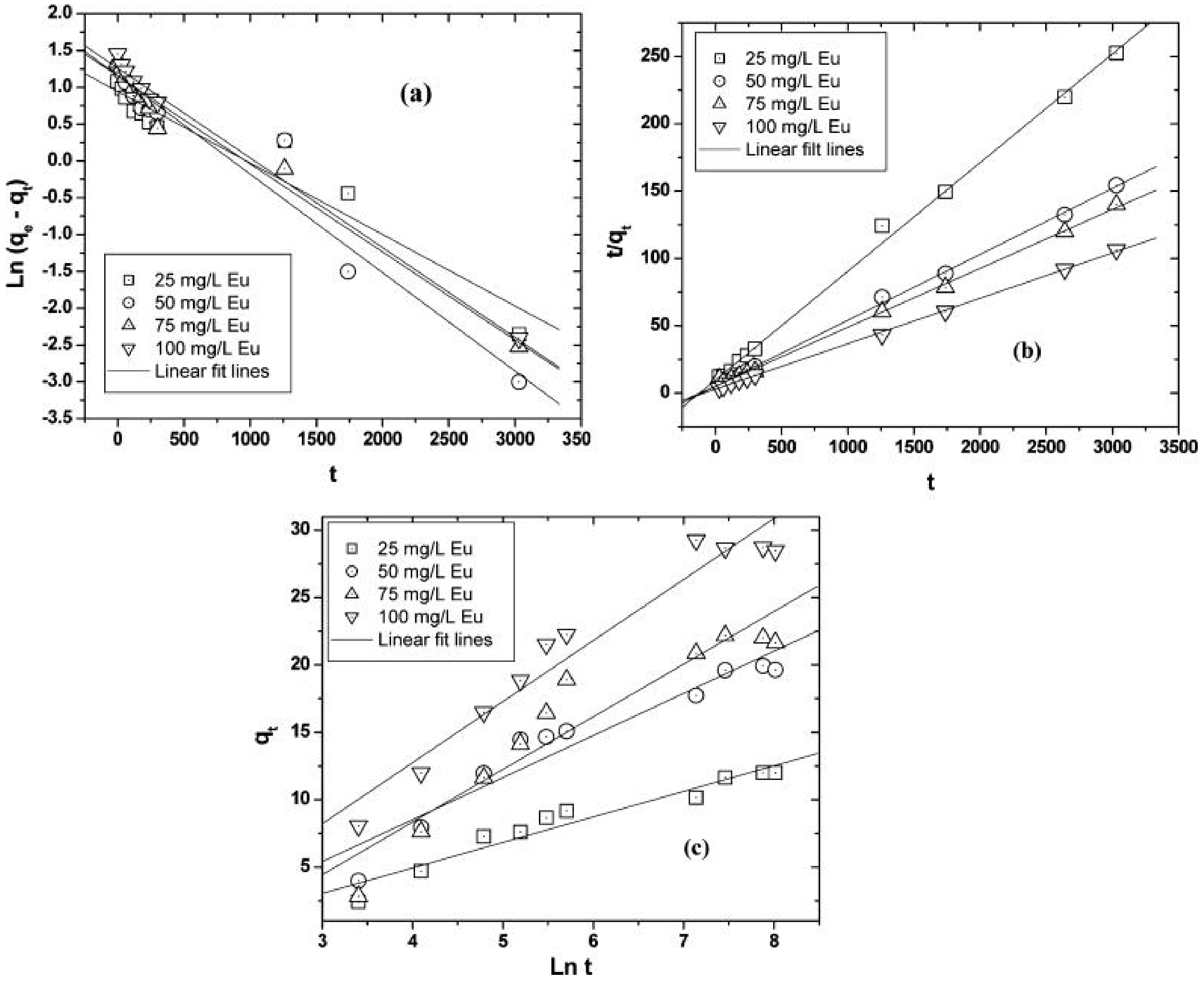

Fig. 3.11. Kinetic model fitting of the linearized equations for the sorption of Eu(III) on PIM: (a) pseudo-first-order model, (b) pseudo-second-order model, (c) Elovich model. PIM composition: 69% T2EHDGA, 17% NPOE, and 14% CTA PIM. Feed acidity: 1 M $HNO_3$.

The rate parameters, α (initial adsorption rate) and β (desorption constant, related to the activation energy of chemisorption) were obtained from the linear plots and are also listed in Table 3.6.

The compliance of the Eu(III) sorption data with the pseudo-second-order and the Elovich model suggested the rapid chemisorption process at the feed-PIM interface per the following equation

$$Eu^{3+}_{(aq)} + 3T2EHDGA_{(M)} + 3NO^{-}_{3(aq)} \leftrightarrow Eu(NO_3)_3.3T2EHDGA_{(M)} \tag{3.4}$$

where the species with the subscripts “(aq)” and “(M)” represent those in the aqueous and the PIM phases, respectively. This equation represents the fast sorption of the metal ion in the initial stages (Fig. 3.10). The fast chemisorption is followed by a slow diffusion reaction in which the uncomplexed carrier ligands are diffused out from the bulk to the periphery of the PIM while at the same time the $Eu^{3+}$-T2EHDGA complex is diffused from the periphery into the bulk of the PIM. Subsequent uptake of the metal ions and loading of the PIM with Eu(III) ions is a slow process which is reflected in the slow increase in the Eu(III) uptake leading to the plateau (Fig. 3.10).

### 3.3.4.2. Eu sorption isotherm modeling

The uptake data were also fitted to different sorption isotherms, viz., Langmuir, Freundlich, and Dubinin−Radushkevich (D-R) isotherm models and the fitting results are shown in Fig. 3.12. The fittings were reasonably good with the Langmuir (Fig. 3.12a) and the Freundlich (Fig. 3.12b) models, whereas the D-R model (Fig. 3.12c) did not yield satisfactory fit. The parameters obtained from the different isotherm models are listed in Table 3.7.

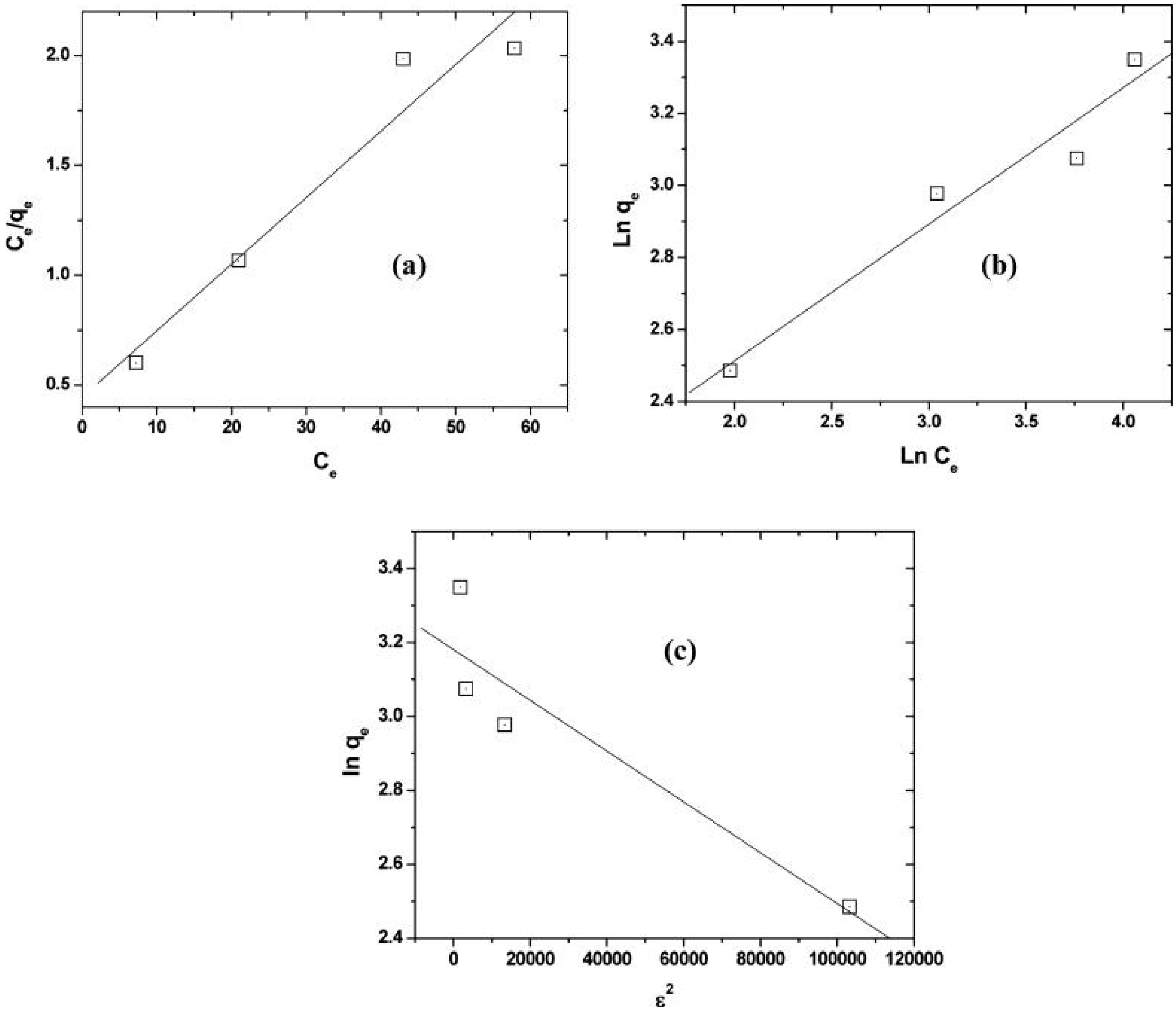

Fig. 3.12. Sorption isotherm fittings using linearized equations: (a) Langmuir, (b) Freundlich, and (c) Dubinin−Radushkevich isotherms. PIM composition: 69% T2EHDGA, 17% NPOE, and 14% CTA PIM. Feed acidity: 1 M $HNO_3$.

The Langmuir isotherm is given by the following equation:

$$\frac{1}{q_e} = \frac{1}{q_m} + \frac{1}{q_m.K_L.C_e} \tag{3.5}$$

where $K_L$ is the Langmuir constant (L/mg) and $C_e$ is the equilibrium concentration of the metal ion (mg/L) while $q_e$ and $q_m$ are the equilibrium and maximum uptake capacities (both in mg/g), respectively. The Langmiur constant ($K_L$) was between 0 and 1, suggesting a favorable sorption by the monolayer [**136**].

Table 3.7. Sorption isotherm constant for the uptake of Eu(III) on to PIM of the composition 69% T2EHDGA, 17% NPOE, and 14% CTA PIM

| Model | Linearized form | Model constant | Parameters | Statistical analysis | |
|---|---|---|---|---|---|
| | | | | $R^2$ | $\chi^2$ |
| Langmuir[a] | $\frac{C_e}{q_t} = \frac{[1]}{bq_{max}} + \frac{C_e}{q_{max}}$ | $q_m$ = 33.014 mg/g | $K_L$=0.068 L/mg | 0.911 | 0.646 |
| Freundlich[b] | $\log q_e = \log K_f + \frac{1}{n}\log C_e$ | $K_f$ = 5.777 L/mg | N = 0.379 | 0.925 | 0.429 |
| D-R[c] | $\log q_t = \log X_m - \beta\varepsilon^2$ | $q_D = 6.56 \times 10^{-4}$ mol/g | $B_D = 3.42 \times 10^{-9}$ $mol^2/J^2$; E = 12.10 kJ/mol | 0.927 | - |

*[a]Langmuir: slope = 0.0303 ± 0.0054; intercept = 0.444 ± 0.203. [b]Freundlich: slope = 0.379 ± 0.061; intercept = 1.754 ± 0.203. [c]D-R: slope = −6.86 × $10^{-6}$; intercept = 3.18 ± 0.09*

The Freundlich isotherm is given by the following equation

$$\log q_e = \log K_f + \frac{1}{n}\log C_e \tag{3.6}$$

and the slope of the straight line plot (Fig. 3.12b) gives the constant 1/n, which is a function of the strength of adsorption in the adsorption process while the intercept gives the constant $K_f$, which is an approximate indicator of the adsorption capacity of the PIM. It is well known that if n = 1, then the partition between the two phases is independent of the concentration of the metal ion and that 1/n < 1 indicates a normal adsorption. As the value of 1/n was found to be 0.379 ± 0.061 (Table 3.7), a normal adsorption process is expected. In view of the nonlinear nature of the D-R isotherm plot (Figure 3.12c), the results are not discussed any further.

### 3.3.5. Stripping studies and reusability of the PIM

Stripping of the metal ions from the PIMs is required for the recovery of the metal ion for subsequent use. Also, long term applicability depends on the successful reusability of the PIMs as sorbents for the target metal ions. Stripping and reusability studies were carried out with the PIMs containing TODGA and T2EHDGA. The TODGA containing PIMs showed a reasonable back extraction of the actinide ion with the trend: Th(IV) > Pu(IV) > Am(III) > U(VI) while using 1 M α-HIBA as the stripping agent (Table 3.8).

Table 3.8. Uptake and stripping data with TODGA containing PIM of the composition, 58% TODGA + 30% NPOE + 12% CTA; Feed: 1 M $HNO_3$, strippant: 1 M α-HIBA.

| Metal ion | % Uptake of metal ion (2 h) | % Stripping of metal ion (2 h) |
|---|---|---|
| Am(III) | 93.4 | 85.3 |
| Pu(IV) | 91.3 | 88.7 |
| Th(IV) | 66.0 | 92.4 |
| U(VI) | 6.3 | 74.8 |

However, when the reusability studies were carried out with the TODGA containing PIM, it indicated that the PIM resulted in 86.4% Am(III) uptake with the regenerated PIM as against 93.4% uptake with the fresh PIM. The stripping studies indicated about 85.3% back extraction in 2 h with the fresh PIMs. However, >95% stripping (in 2 h) was seen when the regenerated PIM was used which was attributed to higher Am content in the PIM arising due to the unstripped radiotracer from the previous experiment.

Similar stripping studies with T2EHDGA containing PIM suggested quantitative back extraction of Am(III) in about 60 minutes (Fig. 3.13) while using a solution containing 0.01 M EDTA at pH 3.0 as the stripping agent.

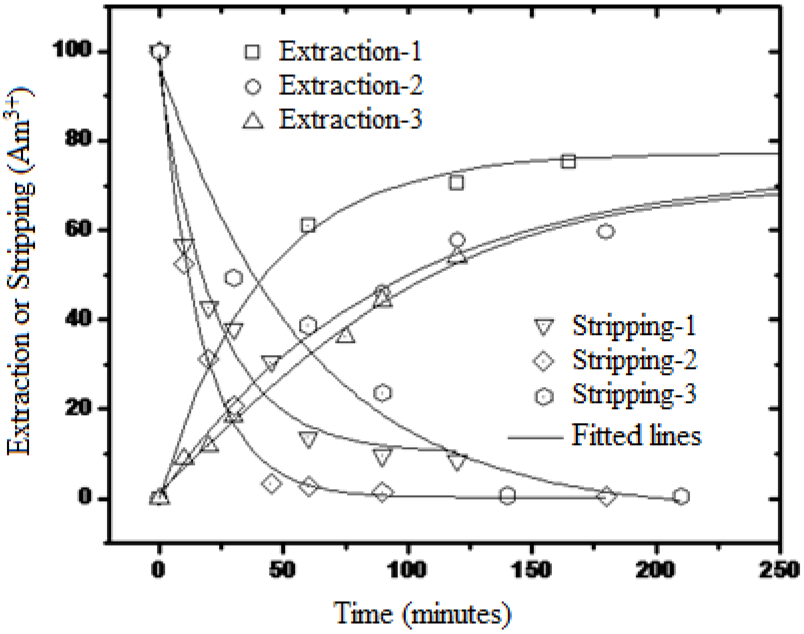

Fig. 3.13. Uptake (from 1 M $HNO_3$) and stripping (using 0.01 M EDTA at pH 3.0) data for three successive experiments. Membrane composition: 68.4% T2EHDGA, 17.9% NPOE and 13.7% CTA

However, when the retrieved PIM was used for the subsequent uptake studies, the profile was significantly lower than that obtained with pristine PIMs (Fig. 3.13). Similarly, the stripping profiles also showed a tendency of deterioration of the PIM. Three successive uptake and stripping profiles are shown in Fig. 3.13 which confirms the fact that the PIMs cannot be reused effectively. These studies suggested that the reusability possibilities of the TODGA (or T2EHDGA) containing PIM as sorbent are limited.

## 3.4. COMPARATIVE EVALUATION OF TRANSPORT DATA FOR VARIOUS ACTINIDE IONS BY PIMs CONTAINING DIFFERENT DGAs

The transport studies were carried out using a two-compartment cell with 1 M nitric acid concentration as the feed containing the target radio tracer and 1 M α-HIBA as the strippant in the receiver compartment. Similar to the uptake studies, no transport of the metal ion was noticed when the carrier extractant was not present in the PIM showing that carrier extractant was primarily responsible for the transport of the metal ions across the PIM. For the transport studies, the PIMs with the optimized composition were used and contained TODGA, T2EHDGA, TPDGA and THDGA as the carrier extractants. TDDGA containing PIMs were not used in view of leaching out of the extractant.

The transport behavior of Am(III), Pu(IV), Th(IV) and U(VI) by the PIMs containing TODGA, T2EHDGA, TPDGA and THDGA was investigated over 24 h and the data are presented in Tables 3.9 and 3.10. The overall mass transport can be summed up as a combination of 3 steps viz., (i) the uptake of the actinide ion from the source solution; (ii) the diffusion of the actinide ion-DGA complex across the PIM and (iii) the release of the actinide ion from the complex into the receiver phase. The mass transport in the case of the PIMs can take place via a mechanism involving the diffusion of the actinide ion-carrier complex or via a ‘fixed-site jumping’ mechanism [**130**]. In the former case, the mass transport does not require a “percolation threshold” of carrier concentration whereas the reverse is true for the latter. Table 3.9 contains the data for the uptake of the actinide ions by the TODGA / T2EHDGA based PIMs from the source solution as well as the data of the transport of the respective ions into the receiving solution. As it can be seen from the Table 3.9, the transport of the metal ion to the receiving solution for the T2EHDGA containing PIM followed the trend: Pu(IV) > Am(III) > Th(IV) > U(VI) while that for the TODGA containing PIM followed the trend: Am(III) > Pu(IV) > Th(IV) > U(VI) (*Annexure-II*, Fig.A2.9, A2.10). This could be explained by taking into account several factors. Firstly, the aggregation tendency of TODGA was significantly higher than that of T2EHDGA, which was attributed to the branched 2-ethylhexyl groups present in the latter. Secondly, though the aggregation has been reported in a non-polar medium [**131**], the same may be unfavorable in a polar medium such as NPOE. Finally, at higher extractant concentration, the aggregation of the diglycolamides may be possible to some extent. Therefore, while the trend of metal ion extraction, seen in the case of PIMs containing TODGA as the extractant, was the same as that reported in *n*-dodecane as the diluent in solvent extraction [**129**], an entirely different trend was seen with the PIMs containing T2EHDGA.

Table 3.9. Comparative transport data of various actinide ions by TODGA and T2EHDGA based PIMs; Feed acidity: 1 M $HNO_3$; Receiver: 1 M α-HIBA.

| Metal ion | TODGA[a] | | T2EHDGA[b] | |
|---|---|---|---|---|
| | % Uptake (2 h)[c] | %T (2 h)[c] | % Uptake (2 h)[c] | %T (2 h)[c] |
| U(VI) | 22.3 | 15.3 | 8.6 (42.9)[c] | 3.6 (32.1)[c] |
| Pu(IV) | 87.1 | 50.4 | 83.6 (96.9)[c] | 27.2 (91.7)[c] |
| Th(IV) | 60.6 | 35.2 | 38.8 (86.5)[c] | -[d] (63.2)[c] |
| Am(III) | 93.8 | 55.9 | 63.8(97.9)[c] | 14.9 (92.3)[c] |

*Note: [a]: PIM composition: 58% TODGA + 30% NPOE + 12% CTA; [b]: PIM composition: 68.4% T2EHDGA + 17.9% NPOE + 13.7% CTA; [c]Data inside parentheses indicate data at 24 h. [d]Not measurable*

On the other hand, the PIMs containing TPDGA and THDGA displayed the following actinide transport trends from the feed side to the receiver side: Pu(IV) > Am(III) > U(VI) > Th(IV) (Table 3.10 and *Annexure-II*, Fig.A2.11, A2.12). The higher transport rate of the tetra-valent actinide (Pu(IV)) than the tri-valent actinide (Am(III)) was also observed with the T2EHDGA based PIM (Table 3.9).

Table 3.10. Transport data of various actinide ions by PIM of the composition: 68.4% Carrier + 17.9% NPOE + 13.7% CTA; Feed acidity: 1 M $HNO_3$; Receiver: 1 M α-HIBA.

| Metal ion | TPDGA[a] | | | | THDGA[a] | | | | TODGA[b] | T2EHDGA[a] |
|---|---|---|---|---|---|---|---|---|---|---|
| | %T (2 h)[c] | P x $10^4$ (cm $s^{-1}$) | k x $10^4$($s^{-1}$) | $J_0$(molcm$^{-2}$s$^{-1}$) | %T (2 h)[c] | P x $10^4$ (cm $s^{-1}$) | k x $10^4$ ($s^{-1}$) | $J_0$(molcm$^{-2}$s$^{-1}$) | P x $10^4$ (cm $s^{-1}$) | P x $10^4$ (cm $s^{-1}$) |
| U(VI) | 13.4 (25.2) | 2.2±0.1[d] | -(0.54 ± 0.02) | (2.2 ± 0.1) x $10^{-12}$ | 9.2 (29.7) | 2.7 ± 0.12[d] | -(0.66 ± 0.03) | (2.7 ± 0.1) x $10^{-12}$ | 0.21 ± 0.01 | 0.63±0.04 |
| Pu(IV) | 49.2 (74.5) | 24.9±2.7 | -(6.1 ± 0.81) | (2.5 ± 0.3) x $10^{-12}$ | 35.0 (74.1) | 25.5 ± 1.2 | -(6.3 ± 0.29) | (2.6 ± 0.3) x $10^{-12}$ | 0.85 ± 0.01 | 11.44±0.80 |
| Th(IV) | 0.77 (4.2) | 3.1±1.3[d] | -(0.76 ± 0.32) | (3.1 ± 1.3) x $10^{-17}$ | 4.5 (16.2) | 4.1±1.2[d] | -(1.0 ± 0.29) | (4.1 ± 1.2) x $10^{-17}$ | 0.65 ± 0.01 | 3.46±0.09 |
| Am(III) | 39. 3 (88.6) | 16.8 ±2.1 | -(4.1 ± 0.5) | (1.7 ± 0.2) x $10^{-13}$ | 19.2 (60.8) | 20.8 ± 4.00 | -(5.1 ± 0.98) | (2.1 ± 0.4) x $10^{-13}$ | 2.11 ± 0.01 | 7.44±0.02 |

*Note: [a] PIM composition: 68.4% Carrier + 17.9% NPOE + 13.7% CTA; [b]PIM composition: 58% TODGA + 30% NPOE + 12% CTA; [c] Values in brackets indicate the respective metal ion transport at 24 h; [d]Higher P values for Th(IV) as compared to U(VI) is due to the higher uptake from the feed even though the transport trend showed an opposite trend*

As seen from Table 3.10 (and also from *Annexure-II*, Fig.A2.11b, A2.12b), the uranyl ion has lower uptake from the source side out of all the actinides but higher cumulative transport to the receiving phase than that of the Th(IV) ion. This may be due to the less number of TPDGA (or THDGA) molecules surrounding the uranyl ion as compared to a large number of ligands coordinating to the Th(IV) ion due to higher ligand to metal ratio (Th(IV) $<10^{-10}$ M) as well as higher ionic potential resulting in slower diffusion of the Th(IV)-DGA complex, in turn resulting in rather slow transport rates.

Comparison of the transport of different actinide ions amongst the PIMs containing T2EHDGA, TPDGA and THDGA indicated that though Pu(IV) showed the highest transport rates, the slower transport rate observed for Th(IV) (another tetravalent ion) could be attributed to very low concentration of the metal ion ($<10^{-10}$ M) resulting in higher ligand to metal ratio. The difference in the % uptake from the feed compartment and that transported into the receiver compartment was accounted for as the metal ion trapped in the PIM (confirmed by gamma counting of the PIMs). As can be seen from Tables 3.9 and 3.10, considerable amount of the actinide ions were found to be trapped within the PIMs containing TODGA, T2EHDGA, TPDGA and THDGA as the carrier extractant (2 h data). As for example the amount of Am(III) was found to be trapped inside TODGA containing PIM was 37.9% while that for T2EHDGA containing PIM was found to be 48.9% at 2 h of transport (Table 3.9). This was because of the slow transport rates due to the higher viscous nature of the PIMs.

### 3.4.1. Calculation of transport parameters

The transport parameters such as the permeability coefficient (P) and the effective diffusion coefficient ($D_{eff}$) were calculated from the transport data as well as from the lag-time ($t_{lag}$)

measurements, respectively. Permeability coefficient values were calculated using Eq. 3.8, and the data are presented in Table 3.10. The transport rate equation is given by

$$\ln (C_{f,t}/ C_{f,0}) = -k.t \qquad (3.7)$$

where, $C_{f,t}$ is the actinide ion concentration at a given time (t) in the feed phase, $C_{f,0}$ is the initial concentration of actinide ion in the feed phase, k is the rate constant ($s^{-1}$), and t is the time of transport (s). The value of k was calculated from the slope of the fitted straight line plot of ln ($C_{f,t}/ C_{f,0}$) vs. time. P can be calculated as follows.

$$P = -(V / Q)^* k \qquad (3.8)$$

where, V is the volume of the feed phase and Q is the membrane effective area obtained from the total exposed membrane surface area A and the porosity ε ($Q=A.\varepsilon$). As the PIMs act like dense membranes, A and Q are same. Initial metal ion flux ($J_0$) can be calculated using equation (3.9)

$$J_0 = P \bullet C_{f,0} \qquad (3.9)$$

The $D_{eff}$ values were calculated involving the metal carrier complex transfer from one end of the PIM (feed-membrane interface) to the other (membrane-receiver interface) from the following expression (3.10) [**137**].

$$D_{eff} = d_o^2/6t_{lag} \qquad (3.10)$$

where, $d_o$ is the membrane thickness in centimeters and $t_{lag}$ is the lag-time defined as the time required for the metal carrier complex to diffuse across the membrane from the feed phase to the receiving phase, which was calculated graphically from the time of detection of the activity of the target radionuclide in the receiver solution from the transport experiment. A typical plot for the determination of lag-time for Pu(IV) transport with TODGA containing

PIM is given in Fig. 3.14. The lag-time plot for other actinide ions with the PIMs containing DGAs are presented in *Annexure-II* (Fig. A2.15). The $D_{eff}$ values are presented in Tables 3.11 and 3.12. As can be seen from Table 3.10, the values of P follow the trend: Pu(IV) > Am(III) > Th(IV) > U(VI) for the PIMs containing T2EHDGA, TPDGA and THDGA while the trend for the TODGA based PIM was: Am(III) > Pu(IV) > Th(IV) > U(VI) which was also found to follow the same trend as that for their uptake from the feed solution.

Table 3.11. Diffusion coefficient data for actinide ions: PIM composition: 68.4% Carrier + 17.9% NPOE + 13.7% CTA.

| Metal ion | TPDGA | | | THDGA | | |
|---|---|---|---|---|---|---|
| | Thickness (cm) | Lag Time (s) | $D_{eff}$ (cm$^2$/s) | Thickness (cm) | Lag Time(s) | $D_{eff}$ (cm$^2$/s) |
| U(VI) | 0.0084 ± 0.0009 | 2280 | $5.16 \times 10^{-9}$ | 0.0081± 0.0009 | 2400 | $4.56 \times 10^{-9}$ |
| Pu(IV) | 0.0084 ± 0.0009 | 1080 | $1.09 \times 10^{-8}$ | 0.0082 ± 0.0009 | 1440 | $7.78 \times 10^{-9}$ |
| Th(IV) | 0.0084 ± 0.0009 | 5940 | $1.98 \times 10^{-9}$ | 0.0081 ± 0.0009 | 3120 | $3.50 \times 10^{-9}$ |
| Am(III) | 0.0084 ± 0.0009 | 1680 | $7.00 \times 10^{-9}$ | 0.0081 ± 0.0009 | 1920 | $5.69 \times 10^{-9}$ |

It can also be seen from Table 3.10 that the P value of the respective ion is higher with the PIMs containing TPDGA or THDGA as compared to those with the PIMs containing T2EHDGA or TODGA. Though the first order rate constant (k), which is related to the P value, also followed the same trend, the flux ($J_0$) values showed a different trend due to the differences in the metal ion concentrations used in the transport experiments (Table 3.10). As seen from Table 3.11, the $D_{eff}$ values followed the trend: Pu(IV) >Am(III) > U(VI) >Th(IV) for the PIMs containing both TPDGA and THDGA. Similar observation was made in studies involving the T2EHDGA based PIMs (Table 3.12). On the other hand, the $D_{eff}$ values obtained for the TODGA based PIM followed the trend: Am(III) > Pu(IV) > Th(IV) > U(VI) (Table 3.12).

Table 3.12. Diffusion coefficient data for actinide ions

| Metal ion | TODGA[a] | | | T2EHDGA[b] | | |
|---|---|---|---|---|---|---|
| | Thickness (cm) | Lag Time (s) | $D_{eff}$ (cm$^2$/s) | Thickness(cm) | Lag Time (s) | $D_{eff}$ (cm$^2$/s) |
| U(VI) | 0.014±0.002 | 1500 | $2.18 \times 10^{-8}$ | 0.0081 ±0.0004 | 1200 | $9.11 \times 10^{-11}$ |
| Pu(IV) | 0.015±0.002 | 900 | $4.16 \times 10^{-8}$ | 0.0081 ±0.0004 | 900 | $1.22 \times 10^{-10}$ |
| Th(IV) | 0.012±0.005 | 840 | $2.86 \times 10^{-8}$ | 0.0087 ±0.0004 | 3000 | $4.21 \times 10^{-11}$ |
| Am(III) | 0.016 ± 0.004 | 480 | $8.89 \times 10^{-8}$ | 0.0087 ±0.0004 | 1380 | $9.14 \times 10^{-11}$ |

*Note: [a]PIM composition: 58% TODGA, 30% NPOE, 12% CTA; [b]PIM composition: 69% T2EHDGA, 17% NPOE, 14% CTA*

Though the TPDGA based PIMs showed higher $D_{eff}$ values as compared to those obtained for the THDGA based PIMs, a reversal in case of Th(IV) transport is not understood (Table 3.10). The $D_{eff}$ values were found to be higher by one order magnitude for the PIMs containing TPDGA and THDGA as compared to those with the T2EHDGA based PIM which in turn were lower by one order of magnitude as compared to the the TODGA based PIMs for all the actinides concerned.

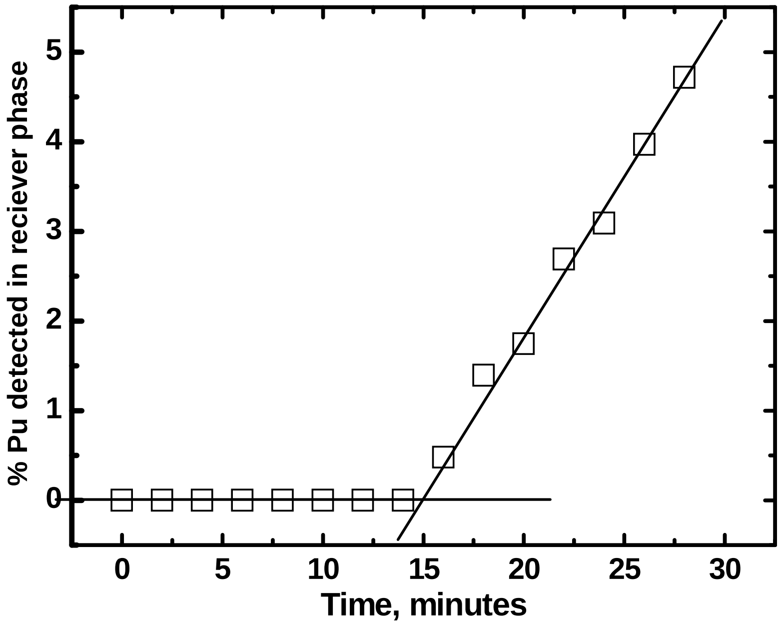

Fig. 3.14. A typical lag-time determination plot for the Pu(IV) transport system. PIM composition: 58% TODGA, 30% NPOE, 12% CTA; Feed: 1 M $HNO_3$; Receiver: 1 M α-HIBA at pH 3.0

### 3.4.2. Effect of the carrier (T2EHDGA) concentration on the transport of Am(III)

To study the effect of T2EHDGA concentration on the metal ion transport rates, PIMs containing varying fractions of T2EHDGA were prepared and employed for the Am(III) transport studies (Fig. 3.15). PIMs prepared in an analogous manner containing 100 mg of T2EHDGA, 80 mg CTA and 105 mg NPOE had a composition of 35% T2EHDGA, 37% NPOE, and 28% CTA, while the PIM prepared with 200 mg of T2EHDGA, 80 mg CTA and 105 mg NPOE corresponded to a composition of 52% T2EHDGA, 27% NPOE, and 21% CTA. As shown in Fig. 3.15, the transport of Am(III) increased with the T2EHDGA content of the PIM. Furthermore, these results suggested the absence of any “percolation threshold” for the transport system.

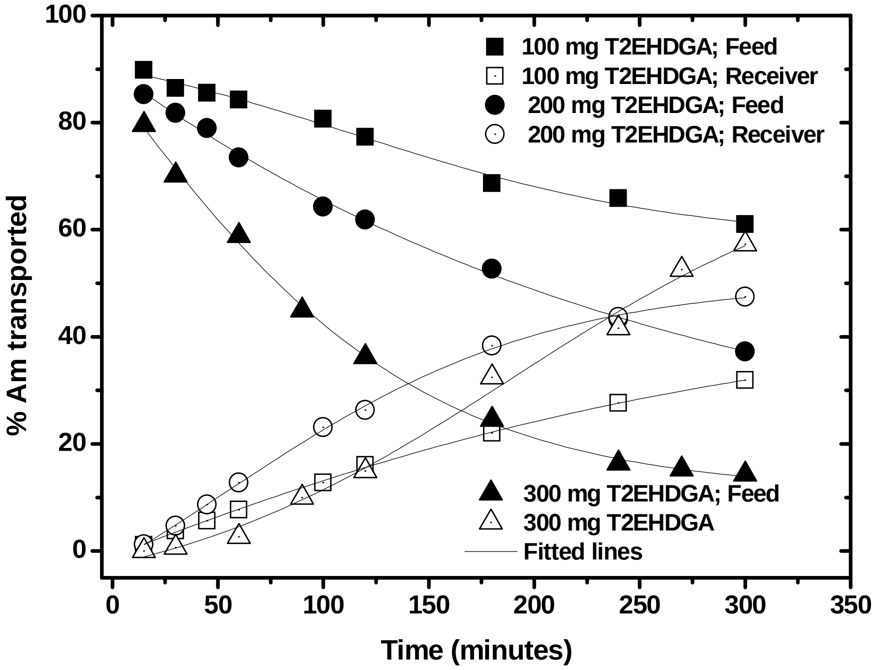

Fig. 3.15. Transport profiles of Am(III) by PIMs containing varying amounts of T2EHDGA. Feed: 1 M $HNO_3$. Receiver: 1 M α-HIBA at pH 3.0.

### 3.4.3. Stability of the membranes

It is reported that the PIMs have better stability as compared to the supported liquid membranes [**138**]. However, there are stray reports of poor stability of the PIMs. It is well-known that CTA-based PIMs have lower hydrolytic stability in acidic or alkaline media as compared to the PVC based PIMs. In view of this, most of the studies in the present work were carried out using 1 M $HNO_3$ and 1 M α-HIBA at pH 3.0 as the feed and receiver solutions, respectively. The PIM stability studies were carried out by using the same PIM while changing the feed and receiver solutions every day where the feed has been spiked with a known amount of $^{241}$Am radiotracer.The transport data are presented in Fig. 3.16 which indicated marginal change in the first 2 days, while slow deterioration of the PIMs was noticed over the next 3 days. This suggested rather poor stability of the T2EHDGA-containing PIMs.

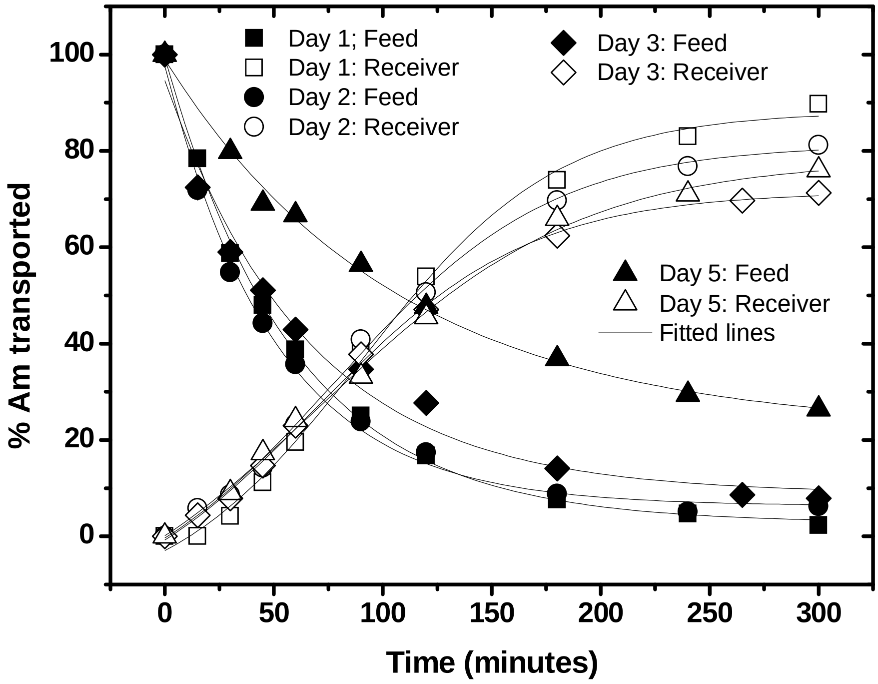

Fig. 3.16. Repeated transport experiments carried out to assess the stability of the T2EHDGA-based PIM. Feed: 1 M $HNO_3$. Receiver: 1 M α-HIBA at pH 3.0.

Though hydrolysis of CTA appeared to be less probable over such a short period of time, the factors responsible were not clearly understood. PVC-based PIMs needed to be evaluated as an alternative in future studies.

## 3.5. CONCLUSIONS

In conclusion, the uptake and transport of actinide ions, viz. U(VI), Pu(IV), Th(IV) and Am(III) by PIMs containing a series of substituted diglycolamide (DGAs) ligands such as TPDGA, THDGA, TODGA and T2EDGA as the carrier extractant were studied in detail while the uptake studies were carried out using TDDGA. Physical characterization of the PIMs using various techniques was carried out which suggested uniform distribution of the extractant in the PIM. Various factors viz., PIM composition, feed acidity, alkyl substitution at the acyl N atom of the DGAs were found to affect the uptake and transport of the actinide ions by the PIMs. The kinetics and isotherm of uptake of metal ion by the PIM have been investigated in detail. The diffusion coefficients were determined from lag-time measurements.

The results suggested that the uptake of the $Am^{3+}$ (taken as a representative actinide ion) decreased continuously when the PIMs were regenerated and reused. Similarly, the transport results obtained with the regenerated PIMs suggested deterioration of the PIMs which was attributed to possible hydrolysis of CTA or leaching of the extractant.

# CHAPTER 4

# SEPARATION OF ACTINIDES BY POLYMER INCLUSION MEMBRANES CONTAINING MULTIPLE DIGLYCOLAMIDE-FUNCTIONALIZED LIGANDS AS THE CARRIER EXTRACTANTS

## 4.1. INTRODUCTION

Diglycolamide (DGA) based extractants such as, *N,N,N',N'*-tetra-*n*-octyl diglycolamide (TODGA) preferentially extracts trivalent actinides over tetravalent or hexavalent actinides which has been attributed to the formation of reverse micellar aggregates at 3 M $HNO_3$ [**139, 140**]. Generally, three to four molecules of TODGA are reported to form an aggregate in the core of which the trivalent actinide ions are preferentially extracted in a size selective manner. This aggregate formation is highly dependent on the diluents properties and hence the extraction behavior of the actinides changes drastically with the diluent polarity. It was therefore, of interest to evaluate the performance of multiple DGA-functionalized extractant for the extraction of the actinide ions in the absence of any diluent enabled aggregation. Moreover, the extraction efficiency also increases due to a cooperative action of in case of multiple DGA-functionalized extractants resulting from a pre-organized structure [**141**]. In the view of these, PIMs containing two typical multiple DGA-functionalized carrier extractants, such as, tripodal diglycolamides (T-DGA, Fig. 4.1a) and DGA-functionalized calix[4]arenes (C4DGA, Fig. 4.1b) based PIMs were evaluated for the uptake and transport of actinide ions from acidic feed solutions. In T-DGA, three DGA units were appended to form a C-pivot tripodal diglycolamide (T-DGA) whereas in C4DGA, four DGA moieties (each containing two *n*-octyl groups at the outer amide group) were appended at the lower rim of the calix[4]arene skeleton [**141-143**]. The actinide ions studied were, Am(III), Pu(IV), Th(IV) and U(VI). This Chapter deals with the characterization of the PIMs using different techniques, such as TGA, XRD, SEM, AFM, FTIR and TIMM. The uptake and transport of actinide ions using CTA based PIMs containing T-DGA or C4DGA as the carrier extractant and NPOE (2-nitrophenyloctyl ether) as the plasticizer are discussed in this Chapter.

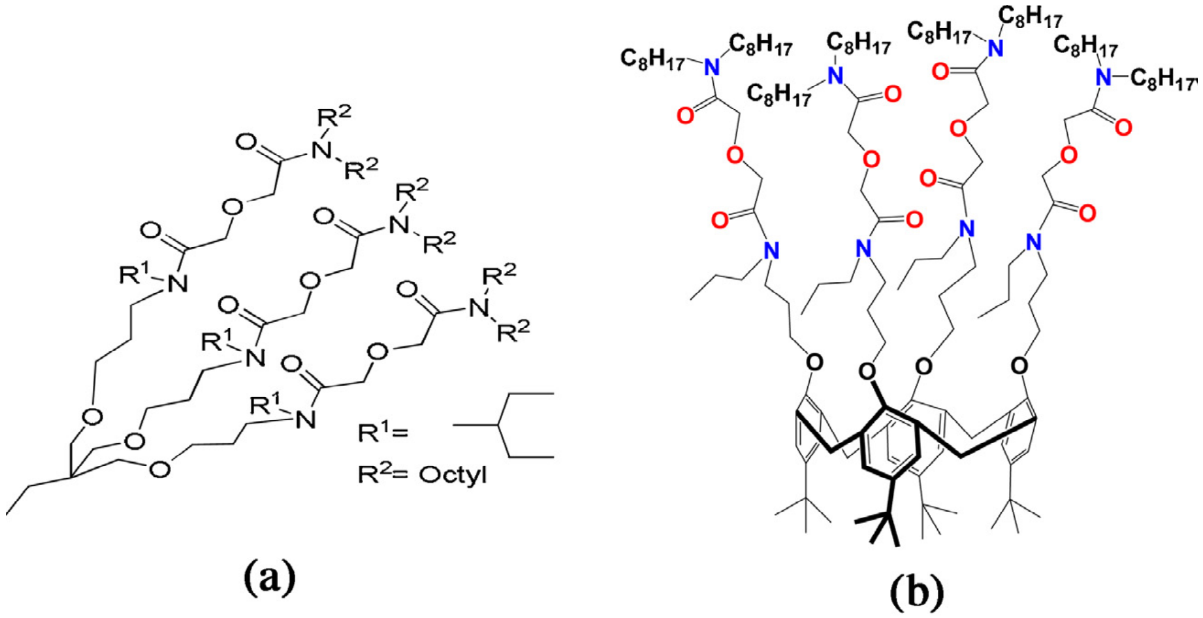

Fig. 4.1. Structural formulae of (a) T-DGA and (b) C4DGA

The effects of the concentrations of the carrier extractants (T-DGA/C4DGA) and NPOE (the plasticizer) in the PIMs on the uptake of Am(III) at 1 M $HNO_3$ were thoroughly investigated in order to optimize the composition of the PIMs for the metal ion uptake. The effect of the feed composition (the feed acidity as well as the salt composition) on Am(III) uptake by the PIMs was also investigated. The results of the comparative uptake and transport studies involving some actinides, viz. U(VI), Pu(IV), Th(IV) and Am(III) using the PIMs containing T-DGA/C4DGA are discussed in this Chapter. Different kinetic parameters for the transport of actinides were determined and compared with those obtained with TODGA and T2EHDGA based PIMs, already discussed in the previous Chapter. This Chapter also describes in detail the batch sorption studies of Eu-radiotracer in the presence of macro concentrations of $Eu^{3+}$ (used as a surrogate of $Am^{3+}$) on to the T-DGA based PIMs. The experimental uptake data were fitted to different isotherms (Langmuir, Freundlich, Dubinin−Radushkevich, Redlich-Peterson) and kinetic (pseudo-first-order, pseudo-second order, Elovich) models. The various parameters of the different model equations were determined from the fitted plots and the results are also included in this Chapter. The stability and reusability possibility of the T-DGA and C4DGA based PIMs, which are crucial for their long term use, are also discussed.

## 4.2. PHYSICAL CHARACTERIZATION OF THE PIMs

Physical characterization of the PIMs containing T-DGA or C4DGA as the carrier extractant was carried out by using a series of experimental techniques, such as TGA, XRD, FTIR, TIMM, SEM and AFM. The details of the experimental techniques are discussed in Chapter 2.

### 4.2.1. TG analysis

Thermogravimetric (TG) technique was used to determine the thermal stability and thermal degradation behaviour of the PIMs. The thermograms of the PIMs are strongly influenced by the behaviour of the components in the PIM. When the plasticizer is present in the PIM, its evolution suffers a delay as compared to when the plasticizer is alone [**144-146**]. Similarly, the base polymer decomposes at a lower temperature when it is present in the PIM as compared to when it is alone. This behaviour is the consequence of the effect of interactions between the plasticizer and the base polymer molecules in the PIM prior to the decomposition process. Both these effects, the delay in the evolution of the plasticizer and the advance in the decomposition of the polymer, are more marked for the more compatible plasticizers [**144-146**]. It is evident from the thermograms (*Annexure-I*, Figs.A1.3a-b) that the freshly prepared PIMs containing T-DGA and C4DGA are thermally stable up to 140°C-150°C after which decomposition takes place in two steps where the first step corresponds to the loss of NPOE and T-DGA (or C4DGA) and the second step corresponds to the degradation of CTA. It was required to understand the thermal decomposition pattern of the used PIMs. Therefore, the pristine PIMs (T-DGA containing PIMs) were contacted with 1 M $HNO_3$ in the presence as well as absence of Eu(III) ions (used as a surrogate of $Am^{3+}$) and the thermograms were recorded subsequently (*Annexure-I*, Figs.A1.4a-f**,**). Thermograms of the Eu(III) loaded as well as the regenerated (the loaded Eu was stripped using 1 M *alpha*-hydroxy-*iso*-butyric acid (α-HIBA) solution) PIMs containing T-DGA were also taken and the results are listed in *Annexure-I*, Figs.A1.4e-f. The nature of the thermograms remained unchanged as that of the pristine PIM, even after immersing the PIM in 1 M $HNO_3$ for 24 h indicating that the integrity of the components in the PIM remained unchanged. On the other hand, the thermogram patterns changed drastically upon contacting the PIM with 1 M $HNO_3$ for a longer period of time (13 days) (*Annexure-I*, Fig.A1.4 (d)), which is attributed to the loss of the carrier and the plasticizer and also to the hydrolysis of CTA. When the thermogram of a freshly regenerated PIM (previously loaded with $Eu^{3+}$) was taken, it resembled that of the pristine PIMs (*Annexure-I*, Fig.A1.4 (a)), indicating that the loaded Eu(III) ions can be quantitatively removed using 1 M α-HIBA.

### 4.2.2. XRD analysis

It was required to understand the XRD pattern of the PIMs in order to get an idea about the possible mechanism of metal ion transport. Two of the most likely mechanistic possibilities of metal ion transport through the PIMs are ‘carrier-diffusion’ [**122**] and ‘fixed-site jumping’ [**130**]. The fixed-site jumping mechanism is favoured for PIMs with a crystalline structure while an amorphous structure of the PIMs favours transport of metal ions via carrier-diffusion mechanism [**126, 147**]. XRD analysis of the PIMs containing T-DGA and C4DGA (*Annexure-I*, Fig.A1.8a-b**,)** showed a broad spectrum with a single maximum at around 20°, which corresponds to van der Waals halo found in all polymers suggesting an amorphous structure [**124, 125**]. It indicated that the possible mechanism of the metal ion transport through the PIMs was via carrier-diffusion. However, to confirm this, a detailed investigation is required which is considered as beyond the scope of the Thesis.

### 4.2.3. FTIR analysis

FTIR analysis of the PIMs would give information regarding covalent bond formation between the carrier, the plasticizer and the base polymer molecules. In the absence of covalent bonding among the components of the PIM, the FTIR spectra of the PIM would show no new bands and they would match with the FTIR spectra of the individual components when they were present alone. FTIR spectroscopy of the PIMs made from pure CTA and NPOE+CTA showed a perfect similarity among the two spectra at all wavelengths except at 1529 $cm^{-1}$ (corresponding to the -NO stretching) where CTA does not absorb (*Annexure-I*, Fig.A1.10a-b). It indicated that CTA and NPOE were present as separate entities in the membrane and any chemical interaction between these components was lacking. Similarly, comparison of the spectra of NPOE + CTA and NPOE + CTA + T-DGA (or C4DGA) showed a perfect matching except at 1652 $cm^{-1}$ (or 1642 $cm^{-1}$ in the case of C4DGA), which corresponded to the >C=O stretching frequency (*Annexure-I*, Fig.A1.10a-b). Thus, the FTIR spectra of the PIMs indicated that all the components, viz., CTA, NPOE, and T-DGA (or C4DGA), existed in the membrane as separate entities without any sort of chemical interactions between them. Although there was no chemical bond formation involving the carrier, the plasticizer and the CTA molecules it was likely that they were bound to one another by a form of secondary bonding such as hydrophobic, van der Waals or hydrogen bonding interactions. These secondary interactions were much stronger than interfacial tension or capillary forces. Consequently, PIMs are considerably more stable than the analogous SLMs (supported liquid membranes) [**31**].

### 4.2.4. TIMM analysis

Transmission Infrared Mapping Microscopy (TIMM) profiles have been employed for characterizing the distribution of the carrier extractant as well as the plasticizer which have a very important role in the metal ion uptake and transport properties of the PIMs. The TIMM analysis can provide the distribution of the components within the PIM unlike SEM and AFM which only give basic information about the surface morphologies of the PIMs. Miguel et al. [**148**] used the TIMM distribution profiles of the components of a PIM containing three plasticizers viz. tris(2-ethylhexyl)phosphate (TEHP), tris(2-butoxyethyl)phosphate(TBEP) and 2-nitrophenyloctylether (NPOE) and the carrier bis(2,4,4-trimethylpentyl)phosphinic acid (CYANEX 272) to explain the differences in the transport mechanism of In(III). The presence of 'percolation thresholds' for the PIMs with TBEP or NPOE as the plasticizers was recognized by their TIMM study whereas carrier diffusion type mechanism was indicated for the PIMs with TEHP as the plasticizer.

In the present study, the distribution profiles of NPOE, T-DGA and C4DGA in the PIMs were obtained from the TIMM mappings and the results are depicted in Fig.A1.18a-c, Fig.A1.19a-b (*Annexure-I*). The distribution profiles of NPOE and CTA could not be monitored alone due to band overlapping (*Annexure-I*, Fig.A1.10a-b) in the PIMs containing T-DGA, NPOE, and CTA or the PIMs containing C4DGA, NPOE, and CTA whereas the distribution profiles of T-DGA and C4DGA in the PIMs could be monitored at 1652 $cm^{-1}$ and 1645 $cm^{-1}$, respectively without the interference of NPOE and CTA [**149**]. It was evident from Figs.A1.18(b) and A1.19(b) (*Annexure-I*) that a homogeneous distribution of carrier (T-DGA or C4DGA) across the membrane was present which indicated that a carrier diffusion type mechanism might be possible for the uptake / transport of metal ions in the PIM and the existence of a 'percolation threshold' was ruled out. An analogous homogeneous distribution of the extractant (T2EHDGA) along the membrane using a TIMM plot and the carrier diffusion type mechanism has been reported by us [**135**]. TIMM profiles of the PIMs taken after contacting with 1 M $HNO_3$ for 24 h indicated no change in the distribution profile of the components compared to the pristine PIMs (*Annexure-I*, Fig.A1.20a-b).

### 4.2.5. AFM analysis

It was also required to measure surface roughness of a PIM which could be correlated with the uptake and transport behavior of metal ions by the PIMs [**150**]. The topographic AFM images of the pristine as well as the used PIMs containing 25.6% T-DGA, 53.9% NPOE, and 20.5% CTA are shown in Figs.A1.22a-b (*Annexure-I*). It was clear from the figures that although the pristine PIMs showed ample roughness, the surfaces of the PIMs appeared to smoothen after it was used several times for Eu(III) ion uptake followed by stripping. As a consequence, the uptake efficiency of the PIMs was found to deteriorate after several uses. The amplitude and phase images are also shown in Fig.A1.23 and Fig.A1.24 (*Annexure-I*) for comparison purpose.

### 4.2.6. SEM analysis

The SEM analysis was required to obtain information about homogeneity, porosity of the PIM surface. The morphology of the surface as well as the cross section of the T-DGA based PIM of the composition, 25.6% T-DGA, 53.9% NPOE, and 20.5% CTA were analyzed by the SEM analysis at 1000X magnification. Figs. A1.26a-c (*Annexure-I*) depicts the SEM images of the bottom surface (the surface of PIM adhered to the glass Petri dish during preparation), the top surface (surface exposed to air during preparation of the PIM) and the cross section of the PIM. All the SEM images of the PIMs showed a uniform dense structure with no apparent porosity. This could be due to the existence of large amounts of the plasticizer, which dissolved the carrier and entangled in the pores of the polymer. A similar filling of porous PIMs, containing only CTA and NPOE as the plasticizer, was reported previously [**150**].

## 4.3. UPTAKE STUDIES

### 4.3.1. Optimization of the composition of PIMs

As already discussed in Chapter 1, the metal ion uptake capacity is unique for a given composition of the PIM. Furthermore, in view of the interactions between the components (the carrier extractant, the plasticizer and CTA), optimization of the PIM composition is required to achieve an efficient metal ion uptake capacity. The effect of the composition of DGA (TODGA, T2EHDGA) based PIMs on the uptake of Am(III) was investigated in detail in Chapter 3. The PIMs described in the present chapter also contain three components, viz., CTA, NPOE and the carrier extractant (T-DGA or C4DGA). PIMs which did not contain NPOE appeared to be brittle and those without any carrier (T-DGA or C4DGA) did not show any uptake of the actinide ions. Though all the three components are important in the PIM, the carrier (T-DGA or C4DGA) plays the most important role in the extraction of the metal ion from its solution by forming a metal-carrier complex at the PIM-solution interface. Once the metal ion is complexed by the carrier molecules present at the PIM surface, it may diffuse into the bulk of the PIM by the “fixed site jumping” [**130**] or the “mobile carrier” mechanism [**122**], reported previously. In both the cases, the metal ion uptake is expected to increase with increasing concentration of the carrier (T-DGA or C4DGA) in the PIM. The metal ion uptake by the PIMs containing T-DGA or C4DGA at the PIM-aqueous feed interface is given by the following equation.

$$M_{aq}^{n+} + mDGA_M + nNO_{3,aq}^{-} \rightleftharpoons M(NO_3)_n{\bullet}mDGA_M \qquad \textbf{(4.1)}$$

where, the species with the subscripts “aq” and “M” represent those in the aqueous and the membrane phases, respectively. DGA indicates T-DGA or C4DGA taking part in the metal ion uptake. The number of nitrate ions (n) taking part in Eq.(4.1) is different for different metal ions and is expected to be 3, 4, 4, and 2, respectively, for Am(III), Pu(IV), Th(IV), and U(VI) which is based on the valency of the metal ion to obtain neutral extractable species.

### 4.3.1.1. Effect of the carrier extractant concentration on the uptake of Am(III)

The effect of T-DGA concentration was studied from a series of experiments by varying the T-DGA content in the PIM in the range of 20-100 mg, while keeping the NPOE (210 mg) and CTA (80 mg) content fixed. Fig. 4.2 depicts the Am(III) uptake results due to concentration variation of T-DGA in the PIMs. The Am(III) uptake profiles (Fig. 4.2) suggested that on increasing the T-DGA content from 6.5% to 12.4%, the Am(III) uptake (after 24 h) improved from 26.6% to 55.4% which was found to increase further to 87.6% when 21.6% T-DGA was used in the PIM. However, any further increase in the T-DGA content to 25.6% has resulted in an unchanged uptake percentage of Am(III) (Table 4.1). Though the initial increase in Am(III) uptake is a consequence of Eq. 4.1, the saturation beyond 21.6% T-DGA may be due to steric hindrance (or entanglement) of the DGA moieties in the rather bulky T-DGA molecule causing some of those not being accessible for metal ion uptake anymore. Salima et al. [**151**] observed a similar increase followed by a plateau in the extraction of methylene blue as a function of the D2EHPA concentration (5-30 μmol/ $cm^2$) of a CTA-based PIM. Similarly, Gherasim et al. [**134**] reported a slight decrease in the sorption capacity of a polyvinyl chloride (PVC) based PIM at higher Aliquat-336 content (>40%) due to increasing steric hindrance.

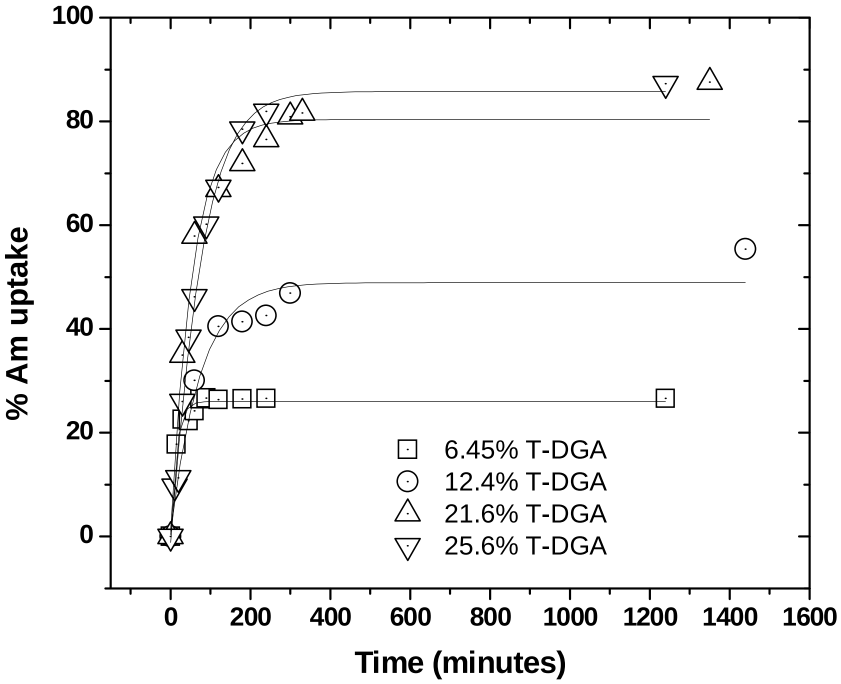

Fig. 4.2. Effect of T-DGA content (in %) on Am(III) uptake by the PIMs prepared with CTA (as the polymer) and NPOE (as the plasticizer). Feed acidity: 1 M $HNO_3$ (20 mL) and 0.020 g of PIM.

Table 4.1. % Am (III) uptake by PIMs containing varying amounts of T-DGA. Feed: 1 M $HNO_3$

| Time (h) | % Am(III) uptake | | | |
|---|---|---|---|---|
| | 6.67% T-DGA | 12.8% T-DGA | 22.4% T-DGA | 26.3% T-DGA |
| 0.5 | 22.6 | 14.3 | 35.0 | 16.3 |
| 1 | 24.2 | 30.3 | 57.9 | 39.3 |
| 2 | 26.4 | 40.5 | 66.9 | 63.1 |
| 3 | 26.5 | 41.5 | 71.9 | 75.7 |
| 4 | 26.6 | 42.6 | 76.5 | 79.5 |
| 24 | 26.6 | 55.4 | 87.6 | 88.4 |

The results of the Am(III) uptake with varying composition of the C4DGA based PIMs are given in Table 4.2. In the case of PIMs containing a comparable NPOE content, the uptake of Am(III) was found to increase with increasing C4DGA content (Table 4.2) which was expected from Eq.4.1. For example, PIMs of the compositions, 5.1% C4DGA, 53.9% NPOE, and 41.0% CTA and 9.8% C4DGA, 51.2% NPOE, and 39.0% CTA showed an uptake of Am(III) of 3.2% and 14.3%, respectively, in 2 h.

Table 4.2. Uptake data of Am(III) at various compositions of C4DGA-containing PIMs. Feed: 5 mL of 1 M $HNO_3$ (values in side parentheses indicate data at 24 h).

| Membrane composition | | | % Am(III) uptake at 2 h (24 h) |
|---|---|---|---|
| % CTA | % NPOE | % C4DGA | |
| 41.0 | 53.9 | 5.1 | 3.2 (4.0) |
| 26.7 | 70.0 | 3.3 | 8.3 (16.3) |
| 15.7 | 82.4 | 1.9 | Nil (11.8) |
| 25.8 | 67.7 | 6.5 | 28.1(46.8) |
| 39.0 | 51.2 | 9.8 | 14.3 (34.5) |

Similarly, PIMs of the composition 3.3% C4DGA, 70.0% NPOE, and 26.7% CTA and 6.5% C4DGA, 67.7% NPOE, and 25.8% CTA showed an uptake of Am(III) of 8.3% and 28.1%, respectively, in 2 h. Here, apart from the carrier extractant concentration, the plasticizer also appears to play an important role (vide infra).

### 4.3.1.2. Effect of NPOE concentration on the uptake of Am(III)

As already discussed before, the plasticizer plays the role of the solvent for ion transport in PIMs and makes the membranes flexible. The effect of plasticizer (NPOE) concentration in the T-DGA based PIM was studied by carrying out Am(III) uptake (2 h) from 1 M $HNO_3$ using the membranes containing a varying NPOE content (24.5-56.8%) at given amounts of

CTA and T-DGA. Fig. 4.3 depicted the Am(III) uptake profiles with varying NPOE content in the T-DGA containing PIMs. An increase in the Am(III) uptake from 77.7% (24.5% NPOE) to 87.1% (39.6% NPOE) was observed (*Annexure-II*, Table A2.2) after 2 h and a further increase in the NPOE content in the PIM to 56.8% resulted in a decrease in the Am(III) uptake efficiency to 66.9% (after 2 h).

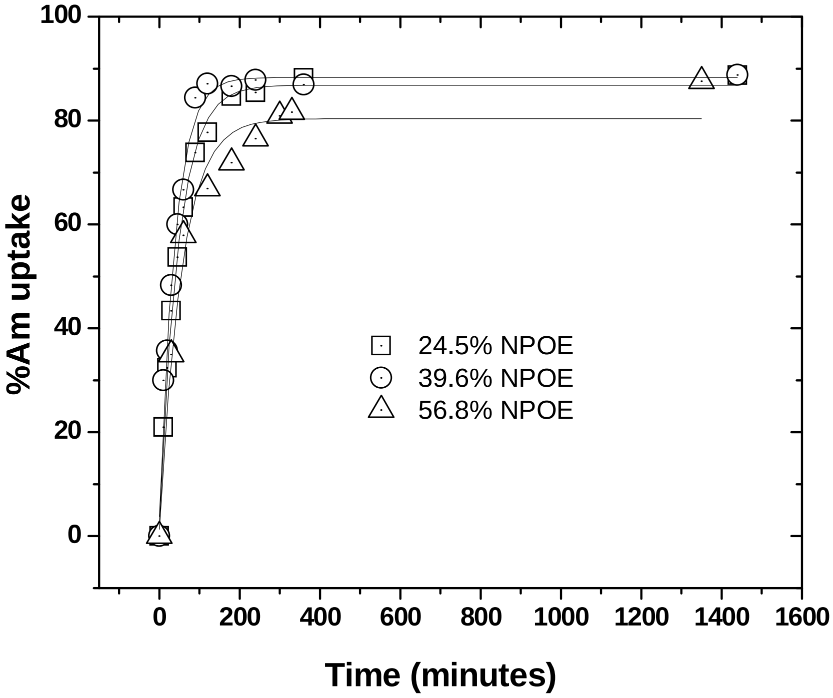

Fig. 4.3. Effect of NPOE content on Am(III) uptake in PIMs with fixed CTA (80 mg) and T-DGA (80 mg) content. Feed: 1 M $HNO_3$ (20 mL) and 0.020 g of PIM.

The increase in the metal ion uptake efficiency with increasing NPOE content is due to plasticization effect, which turns the membrane into a better medium for carrier and plasticizer movements, whereas the decrease in the uptake efficiency at still higher NPOE content may be due to the plasticizer exudation, prevalent in the case of PIMs [**31**]. A similar decrease in the uptake efficiency of a T2EHDGA based PIM in the presence of NPOE as the plasticizer at a much lower concentration (17.9–30.4%) of NPOE was noticed [**152**]. However, with all the PIMs with NPOE content in the range of 24.5–56.8%, the uptake of

Am(III) reached a near constant value of ~88% after 24 h (Fig. 4.3). This shows that the effect of NPOE is more significant initially, while it disappears at higher uptake times. On the basis of these data, the optimized PIM composition was found to be 25.6% T-DGA, 53.9% NPOE, and 20.5% CTA.

Similar to the T-DGA containing PIM as discussed above, the results of the effect of plasticizer concentration on the uptake of Am(III) with the C4DGA containing PIMs are summarized in Table 4.2. The Am(III) uptake increased from 3.2% to 8.3% in 2 h when the NPOE concentration in the PIM increased from 53.9% to 70% with a simultaneous decrease in the C4DGA content from 5.1% to 3.3%. Similarly, in spite of the decrease in the C4DGA content in the PIM, the Am(III) uptake efficiency increased from 14.3% using a PIM containing 9.8% C4DGA, 51.2% NPOE, and 39.0% CTA to 28.1% using a PIM containing 6.5% C4DGA, 67.7% NPOE, and 25.8% CTA. This increase in the Am(III) uptake by the PIMs containing a higher amount of NPOE and a lower amount of C4DGA is the result of the plasticization effect which makes the medium more favorable for carrier as well as carrier-metal ion complex movement. However, the uptake of Am(III) in 2 h becomes negligible (below detection limit) if NPOE content in the PIM was increased to 82.4%, which is partly attributed to the very low C4DGA concentration and also may be due to the plasticizer exudation. Similar effect of the NPOE content on the uptake of Am(III) with T2EHDGA based PIMs [**152**] was observed by us. On the basis of the above studies using varying C4DGA, CTA, and NPOE contents, the optimized composition of PIM was found to contain 6.5% C4DGA, 67.7% NPOE, and 25.8% CTA.

### 4.3.2. Effect of feed composition on the uptake of Am(III) by T-DGA based PIM

Eq. 4.1 indicated that the uptake of the actinide ions is influenced by the nitrate ion concentration in the feed solution. The effect of feed composition on the uptake efficiency of

Am(III) by the PIM was studied by varying the concentrations of $HNO_3$ and $NaNO_3$, while keeping the total nitrate ion concentration fixed at 3 M (Fig. 4.4).

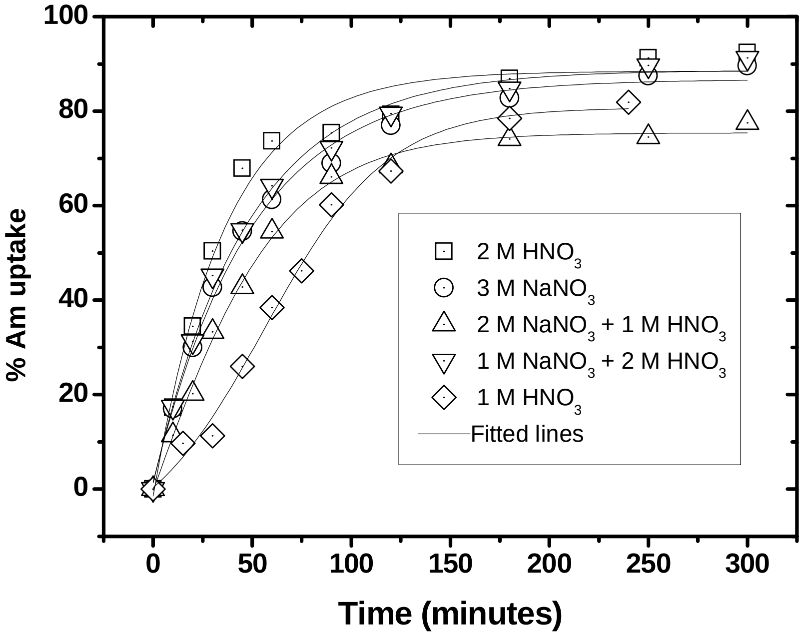

Fig. 4.4. Uptake of Am(III) from feeds containing varying fractions of $HNO_3$ and $NaNO_3$. PIM composition: 25.6% T-DGA, 53.9% NPOE, and 20.5% CTA.

The uptake of Am(III) at 2 M $HNO_3$ (no $NaNO_3$) was also shown in Fig. 4.4 for comparison. 3 M $HNO_3$ was not taken as the feed in view of relatively fast degradation of the PIM (due to CTA hydrolysis). Comparable uptake efficiency of Am(III) for the 3 M $NaNO_3$ (0.01 M $HNO_3$ was added to prevent the hydrolysis of $Am^{3+}$) and 1 M $NaNO_3$ + 2 M $HNO_3$ solutions can be observed in Fig. 4.4. On the other hand, though the best uptake efficiency was observed with 2 M $HNO_3$ (up to 1.5 h), a plateau was reached at 2 h and above, and the uptake efficiency matched well with those observed for 3 M $NaNO_3$ and 1 M $NaNO_3$ + 2 M $HNO_3$. The solution containing 2 M $NaNO_3$ + 1 M $HNO_3$ was found to be the least effective feed composition for Am(III) uptake. It was surprising to find that the uptake efficiency with 1 M $HNO_3$ was inferior to that with 2 M $NaNO_3$ + 1 M $HNO_3$ up to 2 h, beyond which it showed a better uptake efficiency. The uptake data obtained in the present study are in variance with those reported with TODGA [**153**] where 2 M $NaNO_3$ + 1 M $HNO_3$ resulted in the most effective Am(III) uptake. Furthermore, while TODGA based PIMs showed a near quantitative Am(III) uptake at ~2 h, much longer time was needed with T-DGA-based PIMs. These data, though not very conclusive, broadly suggest that (i) nitrate is the key ion for the metal ion uptake, (ii) $HNO_3$ is much more effective that $NaNO_3$, (iii) in some cases, $NaNO_3$ has a negative effect on the metal ion uptake. Though nitric acid assisted reverse micelle formation [**131**] has been reported which perhaps facilitates metal ion extraction, a similar effect is not ruled out with the T-DGA containing PIMs.

### 4.3.3. Comparative uptake behavior of actinides by T-DGA and C4DGA based PIMs

It was required to investigate the uptake of various actinides, viz., Am(III), Pu(IV), Th(IV), and U(VI) in 1 M $HNO_3$ by T-DGA as well as C4DGA based PIMs.

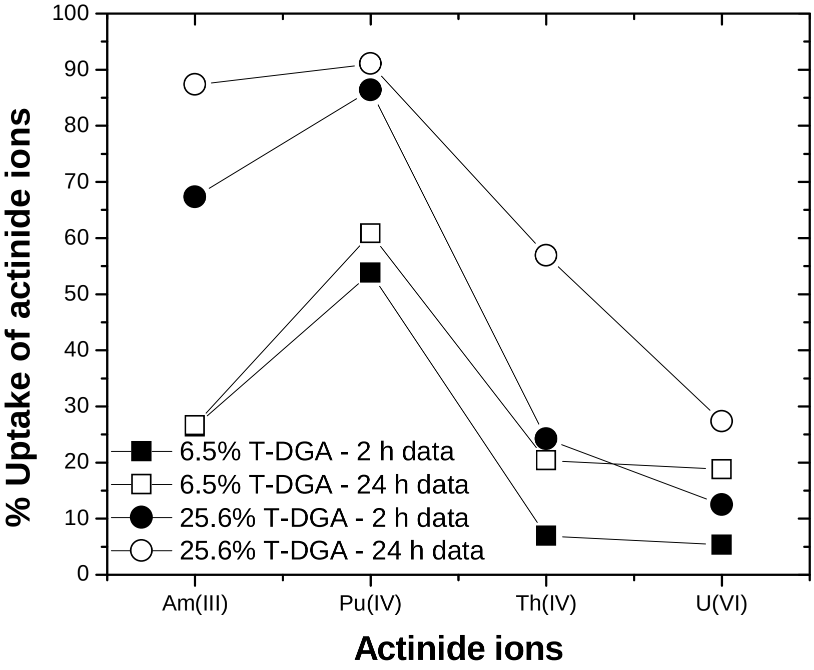

Fig. 4.5. Uptake of actinides by T-DGA-based PIM at two different PIM compositions

The uptake was carried out with two different compositions of the T-DGA containing PIMs and the results are given in Fig. 4.5. It shows that the Am(III) ion uptake with 6.5% T-DGA did not show uptake values $\geq$26% and higher uptake values were obtained with higher T-DGA concentrations (Table 4.1). Fig. 4.6 depicts the uptake profile of the actinides studied with the PIM composition, 25.6% T-DGA, 53.9% NPOE, and 20.5% CTA.

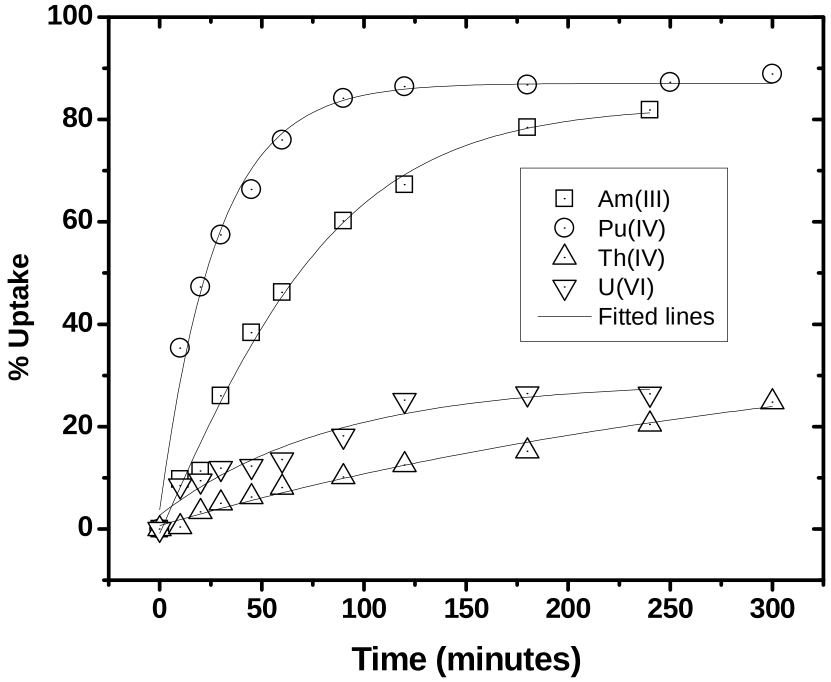

Fig. 4.6. Comparative actinide ion uptake efficiency of T-DGA based PIM of composition: 25.6% T-DGA, 53.9% NPOE, and 20.5% CTA. Feed: 1 M $HNO_3$ (20 mL)

It can be seen from Fig. 4.6 that the trend of actinide ion uptake was: Pu(IV) > Am(III) >> U(VI) > Th(IV). The higher uptake of Pu(IV) as compared to Am(III) is attributed to the higher ionic potential of the former. On the other hand, the relatively low uptake of U(VI) is ascribed to the steric factors associated with the axial ‘O’ atoms which forces complexation only in the equatorial plane. However, the poor extraction of Th(IV) as compared to that of Am(III), though the former has a higher ionic potential, may be due to the larger amount of ligands available for complexation with the Th(IV) ions at a very high ligand to metal ion ratio ($Th^{4+} < 10^{-10}$ M) and the subsequent poor diffusion of the rather bulky complex into the bulk of the PIM (mobile carrier model) thus, resulting in an uptake only on the PIM surface. Our earlier studies with a T2EHDGA based PIMs showed the uptake trend: Pu(IV) > Am(III) > Th(IV) > U(VI) [**152**]. On the other hand, an entirely different trend was observed with the TODGA based PIMs [**153**]. Interestingly, in contrast to the T2EHDGA based PIMs, the uptake of Pu(IV) was found to be significantly higher (~90%) by the T-DGA based PIMs even at a 10 times lower concentration of the carrier present in the PIM [**152**].

The uptake profiles of actinides with C4DGA containing PIMs with composition 6.5% C4DGA, 67.7% NPOE, and 25.8% CTA are given in Fig. 4.7. It indicates the trend of uptake as: Am(III) > Pu(IV) > Th(IV) > U(VI).

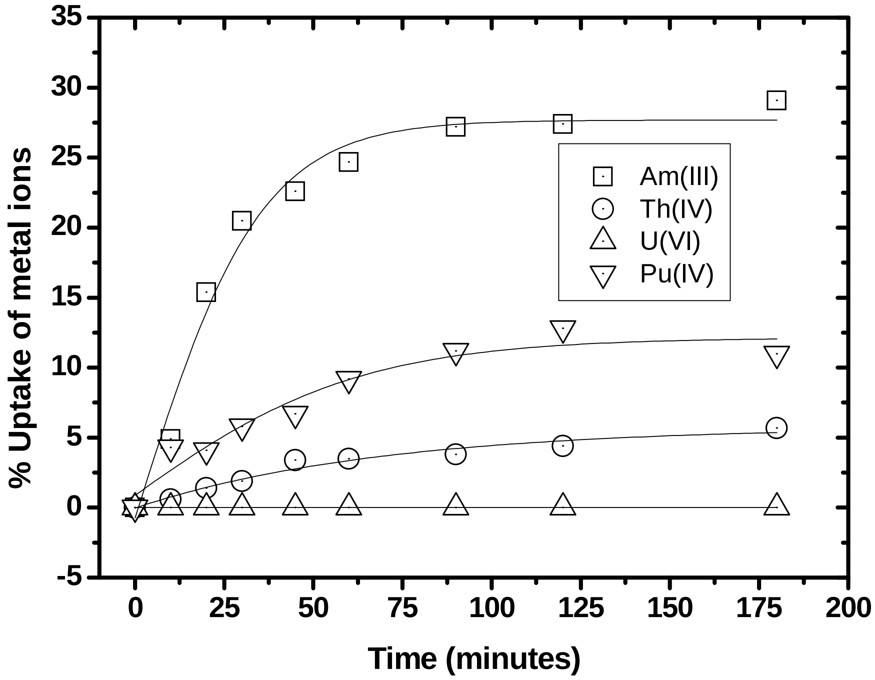

Fig. 4.7. Uptake of actinide ions using a PIM of the composition: 6.5% C4DGA, 67.7% NPOE and 25.8% CTA; feed: 1 M $HNO_3$

The practically no uptake of uranyl ion is due to stereochemical restrictions in accommodating the four DGA units of C4DGA at the equatorial position of the uranyl ion.

This poor extraction of the uranyl ion by the PIMs is quite interesting and can be advantageous for the selective separation of actinides from mixtures containing a bulk of uranium. The trend of uptake of actinides is similar to that observed with TODGA based PIMs [**153**]. The higher uptake of Am(III) than Pu(IV) is the same as that found in the solvent extraction studies involving TODGA [**75**], however opposite of that reported with C4DGA [**143**]. The percentage uptake values of Am(III), Pu(IV) and Th(IV) after 2 h were found to become nearly double after 24 h which indicated that the uptake of actinide by the C4DGA-based PIMs was rather slow.

### 4.3.4. Comparative uptake behavior of actinides by PIMs containing DGA and multiple DGA based carrier ligands

Table 4.3 gives a comparative overview of the uptake data of all the four actinide ions, viz., Am(III), Pu(IV), Th(IV) and U(VI) with DGA (TODGA and T2EHDGA) and multiple DGA (T-DGA and C4DGA) based PIMs. In view of the higher extraction / transport of the actinide ions by T-DGA / C4DGA as compared to that by TODGA / T2EHDGA, the former ligands were kept at much lower concentration in the PIM than the latter ones. The Am(III) uptake trend was found to be TODGA > T2EHDGA > T-DGA > C4DGA which was partly attributed to the fraction of the carrier extractant present in the respective PIMs. However, the kinetic effects due to the presence of three / four DGA moieties present in T-DGA / C4DGA are discounted while making a comparison with TODGA and T2EHDGA based PIMs.

Table 4.3. Comparative uptake of various actinide ions by PIMs containing TODGA, T2EHDGA, or T-DGA, C4DGA after 2 h[a]

| Metal ion | % Uptake (2 h) | | | |
|---|---|---|---|---|
| | TODGA[b] | T2EHDGA[c] | T-DGA[d] | C4DGA[e] |
| U(VI) | 7.4 | 4.8 | 25.2 | Nil |
| Th(IV) | 57.7 | 60.4 | 12.5 | 4.4 |
| Pu(IV) | 95.4 | 72.2 | 86.4 | 12.8 |
| Am(III) | 91.6 | 73.8 | 67.3 | 27.4 |

*Note: [a]Feed solution, 20 mL of 1 M $HNO_3$ using 4 $cm^2$ PIMs; [b]PIM composition: 58% TODGA, 30% NPOE, and 12% CTA; [c]PIM composition: 68.4% T2EHDGA, 17.9% NPOE, and 13.7% CTA; [d]PIM composition: 25.6% T-DGA, 53.9% NPOE, and 20.5% CTA; [e]PIM composition: 6.5% C4DGA, 67.7% NPOE, and 25.8% CTA.*

### 4.3.5. Extraction kinetics and isotherm studies with T-DGA based PIMs

Batch uptake studies of Eu(III) (used as a surrogate of $Am^{3+}$) by T-DGA based PIMs of composition 25.6% T-DGA, 53.9% NPOE, and 20.5% CTA were carried out by equilibrating the feed solution (15 mL) containing the Eu carrier solution (containing 20-100 mg/L Eu), spiked with $^{152}$Eu tracer, in 1.0 M nitric acid with small pieces of the PIM (total area of the PIM was fixed at 2 $cm^2$ with an approximate weight of 18 mg) in a stoppered conical flask at a constant stirring speed of 200 rpm using a high-speed precise magnetic stirrer (Corning) for a total time period of 46.5 h at ambient temperature (ca. 24°C). The percentage uptake of Eu(III) by the PIM at time ‘t’ can be expressed as follows.

$$\% \text{ Uptake} = \frac{C_0 - C_t}{C_0} \text{ X } 100 \qquad (4.2)$$

where, $C_0$ and $C_t$ are the Eu(III) ion concentrations in the aqueous phase at the beginning of the experiment and at time 't', respectively. The uptake studies were carried out in duplicate at ambient temperature (ca. 24 °C); the error in the uptake data was limited to <5%. The sorption capacity ($q_t$) (mg/g) of the PIM for Eu(III) was determined from the uptake of Eu onto the unit mass of the PIM using Eq. (4.2).

#### 4.3.5.1. Comparison of the uptake of Am(III) and Eu(III)

It was of interest to compare the uptake profile of Eu(III) tracer with Am(III) tracer by T-DGA based PIMs under similar experimental conditions with as before Eu(III) being used as the surrogate of Am(III) in the subsequent batch sorption studies. The uptake profiles of both the metal ions with T-DGA containing PIMs are shown in Fig. 4.8 which indicated marginally lower uptake efficiency of the PIM for the Eu(III) tracer as compared to that seen with the Am(III) tracer. This is in sharp contrast to the distribution coefficient values of the metal ions reported in a previous solvent extraction studies using TODGA in *n*-dodecane [75].

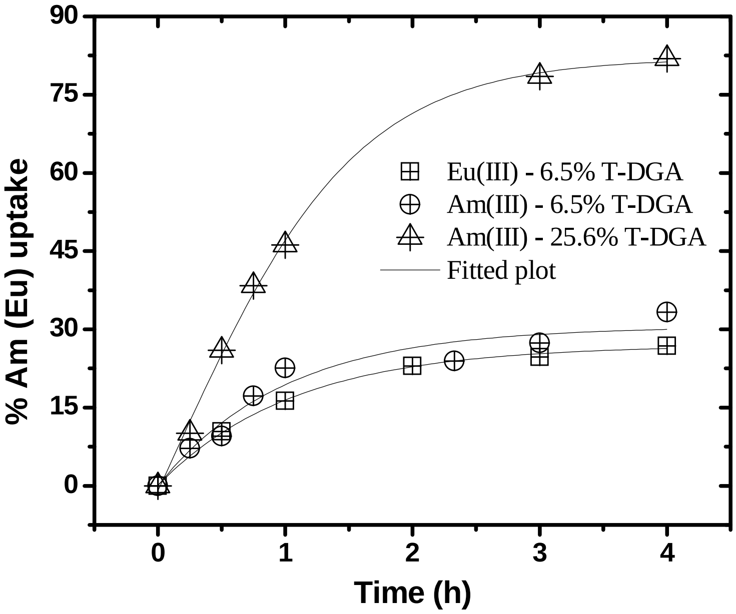

Fig. 4.8. Uptake of Eu(III) and Am(III) using a PIM with composition 6.5% T-DGA, 67.7% NPOE, and 25.8% CTA

Apparently, the T-DGA ligand does not yield the same extraction trend for Am(III) and Eu(III) extraction, at least, not in the plasticized membrane used in the present study. For comparison purpose, the uptake profiles of Am(III) tracer was shown in two different compositions of PIMs containing 6.5% and 25.6% T-DGA which clearly showed much larger metal ion uptake with the PIM containing higher carrier extractant concentration (25.6% T-DGA).

#### 4.3.5.2 Kinetics studies

The kinetics studies were carried out using T-DGA containing PIMs as the sorbents and Eu carrier solutions (20-100 mg/L) spiked with $^{152,154}$Eu tracer at 1 M $HNO_3$ as the feed and the sorption capacities of the PIMs for Eu(III) were plotted as a function of time as shown in Fig. 4.9. It is evident from the figure that the equilibrium condition was reached within 5 h of contact after which negligible changes are seen. The initial rapid increase is due to the presence of a large number of vacant sites present at the PIM surface leading to a high concentration gradient between Eu(III) in solution and on the PIM surface. As the contact time increased, the concentration of Eu(III) in the solution decreased due to the accumulation of the Eu(III) on the vacant sites of the PIM. This gave rise to a decrease in the concentration gradient, subsequently, resulting in a decrease in the sorption rate and eventually leading to the equilibrium sorption state [**149**].

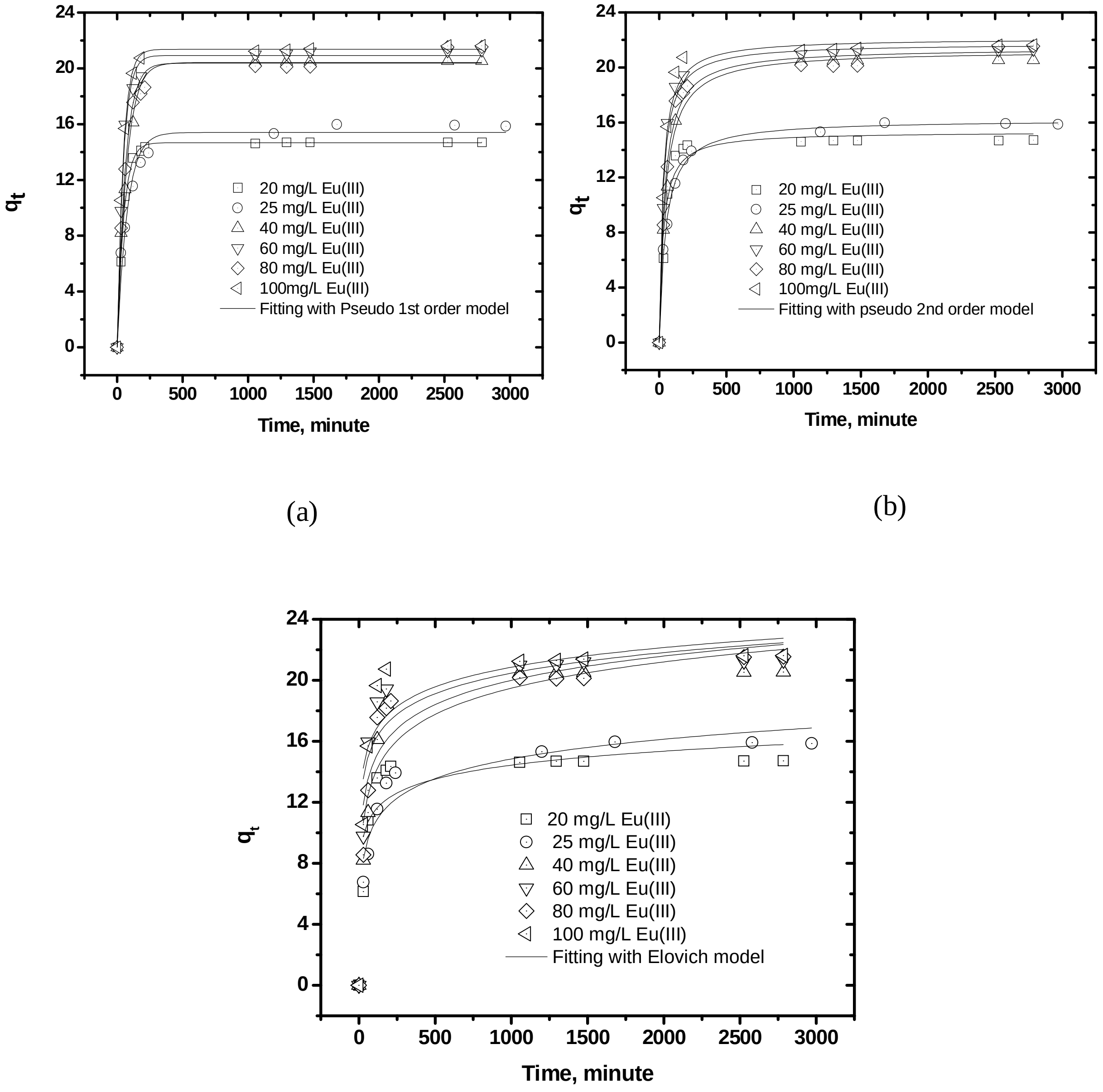

(a) (b)

(c)

Fig. 4.9. Plots on the time dependence of the sorption capacity of the PIMs using varying Eu(III) concentrations in 1 M $HNO_3$ (15 mL samples). PIM composition: 25.6% T-DGA, 53.9% NPOE, and 20.5% CTA; Weight of PIM: 0.018 g.

The experimental uptake data of Eu(III) were fitted with different kinetic model equations, viz., pseudo-first order or Lagergren model [**154**], pseudo-second order or Ho model [**155**], and Elovich models [**156**]. The different equations for the models are given in the following sections.

#### 4.3.5.2.1. The Lagergren's pseudo-first order model

The Lagergren pseudo-first order model [**154**] is given by Eq. (4.3):

$$\frac{dq}{dt} = k_1(q_e - q_t) \tag{4.3}$$

On integrating Eq. (4.3) and applying the boundary conditions, $q_t = 0$ at $t = 0$ and $q_t = q_t$ at a given time 't', the following equation is obtained:

$$q_t = q_e(1 - \exp(-k_1 t)) \tag{4.4}$$

where, $k_1$ ($min^{-1}$) is the pseudo-first order rate constant while $q_e$ and $q_t$ are the sorption capacities expressed as the amount of metal ion retained (in mg) per g of the PIM at equilibrium and at time t, respectively.

Eq. (4.4) can be written in the linearized form as:

$$\log(q_e - q_t) = \log q_e - (\frac{k_1 \cdot t}{2.303}) \tag{4.5}$$

The plot of $\log(q_e$-$q_t)$ vs t gave a straight line plot, whose slopes gave the pseudo-first order rate constant, $k_1$.

#### 4.3.5.2.2. The pseudo-second order model (Ho)

The pseudo-second order or the Ho model [**155**], which is based on the assumption that the rate-limiting step may be chemisorption, is given by Eq. (4.6):

$$q_t = \frac{k_2 q_e^2 t}{1 + k_2 q_e t} \tag{4.6}$$

where, $k_2$ (g/mg min) is the pseudo-second order rate constant, while $q_e$ and $q_t$ have the same meaning as mentioned above. The linearized form of Eq. (4.6) can be expressed as:

$$\frac{t}{q_t} = \frac{1}{k_2 q_e^2} + \frac{1}{q_e} t \qquad (4.7)$$

The rate constant ($k_2$) can be obtained from the straight line plots of $t/q_t$ vs t.

#### 4.3.5.2.3. The Elovich model

When the uptake data do not fit into either of the above two models, the Elovich model [**156**] is used. The basic equation used in the Elovich model is given as,

$$q_t = \frac{1}{\beta}\ln(\alpha\beta) + \frac{1}{\beta}\ln t \qquad (4.8)$$

where, $\alpha$ (mg/g min) is the sorption initial rate and $\beta$ (g/mg) is the desorption constant related to the degree of surface coverage and to the activation energy of chemisorption.

In order to fit Eq. (4.4) (pseudo-first order or Lagergren model), Eq. (4.6) (pseudo-second order or Ho model), and Eq. (4.8) (Elovich model) with the experimental data obtained from the uptake studies using PIMs containing T-DGA or C4DGA, non-linear fitting was executed using the Origin Pro 8.1 program and the fitted plots are shown in Fig. 4.9.

Table 4.4. Kinetic parameters for the sorption of Eu(III) on PIM with composition: 25.6% T-DGA, 53.9% NPOE, and 20.5% CTA.

| $Eu^{3+}$ Initial concent-ration (mg/L) | $q_{e,exp}$ (mg/g) | Removal (%) | Pseudo $1^{st}$ order | | | | Pseudo $2^{nd}$ order | | | | Elovich model | | | |
|---|---|---|---|---|---|---|---|---|---|---|---|---|---|---|
| | | | $q_1$ (mg/g) | $Kp_1$ x$10^3$ ($min^{-1}$) | $R^2$ | $\chi^2$ | $q_2$ (mg/g) | $K_{p2}$ x$10^3$ (g/mg min) | $R^2$ | $\chi^2$ | α (mg/gmin) | β (g/mg) | $R^2$ | $\chi^2$ |
| 20 | 14.7 | 88.3 | 14.671 | 20.40 | 0.997 | 0.078 | 15.325 | 2.3 | 0.967 | 0.671 | 75.084 | 0.758 | 0.868 | 2.455 |
| 25 | 16.0 | 76.1 | 15.405 | 13.26 | 0.975 | 0.754 | 16.209 | 1.34 | 0.996 | 0.085 | 5.386 | 0.537 | 0.949 | 0.999 |
| 40 | 20.5 | 61.6 | 20.416 | 14.08 | 0.996 | 0.223 | 21.254 | 1.07 | 0.99 | 0.255 | 6.341 | 0.403 | 0.931 | 1.926 |
| 60 | 21.3 | 42.6 | 20.923 | 21.49 | 0.993 | 0.146 | 21.750 | 1.68 | 0.987 | 0.365 | 71.554 | 0.514 | 0.926 | 3.522 |
| 80 | 21.5 | 31.6 | 20.373 | 16.19 | 0.986 | 0.325 | 21.423 | 1.24 | 0.988 | 0.307 | 14.007 | 0.436 | 0.927 | 2.065 |
| 100 | 21.6 | 26.0 | 21.363 | 22.12 | 0.999 | 0.014 | 22.122 | 1.78 | 0.984 | 0.403 | 139.363 | 0.538 | 0.916 | 2.087 |

The resulting kinetic parameters are presented in Table 4.4. The correlation coefficients ($R^2$) and the non-linear parameters ($\chi^2$) for the fitting, measure the closeness between the experimental data with the predicted data of the models. The best fitting between the models and the experimental kinetic data is obtained if the value of $R^2$ is close to or equal to 1.0 and the value of $\chi^2$ is close to or equal to zero. The results presented in Table 4.4 indicate best matching with the fittings obtained for the pseudo-first order model i.e., the sorption kinetics conform to the Lagergren model. However, when the experimental data were fitted to the linearized form of the pseudo-first order model, a very poor fitting was obtained (*Annexure-II*, Fig. A2.7a). Analogous good non-linear fitting and poor linear fitting have been reported in the literature [**133**]. On the other hand, reasonably good fittings for both the linearized and the non-linear forms of the pseudo-second order model (*Annexure-II*, Fig.A2.7b) can be seen [**149**]. When the sorption capacity values ($q_1$ or $q_2$), obtained from the kinetic models were compared with the experimentally obtained equilibrium sorption capacities ($q_{e,exp}$) for all the initial concentrations of Eu(III), the $q_1$ values obtained from the pseudo-first order model showed excellent match. The values of $R^2$, $\chi^2$, and the sorption capacity ($q_1$), as obtained with the fitting with the pseudo-first order model (non-linear), validate the pseudo-first order model in this case (Table 4.4).

Eq. (4.1) indicates that the desorbing tendency of the loaded metal ion from the PIM should decrease with increasing concentration of the metal ion in the feed solution. The theoretical maximum sorption capacity of the PIM containing 25.6% T-DGA and assuming 1:1 complex formation with Eu(III) is 25.6 mg/g of the PIM. The total amounts of T-DGA which corresponds to 25.6% T-DGA (100 mg T-DGA taken in the total weight of 390 mg of the PIM) in the PIMs equals to $6.58 \times 10^{-5}$ (M.W.of T-DGA is 1520) moles of T-DGA and thus assuming a 1:1 complex formation with Eu(III) suggests the theoretical maximum sorption capacity is 25.6 mg/g of the PIM. The maximum sorption capacity of the PIM is found to be very close to the experimentally observed sorption capacity of the membrane at equilibrium (27.0 mg/g of PIM) and also very close to the equilibrium sorption capacity obtained by the fitting with the pseudo-second order model for the sorption of Eu(III) with the initial concentration of 100 mg/L. This suggested that not only the kinetics of sorption is pseudo-second order, but also that the rate-limiting step is the chemisorption of Eu(III) by the T-DGA based PIM. This may occur by a 1:1 reaction of Eu(III) and T-DGA as mentioned in Eq. (4.1) (m=1, n=3), on the surface of the PIM, followed by the diffusion of the cation-carrier species to the bulk of the membrane with the simultaneous diffusion of an equivalent amount of the free carrier towards the surface of the membrane to complex more of the cation and eventually leading to the saturation of the membrane at higher Eu(III) concentrations. The TIMM studies also support the carrier diffusion mechanism for the transport of Eu(III) in this case (*vide supra*). We have observed a similar phenomenon with the T2EHDGA based PIMs for the sorption kinetics studies of Eu(III) [**135**]. The gradual saturation of the membrane can also be observed from the decreasing trend of the Eu(III) removal percentage from the solution at higher initial Eu(III) concentrations. The dynamics of Eu(III) sorption onto the T-DGA-based PIM can be summarized as: (a) the sorption of Eu(III) follows pseudo-second order kinetics as well as the Elovich model (Fig.A2.7c, *Annexure-II*) and (b) the rate-limiting step is chemisorption.

### 4.3.5.3. Isotherm studies

The experimentally obtained equilibrium uptake data ($q_e$, $C_e$) of Eu(III) of the T-DGA containing PIMs were fitted with four different isotherm models, namely Langmuir, Freundlich, Dubinin-Radushkevich, and Redlich-Peterson [**135, 157-160**]. The different isotherm model equations are discussed below.

### 4.3.5.3.1. The Langmuir isotherm

Langmuir isotherm model [**161**] is the simplest of the four models which is based on the following assumptions i) adsorption of the sorbate takes place onto the monolayer of the sorbent ii) all the adsorption sites are energetically equivalent with no lateral and steric interactions between the adsorbed metal ions even on the adjacent sites and iii) the enthalpy of adsorption is constant. The Langmuir isotherm model is given by the following equation:

$$q_e = \frac{K_L C_e q_{max}}{1 + K_L C_e} \qquad (4.9)$$

where, $q_e$ is the amount of Eu retained (in mg) per gram of the PIM at equilibrium, i.e., the sorption capacity (mg/g) of the PIM at equilibrium while $q_{max}$ [**136**] is the maximum sorption capacity (in mg/g) of the PIM corresponding to the complete monolayer coverage. On the other hand, $C_e$ is the equilibrium concentration of Eu in solution whereas $K_L$ is the Langmuir constant related to the energy of adsorption. The separation factor or equilibrium parameter ($R_L$) is inversely related to the Langmuir constant and is defined by the equation:

$$R_L = \frac{1}{K_L C_0} \qquad (4.10)$$

where, $C_0$ is the initial Eu concentration in the feed solution. The value of $R_L$ indicates whether the adsorption process is favorable ($0 < R_L < 1$), unfavorable ($R_L > 1$), linear ($R_L = 1$) or irreversible ($R_L = 0$) [**157**].

### 4.3.5.3.2. The Freundlich isotherm

The Freundlich isotherm model [**162**] is based on an empirical equation generally applied for a heterogeneous surface and is based on the assumption that the different adsorptions sites present in the sorbent involve different adsorption energies. This model is not restricted to monolayer adsorption, but the possibility exists for multilayer adsorption when $C_e$ becomes larger. The Freundlich equation is commonly given as:

$$q_e = K_F C_e^N \tag{4.11}$$

where, $K_F$ is the Freundlich constant (L/mg) defined as the sorption capacity of the PIM at the unit equilibrium concentration of Eu(III) in the solution. The value of the exponent 'N' in Eq. (4.11) determines the nature and the extent of the adsorption process as well as the heterogeneity of the surface. When $N < 1$, the adsorption is favorable indicating a chemisorption process, i.e., a chemical reaction is involved. On the other hand, when $N > 1$ the adsorption is weak in nature, while for $N = 1$, all the active centers on the surface are equivalent and follow a linear adsorption isotherm [**163**].

#### 4.3.5.3.3. The Dubinin-Radushkevich isotherm

The Dubinin-Radushkevich isotherm model (D-R model) [**164**] is an empirical model generally applied to describe the adsorption mechanism onto a heterogeneous surface with a Gaussian energy distribution. The model is often fitted with high solute activities as well as intermediate solute concentration ranges. The D-R model is given by the following equation,

$$q_e = q_D \exp\left( -B_D \left[ RT \ln\left(1 + \frac{1}{C_e}\right)\right]^2 \right) \tag{4.12}$$

Or, in the logarithmic form is commonly presented as

$$\ln q_e = \ln q_D - B_D \left[ RT \ln\left(1 + \frac{1}{C_e}\right)\right]^2 \tag{4.13}$$

where, $B_D$ is the D-R isotherm constant ($mol^2/J^2$), $q_D$ is the saturation uptake capacity of the sorbent (in mg/g) (T-DGA-based PIM in the present case), R and T represent the gas constant

(8.314 J/mol K) and the absolute temperature (K), respectively. The mean free energy (E) of the metal ion (energy required to remove a metal ion from its sorption space to infinity) can be computed from the value of $B_D$ given in the following expression:

$$E = \frac{1}{\sqrt{2B_D}} \tag{4.14}$$

The value of E decides the nature of the adsorption process [**165, 166**].

### 4.3.5.3.4. The Redlich-Peterson isotherm

The Redlich-Peterson isotherm is an empirical equation involving three parameters [**158**] widely used as a compromise between the Langmuir and the Freundlich isotherm models. It describes the adsorption equilibrium over a wide concentration range of the solute. The Redlich-Peterson isotherm is given by the following expression:

$$q_e = K_R \frac{C_e}{1 + a_R \cdot C_e^{\beta}} \tag{4.15}$$

where, $K_R$ (L/g), $a_R$ (L/mg), and β represent the Redlich-Peterson constants. The above equation is reduced to the Langmuir isotherm if β=1, and to the Freundlich isotherm when $a_R.C_e.\beta >> 1$.

The non-linear fitting between the experimental data and the different isotherm models was performed using Eqs. (4.9), (4.11), (4.12) and (4.15) and the results are presented in Fig. 4.10 while the different parameters obtained after non-linear curve fitting are listed in Table 4.5.

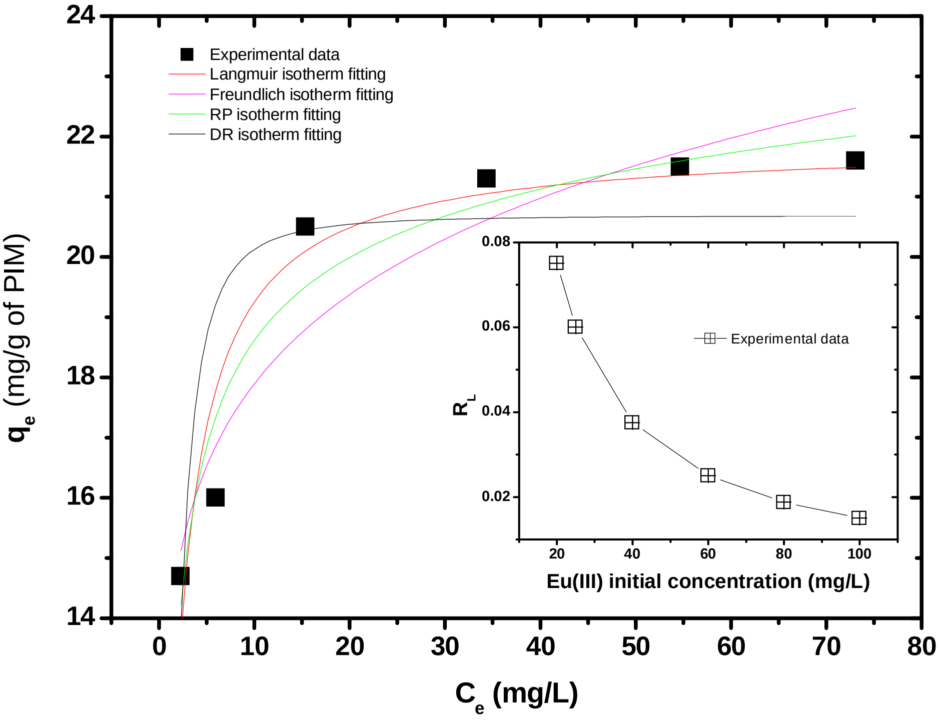

Fig. 4.10. Isotherm fitting for Eu(III) sorption (varying Eu concentrations in 1 M $HNO_3$ (15 mL samples)). PIM composition: 25.6% T-DGA, 53.9% NPOE, and 20.5% CTA; Weight of PIM: 0.018 g. The inset of the figure presents a variation of $R_L$ with the initial concentration of Eu

The straight line fitting plots are presented in *Annexure-II* (Figs. A2.8a-c). It is evident from both Table 4.5 and Fig. 4.10 that the experimental uptake data can be best fitted with the Redlich-Peterson isotherm model, the $R^2$ value being very close to unity (0.946) and the $\chi^2$ value is very small (0.188), while it is worst fitted with the D-R isotherm model, having $R^2$ and $\chi^2$ values of 0.657 and 0.686, respectively [**149**]. Out of the Langmuir and the Freundlich isotherm models, the higher value of the correlation coefficient ($R^2$) and the lower value of the non-linear parameter ($\chi^2$) obtained with the latter isotherm model, reflects the presence of a heterogeneous surface. It is also evident from the inset in Fig. 4.10 that the value of $R_L$ lies between 0.01 and 0.075 and it decreases upon increasing initial concentration of Eu, which indicates that the sorption process is more favorable at higher Eu concentrations.

Table 4.5. Isotherm parameters for the sorption of Eu(III) onto the PIM with the composition: 25.6% T-DGA, 53.9% NPOE, and 20.5% CTA.

| Model | Model constant | | | Statistical analysis | |
|---|---|---|---|---|---|
| Langmuir | $q_m$ (mg/g) | $K_L$ (L/mg) | | $R^2$ | $\chi^2$ |
| | 21.890 | 0.730 | | 0.888 | 0.267 |
| Freundlich | $K_F$ (L/mg) | N | | $R^2$ | $\chi^2$ |
| | 13.744 | 0.114 | | 0.870 | 0.269 |
| D-R | $q_D$ (mg/g) | $B_D$ (mol$^2$/J$^2$) | E (kJ/mol) | $R^2$ | $\chi^2$ |
| | 20.691 | $4.910 \times 10^{-7}$ | 1.009 | 0.657 | 0.686 |
| Redlich-Peterson | $K_R$ (L/g) | $a_R$ (L/mg) | β | $R^2$ | $\chi^2$ |
| | 26.774 | 1.514 | 0.946 | 0.881 | 0.188 |

The results from the Freundlich isotherm fitting show that the value of N is less than unity, which further supports the favorable sorption of Eu(III) onto the PIM. The maximum sorption capacity obtained with the application of the Langmuir model is 21.890 mg Eu(III)/g of PIM, assuming a monolayer sorption process which is closer to the observed sorption capacity (27.0 mg/g) at equilibrium as compared to the value obtained by the D-R isotherm. Also, out of the above mentioned isotherm models, the experimental equilibrium data of Eu(III) sorption onto the T-DGA-based PIM is best fitted with the Redlich-Peterson model.

Table 4.6 gives a comparison of the maximum loading capacities of the T-DGA containing PIM along with that for a T2EHDGA based PIM [**135**]. Though the T2EHDGA based PIM showed a higher loading capacity, the extractant content is about 2.5 times higher. Table 4.6 also lists the loading capacities of some TODGA containing resin materials reported in literature, which are significantly lower, though the extractant loading is significantly higher. This can be attributed to a better extractability of the T-DGA extractant as compared to other DGA extractants such as TODGA or T2EHDGA.

Table 4.6. Comparison of Eu(III) sorption capacities of different DGA-based sorbents

| Sorbent | % DGA loading | Sorption capacity ($q_m$) in mg/g | Reference |
|---|---|---|---|
| T-DGA based PIM | 25.6 | 27.0 | This study |
| T2EHDGA based PIM | 69.0 | 33.0 | [**135**] |
| TODGA resin | 40.0 | 13.07 | [**167**] |
| TODGA resin | 50.0 | 20.0 | [**168**] |

### 4.3.6. Comparative extraction-stripping studies with the T-DGA and C4DGA based PIMs

It was important to investigate the reusability of the PIMs for successive metal ion uptake studies. Therefore, an extraction study of Am(III) was performed in 1 M $HNO_3$ using a 4 $cm^2$ PIM followed by the regeneration of the PIM by stripping the loaded Am(III) with 1 M α-hydroxy-isobutyric acid (α-HIBA) solution. Subsequently, the extraction and stripping studies were carried out for a second or third time using the regenerated PIMs. Fig. 4.11 gives the extraction-stripping profiles of Am(III) with PIMs containing T-DGA as the carrier extractant whereas Fig. 4.12 shows analogous data with the C4DGA based PIMs.

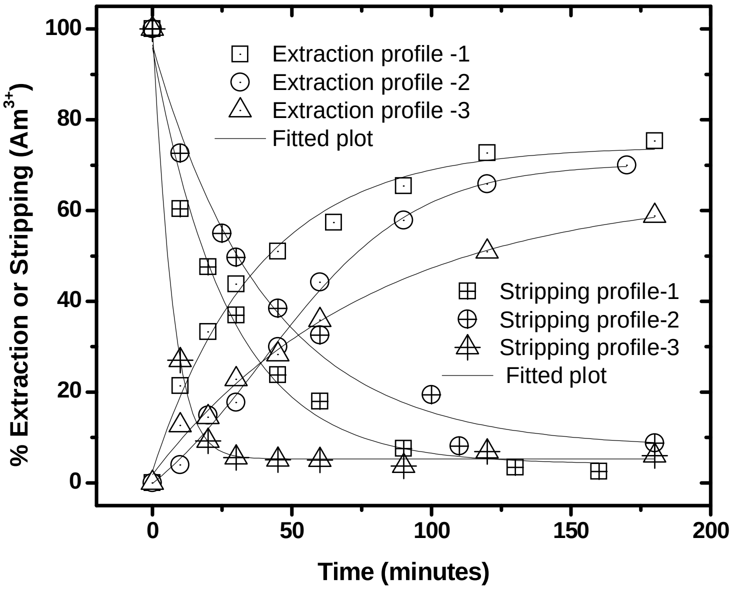

Fig. 4.11. Extraction-stripping profiles for Am(III) uptake using a PIM of composition: 25.6% T-DGA, 53.9% NPOE, and 20.5% CTA. Feed: 1 M $HNO_3$ (20 mL). Stripping was done using 1 M α-HIBA solution (20 mL).

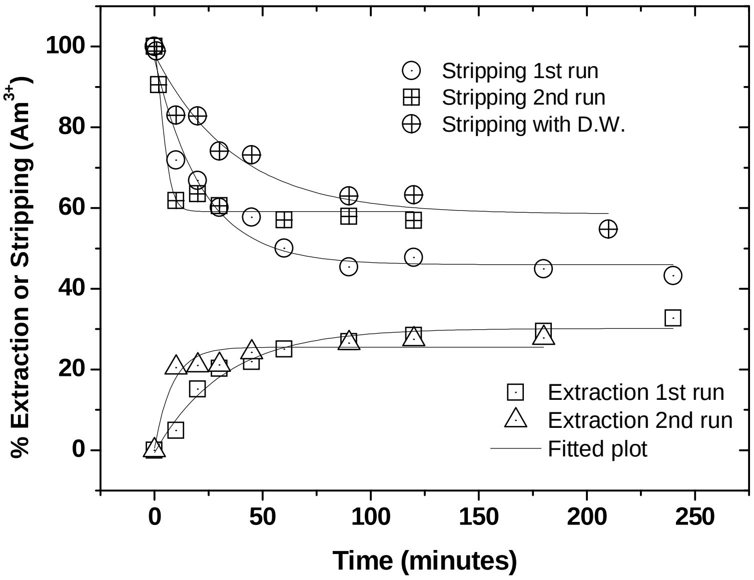

Fig. 4.12. Extraction-stripping profiles for Am(III) uptake using a PIM of composition:: 6.5% C4DGA-octyl, 67.7% NPOE, 25.8% CTA; Uptake: from 1 M $HNO_3$ (5 mL); Stripping: using 1 M α-HIBA (5 mL); Weight of the PIM: 4.0 ± 0.5 mg; D.W.: Distilled water

It is evident from the figures that the uptake efficiency of both the PIMs are best when those are freshly prepared and it deteriorates with successive cycles suggesting the limited reuse possibility of the PIMs as sorbent. The back-extraction studies with 1 M α-HIBA as the stripping agent indicated that although quantitative stripping of Am(III) was possible in ca. 90 minutes with the T-DGA based PIMs, only ca. 45% stripping was seen in 2 h with the C4DGA based PIMs. On the other hand, only around 30% stripping of Am(III) was possible from the C4DGA based PIMs when distilled water was used as the strippant (Fig. 4.12). This indicated that even though α-HIBA was a better stripping agent as compared to distilled water, the former was not able to strip the actinide ion from the C4DGA based PIM quantitatively. The slow kinetics of stripping of the actinide ions by the C4DGA based ligands was attributed to the stronger bonding of the ligand with the actinide ions [**143**].

## 4.4. TRANSPORT STUDIES

The transport behavior of various actinide ions such as U(VI), Th(IV), Pu(IV) and Am(III) by the T-DGA and C4DGA based PIMs were also studied and the results are discussed in detail in this Chapter. The transport experiments were carried out in a two compartment cell with 1 M nitric acid concentration as the feed containing the target radio tracers and 1 M α-HIBA as the strippant in the receiver compartment.

### 4.4.1. Effect of carrier concentration in the PIM

As already discussed before, the carrier extractant plays the most important role amongst all the components of the PIM in the metal ion transport. The complex or ion-pair formed between the metal ion and the carrier at the feed – PIM interface is picked up by the membrane and is subsequently solubilized in the membrane and facilitates the metal ion transport across the membrane. The membrane permeability and selectivity are strongly influenced by both the physicochemical properties of the carrier extractant and the target solute and also on the composition of the PIM as well as those of the feed and the strip phases. In order to understand the mechanism of metal ion transport (whether the carrier-diffusion mechanism [**122**] or the fixed-site jumping mechanism [**130**]) experiments were carried out to study the effect of T-DGA concentration on the transport of Am(III) by varying the T-DGA content from 6.5% to 25.6% in the PIMs (Table 4.7). The respective transport profiles are shown in Fig.A2.13 (*Annexure-II*). It is evident from Table 4.7 that the cumulative transport of Am(III) to the strip phase after 2 h increased from 43.4% to 87.4% when the T-DGA concentration was made to increase from 6.5% to 21.6% in the PIM. A further increase in the T-DGA content to 25.6% slightly decreased the transport to 84.8%. Quantitative (~100%) transport was seen after 24 h with the PIMs containing 21.6% as well as 25.6% T-DGA.

Table 4.7. Effect of T-DGA content in the PIMs on Am(III) transport with fixed CTA(80 mg) and NPOE (210 mg) contents[a]

| T-DGA content (mg) | % Uptake (2 h) | % Transport (2 h) | $P_f$ (cm/s) X $10^5$ |
|---|---|---|---|
| 20 | 60.2 (96.9)[b] | 43.4 (87.2)[b] | 0.691 ± 0.038 |
| 80 | 95.8 (>99.9) | 87.4 (100.0) | 2.893 ± 0.034 |
| 100 | 93.4 (>99.9) | 84.8 (99.9) | 2.367 ± 0.053 |

*Note: [a] Feed: 20 mL 1 M* $HNO_3$*; Strip solution: 20 mL 1 M α-HIBA; PIM: 4.94* $cm^2$ *size with average weight of 62 ± 1 mg; [b]Values in parentheses indicate respective metal ion uptake and transport after 24 h.*

The permeability coefficient (P) values of Am(III) increased significantly when the T-DGA concentration in the PIMs increased from 6.5% to 21.6% after which a slight decrease was observed when T-DGA content in the PIM was further increased to 25.6% (Table 4.7). The TODGA based PIMs containing 58% TODGA showed higher permeability coefficient for Am(III) transport under similar experimental conditions which is in line with the lower transport rates observed in case of T-DGA as compared to TODGA as the carrier extractant

[**153**]. The effective diffusion coefficient ($D_{eff}$) as determined by the lag-time method (*Annexure-II*, Fig.A2.16**)** for the transport of Am(III) by the T-DGA based PIMs ($7.56 \times 10^{-9}$ $cm^2/s$) was found to be about 1 order of magnitude lower than that reported with TODGA-based PIMs ($8.89 \times 10^{-8}$ $cm^2/s$) [**153**]. This was attributed to factors related to the ligand conformational changes during the complex formation and not related to the size of the metal ion-carrier complex where one would expect a bulkier complex with Am(III)-TODGA than that of the Am(III)-TDGA system (assuming 1:1 complexation).

It was also expected that the carrier structure might influence the metal ion transport across the membrane. Walkowiak et al., [**169**] studied the transport of alkali metal cations across PIMs containing a sym-(alkyl)-dibenzo-16-crown-5-oxyacetic acid with side arms of different alkyl chain lengths geminally attached to the lariat ether as the carrier extractant. Maximal flux was found when the alkyl side arm contained nine carbon atoms with considerably lower transport efficiency being seen when the alkyl chain was longer or shorter. The transport data with the PIMs with varying C4DGA content (in %) are included in Table 4.8. It can be seen from the Table 4.8 that ca. 3.4% Am(III) transport was observed (in 2 h) for the PIMs with the composition of 5.1% C4DGA, 53.9% NPOE, and 41.0% CTA, while ca. 5.7% transport of the metal ion was noticed with the PIMs of the composition, 9.8% C4DGA, 51.2% NPOE, and 39.0% CTA in the same time period. Finally, PIMs of the composition, 70% NPOE, 3.3% C4DGA, 26.7% CTA, and 67.7% NPOE, 6.5% C4DGA, and 25.8% CTA showed 1.9% and 13.1% Am(III) transport, respectively in 2 h.

Table 4.8. Transport data of Am(III) with different compositions of C4DGA containing PIMs. Feed: 1 M $HNO_3$; Receiver: 1 M α-HIBA at pH 3.0.

| PIM Composition | | | $P_f$ X $10^5$ (cm/s) | $P_s$ X $10^5$ (cm/s) | % Uptake from source phase at 2h[a] | % Transport to receiver phase at 2h[a] |
|---|---|---|---|---|---|---|
| % CTA | % NPOE | % C4DGA | | | | |
| 15.6 | 82.4 | 2.0 | 2.29 | 2.13 | 6.8 (35.7) | 4.3 (30.3) |
| 26.7 | 70.0 | 3.3 | 3.00 | 1.70 | 4.8 (23.7) | 1.9 (17.9) |
| 41.0 | 53.9 | 5.1 | 3.58 | 2.10 | 12.9 (35.0) | 3.4 (25.1) |
| 39.0 | 51.2 | 9.8 | 5.21 | 2.88 | 12.7 (61.7) | 5.7 (39.2) |
| 25.8 | 67.7 | 6.5 | 11.78 | 10.1 | 18.4 (64.9) | 13.1 (49.9) |

*Note: [a]Values between parentheses refer to the data after 24 h.*

This indicated that at comparable NPOE content, the transport efficiency increased with increasing C4DGA content in the PIM. The same trend was also seen in the permeability coefficient (P) values (Table 4.8). The higher permeability coefficient values from the feed side ($P_f$) than strip side ($P_s$) indicated that the metal ion was trapped inside the membrane during the transport studies.

### 4.4.2. Effect of plasticizer concentration in the PIM

As already discussed, the plasticizer acts as a solvent in the PIM and makes the membrane suitable for metal ion transport. Table 4.8 shows the effect of plasticizer content on the transport of Am(III) by the C4DGA based PIMs. It was evident from the transport data (Table 4.8) that the transport of Am(III) to the strip solution was rather small (2- 4% after 2 h) when the C4DGA content was <5% in the PIM, even though the NPOE content was kept in the range of 50-80%. However, the transport efficiency sharply rose to 13.1% after 2 h with the PIM containing higher C4DGA (6.5% C4DGA and 67% NPOE). Further increase in the C4DGA content to 9.8% with a corresponding decrease in the NPOE content to 51.2%, resulted in a decrease in the transport efficiency of the PIM to 5.7% after 2 h. These results indicated that similar to C4DGA, the NPOE content in the PIM also influences the transport efficiency and as a consequence optimization of the concentration of the latter was required to maximize the transport efficiency.

Therefore, the subsequent transport studies with C4DGA based PIM were carried out with 6.5% C4DGA, 67.7% NPOE, and 25.8% CTA which was also the PIM composition employed for the uptake studies (*vide supra*). Furthermore, in order to assess the possibility of metal ion transport using PIMs containing low amounts of T-DGA, the transport of various actinide ions by T-DGA based PIM was carried out with the PIM composition of 6.5% T-GA, 67.7% NPOE and 25.8% CTA.

### 4.4.3. Comparative transport behavior of actinides with the T-DGA based PIMs

Table 4.9 summarizes the transport data including the permeability coefficient values obtained for the transport of U(VI), Pu(IV), Th(IV) and U(VI) with the PIMs of the composition: 6.5% T-DGA, 67.7% NPOE and 25.8% CTA. The transport of actinide ions into the receiver side after 2 h followed the trend: Am(III) > Pu(IV) ≫ U(VI) ≥ Th(IV), which was contrasting to that observed with the uptake studies (Pu(IV) > Am(III) > Th(IV) ~ U(VI)). The difference between the uptake and the transport processes is that the latter also involved the simultaneous stripping of the metal ions. Since the extraction and the stripping of the metal ions was faster than the transport rates of the metal ions, the rate-determining step was the bulk diffusion of the metal-carrier complex across the thickness of the membrane. Thus, the transport efficiency strongly depended on the bulk diffusion of the metal ion.

Table 4.9. Uptake and transport of various actinide ions by T-DGA based PIMs[a] using 1 M $HNO_3$ as the feed (20 mL) and 1 M α-HIBA as the receiver (20 mL)

| Metal ion | % Uptake (2 h)[b] | % Transport (2 h)[b] | $P_f$ (cm/s) x $10^5$ |
|---|---|---|---|
| U(VI) | 5.3 (31.8)[b] | 2.5 (24.0) | 0.04 ± 0.00 |
| Th(IV) | 15.2 | N.D.[c] | 0.12 ± 0.03 |
| Pu(IV) | 21.5 (86.3) | 18.5 (73.3) | 0.24 ± 0.04 |
| Am(III) | 60.2 (96.9) | 43.2 (87.2) | 0.69 ± 0.04 |

*Note: [a]:PIM (4.94 $cm^2$ with av.wt. 62 ± 1 mg) composition: 6.5% T-DGA, 67.7% NPOE, 25.8% CTA; [b]: Values in parentheses refer to the metal ion uptake and transport after 24 h; [c]N.D.: Not detected.*

It was clear from the mass balance data (Table 4.9) that a considerable amount of the actinide ions was held up within the PIM during the 2 h transport period, indicating slow diffusion of the metal ion through the membrane. This was confirmed by carrying out gamma ray counting of the PIM used for the Am(III) transport, which accounted for the missing counts (total counts at the beginning of the experiment minus the sum of counts in the feed and receiver compartment after 2 h). We have also observed retention of actinides by a CTA-based PIM when TODGA and other several substituted diglycolamides were used as the carrier extractants [**153**]. The P values, as seen from the feed side, followed the trend: Am(III) > Pu(IV) > Th(IV) > U(VI). Surprisingly, Th(IV) ion was not detected in the receiver compartment during 2 h of transport. It appears that in view of the very low concentration of Th ($<10^{-10}$ M), the complex may be having more than one T-DGA molecule per Th(IV) ion, consequently resulting in bulky complexes which are very slow diffusing. On the other hand, uranyl ion complexation may be highly unfavourable which may explain the detection of U in the receiver compartment, while no Th was detected.

### 4.4.4. Comparative transport behavior of actinides with the C4DGA based PIMs

The transport profiles of the actinide ions Am(III), Th(IV), and Pu(IV) as seen with the PIMs containing C4DGA as the carrier extractant are presented in Table 4.10 as well as in Fig.A2.14 (*Annexure-II*). The transport studies involving uranyl ion were not carried out in view of negligible uptake of the metal ion as noted during the uptake studies (*vide supra*). The trend for the transport of the actinide ions into the receiver compartment was found to be Pu(IV) > Am(III) > Th(IV) after 2 h (Table 4.10), which was entirely different from that seen during the uptake studies (Am(III)>Pu(IV)>Th(IV)). This difference in the uptake and the transport behavior of the actinide ions was also seen with the T-DGA based PIMs (*vide supra*). It is reported that the diffusion of the C4DGA-actinide ion complex is slow due to its bulky nature. On the other hand, the stripping of the actinide ions from their respective C4DGA complex is also slow due to kinetic factors well known in macrocyclic ligand complexes [**143**]. Since Am(III) is strongly held in the core of the four DGA arms of the C4DGA, it is more difficult to strip from the metal-carrier complex than the tetravalent Pu(IV) and Th(IV) ions, which are comparatively weakly bound by the ligand. Poor transport of Th(IV) into the receiver side seen in the present study was attributed to a higher ligand to metal ion ratio ($Th^{4+}$ $<10^{-10}$ M), which may cause association of more than one C4DGA molecule in the complex leading to a significant increase in its molar volume [**135, 170**]. Similar reason for the poor transport of Th(IV) ion into the receiver side was also observed in the case of the PIMs containing T-DGA (*vide supra*). In the case of T2EHDGA-based PIMs, a similar trend was found for the transport of the actinide ions [**135**].

Table 4.10. Transport data of actinide ions by the PIMs of optimized composition: 6.5% C4DGA, 67.7% NPOE, 25.8% CTA; Feed: 1 M $HNO_3$; Receiver: 1 M α-HIBA at pH 3.0.

| Actinide ion | % uptake from feed phase at 2h (24 h) | % transport to the receiver phase at 2h (24 h) | $P \times 10^5$ (cm/sec) |
|---|---|---|---|
| Am(III) | 18.4 (64.9) | 13.1 (49.9) | 11.78 ± 1.14 |
| Th(IV) | 13.3 (40.3) | 9.6 (34.6) | 9.56 ± 0.07 |
| Pu(IV) | 46.7 (84.4) | 35.0 (81.4) | 47.5 ± 0.10 |

The determined P values are presented in Table 4.10 which followed the order Pu(IV) > Am(III) > Th(IV). This is the same order as found for the uptake of actinides by the PIMs from the feed solution. The effective diffusion coefficients ($D_{eff}$ values) were determined for Am(III), Pu(IV) and Th(IV) using the lag-time method as already discussed before. The lag-time values for the individual cases were determined graphically (*Annexure-II*, Figs.A2.17-A2.19). The $D_{eff}$ values were found to follow the trend Pu(IV) > Am(III) > Th(IV), which is identical to the transport trend of the actinide ions into the receiver side (Table 4.11).

Table 4.11. $D_{eff}$ values obtained using the optimized PIM composition: 6.5% C4DGA, 67.7% NPOE and 25.8% CTA

| Actinide ion | Thickness of PIM (cm) | Lag Time (min.) | $D_{eff}$ ($cm^2/s$) |
|---|---|---|---|
| Pu(IV) | 0.0085 ± 0.006 | 7.0 | $2.9 \times 10^{-8}$ [a, b] |
| Am(III) | 0.0075 ± 0.006 | 5.0 | $2.7 \times 10^{-8}$ |
| Th(IV) | 0.0075 ± 0.007 | 10.0 | $1.5 \times 10^{-8}$ |

[a] *:TODGA PIM:* $D_{eff} = 4.16 \times 10^{-8}$ $cm^2/s$; [b] *:T2EHDGA PIM:* $D_{eff} = 1.22 \times 10^{-10}$ $cm^2/s$

The $D_{eff}$ values were compared with those obtained with TODGA- and T2EHDGA-based PIMs (Table 4.11). It is clear from the table that the respective $D_{eff}$ values of the actinide ions are smaller with the C4DGA based PIMs as compared to those obtained with the TODGA based PIMs, but higher than those found with the T2EHDGA-based PIMs [**153, 135**]. The higher P values are based on the higher complexation ability of the C4DGA ligand with 4 DGA pendant arms. On the other hand, the lower diffusion coefficient values are due to the slow diffusion of the bulky metal – carrier complexes across the PIMs.

### 4.4.5. Stability of the T-DGA and C4DGA based PIMs

It is very important to evaluate the stability of the PIMs for their long term reusability. The stability studies were performed by using the same PIM repeatedly for the transport of the metal ions while the feed and strippant solutions were replaced with fresh lots in each experiment. The stability of the membrane was assessed by determining the permeability coefficient (P) or the transport efficiency of the transported metal ions for each cycle of operation. In the present study, the stability of the T-DGA and C4DGA based PIMs was assessed by investigating the transport of Am(III) using a feed (1 M $HNO_3$) containing Am(III) tracer and a receiver compartment containing 1 M α-HIBA in a manner analogous to that described above. These studies were conducted for five successive days with 24 h cycles. The transport profiles with the T-DGA and C4DGA based PIMs are shown in Figs.A2.20 and A2.21 (*Annexure-II*) which indicated a continuous decrease in the transport efficiency of Am(III) starting from day 1. The permeability coefficient (P) values also followed the same trend (*Annexure-II*, Tables A2.3 and A2.4). This suggests that the CTA based PIMs containing multiple DGA ligands as the carrier extractant and NPOE as the plasticizer has limited operational life time without any long term reusability possibility. These results are in conformity with the results of the reusability studies involving the PIMs during batch uptake studies by a series of sorption and desorption studies (*vide supra*).

The physical deterioration of the PIMs was also investigated by various characterization techniques as already mentioned before. The FT-IR bands characteristic of T-DGA in the pristine PIMs were found to be present in the PIMs used for stability studies (*Annexure-I*, Fig.A1.11) suggesting insignificant leaching of the extractant. On the other hand, the transmission infrared mapping microscopy (TIMM) profiles, showing the chemical images of the PIMs (*Annexure-I*, Fig.A1.21), suggested significant degradation of CTA. The AFM profiles of the PIMs exposed to 1 M $HNO_3$ for 5 days also showed considerable reduction in the roughness (*Annexure-I*, Fig.A1.25).

## 4.5. CONCLUSIONS

The uptake and transport of various actinides, viz., Am(III), Pu(IV), Th(IV) and U(VI) from acidic feed solution by PIMs containing multiple DGA ligands such as T-DGA and C4DGAwere investigated in detail. The PIMs were characterized by a host of techniques to suggest uniform distribution of the carrier molecules in the bulk of the membranes and also no interaction between the individual components. The sorption kinetics and isotherm with Eu(III) (as a surrogate of $Am^{3+}$) were studied using T-DGA based PIMs and experimental data were fitted with different kinetic model equations as well as sorption isotherms. Transport parameters were obtained by using a two-compartment transport cell containing 1 M $HNO_3$ as the feed and α-HIBA as the receiver phases which gave the trend: Am(III) > Pu(IV) ≫ U(VI) ≥ Th(IV) for the T-DGA containing PIMs while the trend of Pu(IV) > Am(III) >Th(IV) was seen for the C4DGA containing PIMs. The stability and reusability of the PIMs were also investigated though the results were not very promising suggesting that the PIMs cannot be used in metal ion transport for long time.

# CHAPTER 5

# DEVELOPMENT OF AN EUROPIUM(III) ION SENSOR BASED ON TODGA AS THE IONOPHORE

## 5.1. INTRODUCTION

*N,N,N',N'*-tetra-*n*-octyl diglycolamide (TODGA) is widely known as a promising extractant for the extraction of trivalent lanthanides and actinide ions from acidic feed solutions. Sasaki and Chopin [**72**] first reported the tridentate nature of the diglycolamide group where it formed complexes with trivalent metal ions through two carbonyl oxygen and one ether oxygen donor atoms. There are numerous literature reports where an extracting agent can be used as an ionophore in the construction of a potentiometric membrane sensor [**171-174**]. The use of the widely studied extracting agent as an ionophore for the metal ion sensing in polymeric membrane based potentiometric sensor minimizes a great deal of experimental effort in studying the sensitivity, selectivity and stability. A polymeric membrane can become a suitable sensor membrane for a given metal ion, provided it shows very fast interfacial reaction at the membrane - feed interface and very slow transport of the metal ion through the polymeric membrane in a measurable time scale as required for an ion selective electrode [**31**]. It should also possess a preferential interfacial reaction of the given metal ion as compared to other metal ions. Recent studies by us indicated that the TODGA containing polymer inclusion membranes (PIMs) exhibit not only faster extraction kinetics but also preferential extraction of the trivalent actinides over tetravalent and hexavalent actinide ions from dilute nitric acid feed solutions [**153**]. Legin et el., demonstrated the cross-sensitivity of TODGA based membrane sensor towards various lanthanides and thus, suggested the possibility of using it in multi-sensor system of electronic tongue [**175**]. Therefore, it was of interest to evaluate PIMs containing TODGA as a potential membrane for sensing trivalent lanthanide ions from lean acidic feed solutions containing these metal ions. Amongst the lanthanide elements, europium finds wide ranging applications including industrial, nuclear, as well as in house hold appliances [**121, 176-179**]. In view of these, determination of europium, at trace level, is of paramount importance. This Chapter deals with the development of a potentiometric sensor for Europium(III) ion based on PIMs containing TODGA as the ionophore. The first part of this Chapter presents a feasibility study in the construction of a CTA based PIM containing TODGA as the ionophore for the electrochemical sensing of Eu(III) ion from dilute nitric acid solutions. The second part of this Chapter deals with the development of a polyvinyl chloride (PVC) based Eu(III) ion sensor containing TODGA as the ionophore, 2-NPOE as plasticizer and sodium tetra phenyl borate (NaTPB) as the anion excluder. This includes the construction of different membranes containing varying concentrations of the membrane components. The effect of pH, concentration of inner filling solution and the interference effects of different metal ions on the electrode response are presented in the second part of the Chapter. The possibility of the sensor electrode as an indicator electrode for the potentiometric titration of Eu(III) has also been presented in this Chapter. Finally, the determination of Eu(III) in a synthetic mixture containing a known amount of added Eu(III) in the uranyl nitrate sample by the proposed sensor as well as its comparison with ICP-AES result are also discussed.

## 5.2. POTENTIOMETRIC STUDIES

### 5.2.1. Potentiometric studies with the CTA based membranes

#### 5.2.1.1. Effect of inner filling solution

The effect of the inner filling solution on the response of the sensor electrode was studied by using different types of filling solution and recording the potential with respect to changes in the Eu(III) ion concentration (Fig. 5.1).

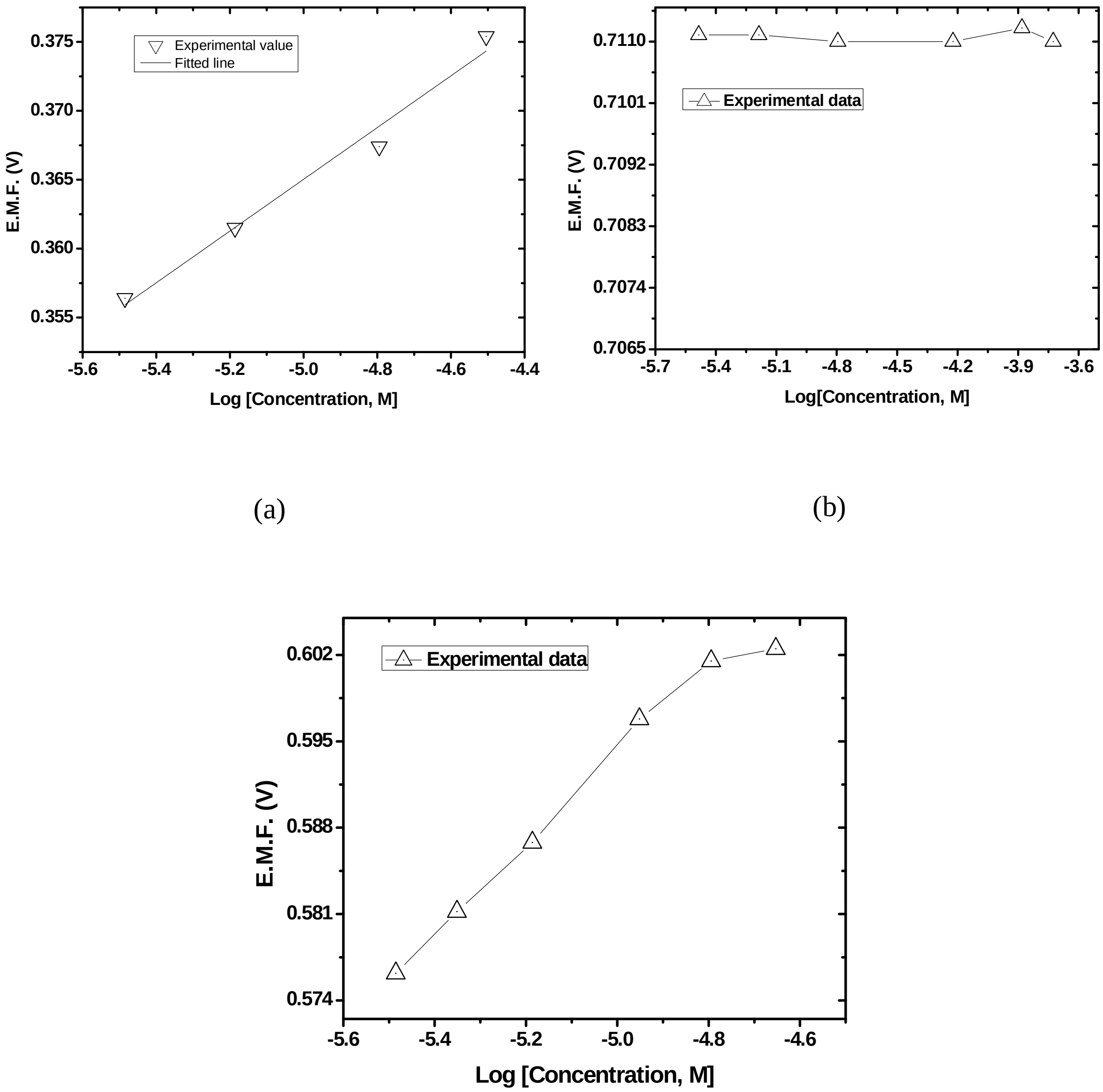

(a) (b)

(c)

Fig. 5.1. Potential response for the TODGA based ion selective electrode for Eu(III) solution in 1 M $HNO_3$; Inner solution (a) 1 M α-HIBA, (b) 1 M $HNO_3$, (c) 100 ppm Eu(III) in 1 M $HNO_3$; Sample solution: Eu(III) in 1 M $HNO_3$; Sample volume: 20 mL; PIM composition: 58% TODGA, 30% NPOE, 12% CTA.

Fig 5.1(a) depicts that when the inner filling solution was 1 M α-HIBA, the slope of the fitted line is 21 mV/decade of concentration for the short linear range of concentration of Eu(III) ($3.3 \times 10^{-6}$ - $3.1 \times 10^{-5}$ M) with a correlation coefficient ($R^2$) of 0.99. However, when the inner filling solution was changed to 1 M $HNO_3$, the potential remained unchanged with the change of Eu(III) concentration (Fig.5.1(b)). This was possibly due to the less tendency of the attachment of $Eu^{3+}$ ion over the membrane due to absence of any driving force exerted by α-HIBA from the inside filling solution. The linear range of potential response further shortened with a corresponding increase in the slope (mV/decade) when 100 ppm Eu(III) in 1 M $HNO_3$ was used as the inner filling solution (Fig.5.1 (c)). Thus, Fig.5.1(a) and Fig.5.1(c) suggest potential developed across the membrane varies linearly with the logarithm of the Eu(III) concentration for a very short range of concentration of Eu(III) in 1 M $HNO_3$ when the polymeric membrane was made with the optimized composition, 58% TODGA, 30% NPOE and 12% CTA.

### 5.2.2. Potentiometric studies with the PVC based membranes

#### 5.2.2.1. Effect of the membrane composition

The details of potential measurement are given in Chapter 2. The electrode potential response was recorded with the addition of Eu(III) in the acetate buffer solution (pH 5.0 ± 0.1) with varying composition of the membrane sensor and the results are summarized in Table 5.1. The membrane sensor without TODGA (S. No. 1; Table 5.1) showed a short linear range ($7.8x10^{-4}$ – $7.3x10^{-3}$ M) and low sensitivity (12.0 ± 0.3 mV/ decade). Increasing the TODGA content in the membrane up to 6.2% did not improve the response of the electrode towards Eu(III) ion (S. No. 2; Table 5.1). When the TODGA content in the membrane was further increased to 12.0 % (S. No. 3; Table 5.1), both the slope and the linear dynamic range were found to increase to become 16.0 ± 0.1 mV/decade and $6.9x10^{-5}$-$1.5x10^{-2}$ M, respectively. A further increase in the TODGA concentration up to 18.5% did not improve the response of the sensor electrode, instead it showed a decrease in the slope (13.0 ± 0.2 mV/decade) and a shorter linear range ($1.5x10^{-4}$-$1.5x10^{-2}$ M) (S. No. 4; Table 5.1). Thus, it showed that the response of the sensor electrode towards Eu(III) ion depends on the optimum concentration of the ionophore in the membrane. The critical micelle concentration (CMC) of TODGA is around 0.1 M [**180**].

Table 5.1. Composition of the membrane ingredients for the europium ion sensor[a,b]

| S. No | Membrane composition (%) | | | | Slope (mV/decade) | LOD (M) | Concentration range (M) |
|---|---|---|---|---|---|---|---|
| | TODGA | PVC | NPOE | NaTPB | | | |
| 1 | - | 26.8 | 69.2 | 4.0 | 12.0±0.3 | $3.8 \times 10^{-4}$ | $7.8 \times 10^{-4}$ - $7.3 \times 10^{-3}$ |
| 2 | 6.2 | 25.6 | 65.6 | 2.6 | 12.0±0.1 | $7.6 \times 10^{-5}$ | $1.5 \times 10^{-4}$ - $9.5 \times 10^{-3}$ |
| 3 | 12.0 | 23.6 | 60.9 | 3.5 | 16.0±0.1 | $6.1 \times 10^{-5}$ | $6.9 \times 10^{-5}$ - $1.5 \times 10^{-2}$ |
| 4 | 18.5 | 31.5 | 47.6 | 2.4 | 13.0±0.2 | $7.5 \times 10^{-5}$ | $1.5 \times 10^{-4}$ - $1.5 \times 10^{-2}$ |
| 5 | 30.3 | 60.6 | - | 9.1 | 17.3±0.1 | $1.2 \times 10^{-6}$ | $1.5 \times 10^{-6}$ - $1.2 \times 10^{-2}$ |

*Note: [a]:0.1 M $Eu(NO_3)_3$ as the inner filling solution; [b]:20 mL acetate buffer at pH 5.0±0.1*

Therefore, with an increase in the TODGA content from 0 to 6.2 % in the PIM does not reach the CMC [**180**]. At 12% TODGA content, the concentration of the extractant is very close to its CMC. It is expected that the PIM be most structured at this TODGA concentration, thus expected to show better sensitivity in the potentiometric measurements. As reported previously, around 3-4 TODGA molecule and 3 nitrate ions are required for binding to a trivalent cation such as Eu(III) [**181, 182**]. At 12 %, which is about 0.12 M of TODGA the effective site for the uptake of Eu(III) is around 0.04 M. The highest concentration at the linear dynamic range of the Eu(III) determined at 12% TODGA concentration was 0.015 M. Therefore, even at the highest Eu(III) concentration, more than 60% of the active site capable of biding with Eu(III) remained vacant. At even higher concentration (more than 12%), additional unstructured TODGA molecule will be present all over the film substrate which, makes the film less sensitive toward potentiometric determination of Eu(III). The best membrane electrode performance out of all the electrodes studied in terms of highest dynamic range ($1.5\text{x}10^{-6}$ – $1.1\text{x}10^{-2}$ M) and slope (17.3±0.1 mV/ decade) was observed with the membrane electrode without any plasticizer (S. No.5; Table 5.1). The detection limit as determined from the intersection point of the two extrapolated segments of the calibration plot was found to be $1.2\text{x}10^{-6}$ M Eu(III) for the electrode (S. No. 5). The improved performance of the membrane potentiometric sensor in the absence of added plasticizer (NPOE) may be due to the presence of higher amount of TODGA where a fraction of the extractant may act as the plasticizer. The thermogravimetric analysis of the PVC based membranes with and without TODGA (*Annexure-I*, Fig.A 1.5a and Fig.A 1.5b) indicated that the presence of TODGA decreased the decomposition temperature of the PVC membranes. Increasing the TODGA content of the membrane to 46.5% further decreased the decomposition temperature of the membrane (*Annexure-I*, Fig.A1.5 c) and a sharp weight loss in the derivative plot was observed. This indicated that the fraction of PVC plasticized by TODGA increased with increasing TODGA content in the membrane. In view of the best response of this sensor electrode (S.No.5; Table 5.1), further study was carried out with this electrode in conjunction with saturated calomel as the reference electrode.

#### 5.2.2.2. Effect of the inner filling solution and the life time of the sensor

The effect of the inner filling solution on the response of the sensor electrode was studied at two different Eu(III) concentrations and the results are depicted in Fig. 5.2. The figure shows that both the slope and the linear dynamic range of the calibration curve are decreased on decreasing the inner concentration of Eu(III) from 0.1 M to 0.01 M and hence, the inner concentration of Eu(III) was fixed at 0.1 M (S.No.5; Table 5.1). It was also observed that overnight soaking was sufficient to get a stable potential with the proposed sensor electrode. The response of the sensor remained unchanged when it was applied with lower to higher or higher to lower concentrations of Eu(III). This indicated the reversible nature of the sensor. The sensor electrode tip was dipped in 0.1 M $Eu(NO_3)_3$ solution when it was not in use. The lifetime of the sensor electrode was found to be one month. The response of the sensor electrode potential after four weeks is shown in Fig. 5.2 which indicated that the sensitivity of the electrode remained good but the linear dynamic range was reduced by around 10 % at the higher concentration.

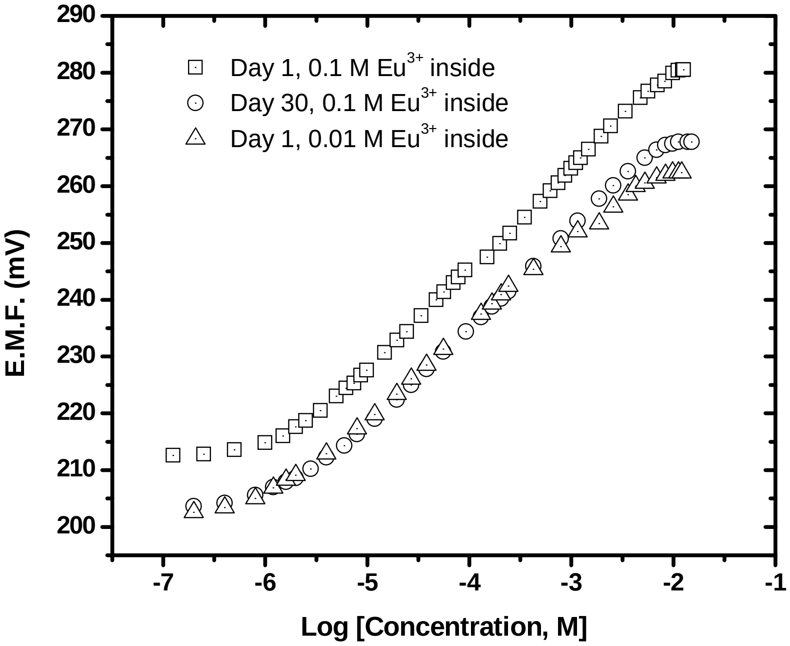

Fig. 5.2. Potential response for the TODGA based electrode for Eu(III) solution in acetate buffer, pH 5.0±0.1; Square: Inner solution: 0.1 M $Eu(NO_3)_3$, day 1; Circle: Inner solution: 0.1 M $Eu(NO_3)_3$, day 30; Triangle: Inner solution: 0.01 M $Eu(NO_3)_3$, day 1; Sample volume: 20 mL; PIM composition: 30.3% TODGA, 9.1% NaTPB and 60.6% PVC

### 5.2.2.3. Effect of pH on the potential response

It was required to investigate the effect of the pH of the solution on the membrane potential response behavior. Fig. 5.3 shows that the membrane potential remained constant in the pH range of 2-6, beyond which a drift in the potential is observed.

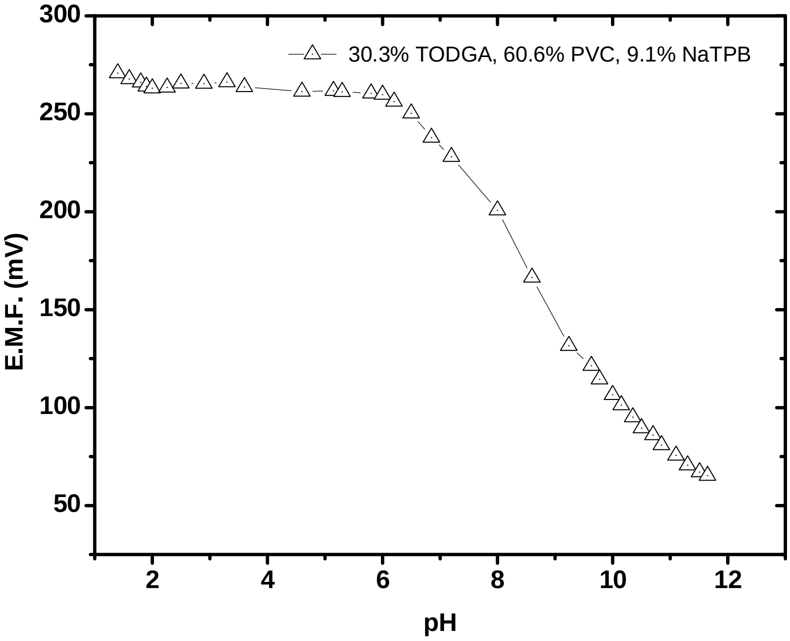

Fig. 5.3. Effect of pH on the potential response of the test solution containing 7.9 X $10^{-4}$ M Eu(III) in Millipore water; Sample volume: 20 mL; PIM composition: 30.3% TODGA, 60.6% PVC, 9.1% NaTPB; Inner solution: 0.1 M $Eu(NO_3)_3$

This is due to the fact that at pH >6.0, the potential decreases due to the formation of hydroxy compounds of Eu(III) resulting in a decrease in the uncomplexed Eu(III). On the other hand, the increase in the potential below pH 2.0 is due to the interference of $H^+$ by the TODGA containing sensor membrane. Therefore, the measurement of potential was carried out at constant pH (5.0 ± 0.1) in acetate buffer solution. The acetate buffer also helps to keep the ionic strength of the solution constant throughout the experiment.

### 5.2.2.4. The response time

Dynamic response time is an important factor for the evaluation of any sensor. Since the potentiometric response only requires ion movement over nanometers at the phase boundary of the sample and the ion-selective membrane, ISEs have inherent fast response times. In general, ISEs have response times ranging from a few milliseconds to few seconds. In this case, the practical response time of the sensor electrode was determined by recording the time required to attain a stable potential over the Eu(III) concentrations in the range, 7.4x10$^{-6}$ M to 2.0x10$^{-5}$ M in the acetate buffer solution (Fig. 5.4). The response time of the sensor electrode was found to be less than 10 s and remained unchanged with different concentrations.

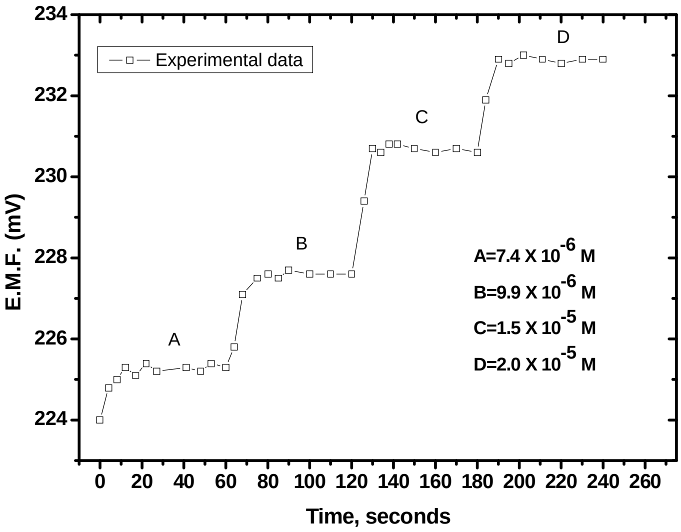

Fig. 5.4. Dynamic response time of the europium sensor electrode for step changes in Eu$^{3+}$ concentration. Membrane composition: 30.3% TODGA, 60.6% PVC, 9.1% NaTPB. Solution volume: 20 mL acetate buffer.

This is probably due to the rapid exchange kinetics of complexation-decomplexation of Eu(III) ion with the ionophore at the sample solution-membrane interface.

### 5.2.2.5. The selectivity coefficient ($K_{i,j}^{pot.}$)

The selectivity coefficient is one of the most important parameters for the membrane based sensor electrode. It measures the response of the primary ion in the presence of other interfering ions. In this matched potential method (MPM) [**183**], the change in potential was recorded upon changing the primary ion activity (concentration) ($\Delta a_i$) in the solution. The interfering ion is then added to an identical reference solution containing constant background of the primary ion until the same potential change is obtained. The selectivity coefficient is given as $K_{i,j}^{pot.} = \Delta a_i/a_j$, where $a_j$ is the activity (concentration) of the interfering ion that produced same change in potential as that obtained with $\Delta a_i$ in the solution.

Table 5.2. Selectivity coefficient data for different interfering ions measured by matched potential method (MPM)[a]

| Ion | Selectivity coefficient, $K^{pot}_{Eu^{3+},B}$ | Ion | Selectivity coefficient, $K^{pot}_{Eu^{3+},B}$ |
|---|---|---|---|
| $Ca^{2+}$ | $5.31 \times 10^{-2}$ | $UO_2^{2+}$ | $1.36 \times 10^{-2}$ |
| $Ba^{2+}$ | $1.14 \times 10^{-3}$ | $Sm^{3+}$ | $8.42 \times 10^{-1}$ |
| $Cu^{2+}$ | $2.43 \times 10^{-3}$ | $Gd^{3+}$ | $9.72 \times 10^{-1}$ |
| $Fe^{3+}$ | $2.86 \times 10^{-2}$ | $Dy^{3+}$ | $8.80 \times 10^{-1}$ |
| $Zr^{4+}$ | $2.52 \times 10^{-1}$ | $Cs^{+}$ | $8.44 \times 10^{-3}$ |

*Note:* [a]*Background concentration of Eu(III) =2.5x10*$^{-6}$ *M in the reference solution*

Table 5.2 gives the selectivity coefficient values measured by matched potential method (MPM). As evident from Table 5.2, the selectivity coefficients of the sensor due to the commonly occurring metal ions such as $Cs^+$, $Cu^{2+}$, $Ca^{2+}$, $Ba^{2+}$ and $Fe^{3+}$ are reasonably high and hence, these metal ions do not interfere even at 100 times higher concentration to the $Eu^{3+}$. The sensor is observed to be interfered due to the presence of other trivalent lanthanide ions such as $Sm^{3+}$, $Gd^{3+}$ and $Dy^{3+}$ and tetravalent $Zr^{4+}$ at 10 times higher concentration of that of the $Eu^{3+}$ ion. This investigation and the determination of selectivity coefficient values indicate that the interference pattern of different metal ions with the determination of Eu(III) and it could be suggested that Eu(III) could be determined effectively in the presence of normally occurring interfering ions and even in the presence of uranyl ion with the TODGA containing PIM.

### 5.2.2.6. Analytical applications

#### 5.2.2.6.1. Determination of Eu(III) ion in lean solutions

The proposed sensor was employed as an indicator electrode to determine Eu(III) concentration in a lean solution containing the metal ion by performing potentiometric titration using a standard solution of EDTA. A known volume (0.1 mL) of the stock Eu(III) solution (8 x $10^{-2}$ M) in 20 mL acetate buffer was taken in 50 mL beaker and was titrated with 0.02 M standard EDTA solution.

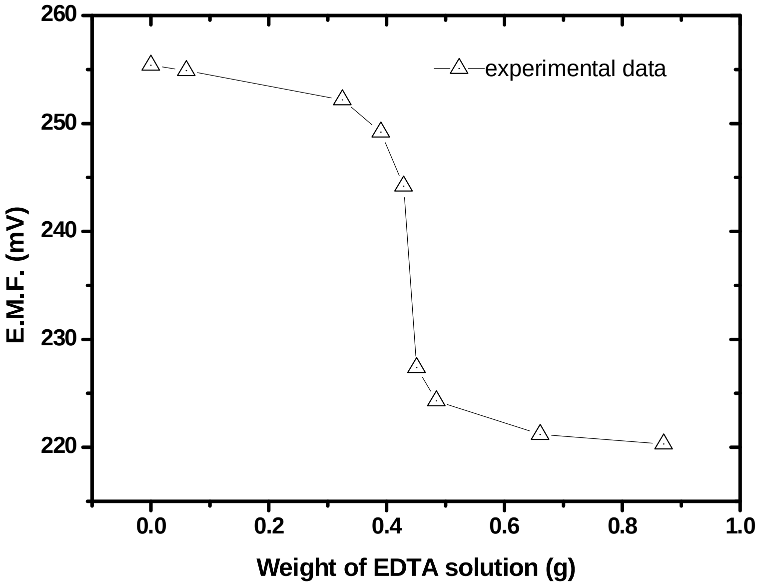

Fig. 5.5. Potentiometric titration curve of 8 x $10^{-2}$ M $Eu^{3+}$ with 0.02 M EDTA solution in acetate buffer (pH 5.0 ± 0.1) using the membrane electrode as indicator electrode; Membrane composition: 30.3% TODGA, 60.6% PVC, 9.1% NaTPB. Solution volume: 20 mL. Inner solution: 0.1 M $Eu(NO_3)_3$.

The corresponding titration curve is shown in Fig. 5.5 which indicates a sigmoidal shape and showed a sharp inflection point at the end point of the titration. The amount of Eu(III) as obtained from the titration curve was compared with the result obtained from an independent measurement using ICP-AES and a good match validated the present method. (Table 5.3).

Table 5.3. Determination of Eu(III) in Millipore water by the proposed sensor using potentiometric titration and comparison with the result of ICP-AES.

| Sample | Eu(III) added (M) | Eu(III) found (M) (proposed sensor)[a] | Eu(III) found (M) (ICP-AES)[a] |
|---|---|---|---|
| Millipore water | 0.08 | 0.088 ± 0.004 | 0.081 ± 0.002 |

Note: [a]Mean ± standard deviation, three results

#### 5.2.2.6.2. Determination of Eu(III) in a synthetic sample

$Eu^{3+}$ ion concentration in a synthetic sample containing known amounts of uranyl nitrate and europium nitrate was determined by the proposed sensor electrode by the direct potentiometric method. The synthetic mixture was prepared by mixing europium nitrate and uranyl nitrate solution in 10 mL volumetric flask which contained 100 mg $L^{-1}$ Eu(III) and uranyl nitrate (containing 1.76 g uranium) solution at 4 M $HNO_3$. The major part of the uranium from the solution was separated by the conventional solvent extraction technique using 30% TBP in *n*-dodecane at 4 M $HNO_3$ [**184-186**]. Subsequently, the aqueous acidic phase containing Eu(III) and other metallic impurities was collected and brought to the aqueous phase with Millipore water in a 10 mL volumetric flask. This solution was considered as the test solution and Eu(III) concentration in the test solution was determined by adding a known quantity (0.2 mL) of the solution in the 20 mL acetate buffer solution followed by the measurement of the potential by the proposed sensor in conjunction with saturated calomel as the reference electrode. Eu(III) concentration was determined using the calibration plot. The Eu(III) concentration determination in the uranyl nitrate blank (without adding $Eu^{3+}$) was carried out in a similar fashion. The results were compared with the results obtained by ICP-AES and are presented in Table 5.4. It is evident from the table that the results obtained by the proposed sensor are in good agreement with those obtained by the ICP-AES technique. The other metallic impurities present in the synthetic mixture were also determined by ICP-AES and are given in Table 5.5 which indicated that the proposed sensor is able to determine Eu(III) in the synthetic sample very accurately in the presence of other metallic impurities and uranium (108.36 ppm).

Table 5.4. Determination of Eu(III) concentration in the uranyl nitrate solution by the proposed sensor using direct potentiometric method

| Sample | Eu(III) added (mg $L^{-1}$) | Eu(III) found[a] (proposed sensor) (mg $L^{-1}$) | Eu(III) found[a] (ICP-AES) (mg $L^{-1}$) |
|---|---|---|---|
| Uranyl nitrate solution | 100.0 | 98.5 ± 4.9 | 100.7 ± 2.0 |
| Uranyl nitrate solution | ------- | BDL | BDL |

*Note: BDL: Below detection limit; [a]Mean ± standard deviation, three results*

Table 5.5. Determination of metallic impurities in the synthetic mixture of uranyl nitrate by ICP-AES after separation of uranium by 30% TBP-n-dodecane

| Element | Concentration, (ppm) | Element | Concentration (ppm) | Element | Concentration (ppm) |
|---|---|---|---|---|---|
| Cr | 0.53 | Mn | 0.462 | Ag | 0.47 |
| Ca | 16.62 | Fe | 14.22 | Gd | 0 |
| W | 0 | Mg | 7.82 | Dy | 1.43 |
| Zn | 0.60 | Mo | 17.06 | Sm | 0.43 |
| Ni | 0.80 | Pb | 3.32 | Eu | 100.72 |
| Cd | 0.13 | Si | 2.84 | U | 108.36 |
| Be | 0 | Al | 5.52 | | |
| Co | 0 | V | 2.56 | | |
| B | 0.83 | Cu | 1.168 | | |

## 5.3. CONCLUSIONS

In conclusion, TODGA based sensor membranes were fabricated with either CTA or PVC as the base polymer to study the potential response of $Eu^{3+}$ ion in acidic feed solutions. The sensor potential response due to the $Eu^{3+}$ ion was found to depend on the composition of the membrane and the optimized membrane composition of the sensor was found to be 30.3% TODGA, 9.1% NaTPB and 60.6% PVC. The PVC based optimized membrane sensor for $Eu^{3+}$ ion was pH sensitive beyond the range of pH 2-6 and showed a slope of 17.3 ± 0.1 mV/decade, low detection limit ($1.2x10^{-6}$ M of $Eu^{3+}$), wide linear dynamic range ($1.5x10^{-6}$ - $1.2x10^{-2}$ M of $Eu^{3+}$) and fast response (<10 s). The selectivity coefficient values were determined by matched potential method and showed that other than trivalent rare earth ions the sensor is interference free from the commonly occurring mono and divalent metal ions. The sensor was used as an indicator electrode in the potentiometric titration of $Eu^{3+}$ ion with EDTA solution in acetate buffer solution and also in the determination of $Eu^{3+}$ ion in a synthetic mixture of uranyl nitrate and europium nitrate solution. The results obtained using the proposed sensor were compared with those obtained by the ICP-AES technique which indicated reasonably good agreement.

# CHAPTER 6

# SUMMARY AND CONCLUSIONS

The long term radiation hazards to the environment by the long lived actinides is due to the possible release of radioactivity during nuclear weapon testing, accidents at nuclear plant site or leaching from vitrified waste blocks containing radionuclides due to possible failures, phase incompatibility, etc. In order to detect and estimate these actinide ions, suitable sensors are needed to be developed for a variety of samples. It is, therefore, required to develop an efficient separation method for the removal of long lived actinides from a variety of samples such as soil, rock, food, air, biological samples, radioactive waste, etc. All these separations involve dilute to moderate nitric acid feed solutions. Amongst the various techniques that can be applied for actinide ion separation and detection, liquid membrane based methods appear to be the most promising. In view of the poor stability of liquid membranes, polymer inclusion membranes are suggested to be a viable alternative and hence, have been used in this Thesis for actinide / lanthanide ion detection and sensing. This Thesis work has extensively dealt with Polymer Inclusion Membranes containing actinide ion selective ligands, mainly diglycolamide (DGA) derivatives, which have previously been found to be highly efficient from solvent extraction studies.

The work reported in this thesis can be summarized as follows.

**(i)** The uptake and transport behaviour of PIMs containing simple tetraalkyl DGA (TODGA / T2EHDGA / TPDGA / THDGA / TDDGA) ligands as the carrier extractants for the separation of actinide ions such as Am(III), Pu(IV), Th(IV) and U(VI) from lean acidic feed solutions was systematically investigated. The PIM composition has a significant effect on the uptake and transport behaviour of the actinide ions and hence, proper optimization of the concentrations of the carrier, plasticizer and base polymer in the PIM is mandatory. The uptake efficiency of the actinide ions by the PIMs also depends on the feed acidity and generally increases with an increase in the feed acid concentration up to 2 M $HNO_3$ as observed with the TODGA containing PIMs. In such cases, slight decrease in the uptake efficiency was found at $\geq$3 M $HNO_3$. The TODGA based PIMs followed the uptake and transport trends as Am(III) > Pu(IV) > Th(IV) > U(VI) whereas T2EHDGA (the branched homolog of TODGA) based PIMs followed an entirely different trend: Pu(IV) > Am(III) > Th(IV) > U(VI). The higher uptake of Am(III) over Pu(IV) indicated that reverse micellar mechanism is prevalent in the TODGA based PIMs whereas it may be operative to a much lesser extent in case of the branched DGA, T2EHDGA, especially in the PIM matrix containing NPOE, a relatively polar diluent, which acted as the solvent medium. Uranyl ion was found to be poorly extracted by all the DGA based PIMs and its uptake by the PIMs at 1 M $HNO_3$ followed the trend: TPDGA > THDGA ~ TODGA > TDDGA > T2EHDGA. The poor uptake of $UO_2^{2+}$ ion by all the PIMs has been attributed to steric constraints associated with the uranyl ion while accommodating the coordinating ligands along the equatorial plane. On the other hand, the Am(III) uptake was found to follow the trend: TODGA > TPDGA ~ THDGA > TDDGA > T2EHDGA at 1 M $HNO_3$. TODGA was found to be the most efficient while T2EHDGA was the least efficient in view of the additional steric requirements of the branched DGA ligand. Amongst the PIMs prepared with the three remaining DGA ligands, it was seen that around 90% uptake of Am(III), Pu(IV) and Th(IV) was possible in ca. 2 h with the TPDGA and THDGA based PIMs whereas with the TDDGA based PIM the uptake of Pu(IV) and Th(IV) was comparatively lower. The transport studies were not carried out with the TDDGA based PIMs in view of leaching out of the extractant from the PIM. The transport of the actinide ions into the receiver phase (1 M α-HIBA) by the TPDGA and THDGA based PIMs followed the trend: Pu(IV) > Am(III) > U(VI) > Th(IV) after 2 h. The poor transport rates seen for Th(IV) ion may be due to the presence of bulkier metal-carrier complexes in the membrane due to a higher ligand to metal ratio (Th concentration: $<10^{-10}$ M). The diffusion coefficient values of the metal – carrier complexes obtained with the

TPDGA and THDGA based PIMs were found to be higher than those found with the T2EHDGA based PIMs but significantly lower than those observed with the TODGA based PIMs. The sorption-desorption studies with the T2EHDGA containing PIMs indicated the limited reuse possibility of the PIMs as the sorbent. Similarly, the PIM stability studies indicated that the permeability coefficient values for the transport of Am(III) decreased from the first day of transport indicating limited reusability of the PIMs for the transport of the metal ion.

**(ii)** In view of superior extraction behaviour of multiple diglycolamide ligands such as T-DGA and C4DGA, the actinide ion uptake and transport studies were also carried out from acidic feed solutions by PIMs containing T-DGA / C4DGA. The actinide ion uptake by T-DGA based PIMs showed the uptake trend: Pu(IV) > Am(III) >> Th(IV) > U(VI) in ca, 2 h which was slightly different from that seen with the TODGA containing PIMs (Am(III) > Pu(IV) > Th(IV) > U(VI)). The sorbed actinide ions could be quantitatively desorbed from the T-DGA based PIMs using 1 M α-HIBA solution. A comparable uptake (~90%) of Pu(IV) was observed at 10 times lower ligand concentration with the T-DGA based PIM as compared to that observed with TODGA / T2EHDGA / TPPDGA / THDGA / TDDGA containing PIMs. Transport studies carried out with 1 M $HNO_3$ as the feed and 1 M α-HIBA (at pH 3.0) as the receiver phase showed the trend: Am(III) > Pu(IV) >> U(VI) > Th(IV) after 2 h of operation, which was different than that observed during the uptake studies. The transport studies also suggested that a significant amount of the actinide ions were trapped inside the membrane. The stability study with T-DGA based PIMs indicated a sharp deterioration in the permeability coefficient values from day 1 of the transport study and thus, limited reuse possibility of the PIMs. The physical characterization of the T-DGA containing PIM was carried out using techniques, such as TGA, XRD, SEM, AFM, FTIR and TIMM.

TGA showed that the integrity of the PIM was not lost even after 48 h of contacting with 1 M $HNO_3$. The TIMM plot of the PIMs revealed a uniform distribution of carrier along the PIM, which indicated a "carrier diffusion model" for the transport of the metal ions. XRD indicated an amorphous structure of the PIMs, whereas SEM profiles showed a dense microstructure and AFM images indicate rough surfaces of the pristine PIMs.

The uptake studies by PIMs containing 6.5% C4DGA, 67.7% NPOE, and 25.8% CTA showed poor extraction of the uranyl ion and poor uptake kinetics of the other actinide ions as compared to those seen with the respective TODGA / T2EHDGA-containing PIMs and the corresponding uptake trend was observed to be as Am(III) > Pu(IV) > Th(IV) >> U(VI) from 1 M $HNO_3$ as the feed acidity. The negligible uptake of uranyl ion by the C4DGA based PIM indicated the steric effects associated with the accommodation of the DGA moieties from the bulky C4DGA ligand at the equatorial plane of the ion. The transport studies of the actinide ions using PIMs of the composition, 6.5% C4DGA, 67.7% NPOE, and 25.8% CTA resulted in the trend, Pu(IV) > Am(III) > Th(IV) when the feed solution contained 1 M $HNO_3$ and the respective actinide tracer while 1 M α-HIBA was used as strip solution in the receiver compartment. The transport of the uranyl ion was not investigated in view of negligible uptake of the actinide ion by the PIM. As already mentioned above, the very low transport of Th(IV) ion may be due to the presence of the bulkier metal ion-carrier complex due to the higher ligand to metal ratio (Th concentration $<10^{-10}$ M). The stripping studies indicated a slow stripping rate of the actinide ions from the PIMs, and only around 45% stripping of Am(III) was seen in ca. 2 h with C4DGA based PIMs in the presence of 1 M α-HIBA as the stripping agent. The $D_{eff}$ values obtained from the lag time experiments of Am(III), Pu(IV) and Th(IV) observed with C4DGA based PIMs were smaller than those obtained with TODGA based PIMs. The respective $D_{eff}$ values with the C4DGA containing PIMs, however, were higher than those found with the T2EHDGA-based PIMs.

**(iii)** The batch uptake data of macro concentrations of Eu(III) (used as a surrogate of $Am^{3+}$) with T2EHDGA containing PIMs conformed to the pseudo-second order model which indicated a chemisorptions process and the isotherm study results conformed to the Langmuir isotherm model. The maximum sorption capacity ($q_m$) of Eu(III) as found by fitting with the Langmuir model was 33.014 mg/g of the PIM which contained 69% T2EHDGA, 17% NPOE and 14% NPOE at room temperature (24°C). A separate batch sorption study involving Eu(III) uptake by T-DGA based PIM containing 25.6% T-DGA, 53.9% NPOE, and 20.5% CTA indicated that the sorption kinetics was best explained by the pseudo-second order model whereas the sorption behaviour was best explained by Redlich-Petersion isotherm. The maximum sorption capacity at equilibrium was found to be 27.0 mg/g of the PIM.

**(iv)** A Polymeric membrane based electrodes containing *N,N,N',N'*-tetraoctyl diglycolamide (TODGA) as the ionophore, polyvinyl chloride (PVC) as the base polymer and sodium tetraphenyl borate (NaTPB) as the ionic additive were fabricated for the potentiometric determination of $Eu^{3+}$ ion in acidic lean solutions. It was found that the membrane with a composition of 30.3% TODGA, 9.1% NaTPB and 60.6% PVC showed a wide linear dynamic range ($1.5 \times 10^{-6}$ M to $1.2 \times 10^{-2}$ M) with a slope of 17.3 ± 0.1 mV per decade with $1.2 \times 10^{-6}$ M as the limit of detection for Eu(III). The proposed sensor was successfully used as an indicator electrode for the potentiometric titration of $Eu^{3+}$ ion at pH 5.0±0.1. However, the sensor response was found to be seriously interfered by the presence of rare earth ions, such as Gd(III), Sm(III) and Dy(III).

**The results obtained during the studies carried out during this Thesis work clearly demonstrated the feasibility of PIM technique for actinide ion uptake and transport from acidic feed solutions using diglycolamides as the carrier extractants. The stability**

**and reusability studies indicated the transport studies can not be carried out over a longer period of time. On the other hand, large scale applications may be possible using hollow fiber polymer inclusion membrane technique. The DGA ligand containing PIMs, however, can be used for the development of sensors for the lanthanide / actinides.**

# REFERENCES

## References

1. N. M. Edelstein and L. R. Morss, Radiochemistry and Nuclear chemistry-Vol.II-Chemistry of the actinide elements.
2. Bennett, Burton, et al. "Chernobyl accident: exposures and effects."Proceedings of the 10th International Congress of the International Radiation Protection Association (IRPA-10). Paper T-12-1. Hiroshima, Japan. 2000.
3. K. R. Rao, "Radioactive waste: The problem and its management." *Current Science* 81.12 (2001)1534.
4. W. E. Kastenberg and L. J. Gratton, Hazardous of managing and disposing of nuclear wastes, *Physics Today*, 50 (1997) 41.
5. Charles McCombie, Nuclear waste management worldwide, *Physics Today*, 50 (1997) 56.
6. N. N. Egorov, M. A. Zakharov, C. N. Lazarev, R. I. Lyubtsev, A. S. Nikiforov, M. V. Strakhov and E. A. Filippov, “New approaches to solving the management problem of long lived radionuclides”, In proceedings of the third international conference on nuclear fuel reprocessing and waste management, RECOD-91, Vol. 1, P. 357.
7. Actinide and Fission Product Partitioning and Transmutation, Status and Assessment report, OECD/NEA, 1999.
8. L. H. Baestle, Burning of Actinides: A complementary waste management option? *IAEA Bulletin*, 34 (1992) 32.
9. J. C. McLean, A. B. McLay and H.G. Smith, *Proc. Roy. Soc. (London)*, 112 (1926) 76.
10. G. T. Seaborg, *Chem. Eng. News*, 23 (1945) 2190.
11. M. S. Milyukova, N. I. Gusev, I. G. Sentyurin and I. S. Skyarenko, Analytical Chemistry of Plutonium, *Israel Prog. for Sci. Translation*, Jerusalem (1967) 5.
12. M. Taube, “Plutonium”, Pergamon Press, Oxford (1964) 5.

**13.** S. Ahrland, J. O. Liljenzin and J. Rydberg, Solution Chemistry, In “Comprehensive Inorganic Chemistry”, J.C. Bailar Jr., H.J. Emeleus, R. Nyhlom and A.F.T. Dickenson (Eds.), Pergamon Press, Oxford 5 (1973) 465-535.

**14.** B. B. Cunningham, “Proc. of XVII international congress of pure and applied chemistry”, Butterworths, London. Vol. 1, 64.

**15.** V. I. Spitsyn, A. D. Gelman, N. N. Krot, M. P. Mefodiyeva, F. A. Zacharova, Y.A. Komokov, V.P. Shilov and I.V. Smirnovam, *J. Inorg. Nucl. Chem*., 31 **(**1969**)** 2733.

**16.** W. M. Latinmer, “Oxidation Potentials”, 2nd Ed., Prentice Hall (1952) 299.

**17.** J. J. Katz and G. T. Seaborg, “The chemistry of actinide elements”, *Willy Publications* (1957) 315.

**18.** K. A. Kraus, Proc. First U.N. Conference on Peaceful Uses of Atomic Energy, 7 (1956) 245.

**19.** M. Haissinsky, “Nuclear chemistry and its applications” (English ed.), Addison-Wesley (1964) 233.

**20.** A. D. Janes and G. R. Choppin, *Actinides Rev.,* 1 (1969) 311.

**21.** W. S. W. Ho and K. K. Sirkar, Membrane Handbook. Chapman & Hall, New York (1992).

**22.** T. Araki and H. Tsukube, Liquid Membranes: Chemical Applications. CRC Press, FL (1990).

**23.** H. J. Fendler, *J. Membr. Sci.*, 30 (1987) 323.

**24.** R. D. Noble, *Sep. Sci. Technol.,* 22 (1987) 731.

**25.** J. P. Shukla, A. Kumar and R. K. Singh, *Sep. Sci. Technol.*, 27 (1992) 447.

**26.** Y. Zhu, J. Chen, and R. Jiao; *Solv. Extr. Ion Exch.,* 14(4) (1996) 555.

**27.** I. J. Youri, P. J. Harrington and G. W. Stevens, *Solv. Extr. Ion Exch.*, 18 (2000) 933.

**28.** N. S. Rathore, J. V. Sonawane, A. Kumar, A. K. Venugopalan, R. K. Singh, D. D. Bajpai and J. P. Shukla, *J. Membr. Sci.*, 189 (2001) 119.

**29.** A. Geist, M. Weigl U. Muellich and K. Gompper, *Memb. Technol.*, 5 (2003) 5.

**30.** A. Geist, M. Weigl and K. Gompper, *Sep. Sci. Technol.*, 37 (2002) 3369.

**31.** L. D. Nghiem, P. Mornane, I. D Potter, J. M. Perera, R. W. Cattrall and S. D. Kolev, *J. Membr. Sci.,* 281 (2006) 7.

**32.** A. Uheida, Y. Zhang and M. Muhammed, *J. Membr. Sci.*, 241 (2004) 289.

**33.** P. R. Danesi, *J. Membr. Sci.*, 20 (1984) 231.

**34.** P. R. Danesi, *Solv. Extr. Ion Exch.*, 2 (1984) 115.

**35.** E. L. Cussler and D. F. Evans, *Sep. Purif. Meth.*, 3 (1974) 399.

**36.** R. Marr and A. Kopp, *Int. Chem. Eng.*, 22 (1982) 44.

**37.** P. R. Danesi, E. P. Horwitz and P. G. Rickert, *J. Phys. Chem.*, 87 (1983) 4708.

**38.** R. P. Wool, Polymer entanglements, *Macromolecules* 26 (7) (1993)1564.

**39.** J. K. Sears and J. R. Darby, Technology of Plasticizers, John Wiley & Sons, New York, (1982) 1174.

**40.** D.A. Lannon and E.J. Hoskins, Effect of plasticizers, fillers, and other additives on physical properties, in: P.D. Ritchie (Ed.), Physics of Plastics, Iliffe Books Ltd., London, 1965.

**41.** Y. M. Scindia, A. K. Pandey and A. V. R. Reddy, *J. Membr. Sci.* 249 (1/2) (2005)143.

**42.** M. E. Duffey, D. F. Evans and E. L. Cussler, *J. Membr. Sci.* 3 (1) (1978)1.

**43.** J. C. Aguilar, M. Sanchez-Castellanos, E. R.D.S. Miguel and J. de Gyves, *J. Membr. Sci.* 190 (1) (2001) 107.

**44.** J. de Gyves, A. M. Hernandez-Andaluz and E.R.D.S. Miguel, *J. Membr. Sci.* 268 (2) (2006) 142.

**45.** E. L. Cussler, R. Aris and A. Bhown, *J. Membr. Sci*. 43 (2/3) (1989) 149.

**46.** N. A. Plate, T. L. Lebedeva, G. A. Shandryuk, L. M. Kardivarenko and V. V. Bagreev, *J. Membr. Sci*. 104 (3) (1995) 197.

**47.** K. M. White, B. D. Smith, P. J. Duggan, S. L. Sheahan and E. M. Tyndall, *J. Membr. Sci*. 194 (2) (2001) 165.

**48.** B. M. Rapko, Synthesis, characterization and actinide extraction behaviour of bridge modified carbamoyl methyl phosphonates and phosphine oxides, In "*Separation of f-elements*", K.L. Nash and G.R. Choppin (eds.), Plenum Press, NY (1995) 99.

**49.** E. P. Horwitz, D. G. Kalina, G. F. Vandrift and W. W. Schulz, *Solv. Extr. Ion Exch.*, 3 (1985) 75.

**50.** W. W. Schultz and E. P. Horwitz, *Sep. Sci. Technol.*, 23 (1988) 1191.

**51.** R. R. Chitnis, P. K. Wattal, A. Ramanujam, P. S. Dhami, V. Goparkrishnan, A. K. Bauri and A. Banergy, *J. Radioanal. Nucl. Chem*., 240 (1999) 721.

**52.** R.R. Chitnis, P.K. Wattal, A. Ramanujam, P.S. Dhami, V. Goparkrishnan, A.K. Bauri and A. Banergy, *J. Radioanal. Nucl. Chem.*, 240 (1999) 727.

**53.** Y. Zhu, R. Jio, S. Wang, S. Fan, B. Leu, H. Zheng, S. Zhou and S. Chen, An extractant (TRPO) for the removal and recovery of actinides from high level radioactive liquid waste, *ISEC-1983*, Denver, Colorado, USA.

**54.** Y. Zhu and R. Jiao, *Nucl. Technol.*, 108 (1994) 361.

**55.** R. Jiao, S. Wang, S. Fan, B. Liu and Y. Zhu, *J. Nucl. Radiochem.*, 7 (1985) 65.

**56.** Y. Morita and M. Kubota, *J. Nucl. Sci. Technol.*, 24 (1987) 227.

**57.** Y. Morita, I. Yamaguchi, Y. Kondo, K. Shirahashi, I. Yamagishi, T. Fujirawa and M. Kubota, Safety and environmental aspects of partitioning and transmutation of actinides and fission products, IAEA-TECDOC-783, IAEA ,Vienna (1995) 93.

**58.** C. Cuillerdier, C. Musikas, P. Hoel, L. Nigond and X. Vitart, *Sep. Sci. Technol.*, 26 (1991) 1229.

**59.** C. Cuillerdier, C. Musikas and L. Nigond, *Sep. Sci. Technol.*, 28 (1993) 155.

**60.** L. Nigond, C. Musikas and C. Cuillerdier, *Solv. Extr. Ion Exch.*, 12 (1994) 261.

**61.** L. Nigond, C. Musikas and C. Cuillerdier, *Solv. Extr. Ion Exch.*, 12 (1994) 297.

**62.** G. R. Mahajan, D. R. Prabhu, V. K. Manchanda and L. P. Badheka, *Waste Management*, 18 (1998) 125.

**63.** L. B. Kumbhare, D. R. Prabhu, G. R. Mahajan, S. Sriram and V. K. Manchanda, *Nucl. Technol.*, 139 (2002) 253.

**64.** D. S. Purroy, P. Baron, B. Christiansen, J. P. Glatz, C. Madic, R. Malmbeck and G. Modolo, *Sep. Purif. Technol.*, 45 (2005) 157.

**65.** L. Spjuth, J. O. Liljenzin, M. J. Hudson, M. G. B. Drew, B. P. Iveson and C. Madic, *Solv. Extr. Ion Exch.*, 18 (2000) 1.

**66.** H. Stephan, K. Gloe, J. Bager and P. Muhl, *Solv. Extr. Ion Exch.*, 9 (1991) 435.

**67.** H. Stephan, K. Gloe, J. Bager and P. Muhl, *Solv. Extr. Ion Exch.*, 9 (1991) 459.

**68.** Y. Sasaki and G. R. Choppin, *Anal. Sci.,* 12 (1996) 225.

**69.** Y. Sasaki and G. R. Choppin, *J. Radioanal. Nucl. Chem.*, 207 (1997) 383.

**70.** Y. Sasaki, T. Adachi and G. R. Choppin, *J. Alloy comp.,* 271-273 (1998) 799.

**71.** Y. Sasaki and G. R. Choppin, *Radiochim. Acta*, 80 (1998) 85.

**72.** Y. Sasaki and G. R. Choppin, *J. Radioanal. Nucl. Chem.*, 246 (2000) 267.

**73.** H. Narita, T. Yaita, K. Tamura and S. Tachimori, *Radiochim. Acta,* 81 (1998) 223.

**74.** H. Narita, T. Yaita and S. Tachimori, Extraction Behavior for Trivalent Lanthanides with Amides and EXAFS Study of their Complexes. In Solvent Extraction for the 21st

Century, Proceedings of ISEC‘99, Barcelona, Spain, July, 1999; M. Cox, M. Hidalgo, and M. Valiente (Eds.), Society of Chemical Industry: London (2001), Vol. 1, P. 693.

**75.** Y. Sasaki, Y. Sugo, S. Suzuki and S. Tachimori, *Solv. Extr. Ion Exch.*, 19 (2001) 91.

**76.** R. B. Gujar, S. A. Ansari, D. R. Prabhu, D. R. Raut, P. N. Pathak, A. Sengupta, S. K. Thulasidas, P. K. Mohapatra and V. K. Manchanda, *Solv. Extr. Ion Exch.*, 28(2010) 764.

**77.** R. P. Buck, K. Toth, E. Graf, G. Horvai and E. Pungor, *J. Electroanal. Chem.*, 223 (1987) 51.

**78.** S. Yajima, K. Tohda, P. B¨uhlmann and Y. Umezawa, *Anal.Chem.*, 69 (1997) 1919

**79.** E. Bakker, P Bühlmann and E. Pretsch, *Chem. Rev.* 97(1997) 3083

**80.** K. N. Mikhelson, A. Lewenstan and S. E. Didina, *Electroanalysis* 11 (1999) 793.

**81.** G. G. Guilbault, R. A. Durst, M. S. Frant, H. Freiser, E.H. Hansen, T.S. Light, E. Purgor, G. Rechnitz, N. M. Rice, T. J. Rohm, W. Simon and J. D. R. Thomas, *Pure and Applied Chemistry* 48(1976) 127.

**82.** G. G. Guilbault, International Union of Pure and Applied Chemistry. Information Bulletin 1(1978) 69.

**83.** D. Janczewski, D. N. Reinhoudt, W. Verboom, C. Hill, C. Allignol and M. T. Duchesne, *New J. Chem.* 32 (2008) 490.

**84.** N. Srinivasan, M. N. Nadkarni, G. R. Balasubramanian, R. T. Chitnis and H. R. Siddiqui, BARC Report, Report-643, Bhabha Atomic Research Centre, Mumbai, India (1972).

**85.** S. S. Rattan, A. V. R. Reddy, V. S. Mallapurkar, R. J. Singh and S. Prakash, *J. Radioanal. Chem.*, 67 (1981) 95.

**86.** D. Alamelu and S. K. Aggarwal, BARC News letter, Mumbai, Issue no. 313 (2010) 23.

**87.** D. E. Ryan and A. W. Wheelright, *Ind. Eng. Chem.,* 51 (1959) 60.

**88.** M. Sugiura and M. Kikawaqa, *J. Membr. Sci.* 42 (1989) 47.

**89.** W. J. McDowell, *"Organic scintillators and liquid scintillation counting*", D.L. Horrocks, L.T. Peng (Eds.), Academic Press, Inc., New York (1971) 937.

**90.** H. Ihle, M. Karayannis and A. Murrenhoff, *"Organic scintillators and liquid scintillation counting*", D.L. Horrocks, L.T. Peng (Eds.), Academic Press, Inc., New York (1971) 879.

**91.** G. F. Knoll, *J. Radioanal. Nucl. Chem*., 243 (2000) 125.

**92.** D. D. Sood, A. V. R. Reddy and N. Ramamoorthy, *"Fundamentals of Radiochemistry"*, 2nd ed., IANCAS publication, BARC, Mumbai (2004) 115.

**93.** M. Thompson and J. N. Walsh, 'Inductively Coupled Plasma Spectrometry', Blackie (1989).

**94.** G. L. Moore, 'Introduction to Inductively Coupled Plasma Atomic Emission Spectrometry, Elsevier.

**95.** E. P., Horwitz and D. G. Kalina, *Solv. Extr. Ion Exch.* 2 (1984) 179.

**96.** S. A. Ansari, P. N. Pathak, P. K. Mohapatra and V. K. Manchanda, *Sep. Purif. Rev*. 40 (2011) 43.

**97.** K. L. Nash, C. Madic, J. N. Mathur and J. Lacquement, Actinide separation and technology. In: *The Chemistry of the Actinide and Transactinide Elements.* 3rd Ed. (Morss, L. R., Edelstein, N. M., Fuger, J., Katz, J. J., eds) Springer, The Netherlands, 4 (2006) 2622.

**98.** J. N. Mathur, M. S. Murali and K. L. Nash, *Solv. Extr. Ion Exch.* 19 (2001) 357

**99.** T. H. Siddall, *J. Phys. Chem.*, 64 (1960) 1863.

**100.** C. Musikas, *Inorg. Chim. Acta*, 140 (1987) 197.

**101.** C. Musikas, *Sep. Sci. Technol.*, 23 (1988) 1211.

**102.** K. Matloka, A. Gelis, M. Regalbuto, G. Vandegrift and M. J. Scott, *Dalton Trans.* (2005) 3719.

**103.** M. Hirata, P. Guilbaud, M. Dobler and S. Tachimori, *Phys. Chem. Chem. Phys.*, 5 (2005) 691.

**104.** Z. Zhu, Y. Sasaki, H. Suzuki and T. Kimura, *Anal. Chim. Acta*, 527 (2004) 163.

**105.** S. P. Kusumocahyo, T. Kanamori, T. Iwatsubo, K. Sumaru, T. Shinbo, H. Matsuyama and M. Teramoto, *J. Appl. Polym. Sci.*, 102 (2006) 4372.

**106.** E. A. Mowafy and H. F. Aly, *Solv. Extr. Ion Exch.*, 25 (2007) 205.

**107.** Y. Sasaki, H. Suzuki, Y. Sugo, T. Kimura and G. R. Choppin, *Chem. Lett.*, 35 (2006) 256.

**108.** R. A. Bartsch, J. D. Way, L. A. J. Chrisstoffels, F. de Jong and D. N Reinhouldt, Chemical separations with liquid membranes. In: ACS Symposium Series Number 642. (Bartsch, R. A., Way, J. D., eds.) ACS, Washington, DC (1996).

**109.** P. K. Mohapatra and V. K. Manchanda, *Indian J. Chem. A* 42 (2003) 2925.

**110.** N. M. Kocherginsky, Q. Yang and L. Seelam, *Sep. Purif. Technol.* 53 (2007) 171.

**111.** L. Boyadzhiev, Z. Lazarova, In: *Membrane Separations Technology: Principles and Applications*. (Noble, R. D., Stern, S. A., eds.) Elsevier Science, B. V., Amsterdam (1995) 283.

**112.** P. Religa, J. Rajewski, P. Gierycz, *Pol. J. Environ. Stud.* 24 (2015) 1283.

**113.** C. Fontas, R. Tayeb, M. Dhahbi, E. Gaudichet, F. Thominette, P. Roy, K. Steenkeste, M. P. Fontaine-Aupart, S. Tingry, E. Tronel-Peyroz and P. Seta, *J. Membr. Sci.* 290 (2007) 62

**114.** M. Ulewicz and E. Radzymińska-Lenarcik, *Physicochem.Probl. Miner. Process.* 46 (2011) 119

**115.** S. A. Ansari, P. K. Mohapatra, D. R. Prabhu and V. K. Manchanda, *J. Membr. Sci.* 282 (2006) 133.

**116.** S. A. Ansari, P. K. Mohapatra, D. R. Prabhu and V. K. Manchanda, *J. Membr. Sci.* 298 (2007) 169.

**117.** S. A. Ansari, P. K. Mohapatra, D. R. Prabhu and V. K. Manchanda, *Ind. Eng. Chem. Res.* 48 (2009) 8605.

**118.** S. Panja, P. K. Mohapatra, S. C. Tripathi and V. K. Manchanda, *J. Membr. Sci.* 337 (2009) 274

**119.** S. Panja, R. Ruhela, S. K. Misra, J. N. Sharma, S. C. Tripathi and A. Dakshinamoorthy, *J. Membr. Sci.* 325 (2008) 158

**120.** S. Panja, P. K. Mohapatra, S. C. Tripathi and V. K. Manchanda, Sep. Sci. Technol. 46 (2011) 94

**121.** S. Panja, P. K. Mohapatra, S. C. Tripathi, G. D. Dhekane, P. M. Gandhi and P. Janardan, *Sep. Sci.Technol.* 48 (2013) 2179

**122.** S. P. Kusumocahyo, T. Kanamori, K. Sumaru, S. Aomatsu, H. Matsuyama, M. Teramoto and T. Shinbo, *J. Membr. Sci.* 244 (2004) 251

**123.** S. A. Ansari, P. K. Mohapatra and V. K. Manchanda, *Desalination*, 262 (2010) 196

**124.** N.S. Murthy, S.T. Correal and H. Minor, *Macromolecules* 24 (1991) 1185.

**125.** G. Vancso, D. Snetvy and I. Tomka, *J. Appl. Polym. Sci.* 42 (1991) 1351.

**126.** O. Arous, F.S. Saoud, M. Amara and H. Kerdjoudj, *Mater. Sci. Appl.* 2 (2011) 615.

**127.** E. R. D. S. Miguel, A. Ma. Hernández-Andaluz, J. G. Bañuelos, J. M. Saniger, J. C. Aguilar and J. de Gyves, *Mater. Sci. Eng. A* 434 (2006) 30.

**128.** A. Bhattacharyya, P. K. Mohapatra, P. A. Hassan and V. K. Manchanda, *J. Hazard. Mater.* 192 (2011) 116.

**129.** S. A. Ansari, P. Pathak, P. K. Mohapatra and V. K. Manchanda, *Chem. Rev.* 112, (2012) 1751

**130.** J. A. Riggs and B. D. Smith, *J. Am. Chem. Soc.* 119 (1997) 2765.

**131.** M. P. Jensen, T. Yaita and R. Chiarizia, *Langmuir* 23 (2007) 4765.

**132.** S. Panja, P. K. Mohapatra, S. C. Tripathi, G. D. Dhekane, P. M. Gandhi and P. Janardan, *J. Membr. Sci.* 399-400 (2012) 28.

**133.** C. V. Gherasim, G. Bourceanu and D. Timpu, *Chem. Eng. J.* 172 (2011) 817.

**134.** C. V. Gherasim and G. Bourceanu, *Chem. Eng. J.* 220 (2013) 24.

**135.** B. N. Mahanty, P. K. Mohapatra, D. R. Raut, D. K. Das, P. G. Behere and Md. Afzal, Ind. Eng. Chem. Res. 54 (2015) 3237. .

**136.** I. Langmuir, *J. Am. Chem. Soc.* 38 (1916) 2221.

**137.** J. Crank, The Mathematics of Diffusion, second ed., Oxford University Press Inc, New York, (1975) 414.

**138.** A. Tor, G. Arslan, H. Muslu, A. Celiktas, Y. Cengeloglu and M. Ersoz, *J. Membr. Sci.* 329 (2009) 169.

**139.** P. N. Pathak, S. A. Ansari, P. K. Mohapatra, V. K. Manchanda, A. K. Patra and V. K. Aswal, *J. Colloid Intef. Sci.* 393 (2013) 347

**140.** P. N. Pathak, S. A. Ansari, S. Kumar, B. S. Tomar and V. K. Manchanda, *J. Colloid Intef. Sci.*, 342 (2010) 114.

**141.** P. K. Mohapatra, M. Iqbal, D. R. Raut, W. Verboom, J. Huskens and V. K. Manchanda, *J. Membr. Sci.* 375 (2011) 141.

**142.** M. Iqbal, P.K. Mohapatra, S.A. Ansari, J. Huskens and W. Verboom, *Tetrahedron* 68 (2012) 7840.

**143.** P. K. Mohapatra, M. Iqbal, D. R. Raut, J. Huskens and W. Verboom, *J. Membr. Sci.* 411–412 (2012) 64.

**144.** A. Marcilla and M. Beltran, *Polymer Degradation and Stability* 53 (1996) 261

**145.** M. Beltran and A. Marcilla, *Polymer Degradation and Stability* 55 (1997) 73.

**146.** A. Marcilla and M. Beltran, *Polymer Degradation and Stability* 60 (1998) 1.

**147.** F. Smail, O. Arous, M. Amara and H. Kerdjoudj, *C. R. Chimie* 16 (2013) 605.

**148.** E. R. de San Miguel, J. C. Aguilar, J. de Gyves, *J. Membr.sci.* 307 (2008) 105.

**149.** B. N. Mahanty, P. K. Mohapatra, D. R. Raut, D. K. Das, P. G. Behere, Md. Afzal, W. Verboom, *J. Environ. Chem. Eng.* 4 (2016) 1826–1838.

**150.** O. Arous, H. Kerdjoudj and P. Seta, *J. Membr. Sci.* 241 (2004) 177.

**151.** A. Salima, K. S. Ounissa, M. Lynda and B. Mohamed, *Procedia Eng.* 33 (2012) 38.

**152.** B. N. Mahanty, P. K. Mohapatra, D. R. Raut, D. K. Das, P. G. Behere and Md. Afzal, *Radiochim. Acta* 103 (2015) 257.

**153.** B. N. Mahanty, D. R. Raut, P. K. Mohapatra, D. K. Das, P. G. Behere and Md. Afzal, *J. Hazard. Mater.* 275 (2014) 146.

**154.** S. Lagergren, Zur theorie der sogenannten adsorption gelöster stoffe: kungliga Svenska Vetenskapsakademiens, Handlingar 24 (1898) 1.

**155.** Y. S. Ho, *Water Res.* 40 (2006) 119.

**156.** S. H. Chien and W. R. Clayton, *Soil Sci. Soc. Am. J.* 44 (1980) 265.

**157.** K.Y. Foo and B. H. Hameed, *Chem. Eng. J.* 156 (2010) 2.

**158.** O. Redlich and D. L. Peterson, *J. Phys. Chem.* 63 (1959) 1024.

**159.** B. Armagan and F. Toprak, *Pol. J. Environ. Stud.* 22 (2013) 1007.

**160.** C. Chen, *Open Chem. Eng. J.* 7 (2013) 24.

**161.** G. Limousin, J. P. Gaudet, L. Charlet, S. Szenknect, V. Barthes and M. Krimissa, *Appl. Geochem.* 22 (2007) 249.

**162.** H. M. F. Freundlich, Z. *Phys. Chem.* 57A (1906) 385.

**163.** M. V. Dinu, E. S. Dragan and A. W. Trochimczuk, *Desalination* 249 (2009) 374

**164.** A. Gunay, E. Arslankaya, I. Tosun, *J. Hazard. Mater.* 146 (2007) 362.

**165.** M. M. Dubinin, *Chem. Rev.* 60 (1960) 235.

**166.** J. P. Hobson, *J. Phys. Chem.* 73 (1969) 2720.

**167.** E. P. Horwitz, D. R. McAlister, A. H. Bond and R. E. Barrans Jr., *Solv. Extr. Ion Exch.* 23 (2005) 319.

**168.** S. A. Ansari, P. N. Pathak, M. Husain, A. K. Prasad, V. S. Parmar and V. K. Manchanda, *Talanta* 68 (2006) 1273.

**169.** W. Walkowiak, R. A. Bartsch, C. Kozlowski, J. Gega, W. A. Charewicz and B. Amiri-Eliasi, *J. Radioanal. Nucl. Chem.* 246 (2000) 643.

**170.** B. N. Mahanty, P. K.Mohapatra, D. R.Raut, D. K. Das, P. G. Behere and Md. Afzal, *J. Membr. Sci.* 501 (2016) 134.

**171.** G. W. Gokel, W. M. Leevy and M. E. Weber, *Chem. Rev.* 104 (2004) 2723.

**172.** P. B¨uhlmann, E. Pretsch and E. Bakker, *Chem. Rev.* 98 (1998) 1593.

**173.** A. Casnati, F. Sansone, J. F. Dozol, H. Rouquette, F. Arnaud-Neu, D. Byrne, S. Fuangswasdi, M. J. Schwing-Weill, R. Ungaro, *J. Incl. Phenomen. Macrocyclic Chem.* 41 (2001) 193.

**174.** F. Cadogan, K. Nolan and D. Diamond, in: Z. Asfari,V. Bohmer, J. Harrowfield, J. Vicens (Eds.), Calixarenes 2001, Kluwer Academic Press, Dordrecht, The Netherlands, 2001, Ch. 34, 627.

**175.** A.V. Legin, V. A. Babain, D.O. Kirsanov and O. V. Mednova, *Sensors and Actuators B* 131 (2008) 29.

**176.** A. M. Srivastava and C. R. Ronda, *The Electrochemical Society Interface* 12 (2003) 48.

**177.** M. Bralic, N. Radi, S. Brini and E. Generalic; *Talanta* 55 (2001) 581.

**178.** R. J. Beaver and M. M. Martin, ORNL-4368, 1969.

**179.** M. V. Ramaniah, *Pure & Appl.Chem*, 54 (1982) 889.

**180.** S. Nave, G. Modolo, C. Madic and F. Testard, *Solv. Extr. Ion Exch* 22 (2004) 527.

**181.** E. Metwally, A. Sh. Saleh and H. A. El-Naggar, *Journal of Nuclear and Radiochemical Sciences* 13 (2013) 1.

**182.** P. N. Pathak, S. A. Ansari, S. V. Godbole, A. R. Dhobale and V. K. Manchanda, SESTEC-2008 symposium, India.

**183.** Y. Umezawa, K. Umezawa and H. Sato; *Pure & Appl. Chern.*, 67 (1995) 507

**184.** J. Stas, A. Dahdouh and H. Shlewit, *Periodica polytechnica ser. chem. eng.* 49 (2005) 3.

**185.** A. Kelkar, A. Prakash, Md. Afzal, J. P. Panakkal and H. S. Kamath, J. *Radioanal. Nucl. Chem.*, 287 (2011) 595

**186.** A. Kelkar, A. Prakash, Md. Afzal, J. P. Panakkal and H. S. Kamath, *J. Radioanal. Nucl. Chem.*, 284 (2010) 443.

# *ANNEXURES*

## List of figures

## List of tables

# PHYSICAL CHARACTERIZATION OF THE POLYMER INCLUSION MEMBRANES CONTAINING DIFFERENT SUBSTITUTED DIGLYCOLAMIDES / MULTIPLE DIGLYCOLAMIDE LIGANDS AS THE CARRIER EXTRACTANTS

Physical characterization of the TODGA / T2EHDGA / TPDGA / THDGA / TDDGA / T-DGA / C4DGA containing PIMs were carried out using techniques such as thermal analysis (TGA), x-ray diffraction (XRD), Fourier transform infrared spectroscopy (FTIR), transmission infrared mapping microscopy (TIMM), scanning electron microscopy (SEM) and atomic force microscopy (AFM).

## A1.1. Thermal analysis

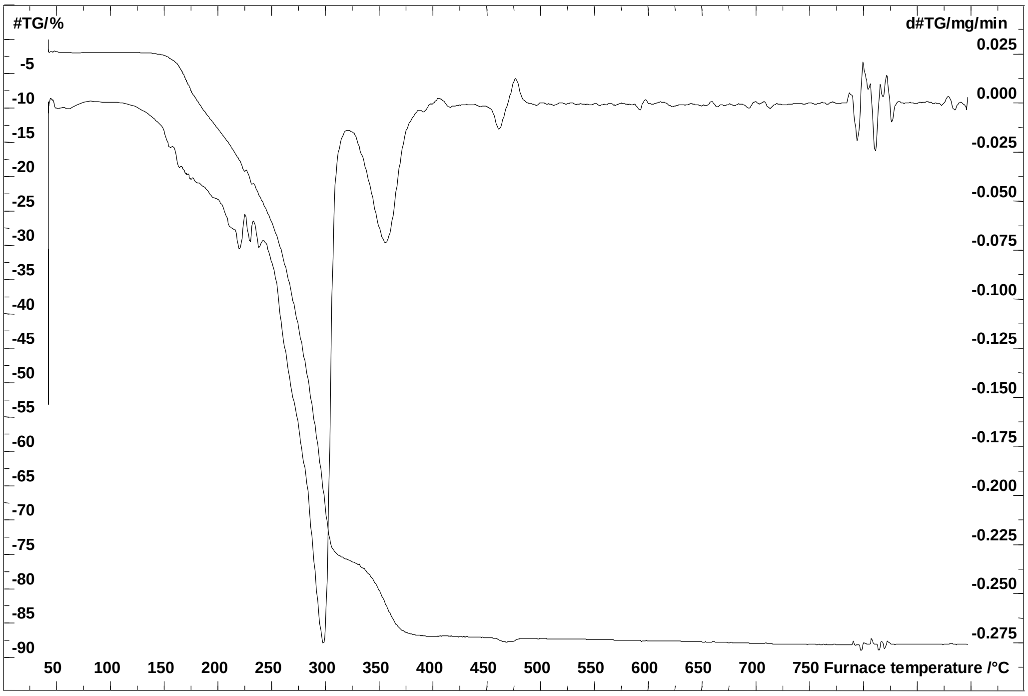

Fig. A1.1: TG-DTG profile of the PIM containing 68.4% T2EHDGA, 17.9% NPOE and 13.7% CTA; Heating rate: 10 °C per min.; Carrier gas: high purity Ar, flow rate 100 mL/min.

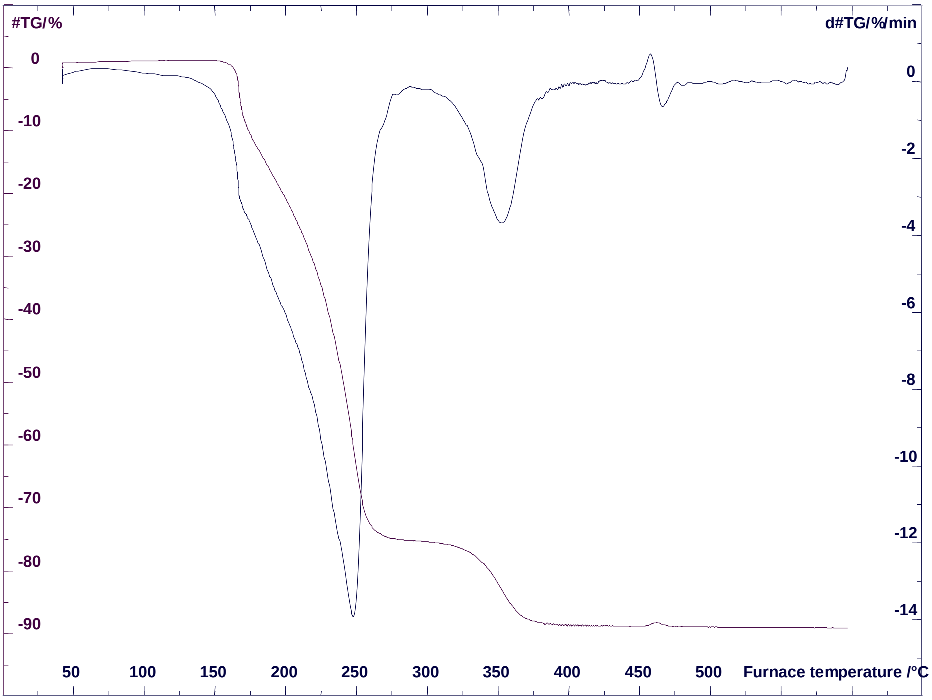

Fig. A1.2(a). TG-DTG profile of the PIMs containing 68.4% TPDGA, 17.9% NPOE, and 13.7% CTA Carrier gas: high purity Ar; Flow rate: 100 mL/min; Heating rate: 10°C/min.

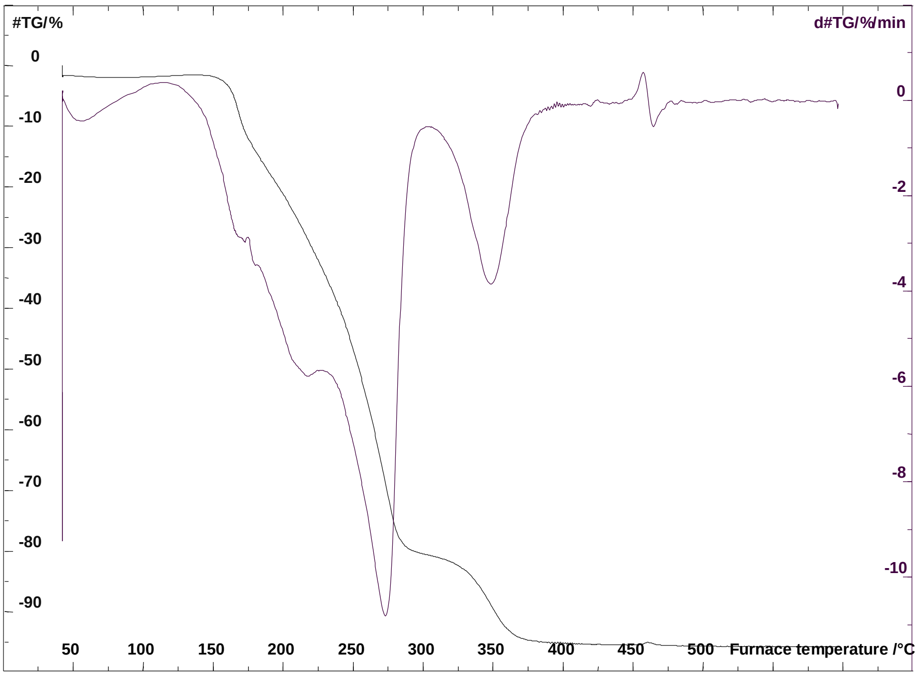

Fig. A1.2(b). TG-DTG profile of the PIMs containing 68.4% THDGA, 17.9% NPOE, and 13.7% CTA Carrier gas: high purity Ar; Flow rate: 100 mL/min; Heating rate: 10°C/min

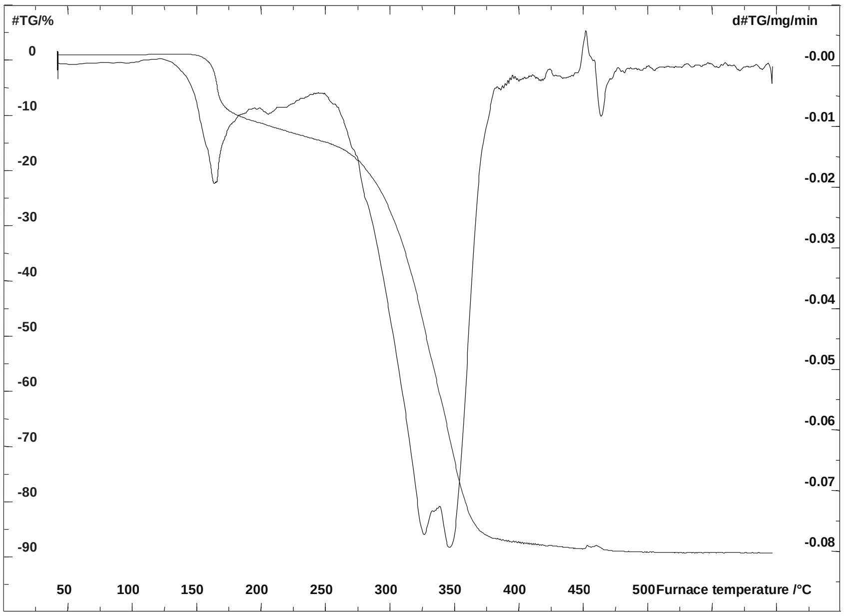

Fig. A1.2(c). TG-DTG profile of the PIMs containing 68.4% TDDGA, 17.9% NPOE, and 13.7% CTA Carrier gas: high purity Ar; Flow rate: 100 mL/min; Heating rate: 10°C/min.

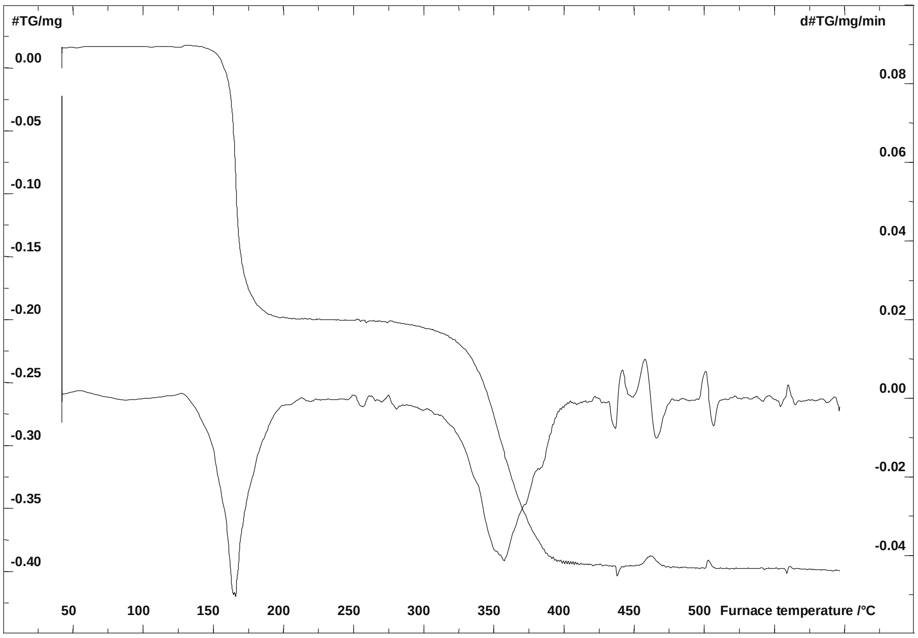

Fig.A1.3(a). TG-DTG profile of the pristine PIM containing 25.6% T-DGA, 53.9% NPOE, and 20.5% CTA; heating rate: 10°C/min.; carrier gas: high purity Ar, flow rate: 100 mL/min.

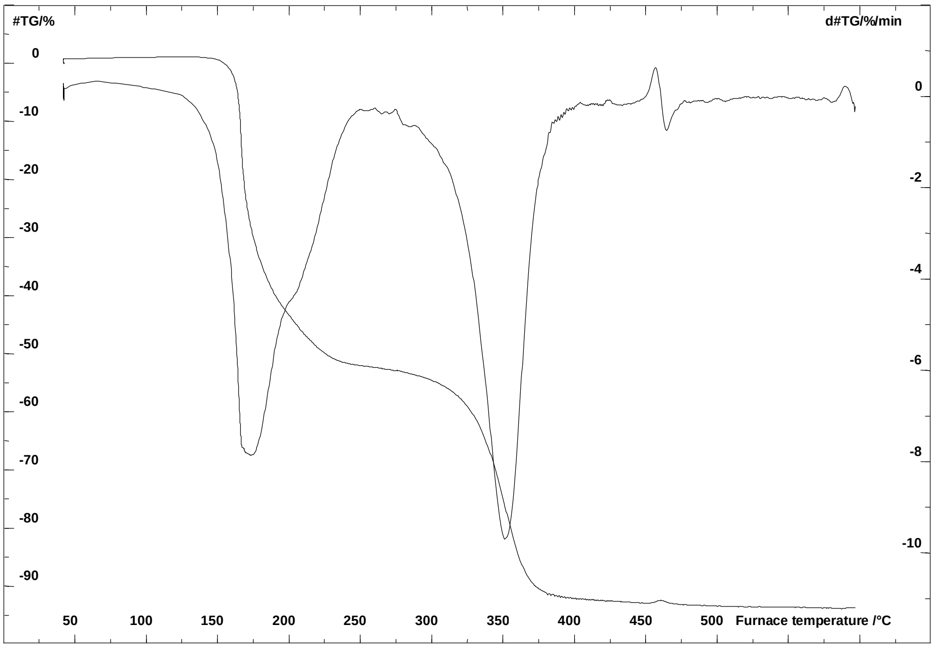

Fig.A1.3(b). TG-DTG profile of the pristine PIM containing 6.5% C4DGA-octyl, 67.7% NPOE, and 25.8% CTA; heating rate: 10°C/min.; carrier gas: high purity Ar, flow rate: 100 mL/min.

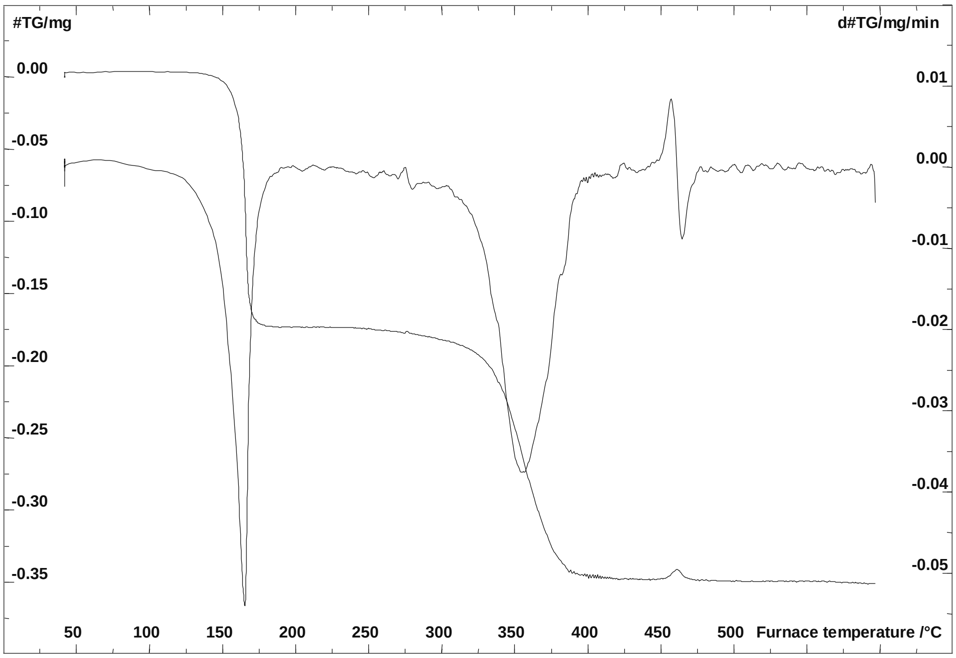

Fig. A1.4(a). TG-DTG profiles of the PIM containing 25.6% T-DGA, 53.9% NPOE and 20.5% CTA; PIM immersed in 1 M $HNO_3$ for 24 h Heating rate: 10°C $min^{-1}$.Carrier gas: high purity Ar, flow rate: 100 mL $min^{-1}$.

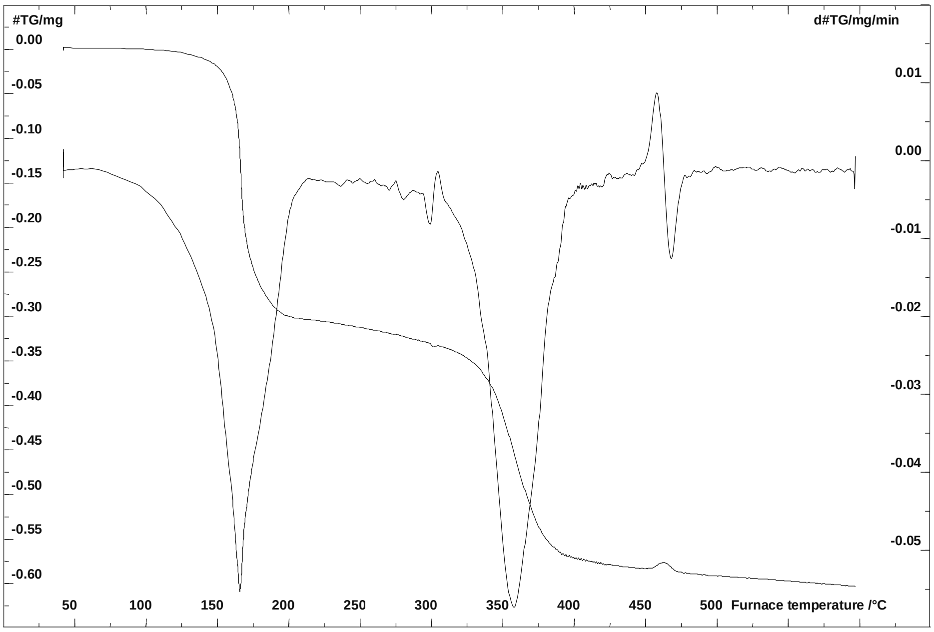

Fig. A1.4(b). TG-DTG profiles of the PIM containing 25.6% T-DGA, 53.9% NPOE and 20.5% CTA; PIM immersed in 1 M $HNO_3$ for 48 h. Heating rate: 10°C $min^{-1}$. Carrier gas: high purity Ar, flow rate: 100 mL $min^{-1}$.

Fig. A1.4(c). TG-DTG profiles of the PIM containing 25.6% T-DGA, 53.9% NPOE and 20.5% CTA; PIM immersed in 1 M $HNO_3$ for 72 h. Heating rate: 10°C $min^{-1}$. Carrier gas: high purity Ar, flow rate: 100 mL $min^{-1}$

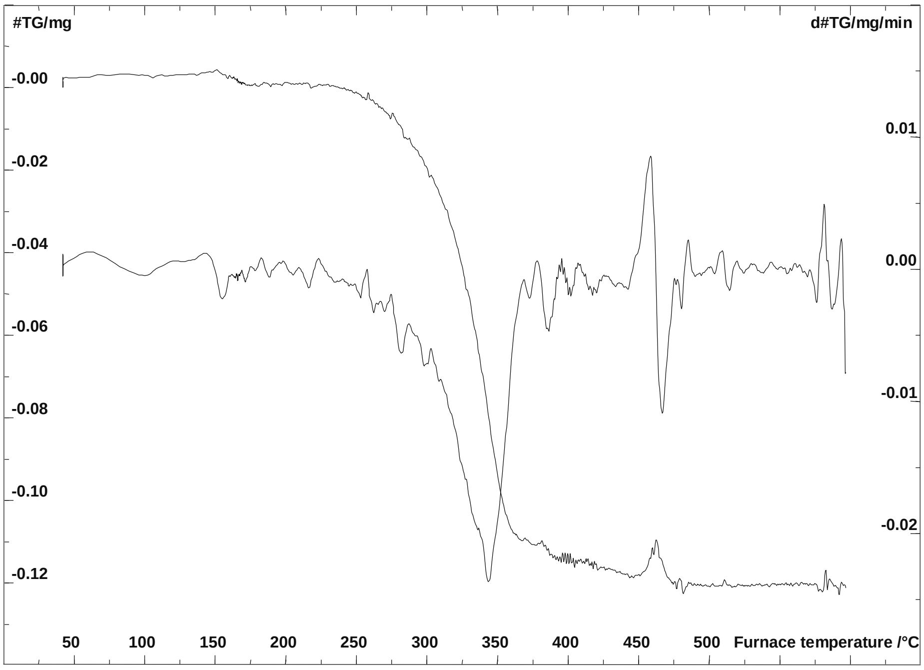

Fig.A1.4(d). TG-DTG profiles of the PIM containing 25.6% T-DGA, 53.9% NPOE and 20.5% CTA; PIM immersed in 1 M $HNO_3$ for 312 h. Heating rate: 10°C $min^{-1}$. Carrier gas: high purity Ar, flow rate: 100 mL $min^{-1}$.

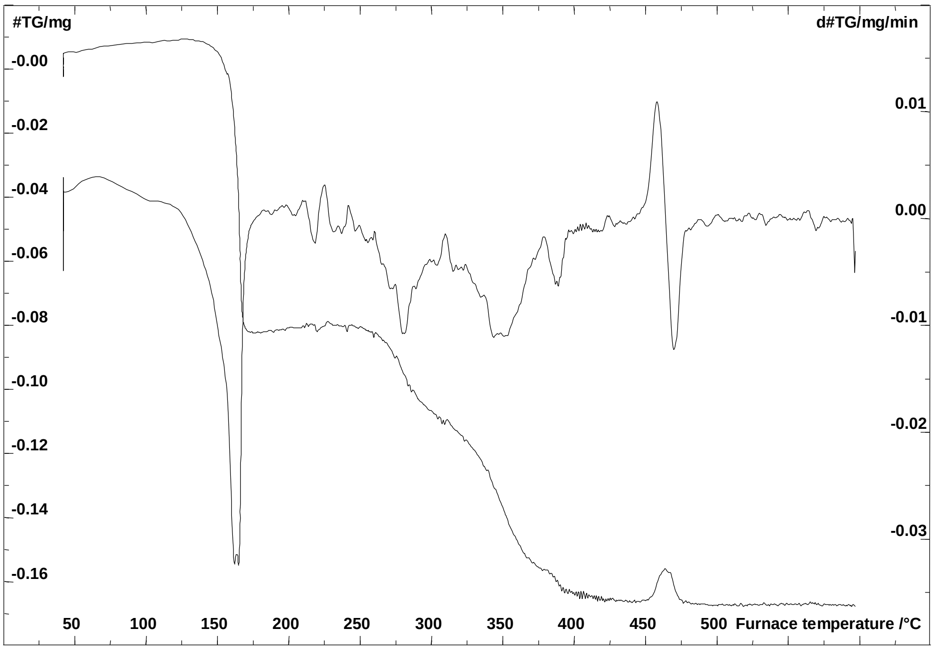

Fig.A1.4(e). TG-DTG profiles of the PIM containing 25.6% T-DGA, 53.9% NPOE and 20.5% CTA. PIM immersed in Eu(III) solution in 1 M $HNO_3$ for 24 h. Heating rate: 10°C $min^{-1}$. Carrier gas: high purity Ar, flow rate: 100 mL $min^{-1}$.

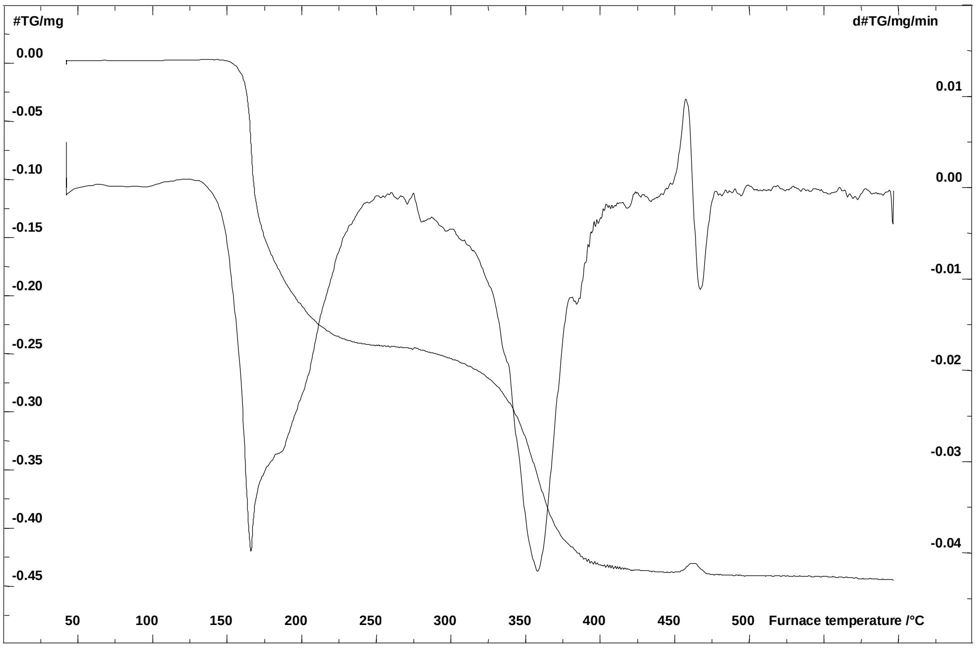

Fig.A1.4 (f). TG-DTG profiles of the PIM containing 25.6% T-DGA, 53.9% NPOE and 20.5% CTA. PIM after stripping off loaded Eu(III) using 1 M α-HIBA for 24 h. Heating rate: 10°C min$^{-1}$. Carrier gas: high purity Ar, flow rate: 100 mL min$^{-1}$.

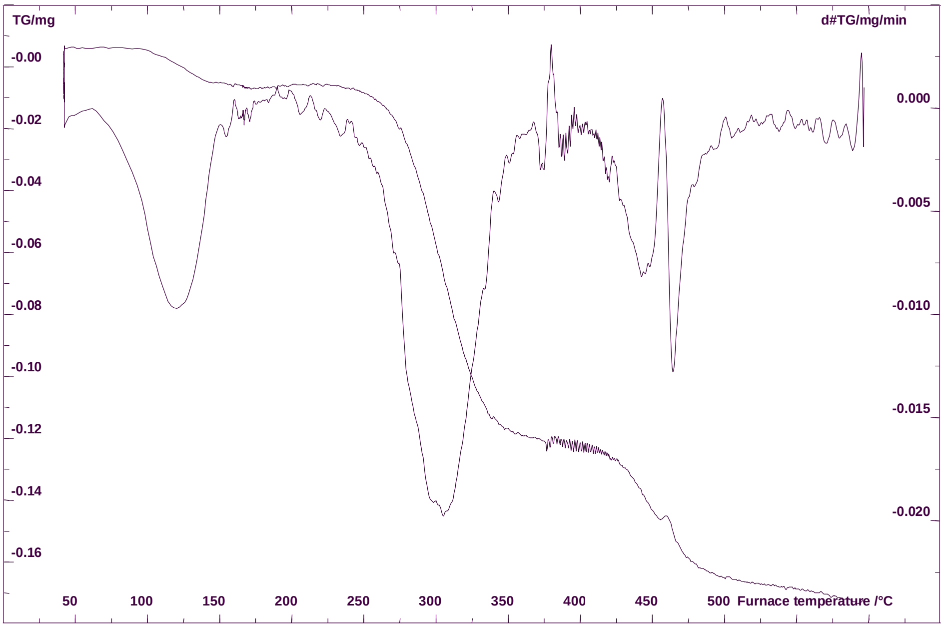

Fig. A1.5(a). TG-DTG profiles of the PVC membrane; Heating rate: 10°C min$^{-1}$. Heating rate: 10°C min$^{-1}$. Carrier gas: high purity Ar, flow rate: 100 mL min$^{-1}$.

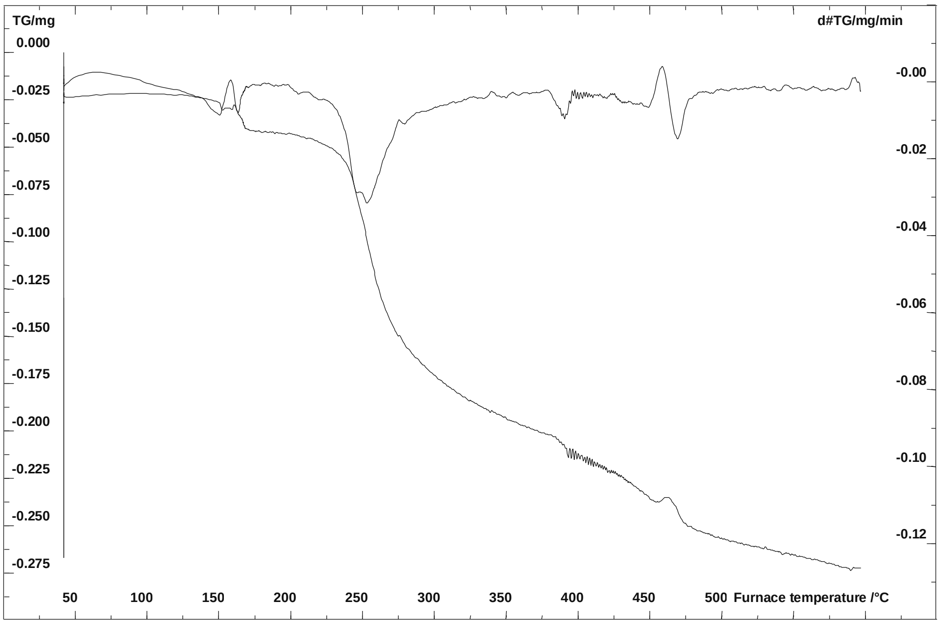

Fig. A1.5(b). TG-DTG profiles of the PIM containing 30.3% TODGA, 60.6% PVC and 9.1% NaTPB. Heating rate: 10°C min$^{-1}$. Carrier gas: high purity Ar, flow rate: 100 mL min$^{-1}$.

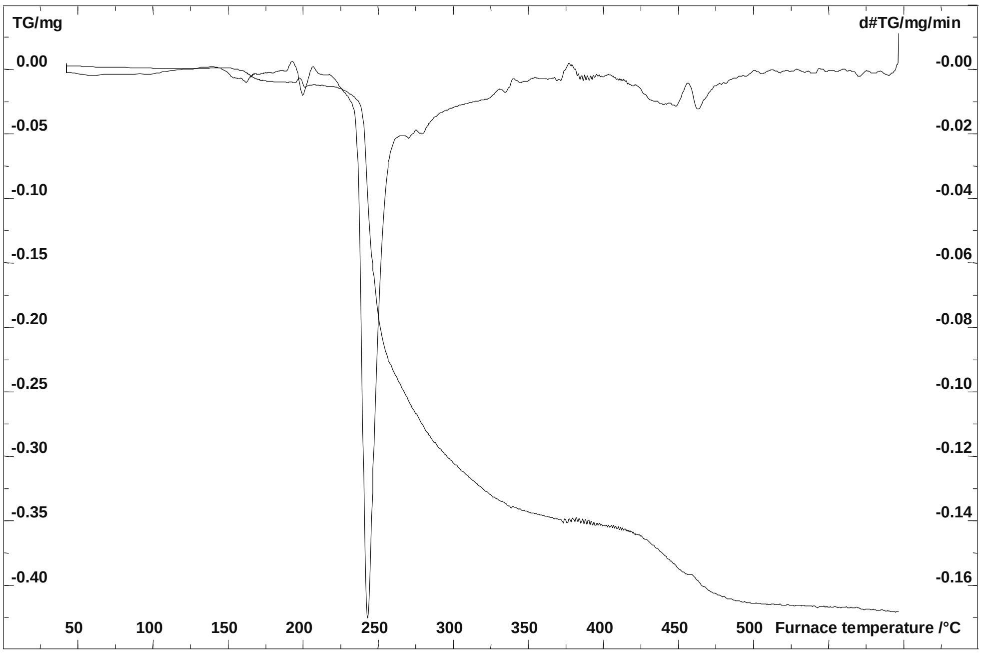

Fig. A1.5(c). TG-DTG profiles of the PIM containing 46.5% TODGA, 46.5% PVC and 7.0% NaTPB; Heating rate: 10°C min$^{-1}$. Carrier gas: high purity Ar, flow rate: 100 mL min$^{-1}$

A1.2. X-ray diffraction studies

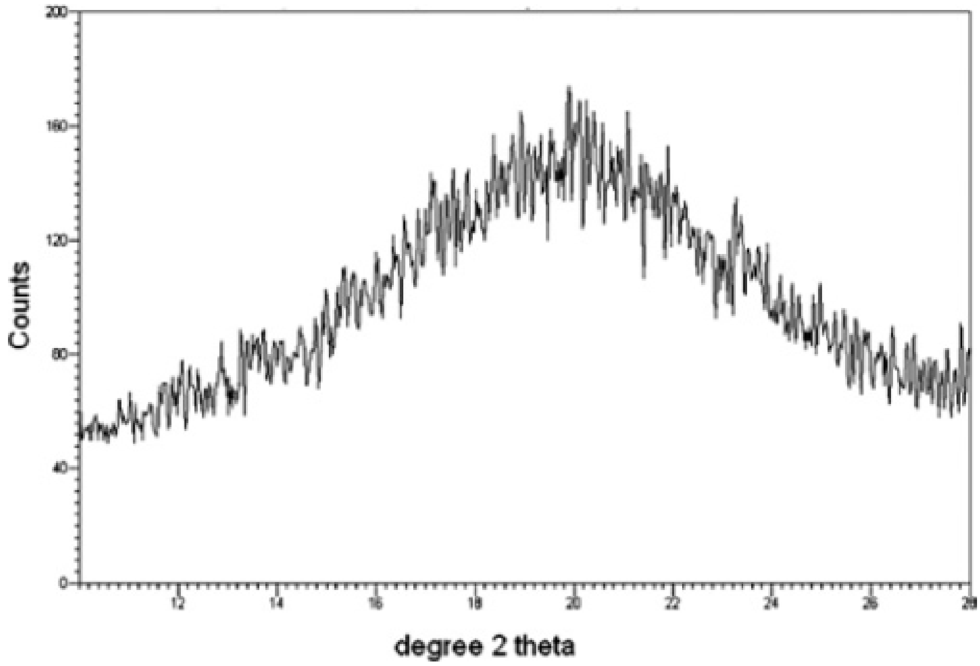

Fig. A1.6. XRD of PIM of the composition: 68.4% T2EHDGA, 17.9% NPOE and 13.7% CTA.

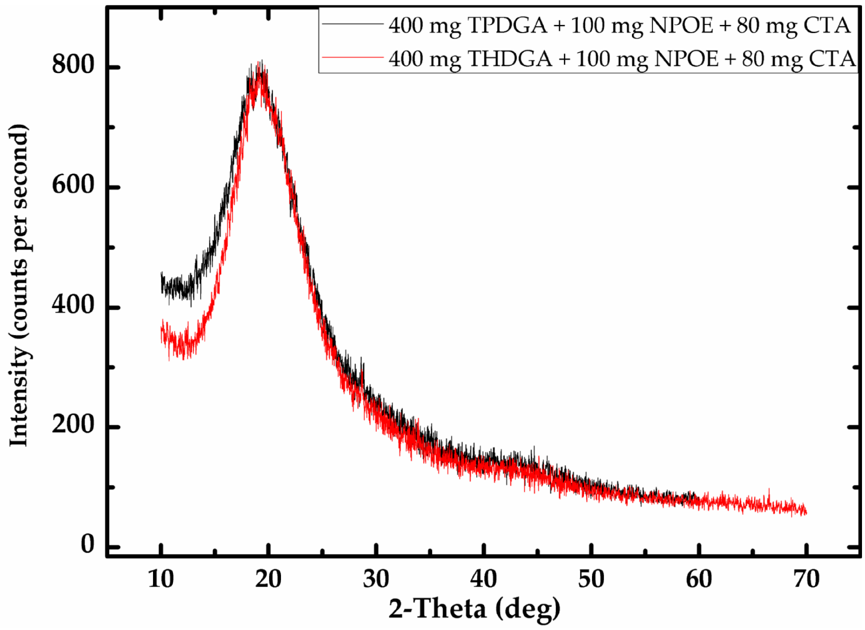

Fig.A1.7. XRD of TPDGA and THDGA containing PIMs of the composition: 68.4% TPDGA (or THDGA), 17.9% NPOE and 13.7% CTA.

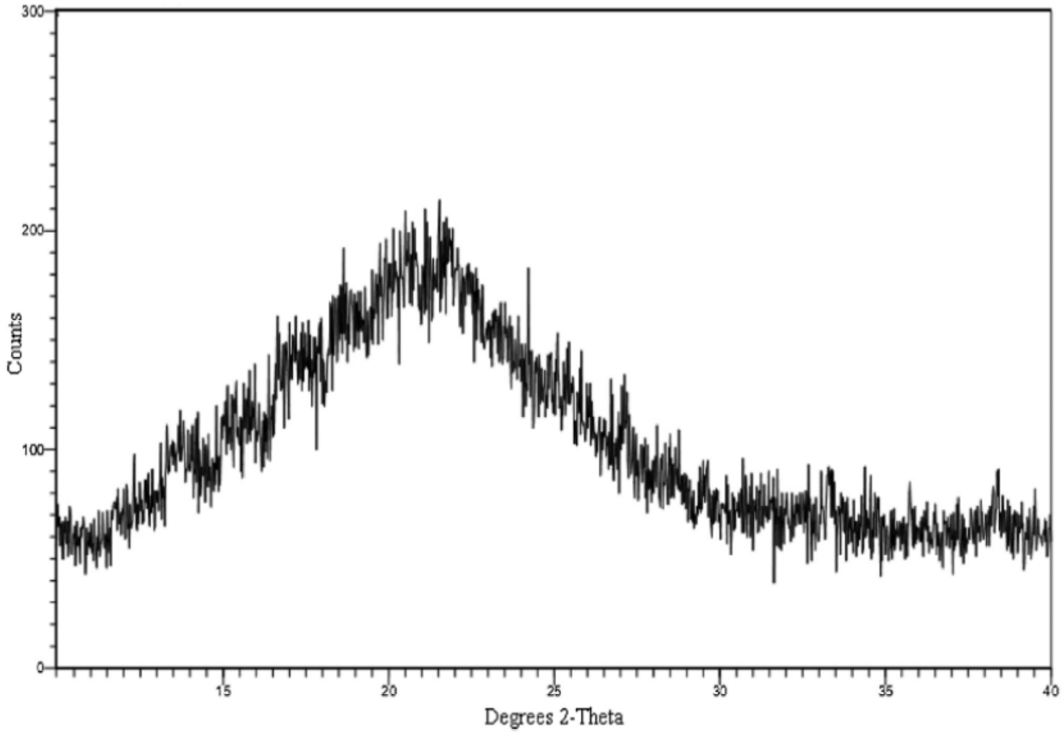

Fig.A1.8 (a). XRD of pristine PIM with composition 25.6% T-DGA, 53.9% NPOE, and 20.5% CTA.

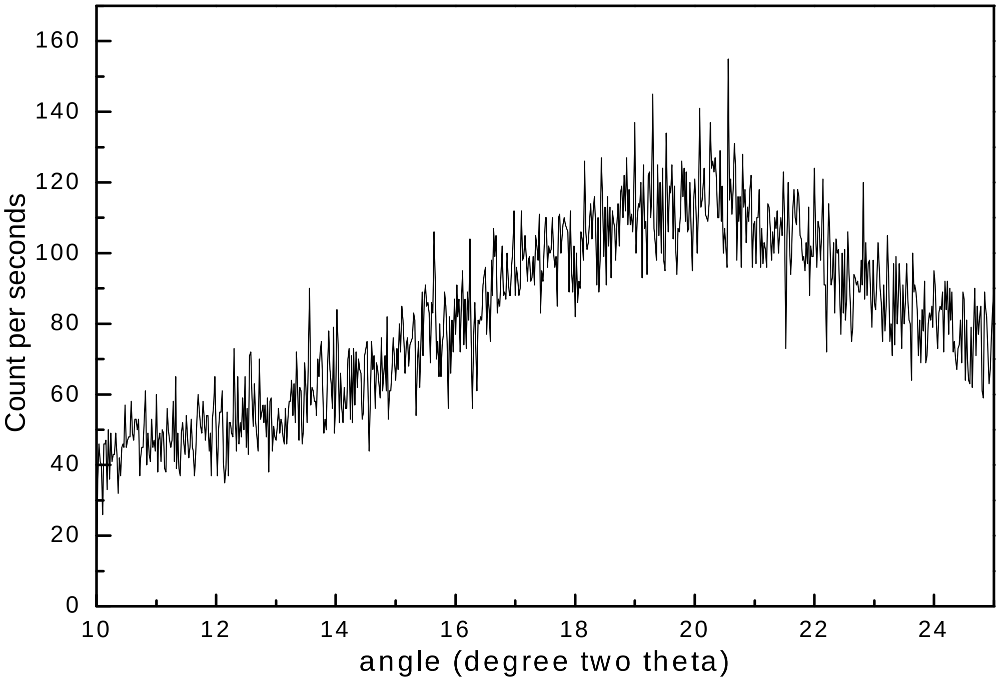

Fig.A1.8 (b). XRD of the PIM of composition: 6.5% C4DGA, 67.7% NPOE, and 25.8% CTA.

## A1.3. FTIR analysis

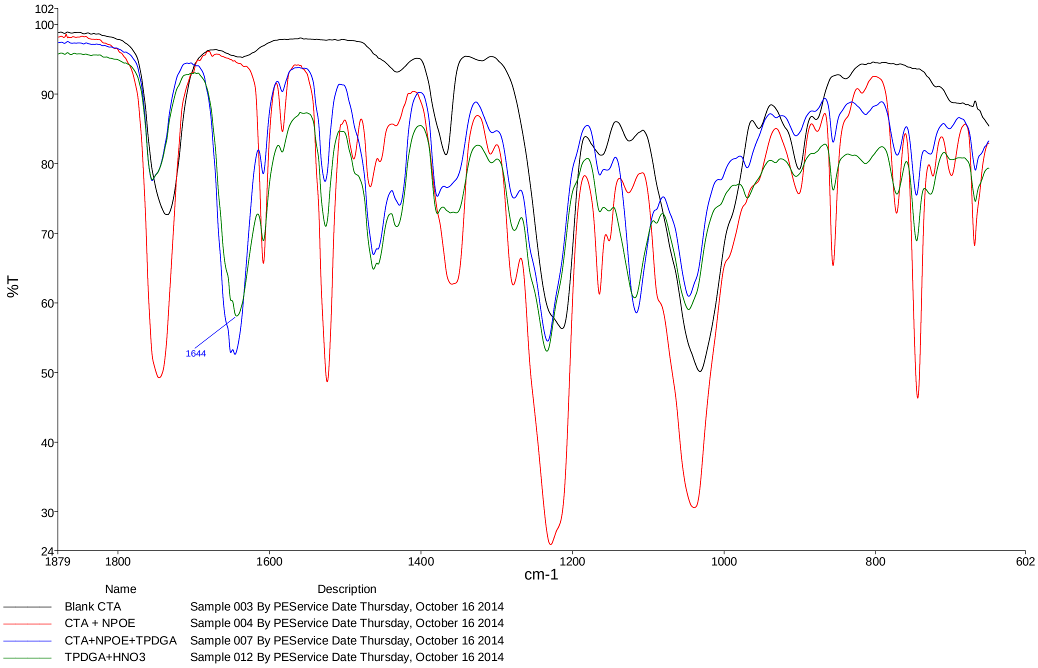

Fig. A1.9(a). FT-IR spectra of PIMs containing: i) CTA alone (black line), ii) CTA + NPOE (red line), iii) CTA + NPOE + TPDGA (blue line) and iv) TPDGA + $HNO_3$ (green line)

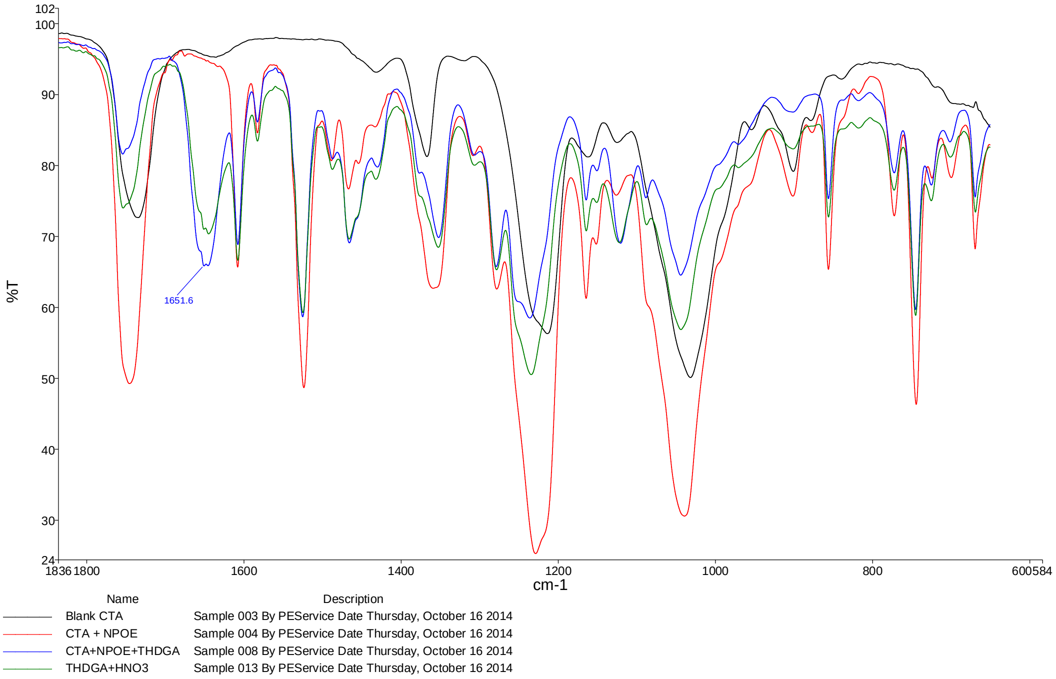

Fig. A1.9(b). FT-IR spectra of PIMs containing i) CTA alone (black line), ii) CTA + NPOE (red line), iii) CTA + NPOE + THDGA (blue line) and iv) THDGA + $HNO_3$ (green line)

The FT-IR spectra of the blank membrane made from CTA as well as other membranes were also recorded in order to see the band interference of CTA, NPOE and TPDGA / THDGA-carrier (Fig. A1.9). As can be seen from the figures, the band over lapping of CTA and NPOE at all wavelengths except at 1529 cm$^{-1}$ where CTA does not absorb. Thus, the IR microscopy studies for NPOE distribution profile were carried out at 1529 cm$^{-1}$ (vide infra). Similarly, the distribution profile of TPDGA and THDGA were monitored at 1645 cm$^{-1}$ and 1651 cm$^{-1}$, respectively (where CTA and NPOE do not interfere) in the membranes containing carrier, NPOE and CTA. The FT-IR spectra of all the membrane indicates that all the membrane components, viz., CTA, NPOE and TPDGA (or THDGA) exist in the membrane as separate entity and no chemical interaction is taking place among them (Fig.A1.9). As TDDGA based PIMs appeared inhomogeneous with subsequent evidence of extractant leaching out of the PIM and hence, not used for FTIR and IR microscopy mapping.

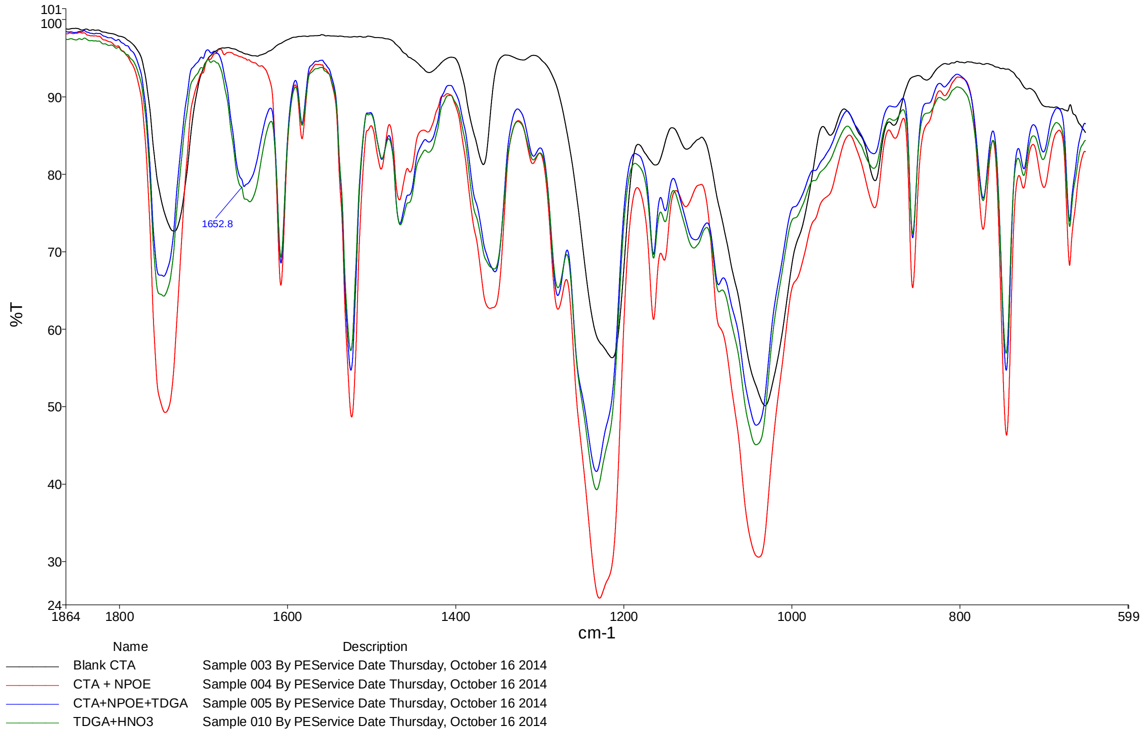

Fig.A1.10(a). FT-IR spectra of the PIM of the composition: 25.6% T-DGA, 53.9% NPOE and 20.5% CTA and the PIM dipped in 1 M $HNO_3$ for 24 h.

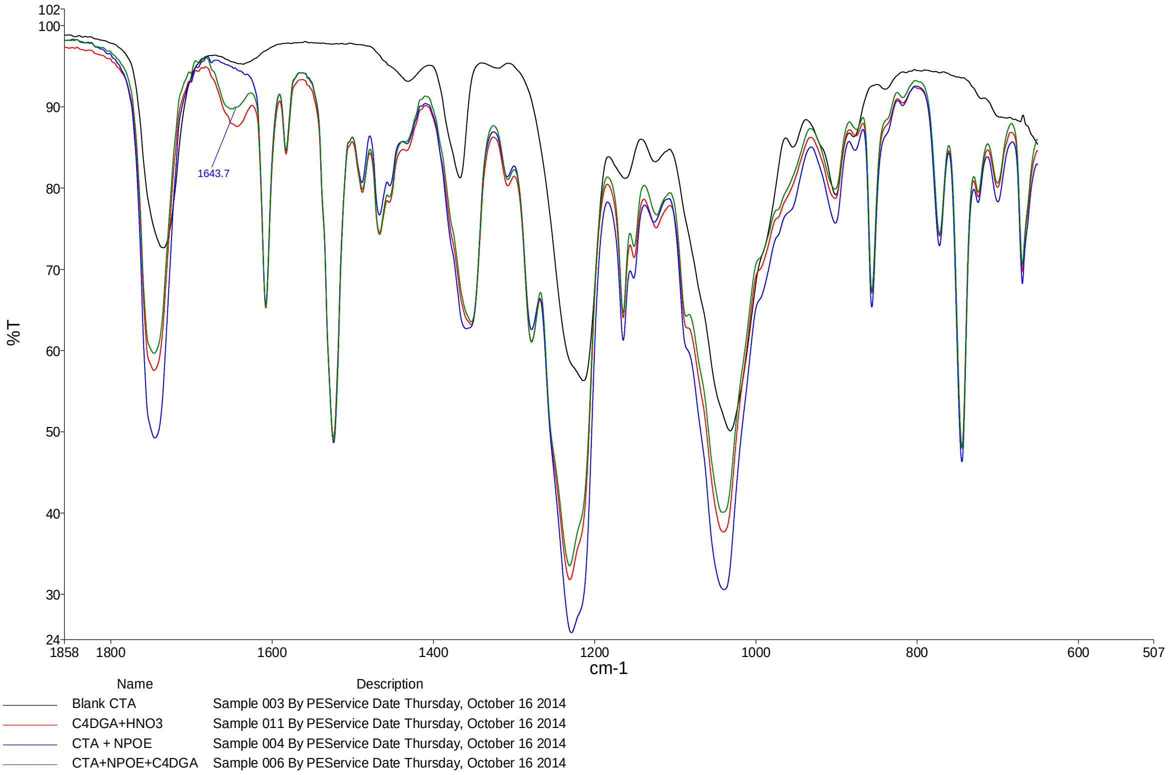

Fig. A1.10(b). FTIR of the PIM of composition 6.5% C4DGA, 67.7% NPOE, and 25.8% CTA and the PIM dipped in 1 M $HNO_3$ for 24 h.

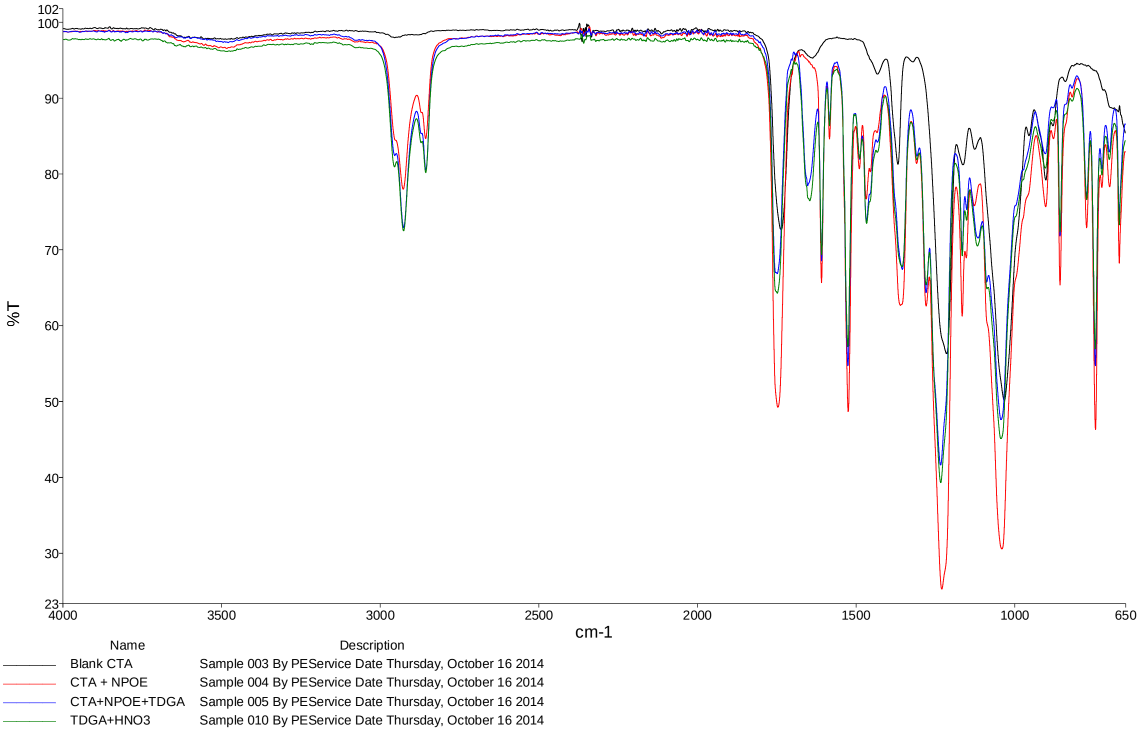

Fig.A1.11. FT-IR spectra of pristine T-DGA containing PIM (blue) and the reused PIM (green).

## A1.4. TIMM studies

The TIMM plots are depicted in Figs.A1.12-A1.15 for PIMs containing the TPDGA (or THDGA) as carrier extractants. TIMM profiles for the mapping of the DGA ligands are presented in Figs.A1.12(a) and A1.13(a) while those for the mapping of NPOE in the same PIMs are shown in Figs. A1.12(b) and A1.13(b).

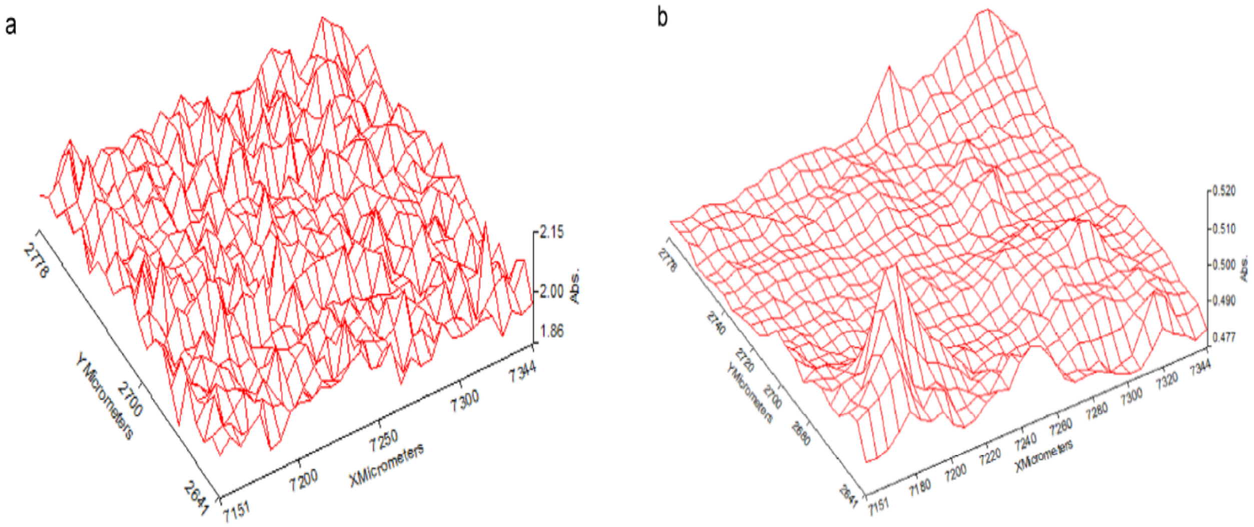

Fig.A1.12 TIMM distribution profile of PIMs containing TPDGA (400 mg TPDGA+ 80 mg CTA+105 mg NPOE), (a) TPDGA at 1645 cm$^{-1}$; (b) NPOE at 1529 cm$^{-1}$.

As seen from Figs. A1.12(a) and A1.13(a), the distribution of the carriers TPDGA (at 1645 cm$^{-1}$) and THDGA (at 1651 cm$^{-1}$), respectively was homogeneous. On the other hand, the distribution of NPOE (as monitored by the 1529 cm$^{-1}$ band, Figs. A1.12(b) and A1.13(b)) is not homogeneous and shows occasional higher distributions (also confirmed by the chemicals distribution contour plots in Fig.A1.14 and Fig.A1.15). TIMM studies were also carried out with the PIMs kept in 1 M $HNO_3$ for 24 h and the results showed no significant change suggesting no leaching out of carrier or plasticizer from the PIMs (Fig.A1.16 and Fig.A1.17).

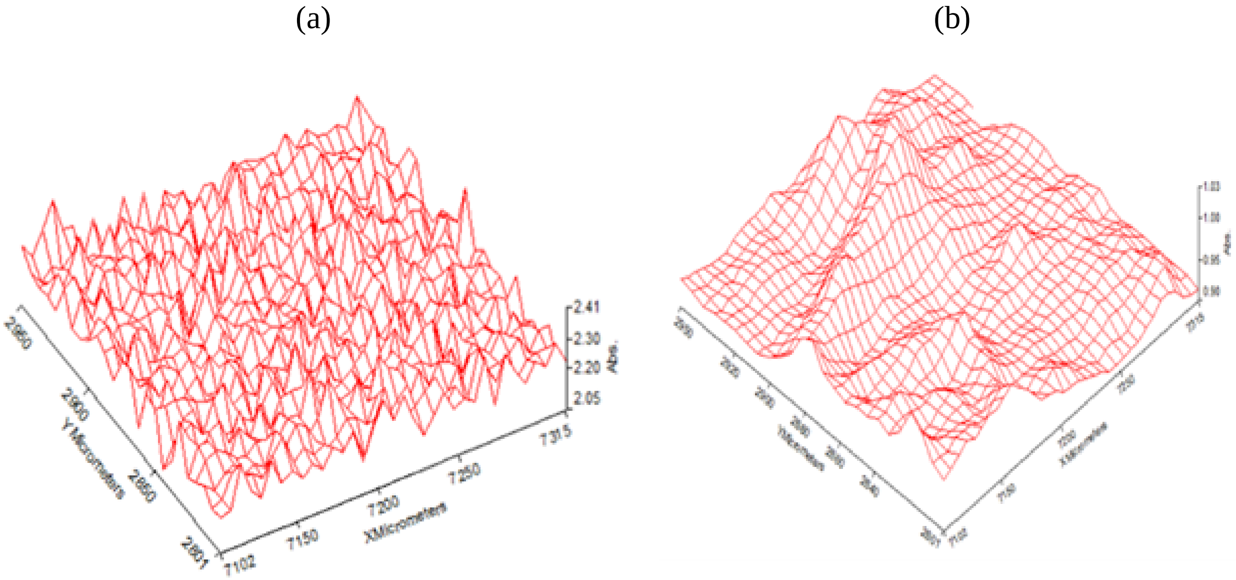

Fig. A1.13: TIMM distribution profile of PIMs containing THDGA (400 mg TPDGA + 80 mg CTA +105 mg NPOE), (a) THDGA at 1645 cm$^{-1}$; (b) NPOE at 1529 cm$^{-1}$.

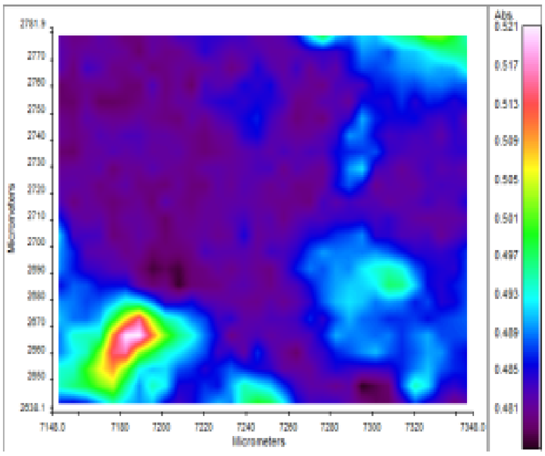

Fig. A1.14: Contour plots of PIM containing TPDGA showing the profiles of NPOE

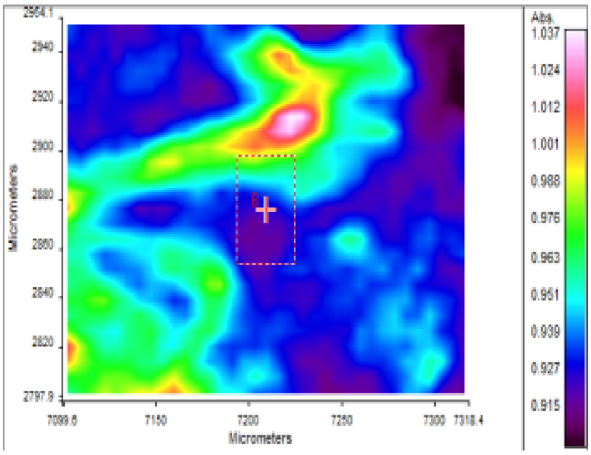

Fig.A1.15: Contour plots of PIM containing THDGA showing the profiles of NPOE

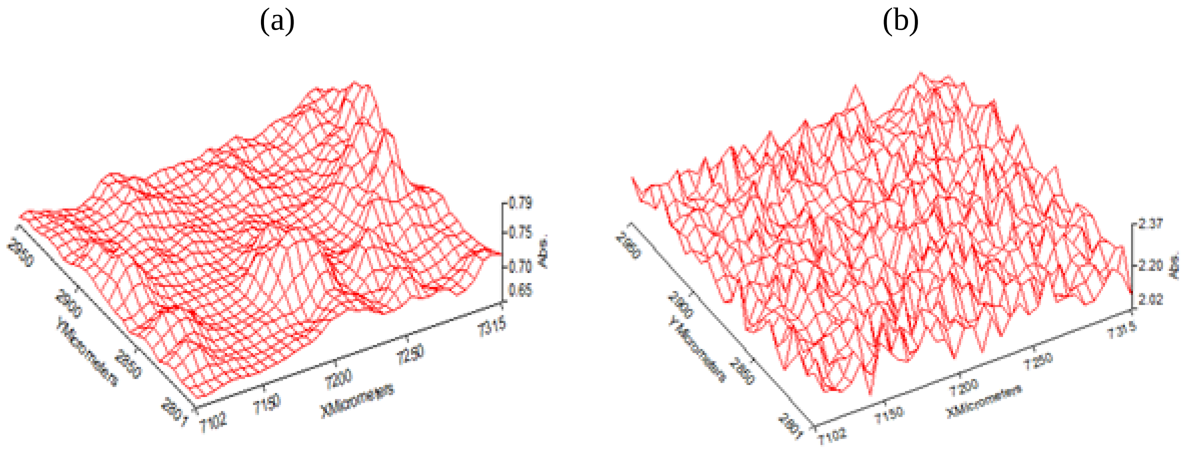
(a) (b)

Fig.A1.16: TIMM plots of (a) NPOE and (b) TPDGA mapping of PIM containing TPDGA after keeping in contact with 1 M $HNO_3$ for 24 h

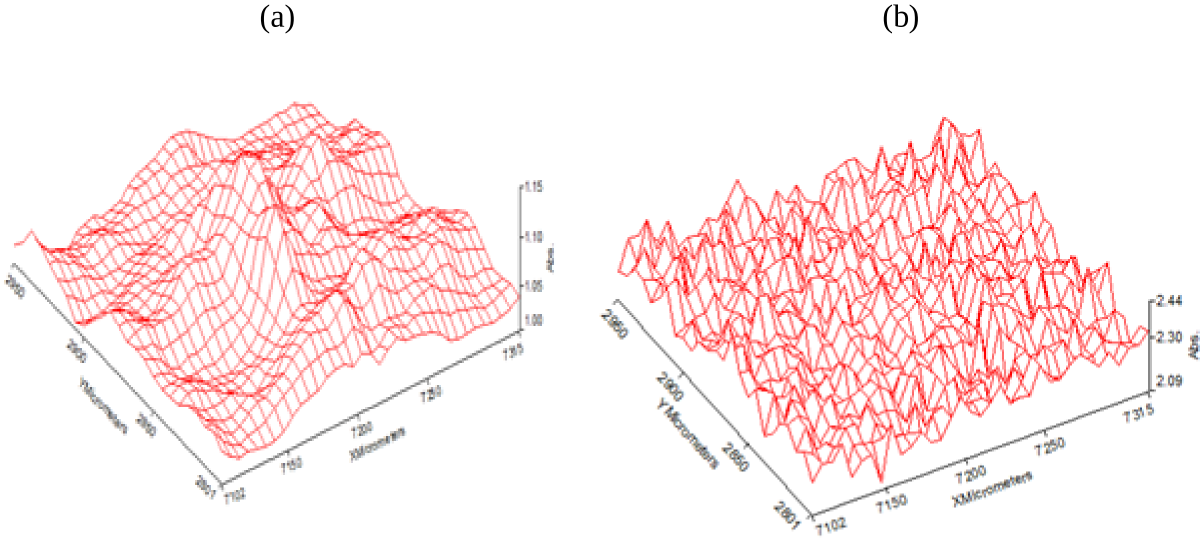
(a) (b)

Fig.A1.17. TIMM plots of (a) NPOE and (b) THDGA mapping of PIM containing THDGA after keeping in contact with 1 M $HNO_3$ for 24 h

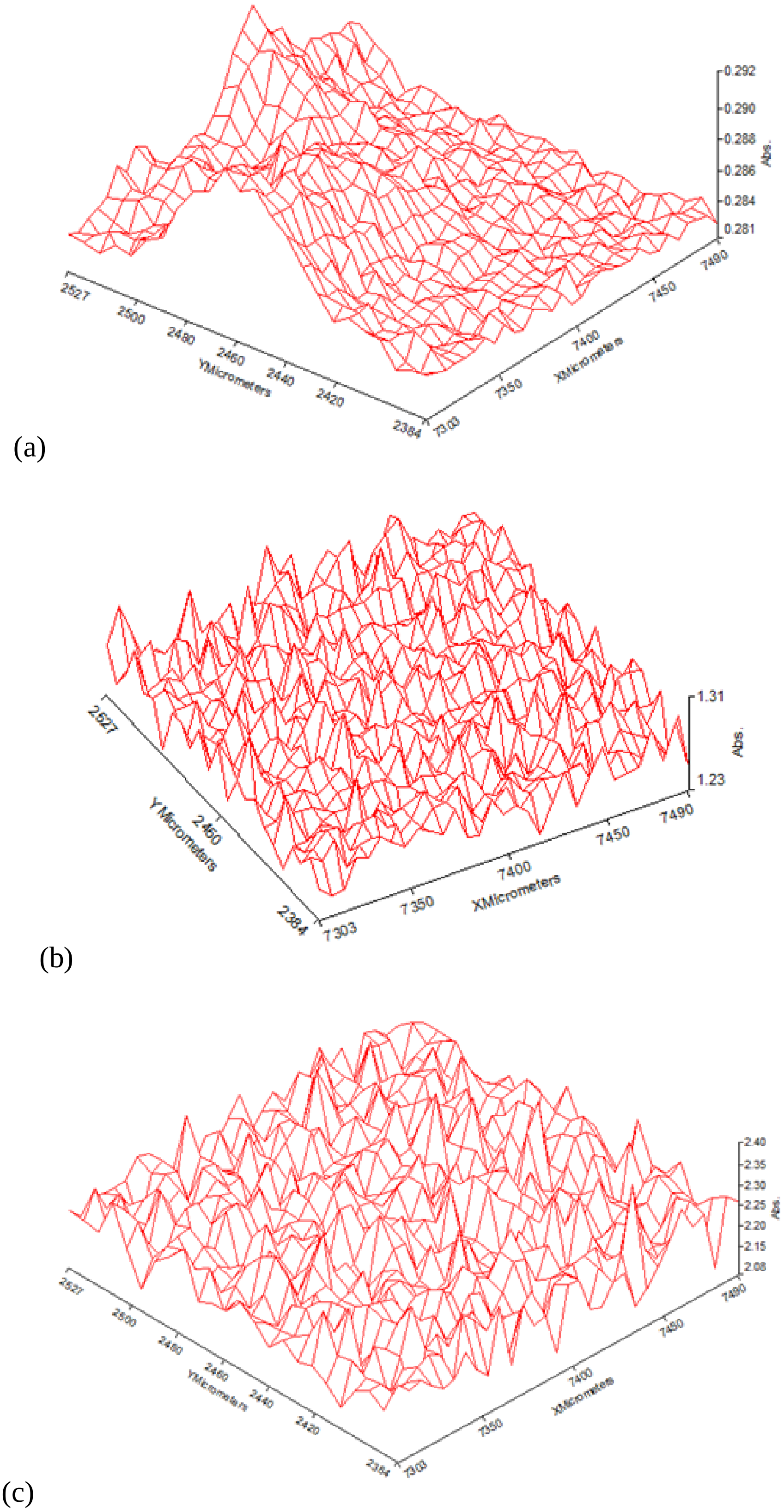

Fig. A1.18. TIMM distribution profile of (a) NPOE at 1529 cm$^{-1}$ (80 mg CTA + 210 mg NPOE); (b) T-DGA at 1652 cm$^{-1}$ (100 mg T-DGA + 80 mg CTA + 210 mg NPOE); (c) T-DGA/NPOE at 1529 cm$^{-1}$ (100 mg T-DGA + 80 mg CTA + 210 mg NPOE).

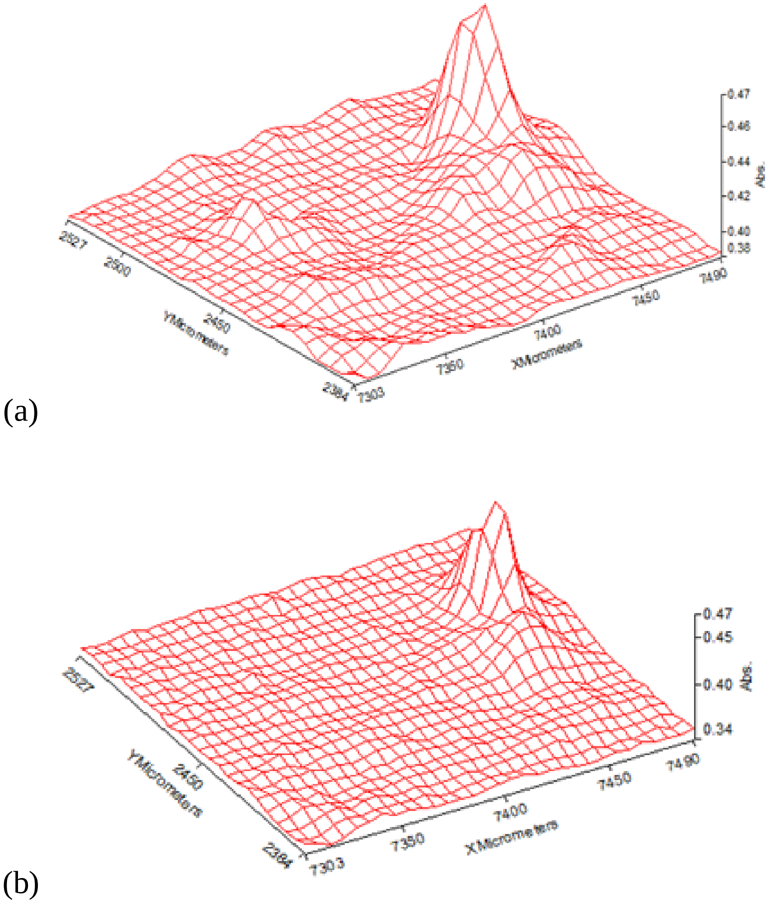

(a)

(b)

Fig. A1.19. TIMM plots of the PIM of the composition: 6.5% C4DGA, 67.7% NPOE, and 25.8% CTA; (a) mapping carried out at 1529 cm$^{-1}$; (b) mapping carried out at 1645 cm$^{-1}$.

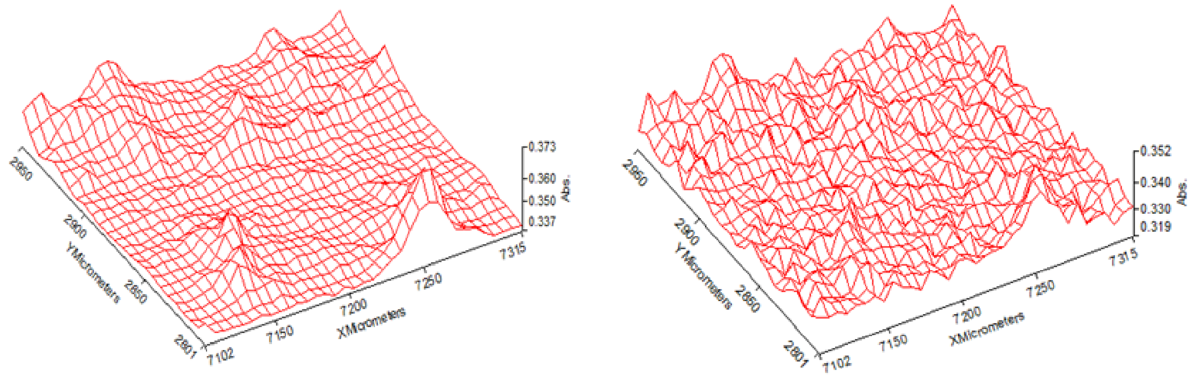

(a)

(b)

Fig.A1.20. TIMM plots of the PIM of composition: 6.5% C4DGA, 67.7% NPOE, and 25.8% CTA dipped in 1 M $HNO_3$ for 24 h; (a) Mapping carried out at 1529 cm$^{-1}$; (b) Mapping carried out at 1645 cm$^{-1}$.

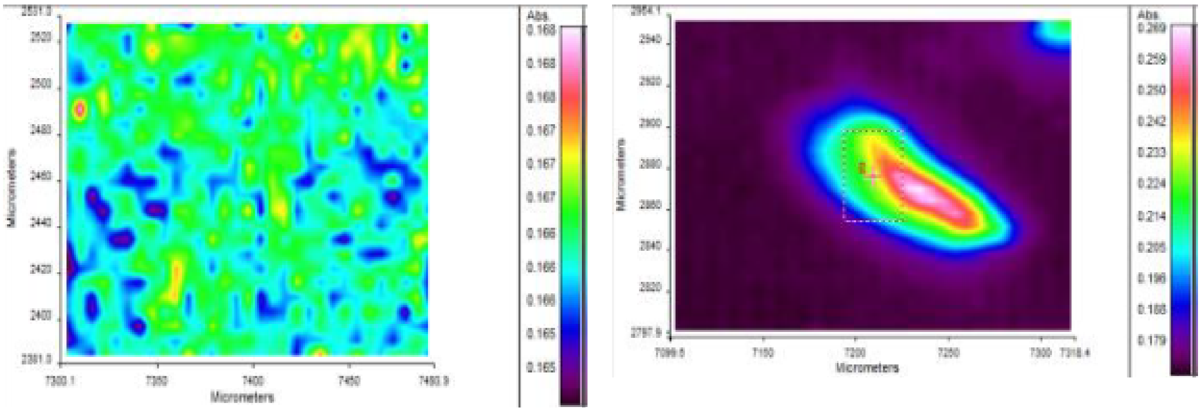

(a) Pristine PIM (only CTA)

(b) Exposed to 1 M $HNO_3$ for 5 days (only CTA)

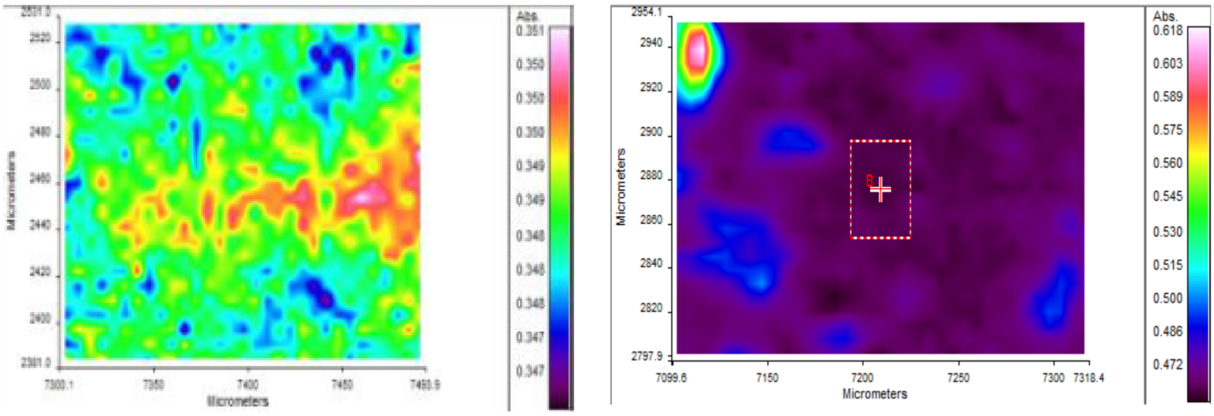

(c) Pristine PIM (CTA+NPOE+T-DGA)

(d) Exposed to 1 M $HNO_3$ for 5 days (CTA+NPOE+T-DGA)

Fig.A1.21. Chemical images of the TIMM plots obtained with a Perkin Elmer Instrument (Spotlight 300 with Spectrum 400 FTIR Spectrometer) operated in the image (transmission) mode. Pixel size: 6.25 μ. Scans per pixel: 16 scans; Resolution: 4 $cm^{-1}$; Detector: Mercury Cadmium Telluride.

## A1.5. AFM studies

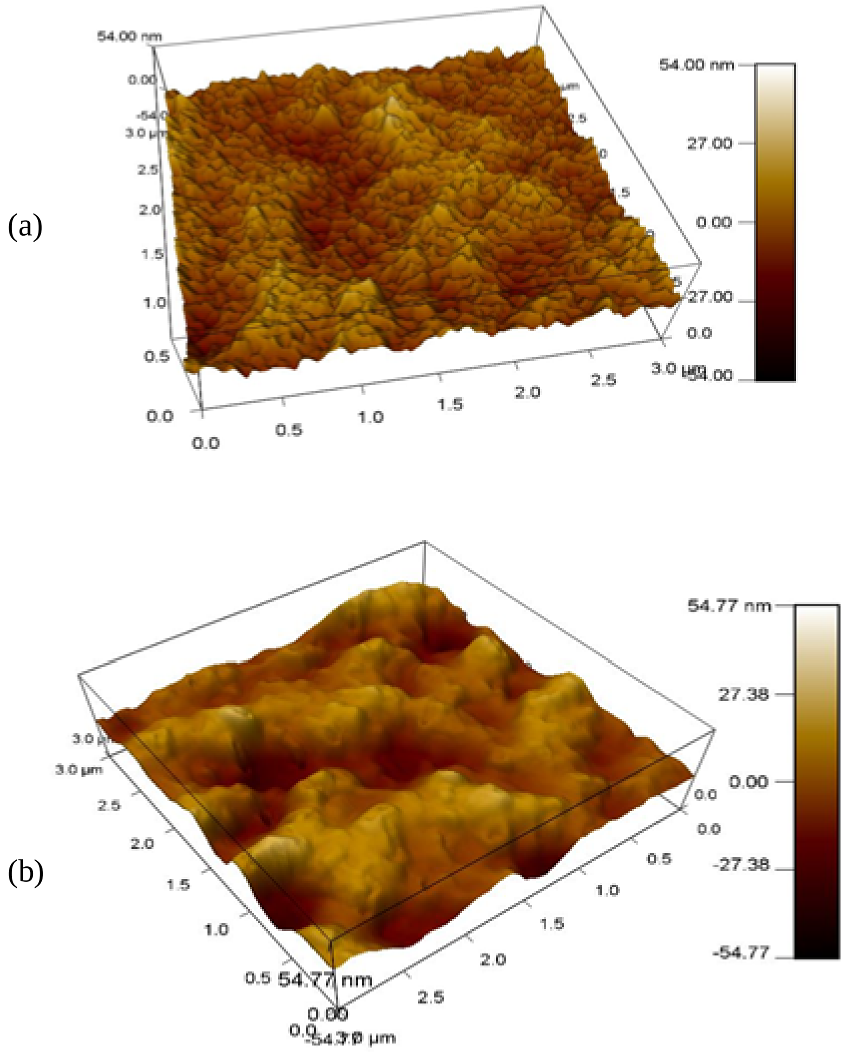

Fig.A1.22. AFM profiles of the PIMs with composition: 25.6% T-DGA, 53.9% NPOE, and 20.5% CTA. (a) Pristine PIM (b) PIM after uptake and stripping.

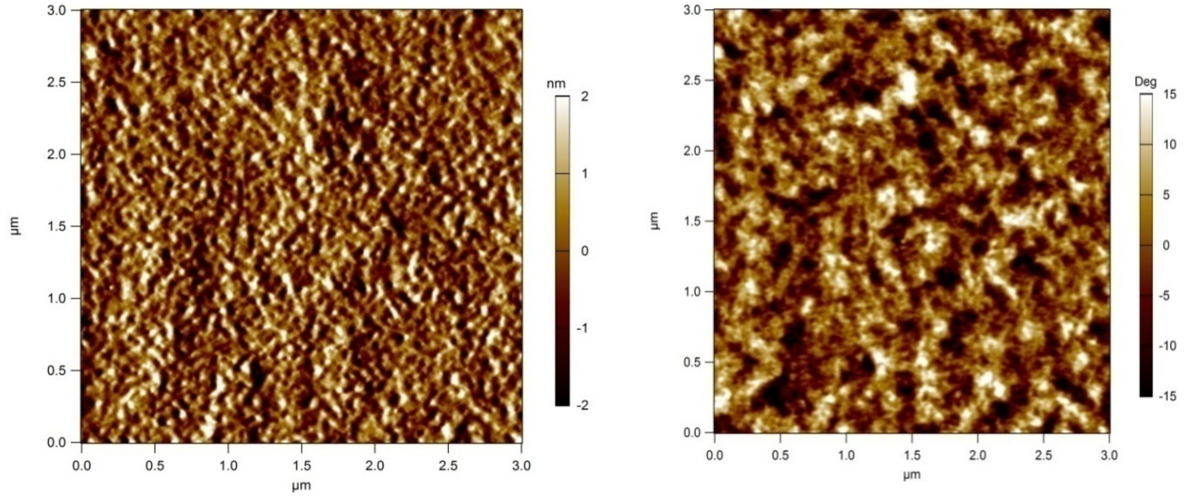

Amplitude image

Phase image

Fig.A1.23. AFM pictures of pristine PIM of the composition: 25.6% T-DGA, 53.9% NPOE, and 20.5% CTA

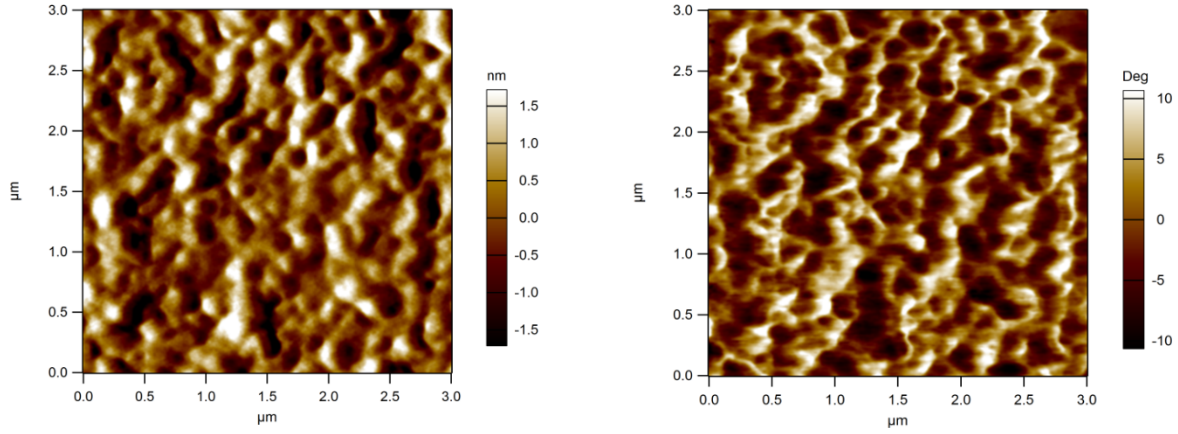

Amplitude image

Phase image

Fig.A1.24. AFM pictures of the PIM of the composition: 25.6% T-DGA, 53.9% NPOE and 20.5% CTA after several use of Eu(III) loading and stripping using α-HIBA.

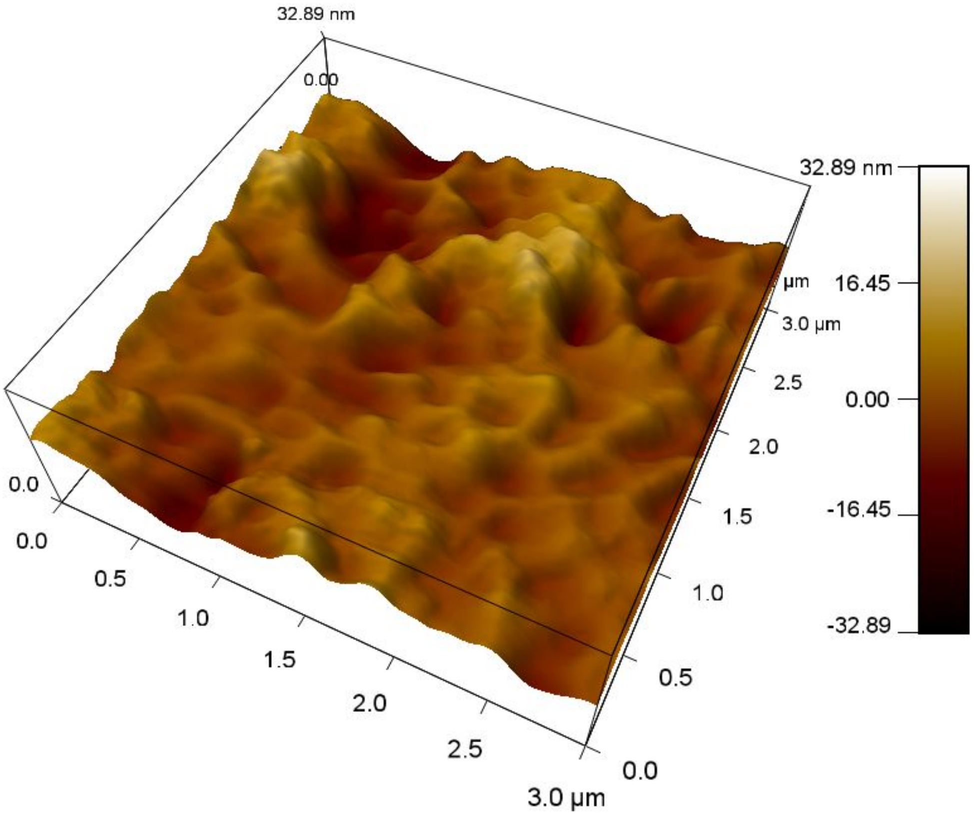

Fig.A1.25. AFM profiles on the surface roughness of the T-DGA containing PIMs after 5 days contact with 1 M $HNO_3$

A1.6. SEM studies

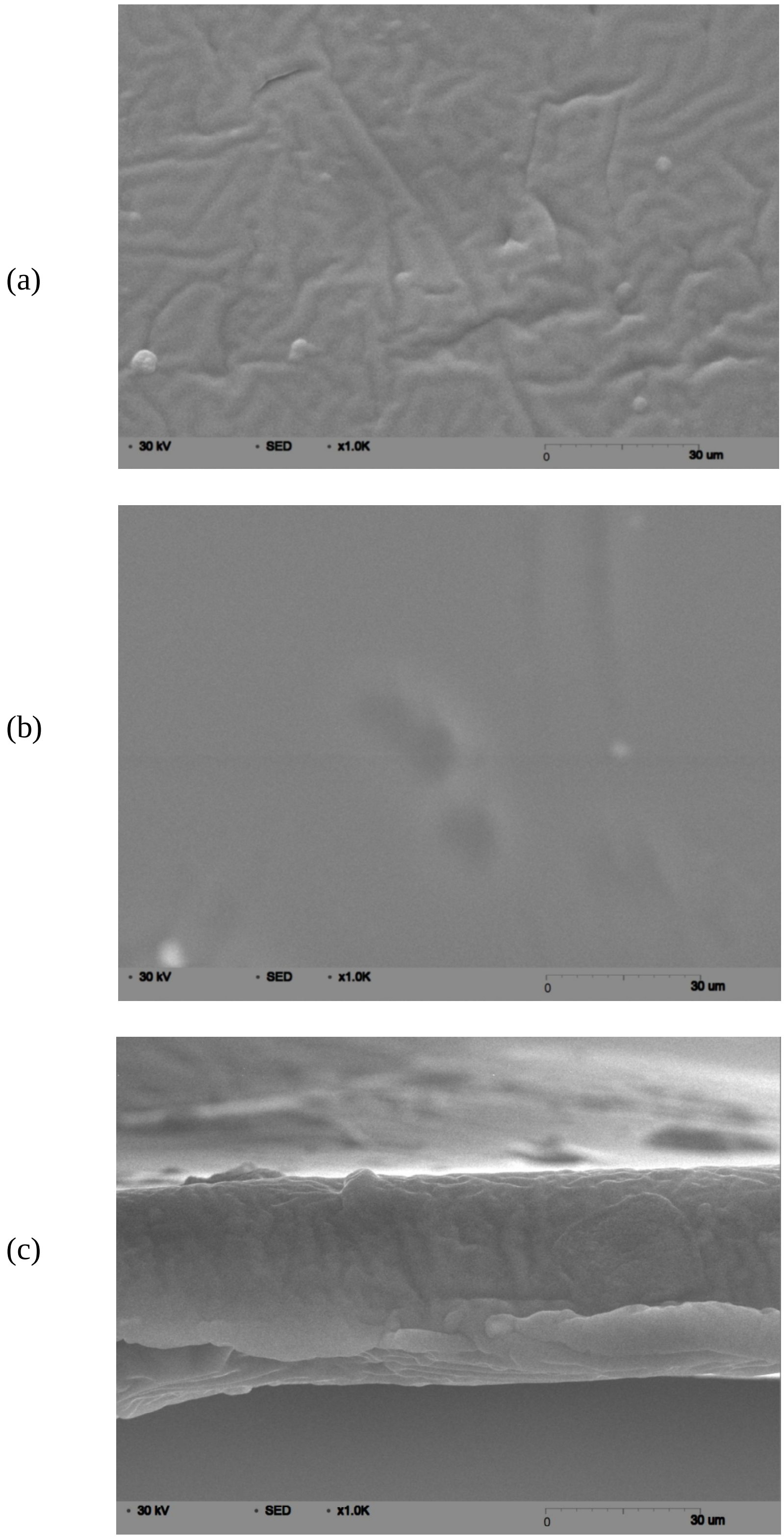

Fig.A1.26. SEM of PIM composition 25.6% T-DGA, 53.9% NPOE, and 20.5% CTA. (a) Lower; (b) Upper; (c) Cross section

# ACTINIDE ION UPTAKE AND TRANSPORT BY THE POLYMER INCLUSION MEMBRANES CONTAINING DIFFERENT SUBSTITUTED DIGLYCOLAMIDES / MULTIPLE DIGLYCOLAMIDE LIGANDS AS THE CARRIER EXTRACTANTS

## A2.1. Uptake Studies

### A2.1.1. Effect of NPOE concentration on the Am(III) uptake

The effect of NPOE concentration in the TODGA containing PIM was studied by varying the NPOE content in casted Polymer Inclusion Sorbent (PIS) from 18% to 39%.

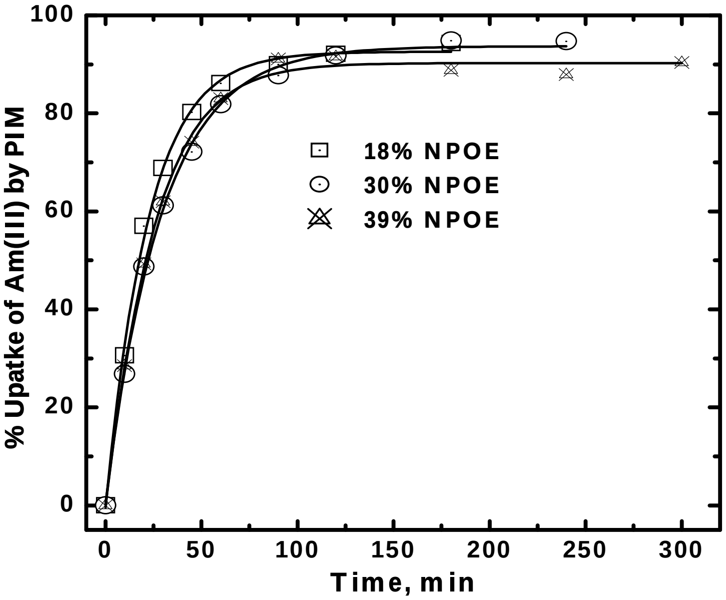

Fig.A2.1. Effect of NPOE content in the PIMs on Am(III) uptake keeping other parameters such as CTA (80 mg) and TODGA (400 mg) content fixed. Feed: 1 M $HNO_3$

There was marginal change in the Am(III) uptake rates suggesting that NPOE concentration (Fig.A2.1) was not very important for PISs containing TODGA as the carrier extractant.

The effect of NPOE concentration in the T2EHDGA containing PIM was studied by varying the NPOE content from 105-315 mg while keeping CTA and T2EHDGA content fixed at 80 mg and 400 mg, respectively which corresponded to 17.9%-39.6% NPOE in the

PIM. A decrease in the Am(III) ion uptake rate with the increasing NPOE concentration was seen (Fig.A2.2).

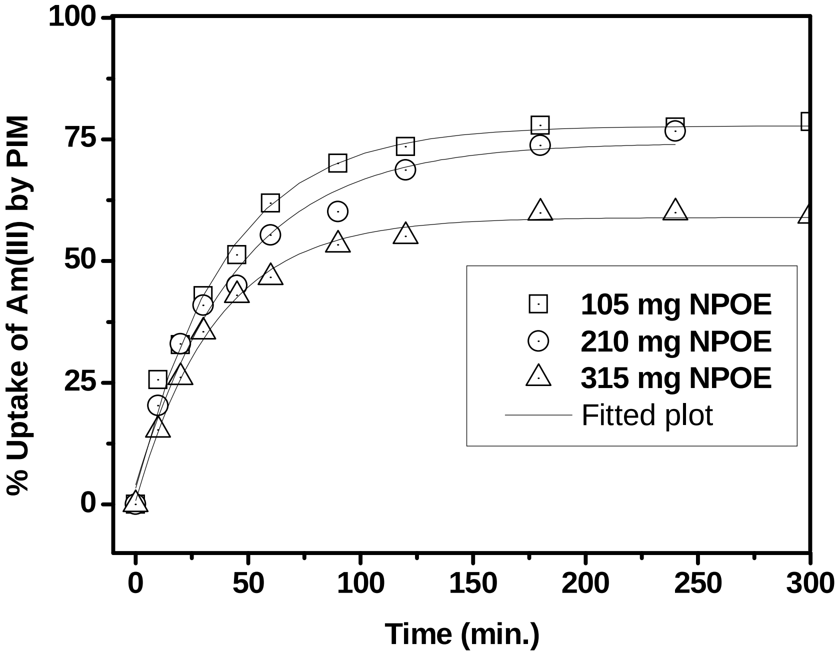

Fig.A 2.2. Effect of NPOE content in the PIMs on Am(III) uptake keeping other parameters such as CTA (80 mg) and T2EHDGA (400 mg) content fixed. Feed: 1 M $HNO_3$.

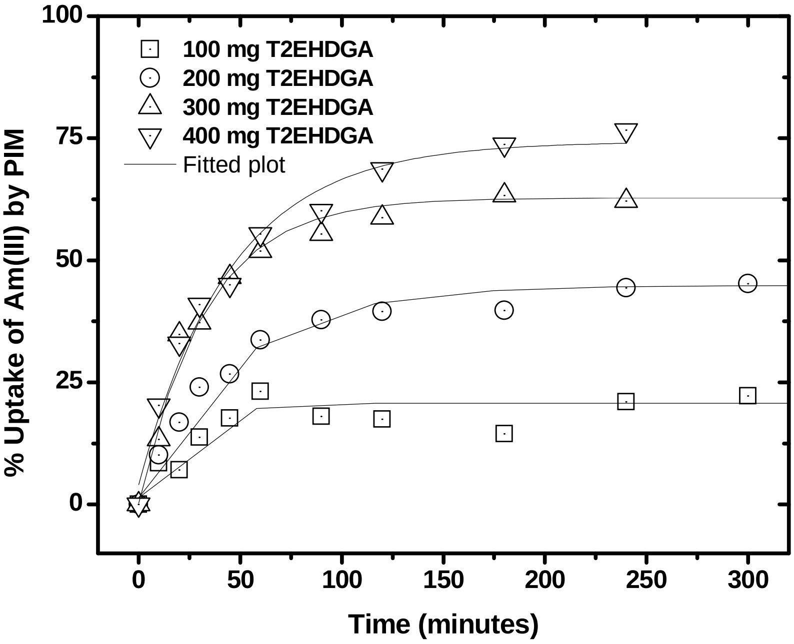

Fig.A 2.3. Effect of T2EHDGA content in the PIMs on Am(III) uptake keeping other parameters such as CTA (80 mg) and NPOE (210 mg) content fixed. Feed: 1 M $HNO_3$.

The effect of NPOE was also confirmed from the uptake study with Am(III) ion using the PIMs containing varying concentrations of T2EHDGA but made with two fixed amounts of NPOE (105 mg and 210 mg). As shown in Fig. 3.7 (Chapter 3) and Fig.A 2.3, the results showed more favourable uptake of Am(III) ion with the PIMs containing lower NPOE content though higher mass transfer rates were seen with higher T2EHDGA content. The % uptake data for Am(III) are presented in Table A2.1.

Table A2.1. Am(III) uptake data (2 h) as a function of various compositions of the T2EHDGA containing PIMs. The weights of the constituents while preparing the PIM are indicated inside the brackets. Feed: 1 M $HNO_3$.

| Composition of PIM | | | % Am uptake (2h) |
|---|---|---|---|
| % CTA (in mg) | % NPOE (in mg) | % T2EHDGA (in mg) | |
| 28.1(80) | 36.8(105) | 35.1(100) | 24.2 |
| 20.8 (80) | 27.3 (105) | 51.9 (200) | 57.9 |
| 16.5 (80) | 21.6 (105) | 61.9 (300) | 67.2 |
| 13.7 (80) | 17.9 (105) | 68.4 (400) | 73.5 |
| 13.6 (80) | 35.6 (210) | 50.8 (300) | 58.7 |
| 16.3 (80) | 42.9 (210) | 40.8 (200) | 39.5 |
| 20.5 (80) | 53.9 (210) | 25.6 (100) | 17.5 |
| 11.6 (80) | 30.4 (210) | 58.0 (400) | 68.7 |
| 10.1 (80) | 39.6 (315) | 50.3 (400) | 55.1 |
| 7.3 (40) | 19.3 (105) | 73.4 (400) | 72.5 |
| 19.2 (120) | 16.8 (105) | 64.0 (400) | 62.9 |
| 24.1 (160) | 15.8 (105) | 60.1 (400) | 60.2 |

It can be seen from the table that under comparable T2EHDGA content, the mass transfer rates were comparable. For example, for two PIMs containing 20.8% CTA, 27.3% NPOE and 51.9% T2EHDGA and 10.1% CTA, 39.6% NPOE and 50.3% T2EHDGA, the Am uptake values were 57.9% and 55.1% suggesting ligand concentration is of paramount importance.

Table A 2.2. % Am(III) uptake by PIMs containing varying amounts of NPOE keeping other parameters such as T-DGA (80 mg) and CTA (80 mg) fixed. Feed: 1 M $HNO_3$

| Time (h) | % Am(III) Uptake | | |
|---|---|---|---|
| | 24.5% NPOE | 39.6% NPOE | 56.8% NPOE |
| 0.5 | 43.4 | 48.3 | 35.0 |
| 1 | 63.3 | 66.7 | 57.9 |
| 2 | 77.7 | 87.1 | 66.9 |
| 3 | 84.7 | 86.6 | 71.9 |
| 4 | 85.4 | 87.8 | 76.5 |
| 6 | 88.2 | 86.9 | 81.6 |
| 24 | 88.7 | 88.8 | 87.6 |

### A2.1.2. Effect of CTA concentration on the Am(III) uptake

As seen in Fig.A2.4, variation in the CTA content did not show any influence on the Am(III) uptake efficiency of the PISs in case of TODGA containing PISs.

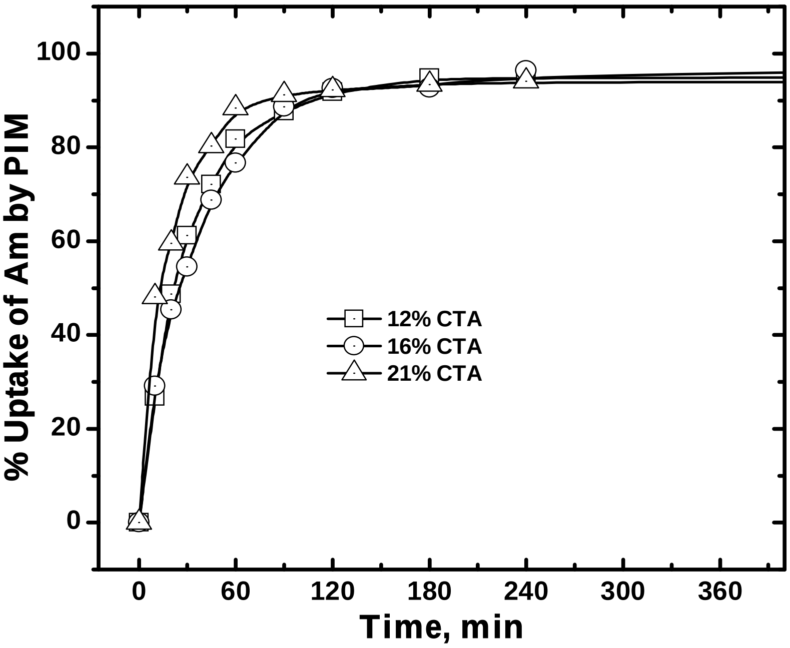

Fig.A2.4. Effect of CTA content in the PIMs on Am(III) uptake keeping other parameters such as TODGA (400 mg) and NPOE (210 mg) content fixed. Feed: 1 M $HNO_3$

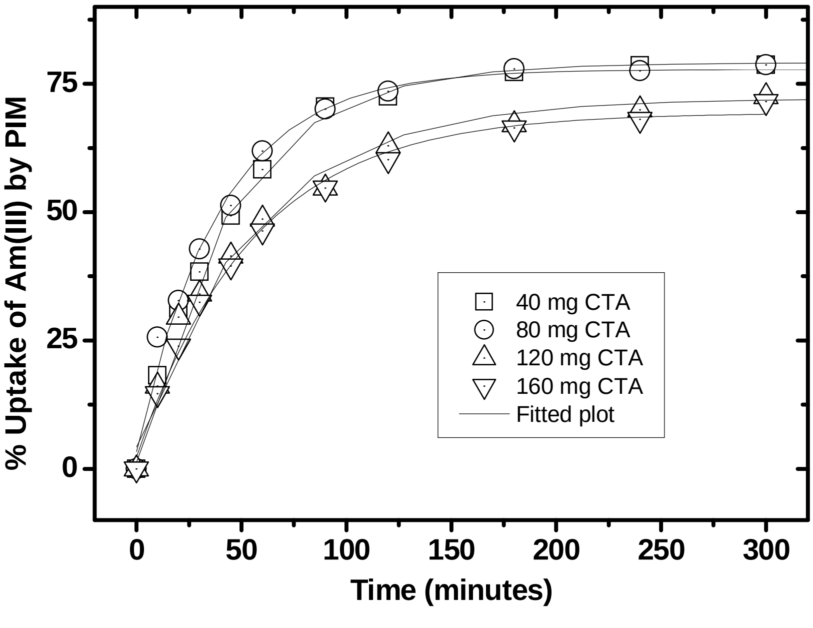

Fig. A2.5. Effect of CTA content in the PIMs on Am(III) uptake keeping other parameters such as T2EHDGA (400 mg) and NPOE (105 mg) content fixed. Feed: 1 M $HNO_3$.

As seen in Fig. A2.5, up to 13.7% CTA content (80 mg) in the T2EHDGA containing PIM, Am(III) ion uptake efficiency was not influenced by the CTA content.

A2.1.3. Effect of carrier extractant

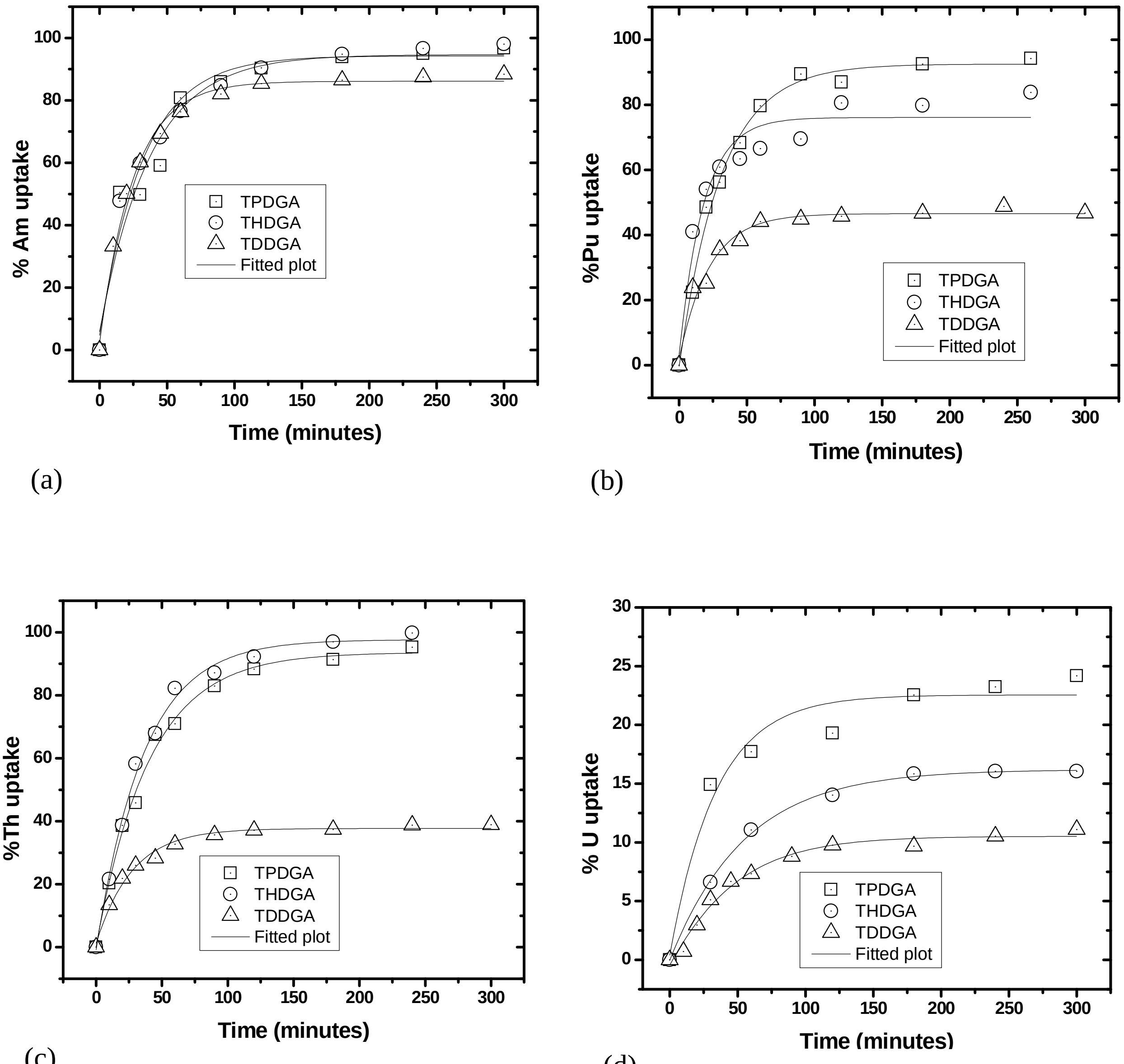

(a) (b)

(c) (d)

Fig.A2.6. Uptake of the actinide ions by various PIMs containing 68.4% carrier, 17.9% NPOE, and 13.7% CTA; Feed solution volume: 20 mL; Acidity:1 M $HNO_3$; (a) Am(III); (b) Pu(IV); (c) Th(IV); (d) U(VI).

A2.1.4. Uptake kinetics and isotherm studies

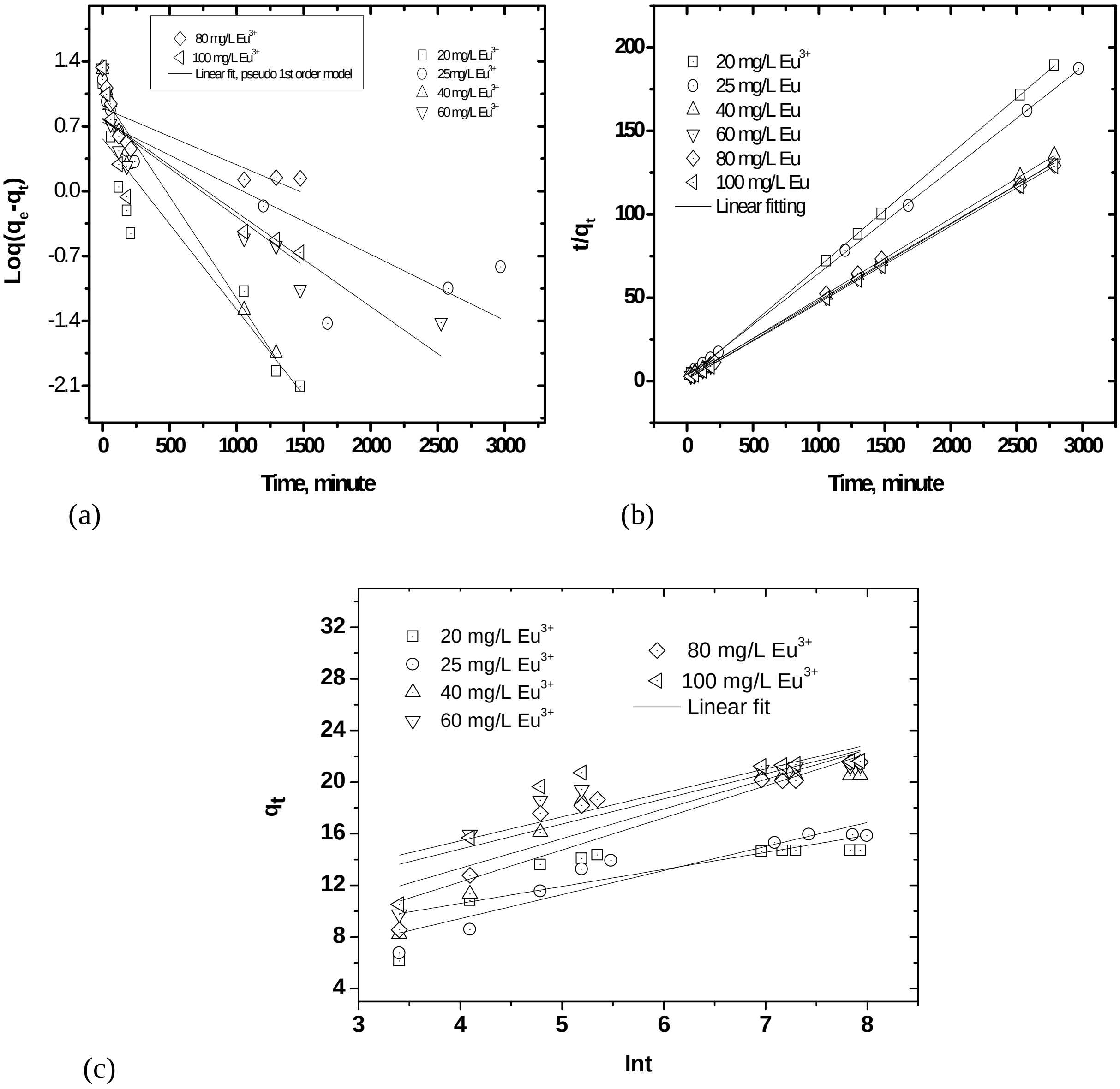

(a) (b)

(c)

Fig.A2.7. Linear fitting of the uptake data to the (a) pseudo-first order Lagergren model (b) pseudo-second order model (c) Elovich model. PIM composition of PIM: 25.6% T-DGA, 53.9% NPOE and 20.5% CTA

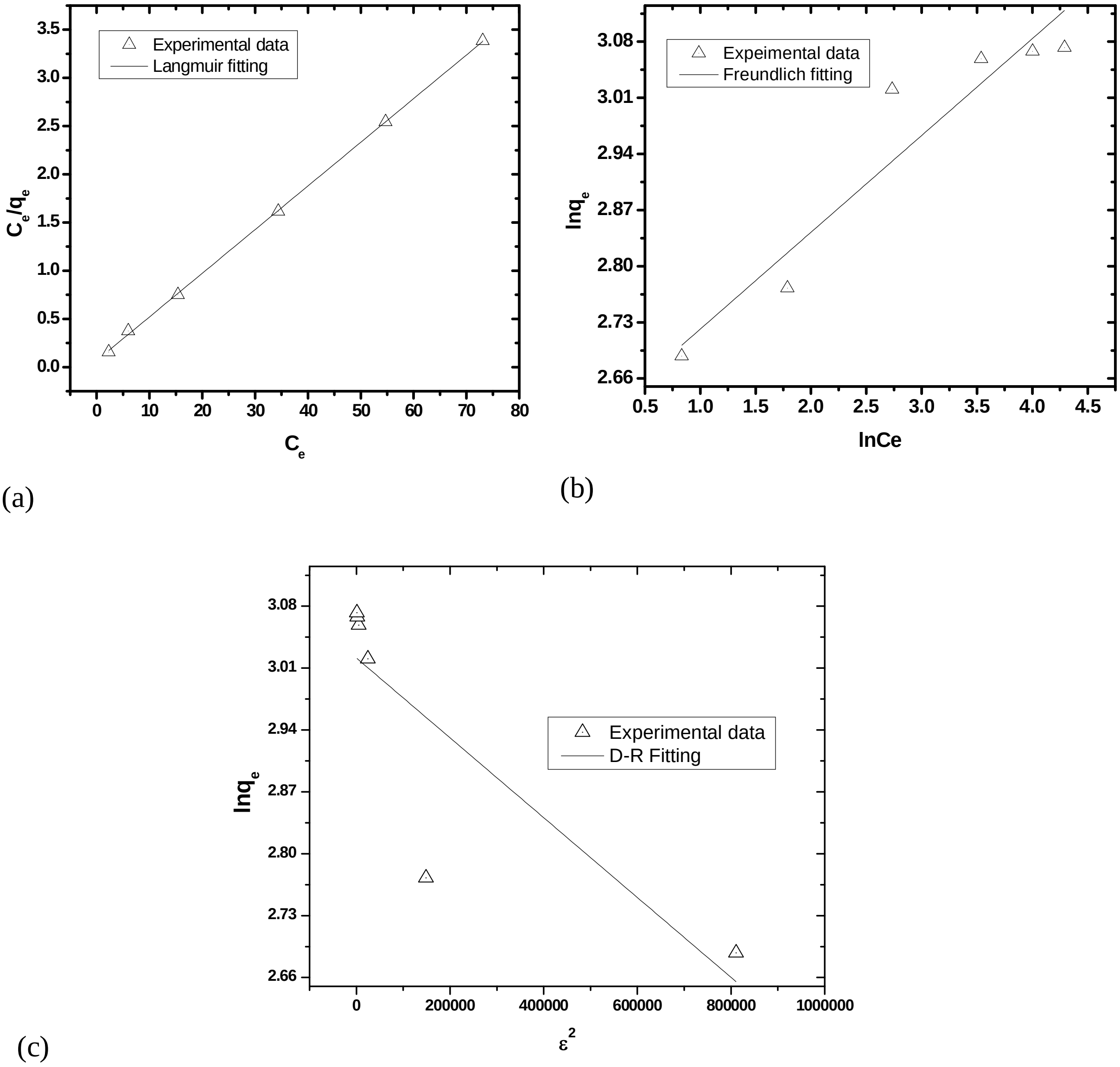

(a)

(b)

(c)

Fig.A2.8. Linear fitting of the uptake data to the (a) Langmuir (b) Freundlich (c) D-R adsorption isotherm model. PIM Composition: 25.6% T-DGA, 53.9% NPOE and 20.5% CTA

## A2.2. Transport studies

Transport profiles for different actinide ions with the TODGA / T2EHDGA / TPDGA / THDGA / T-DGA / C4DGA containing PIMs are given.

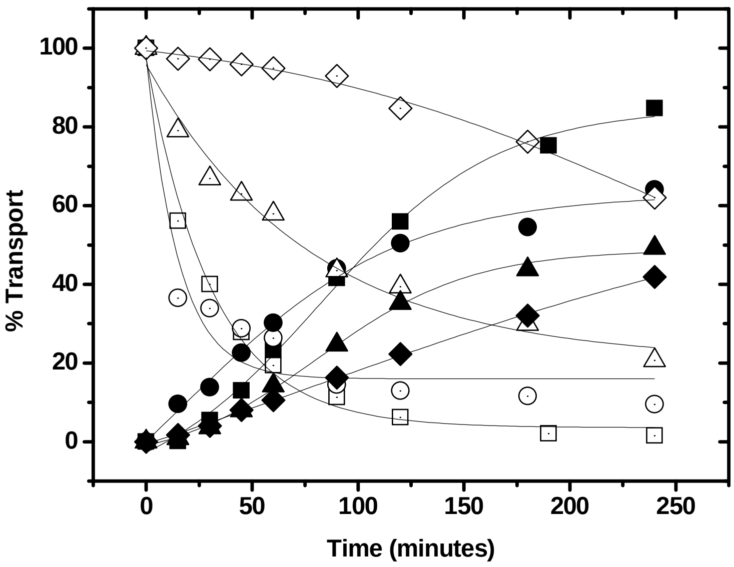

Fig.A2.9. Transport profiles (feed: empty symbol; receiver: filled symbol) of the actinide ions (square: Am(III); circle: Pu(IV); triangle: Th(IV); diamond: U(VI)) using PIMs of the optimized composition: 58% TODGA, 30% NPOE, 12% CTA; Feed: 1 MHNO$_3$; Receiver: 1 M α-HIBA at pH 3.0.

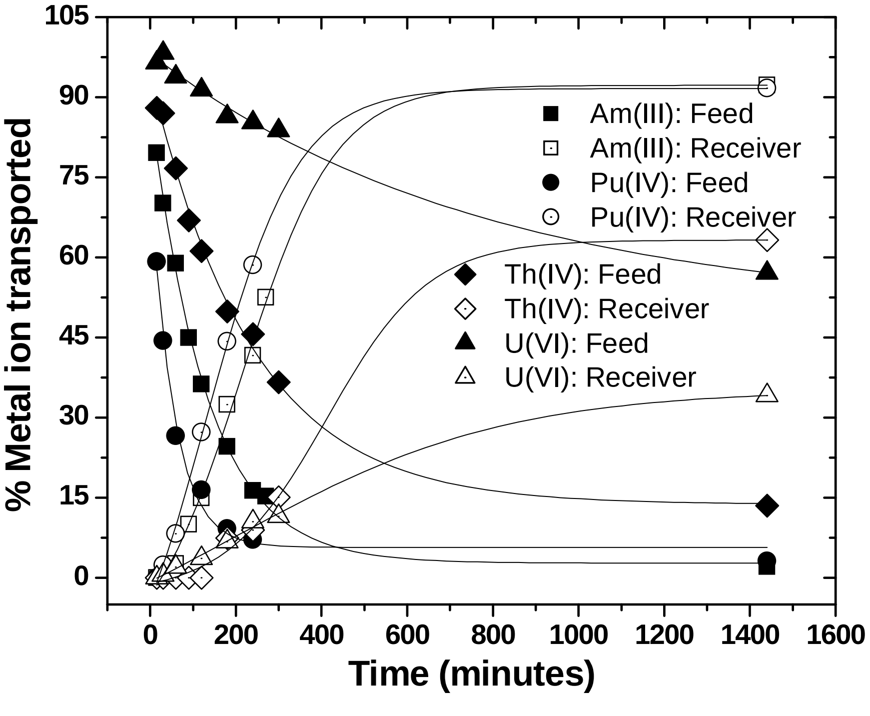

Fig.A2.10. Transport profiles of actinide ions by T2EHDGA-based PIM. Feed: 1 M HNO$_3$. Receiver: 1 M α-HIBA at pH 3.0. PIM composition: 68.4% T2EHDGA, 17.9% NPOE and 13.7% CTA

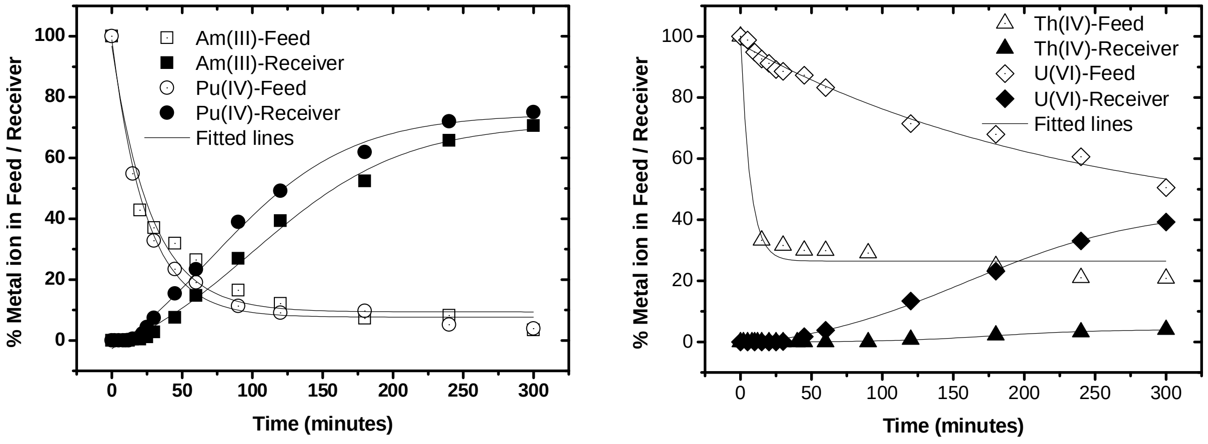

(a) (b)

Fig.A2.11. Transport profiles of the actinide ions using PIMs of the composition: 68.4% TPDGA; 17.9% NPOE; 13.7% CTA; Feed: 1 M $HNO_3$; Receiver: 1 M α-HIBA at pH 3.0.

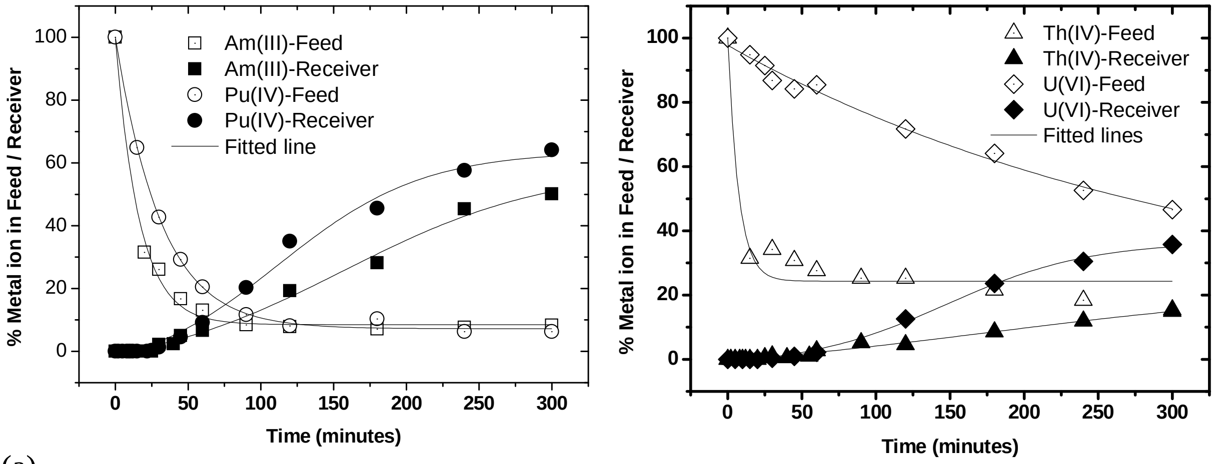

(a) (b)

Fig.A2.12. Transport profiles of the actinide ions using PIMs of the composition: 68.4% THDGA; 17.9% NPOE; 13.7% CTA; Feed: 1 M $HNO_3$; Strip: 1 M α-HIBA at pH 3.0.

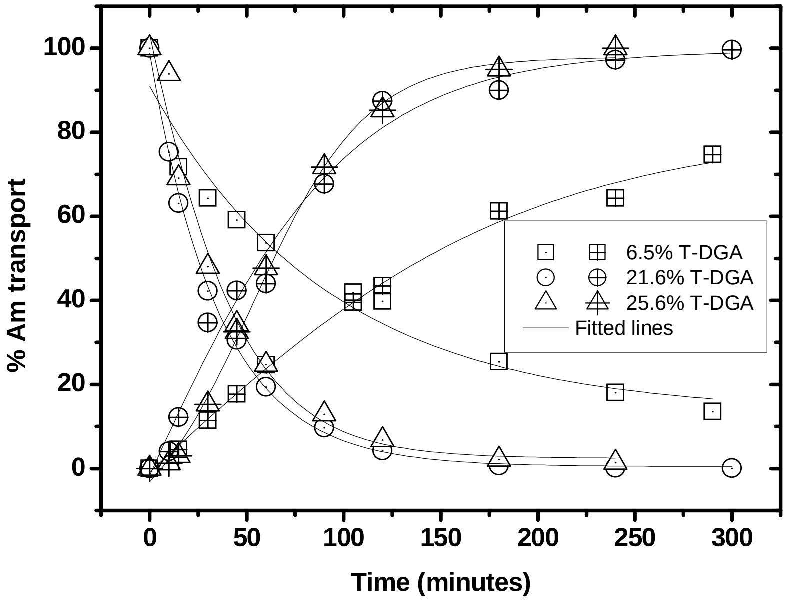

Fig.A2.13. Transport of Am(III) using T-DGA containing PIMs with varying T-DGA content. Feed: 1 M $HNO_3$; Receiver: 1 M α-HIBA.

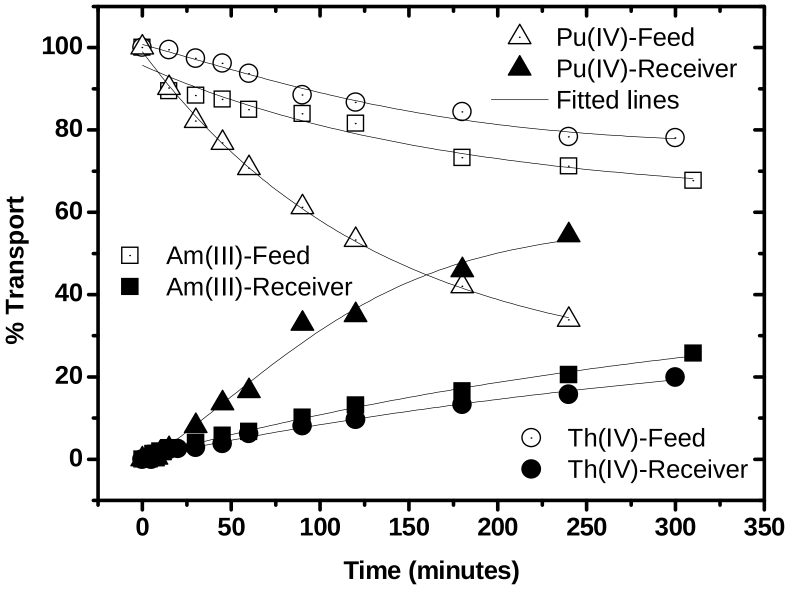

Fig.A2.14. Transport profiles of actinide ions using PIMs of composition: 6.5% C4DGA, 67.7% NPOE, 25.8% CTA; Feed: 1 M $HNO_3$; Receiver: 1 M α-HIBA at pH 3.0.

A2.3. Lag-time studies

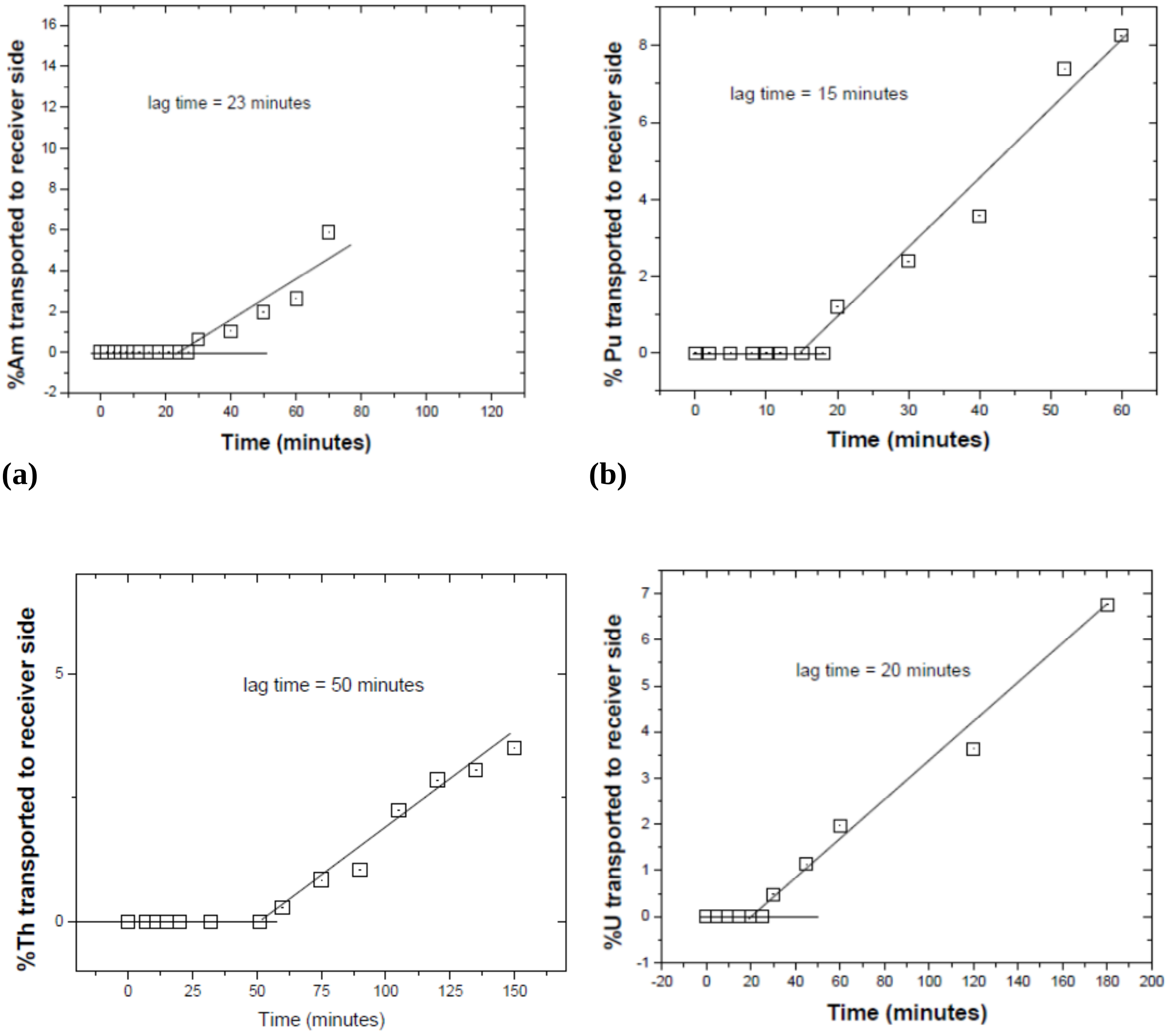

**(a)** **(b)** **(c)** **(d)**

Fig.A2.15. Lag-time plots for actinide ions transport across T2EHDGA containing PIM (a) Am(III) transport (b) Pu(IV) transport (c) Th(IV) transport (d) U(VI) transport

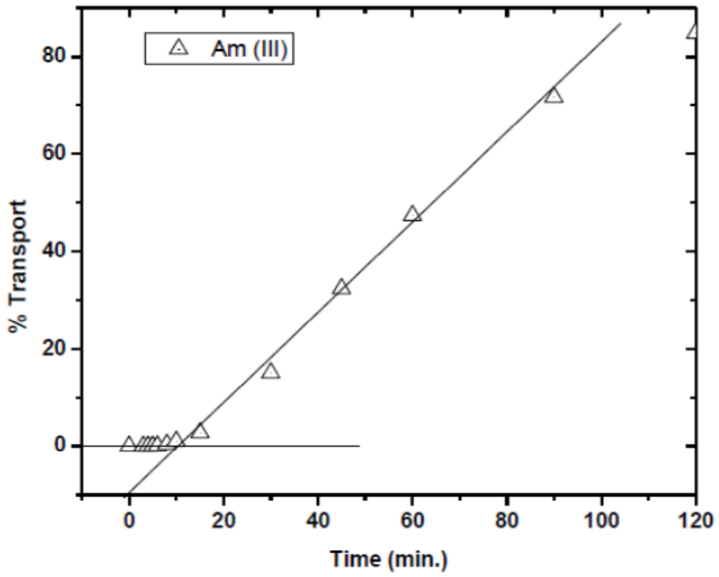

Fig.A2.16. Lag-time plot for Am(III). PIM Composition: 25.6% T-DGA, 53.9% NPOE , and 20.5% CTA. Feed: Am(III) tracer in 1 M $HNO_3$; Receiver: 1 M α-HIBA

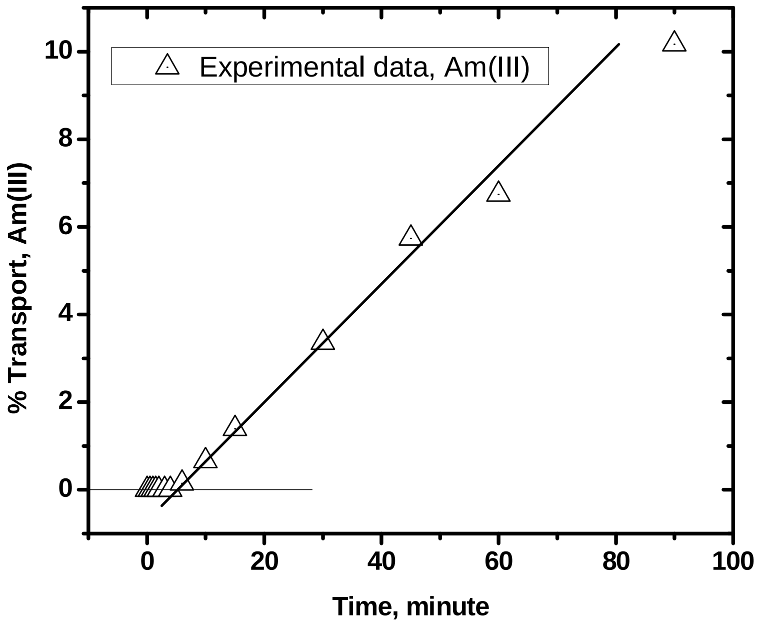

Fig. A2.17. Lag-time plot for Am(III). PIM composition: 6.5% C4DGA, 67.7% NPOE, 25.8% CTA; Feed: Am(III) tracer in 1 M $HNO_3$; Receiver: 1 M α-HIBA

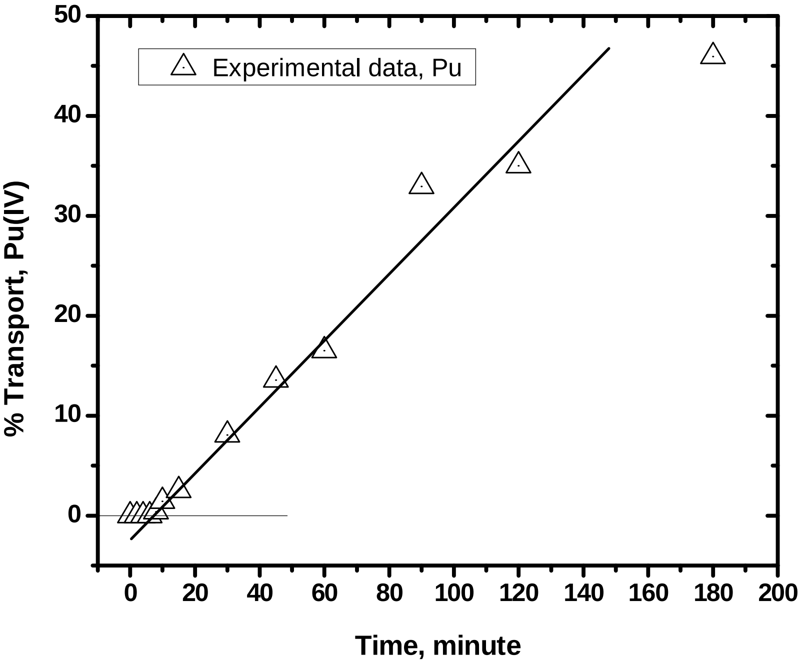

Fig. A2.18. Lag-time plot for Pu(IV). PIM composition: 6.5% C4DGA, 67.7% NPOE, 25.8% CTA; Feed: Pu(IV) tracer in 1 M $HNO_3$; Receiver: 1 M α-HIBA

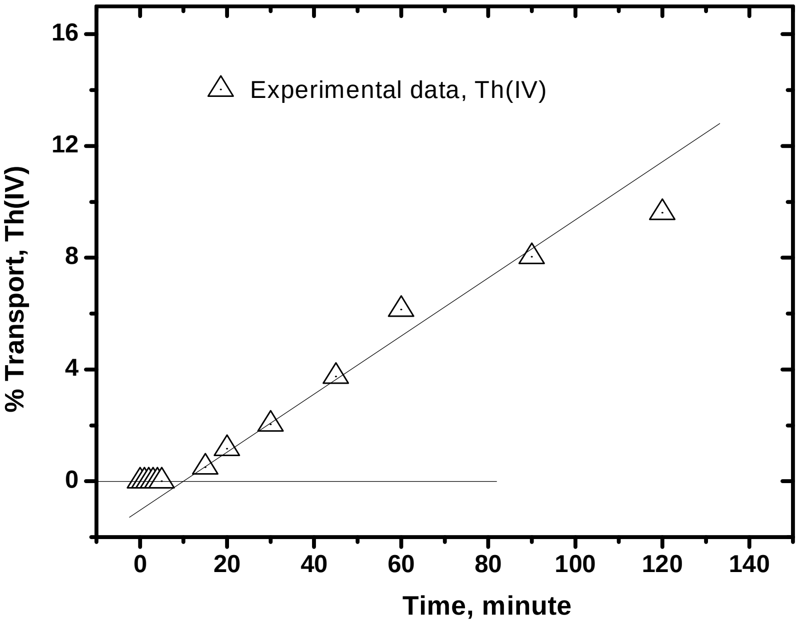

Fig. A2.19. Lag-time plot for Th(IV). PIM composition: 6.5% C4DGA, 67.7% NPOE, 25.8% CTA; Feed: Th(IV) tracer in 1 M $HNO_3$; Receiver: 1 M α-HIBA

## A2.4 Stability studies

### A2.4.1. Stability of the PIMs containing multiple DGA carriers

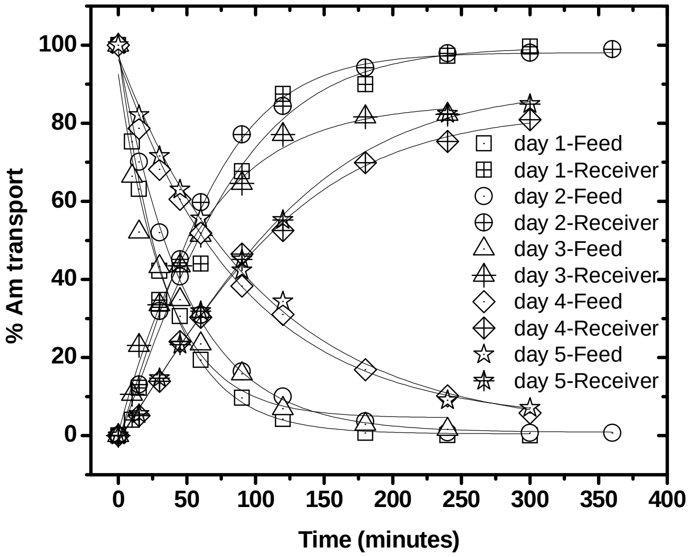

Fig.A2.20. Stability of the T-DGA-containing PIM based on successive Am(III) transport studies. Feed: 1 M $HNO_3$; Receiver: 1 M α-HIBA. PIM composition: 21.6% T-DGA, 56.8% NPOE, 21.6% CTA

Table A2.3. Stability studies of PIM with composition[a]; **[a]**21.6% T-DGA, 56.8% NPOE, 21.6% CTA on Am(III) transport. Feed, 1 M $HNO_3$; Receiver, 1 M α-HIBA at pH 3.0. [b]Data inside parentheses refer to after 24 h

| Day | % Am(III) remained in the feed phase[b] | % of Am(III) transported into the receiver phase[b] | % Am(III) held in PIM[b] | P ($10^{-5}$cm/sec) | % deterioration in P as compared to day 1 |
|---|---|---|---|---|---|
| 1 | 4.2 (nil) | 87.4 (99.9) | 8.4 (0.05) | 2.89 ± 0.03 | 0 |
| 2 | 10.0 (0.3) | 84.4 (95.8) | 5.7 (3.9) | 2.05 ± 0.04 | 29.1 |
| 3 | 6.9 (0.2) | 77.1 (88.0) | 16.1 (11.7) | 1.82 ± 0.08 | 37.0 |
| 4 | 31.0 (0.4) | 52.5 (82.8) | 16.5 (16.8) | 0.99 ± 0.02 | 65.7 |
| 5 | 34.4 (1.0) | 55.2 (88.4) | 10.4 (10.7) | 0.96 ± 0.03 | 66.8 |

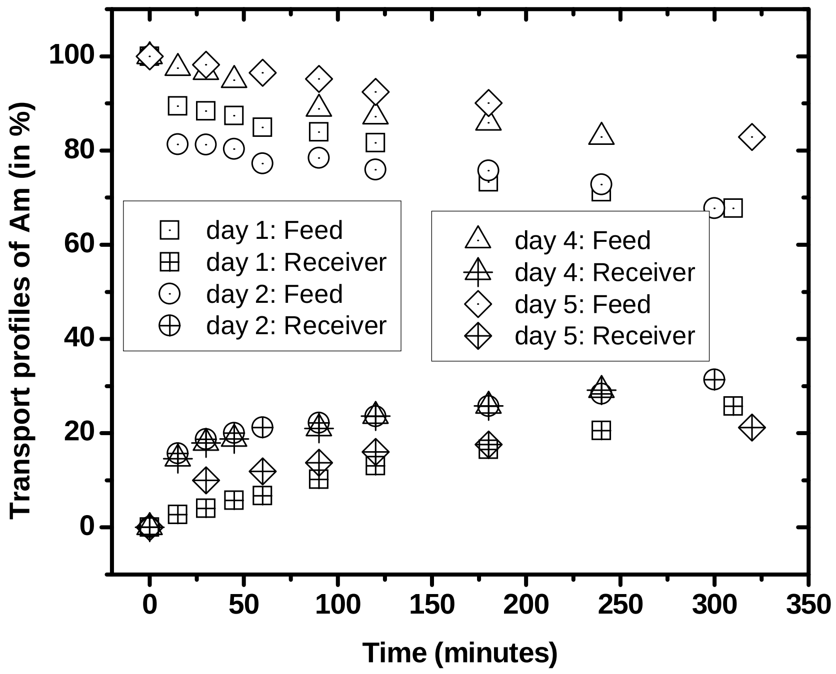

Fig.A2.21. Transport profile of Am(III) for repeated transport experiments for five days consisting of a 24 h cycle to assess the stability of the PIM of composition 6.5% C4DGA octyl, 67.7% NPOE, and 25.8% CTA; Feed:1 M $HNO_3$; Receiver:1 M α-HIBA at pH 3.0.

Table A2.4. Transport data of Am(III) for repeated transport experiments for five days consisting of a 24 h cycle to assess the stability of the PIM of composition 6.5% C4DGA, 67.7% NPOE, and 25.8% CTA; Feed:1 M $HNO_3$; Receiver:1 M α-HIBA at pH 3.0.

| Day | % Uptake from feed phase after 2 h (24 h) | % Transport to the receiver after 2 h (24 h) | P x $10^5$cm/sec |
|---|---|---|---|
| 1 | 18.4 (64.9)[a] | 13.1 (49.9)[a] | 11.78 ± 1.14 |
| 2 | 24.1 (78.0)[b] | 23.6 (63.9)[b] | 8.48 ± 0.22 |
| 4 | 12.8 (50.8)[a] | 23.6 (47.9)[a] | 8.28 ± 0.92 |
| 5 | 7.5 (40.0)[a] | 16.1 (36.8)[a] | 6.23 ± 0.16 |

[a] 24 h data; [b] 48 h data.

## Abbreviations

| | |
|---|---|
| AFM | Atomic force microscopy |
| α-HIBA | Alpha-hydroxy-iso-butyric acid |
| α | Initial absorption rate in Elovich kinetic model |
| A | Total exposed membrane surface area towards solution phase |
| β | Desorption constant in Elovich kinetic model |
| CTA | Cellulose triacetate |
| C4DGA | DGA-functionalized calix[4]arene |
| $C_0$ | Initial concentration of metal ion in feed |
| $C_e$ | Equilibrium concentration of $Eu^{3+}$ in solution |
| $C_t$ | Concentration of metal ion in feed after time 't' |
| CMC | Critical micelle concentration |
| $B_D$ | D-R isotherm constant |
| DGA | Diglycolamide |
| D | Diffusion coefficient |
| D-R | Dubinin−Radushkevich |
| $D_{eff}$ | Effective diffusion coefficient |
| $d_0$ | Membrane thickness |
| EMF | Electromotive force |
| FTIR | Fourier transform infrared spectroscopy |
| HLW | High level waste |
| ISE | Ion selective electrode |
| ICP-AES | Inductively coupled plasma-atomic emission spectroscopy |
| $J_0$ | Membrane initial flux |

| | |
|---|---|
| $k_1$ | Pseudo-first-order rate constant |
| $k_2$ | Pseudosecond-order rate constant |
| $K_{A,B}^{Pot}$ | Selectivity coefficient |
| $K_d$ | Distribution ratio |
| $K_F$ | Freundlich constant |
| $K_L$ | Langmuir constant |
| $K_R$ | Redlich-Peterson constant |
| LSC | Liquid scintillation counter |
| LOD | Limit of detection |
| NaTPB | Sodium tetraphenyl borate |
| NPOE | 2-Nitrophenyl octyl ether |
| P | Permeability coefficient |
| PVC | Poly(vinyl chloride) |
| PIM | Polymer inclusion membrane |
| $q_e$ | Sorption capacity of PIM at equilibrium |
| $q_{max}$, | Maximum sorption capacity |
| $q_t$, | Sorption capacity of PIM at time t |
| $R^2$ | Correlation coefficient |
| SEM | Scanning electron microscopy |
| t | Time |
| T | Absolute temperature in Kelvin |
| $t_{lag}$ | Lag-time |
| TODGA | *N*,*N*,*N'*,*N'*-tetra-*n*-octyl diglycolamide |
| T2EHDGA | *N*,*N*,*N'*,*N'*-tetra-(2-ethylhexyl) diglycolamide |

| | |
|---|---|
| THDGA | *N*,*N*,*N'*,*N'*-tetra-*n*-hexyl diglycolamide |
| TPDGA | *N*,*N*,*N'*,*N'*-tetra-*n*-pentyl diglycolamide |
| TDDGA | *N*,*N*,*N'*,*N'*-tetra-*n*-decyl diglycolamide |
| T-DGA | Tripodal diglycolamide |
| TGA | Thermogravimetric analysis |
| TIMM | Transmission infrared mapping microscopy |
| $T_g$ | Glass transition temperature |
| $T_m$ | Melting temperature |
| TTA | 2-Thenoyltrifluoro acetone |
| THF | Tetrahydrofuran |
| V | Volume of the feed phase |
| XRD | X-ray diffraction |
| $\chi^2$ | Non-linear parameter |